ULTRAFAST CARRIER DYNAMICS AND CHARGE TRANSFER PROCESSES IN PHOTOEXCITED PEROVSKITE NANOCRYSTALS

A Thesis Submitted for the Degree of
Doctor of Philosophy
by

Mr. Apurba De

School of Chemistry
University of Hyderabad
(P.O.) Central University, Gachibowli
Hyderabad- 500 046
Telangana, India

Dedicated to

Amal Sir, Uttam Babu, Nabo Sir

&

my 'family'

A man would do nothing, if he waited until he could do it so well that no one would find fault with what he has done.

John Henry Newman

(1801-1890)

Contents

Declaration

I hereby declare that the matter embodied in the thesis entitled "***Ultrafast Carrier Dynamics and Charge Transfer Processes in Photoexcited Perovskite Nanocrystals***" is the result of investigations carried out by me in the School of Chemistry, University of Hyderabad, India under the supervision of Prof. Anunay Samanta.

In keeping with the general practice of reporting scientific investigations, acknowledgements have been made wherever the work described is based on the findings of other investigators. Any omission or error that might have crept is regretted.

Apurba De.

University of Hyderabad, India

October, 2020

Apurba De

SCHOOL OF CHEMISTRY
UNIVERSITY OF HYDERABAD
HYDERABAD- 500 046, INDIA

Phone: +91-40-2313 4513 (O)
+91-40-2313 0715 (R)
Fax: +91-40-2301 1594
Email: anunay@uohyd.ac.in

Professor Anunay Samanta

Certificate

This is to certify that the thesis entitled **"*Ultrafast Carrier Dynamics and Charge Transfer Processes in Photoexcited Perovskite Nanocrystals*"** submitted by *Mr. Apurba De* bearing the registration number 15CHPH01 in partial fulfilment of the requirements for the award of Doctor of Philosophy (Ph.D.) in the School of Chemistry, University of Hyderabad, India under my supervision and guidance. This thesis is free from plagiarism and has not been submitted previously in part or full to this or other University/Institution for any degree or diploma. Further, the student has following publications before submission of the thesis for adjudication and has produced evidences for the same in the form of reprints.

Parts of this thesis have been published in the following publications:

1. Apurba De, Navendu Mondal and Anunay Samanta, Luminescence Tuning and Exciton Dynamics of Mn-Doped $CsPbCl_3$ Nanocrystals. *Nanoscale* **2017**, *9*, 16722-16727. *(Chapter 1)*

2. Apurba De, Somnath Das, Navendu Mondal and Anunay Samanta, Highly Luminescent Violet- and Blue-Emitting Stable Perovskite Nanocrystals. *ACS Materials Lett.* **2019**, *1,* 116-122. *(Chapter 2)*

3. Apurba De, Navendu Mondal and Anunay Samanta, Hole Transfer Dynamics from Photoexcited Cesium Lead Halide Perovskite Nanocrystals: 1-Aminopyrene as Hole Acceptor. *J. Phys. Chem. C* **2018**, *122*, 13617-13623. *(Chapter 3)*

4. Apurba De, Somnath Das, and Anunay Samanta, Hot Hole Transfer Dynamics from $CsPbBr_3$ Perovskite Nanocrystals. *ACS Energy Lett.* **2020**, *5*, 2246-2252. *(Chapter 4)*

The student has made presentation in the following conferences:

1. "Hot Carrier Extraction from $CsPbBr_3$ Perovskite Nanocrystals", **International Conference on Nano Science and Technology- (ICONSAT-2020)**, S. N. Bose National Centre for Basic Sciences, Kolkata - 700 106, India, March 5-7, 2020. (*Poster Presentation*)
2. "Efficient Extraction of Hot Holes from $CsPbBr_3$ Perovskite Nanocrystals", **Chemfest-2020, 17th Annual In-House Symposium of the School of Chemistry,** University of Hyderabad, Hyderabad, India, February 27-28 , 2020. (*Oral Presentation*)
3. "Impact of B-cation doping on the Photoluminescence Properties of $CsPbCl_3$ Perovskite Nanocrystals: Investigating the Carrier Dynamics", **Theme meeting on Ultrafast Science (UFS 2019),** Indian Institute of Technology, Bombay, India, November 7-9, 2019. (*Poster Presentation*)
4. "Post-synthetic Treatment Yielding Blue-violet Emitting Perovskite Nanocrystals with Near-unity Photoluminescence Quantum Yield and Superior Stability", **The 10th Asian Photochemistry Conference- (APC-2018)** at Taipei, Taiwan, December 16-20, 2018. (*Poster Presentation*)
5. "Photoinduced Hole Transfer Dynamics from Perovskite Nanocrystals ($CsPbX_3$: X=Br, I) to 1-Aminopyrene as Molecular Acceptor", **Chemfest-2018, 15th Annual In-House Symposium of the School of Chemistry,** University of Hyderabad, Hyderabad, India, March 9-10, 2018. (*Poster Presentation*)
6. "Luminescence Tuning and Exciton Dynamics of Mn-doped $CsPbCl_3$ Nanocrystals", **14th Trombay Symposium on Radiation and Photochemistry (TSRP 2018), Bhabha Atomic Research Centre (BARC),** Mumbai, India, January 3-7, 2018. (*Poster Presentation*)

The student has passed the following courses towards the fulfilment of the coursework requirement for Ph.D. degree:

Sl. No.	Course Code	Title	Credits	Grade/Status
1.	CY801	Research Proposal	3	B+/Pass
2.	CY805	Instrumental Methods-A	3	B+/Pass
3.	CY806	Instrumental Methods-B	3	B+/Pass
4.	CY453	Molecular Spectroscopy	4	B+/Pass

28·10·2020

Anunay Samanta

Thesis Supervisor

PROF. ANUNAY SAMANTA
SCHOOL OF CHEMISTRY
UNIVERSITY OF HYDERABAD
HYDERABAD - 500 046

28·10·2020

Dean

School of Chemistry
University of Hyderabad

Dean
School of Chemistry
University of Hyderabad
Hyderabad - 500 046

Acknowledgements

Surely, I didn't expect to grow in a way that I have grown during the last five years, but here I am. Thanks to all those incredible people whom I met here in Hyderabad.

First and foremost, I cannot have a better mentor like Sir, Professor Anunay Samanta, for which I am really grateful. I am humbled for his belief in giving me an opportunity to be a part of his group and I have tried my best to fulfil the expectations. He has been there always in guiding me in proper direction whether academic or personal. His enormous effort to make our work move smoothly is difficult to describe. Virtues like time management, giving 'the best' in every work, no matter how small, are something I wish to adopt from him.

I would like to thank the former and present Dean(s), School of Chemistry, for their constant support and for all the facilities which have accelerated my work. Along with all faculty members, I specially acknowledge my doctoral committee members, Professor Musti J. Swamy and Professor Susanta Mahapatra for their help, cooperation and encouragement. Questions asked by them during various context like in work progress seminar, Chemfest were extremely valuable and made me to re-think the subject from a different perspective.

Acknowledges are also due to Center for Nanotechnology and Central Instrumental Facility, University of Hyderabad for allowing me to avail the facilities. Cooperation that I received from Druga Prasad and Sunil is not limited to just sample measurements. Also, I am grateful to Anil anna and Surya anna (from Prof. Nagia's Lab) for their kind help in many occasions.

I would also like to thank Morrision, Yoganath, Rajesh, Navaneethan and others in LSS, for their constant cooperation and effort, related to our femtosecond-laser setup, whenever needed. I must mention about Shiva, Radhika, Mahesh, Srinivas, and Naresh as well for their enormous efforts in various occasions. Without you all, I cannot imagine how difficult it would have been.

Financial assistance from DST and UGC, New Delhi is greatly acknowledged. Special thanks are due to UGC-BSR for providing me a research fellowship during my Ph.D.

tenure. I also thank SERB for the grant that I received under 'International Travel Support' scheme to attend the overseas conference, APC-2019 in Taipei, Taiwan.

Those without whom I wouldn't be writing today are Amal Sir, Uttam babu and Nabo Sir; the builders of my academic root. From childhood days (when I was in class 6), I have been in associated with Amal Sir and now I realize how valuable those early-periods were. At that age what I learnt from you is more than just academics. All ethical values that I endow today, were taught by you. Thank you for enriching me with those valuable lessons. My love for Physics/Chemistry starts building around an exceptional teacher, Uttam babu during my high-school. Your 'my way or highway' attitude may appear a little unorthodox but that is what I admire most. Your straight-forward way of talking without having any drama is what I always try to follow. My choice of taking Chemistry become worthy when I met Nabo Sir, one of the exceptional Physical-chemistry teachers I ever met. Besides your teaching, your way of interaction with students and your end-less efforts for their success is something I admire the most. I shall always remember those conversations with you (which still motivates me) whether it was while having tea in 'Birati' railway station or over phone. Pure love for academics is always felt whenever I interact with you. Finally, I am humble and proud that I can call myself 'a student' of you three; but at the same time, every now and then, I feel that I have failed to give proper value to what you all expected from me. May be, I didn't tried my best then, but now I am.

I am lucky that throughout my academic journey so far, I have always been surrounded by exceptional teachers which started at 'prathamic bidyalaya' where I met Maharaj, Tapan Sir, Sahadeb Sir. 'Singur Mahamaya High School' is a place very close to me and still today, I enjoy remembering every possible moments that I spent there. The love that I got from all the teachers and staffs in there was something special. It is really difficult to name all of them (almost 40!), but I must name a few. Amitabha babu, Sanchita madam, Piyali madam, Kalyani madam, Prabir babu, Debi babu, Mrinmoy babu, Srikanta babu were exceptional. Especially, the Bengali lesson (not limited to just textbook) that I got from Sanchita madam, is something unparallel and those were the time when I enjoyed my school-life most. I felt sad that I had to leave the school after 10th, but new school brought opportunity to meet new teachers like Uttam babu, Rabin babu and Swadesh babu. I must mention Arun babu, from whom I took Maths lessons, a great teacher who always believed in me and encouraged me to move forward.

Again, it is really difficult to name never-ending list of friends but Milan, Gopi, Saptarshi, Tanmoy, Aniruddha, Prittwish, Subhashis, Ripan, Sumana, Sangita, Suraiya, Chanchal, Niladri, Surajit are few of them. Kuntal and Arnab are there from my childhood days (from class 5!). Kuntal, I never thought that we will have a journey so parallel for such a long period (18 years almost!), starting from school thought college to finally here in Hyderabad. Arnab has always been a special friend of mine. I still remember the fun that we had together whether it was in the 'Ogilvie hostel' of Scottish Church College or when we visited in Delhi. Still a long way to go! Another 'mohan bekti' is Anik! I still remember the gossip that we (you, me, Kuntal and Arijit) used to have in your mess in Kestopur. The cooking and other experiences that we had in your place and in Arijit's flat is something better not to mention here but to cherish forever.

Sauvik, Runa, Kajari, Suvoshree, Joydeb were some extraordinary people whom I met during my college. The fun that we had whether in was Holi celebration or Durga puja outing or going for IPL match in Eden Gardens is unforgettable. Sauvik is someone who is always an inspiration to me. Besides your charming character, your steely focus to achieve something is admirable. I am grateful to kaku-kakima (Sauvik's parents), from whom I got so much love. The excellent home-made food that I had while staying you home occasionally is something I can never forget. I am also fortunate to have friends like Rudra, Agniv, Rajdip, Bratati, Arpita, Anupam da, Rituparna. I am lucky to have Malay da as a brother with whom I spend quite a significant time as roommate during B.Sc. I must mention Rakesh da whose simplicity I admire most. Nithun, Ankan, Sourav, Naren, Pritam, Saptarshi, Subhojit-my M.Sc. buddies; I am thankful to you all. I am grateful to Mithu, Subhendu, Poulami and Munia; though our interaction was limited, but knowingly or unknowingly you all be have been a great motivator for me. I must mention Subho; one of the most talented and versatile characters I ever met; I understand why you disconnected yourself from all of us but I'm sure you will be (or are) doing great and I owe you a lot.

It is really difficult to summarize how grateful I am to my lab-mates. To be very honest, I sometimes doubted on myself whether among you all (with such exceptional qualities), I would be a fit here or not! But, somehow I managed. I still remember my very first conversation with Ashok anna when I first came to the lab. Chandu anna had been a wonderful senior from whom I learnt the synthesis of quantum dots in my initial days. Your involvement in other things like sports, social activity is something I admire.

Shalini di, though our interaction had been limited, but your presence in the lab was something difficult to forget. How much I owe from Navendu da, is not possible for me to gist. Those were my best time in the lab, discussing with you on endless topics. Your patience (which I lack most) and ability of explaining things in very simple way is something I found unparallel. I am fortunate and shall cherries the fact that I worked with you so closely. Your encouragement has always been special to me to motivate myself. Sudipta da, with whom not only I shared the lab but had been a great room-mate as well during my initial days at HCU; I get to learn many things from you. Your straightforward, frank opinion always helps. Your courage of jumping into new avenue is very admirable to me. Sneha di, you had been an excellent senior to me; starting from understanding the instruments to discuss about foods, places, movies, trekking were exciting and mostly, relaxing. I have always followed you trying to adopt your communication skill which I found the best. Saddam has been more than a lab mate to me. I (we) cannot forget the moment of our very first conversion (in English surprisingly!) during our admission. I really respect you in many ways starting from your endless effort in maintaining discipline in the lab to your capability of carrying responsibilities in many occasions. Tasnim, I really enjoyed working with you, especially during the recent past time. I am glad for our occasional discussions on both academic & non-academic context, where in many cases conflicts were raised within me, which however gave me an opportunity to re-evaluate myself; I am thankful for that. Somnath has been an excellent junior to me. Special thanks to you for handling the 'behind the scene' job in the lab which takes enormous efforts that many wouldn't even realize. Sumanta, thank you to for the time-to-time discussions and there is a lot to learn from you for me, but my time here is about to end. Rajesh, your determination of executing work in the lab is admirable. Alila, though your staying here in the lab was short but I shall always remember your treat of pork-my very first time. At last, I must say that you all had been so lovely to me always, and I learnt a lot from each one of you, but in several occasions, I lost my temper (which I guess is not so uncommon!) and had been rude to many; I apologize for that. I tried my best to adopt myself with you all.

I am very glad that I meet Sunanda di. The delicious foodsthat I had in your home was something I'm going to remember for long. It was fun too to have you on lab parties and wish we could have arranged a lab trip along with you that you asked for.

My sincere gratitude to madam, Ani da and Boni. I enjoyed the time being associated with you all, whether it was in lab party or in Ani da's marriage. I shall never forget the fun that I had in Taiwan with Sir and madam. Specially visiting Yehliu Geopark (Sir's idea) was something I am going to remember forever.

Any formal writing is not adequate enough to describe our 'gang' in HCU. Sudipta da, Bappa, Arijit, Kuntal, you all are phenomenon and I feel really sad thinking that our journey together is going to end here. Speaking of each one of you, will be too formal (you all know that), thus just skipping that part. What I am going to miss mostly is our 'Sonibarer adda'; which started with Rabindranath and ended with Joy Goswami; and remembering endless topics discussed in-between, just make me smile today. Starting from the Annexe to NRS, 8, 13, F-205, F-202 are more than just room numbers, those are 'our places'. The fun that we had there is something I am going to remember forever. The adventure that I experienced during trekking to Roopkund and Rupin pass were unparallel; a special 'dhonnobad' to 'vai'. I guess, 'Kodaikanal' has become a new crush for all of us and will make that place as our destination 'reunion-place' for sure. Talking of our 'gang', I must mention Debika (though you don't have permanent membership). A big thank to you for your time-to-time visit and preparing exceptionally delicious homey-foods (specially 'pantua') which I couldn't believe to have here in Hyderabad.

I also thank my hostel wing-mates Kailash, Tushar, Deba, Anand and Ram; especially for bearing the 'hottogol' in almost every Saturday. I am also thankful to have friends like Subrata da, Golu, Anna, Hemant, Razi, Nilanjan (from Physics). I am fortunate to meet Anjan, Chapu and Kushal, who all are amazing people in their respective way.

I consider myself lucky to have seniors like Santanu da, Arpita di, Karunamoy da, Sugata da, Rudra da, Olivia di, Debparna di, Arpita di (from Chemistry), Suman da, Kaushik da, Subho da, Sabari di and Kollol da. Though I had limited interaction but I shall cherish every moment spent with Arup, Suranjan, Rajib, Sritam, Mainak, Aranya here in HCU. It was great to have juniors like Soutrick, Subham, Tausif, Anupam, Nilanjan, Alim, Hafizur, Debu, Pritam, Sarada and Olivia. Fun that we had on our NRS roof-top on several occasions are better not to describe here! I am going to miss that very badly. Going early morning in the vegetable market for 'Saraswati puja' was a special experience for me and I shall never forget that. Events such as Saraswati Puja, BPL, and Knight Cup were full of fun to be associated with, whether actively or just being there.

I am lucky to have batch mates like Senthil, Ankit, Venky, Sankar, Arun, Manish, Harilal, Ramesh, Tanmay, Manzoor, Anif, Mou, Sameeta, Sipra. I enjoyed the time with you all, specially organizing the Ph.D. freshers' party was fun.

Gratitude to my family members is difficult to express. Sacrifice of my 'maa-baba' is beyond words and I sincerely thank them for letting me do what I asked for. A big thank to my 'didi' who I can say was my idol in my childhood days. I still remember the day when I cried so much just because you were not there in helping me in English lessons (you got married couple of days back from then); today it may sound silly but it is what it is. Another person I must mention is my 'jethu'; wish you were alive today. Mentioning everyone in my family is difficult but I thank you all for being there.

I must mention about the 'campus' itself which will stay in my memory forever. I really enjoyed my time here whether it was roaming with friends at night or while clicking some photographs. I couldn't imagine a more calm and vibrant campus than here in 'HCU' and I am lucky that I got the opportunity to spent significant time here.

At last, I must say that I have lived my Ph.D. journey with utmost joy and one way or another, I am grateful to you all.

Cheers!

Apurba
October, 2020

List of Publications

Thesis Chapters Publications

1. Apurba De, Somnath Das, and Anunay Samanta, Hot Hole Transfer Dynamics from $CsPbBr_3$ Perovskite Nanocrystals. *ACS Energy Lett.* **2020**, *5*, 2246-2252. *(Chapter 4)*
2. Apurba De, Somnath Das, Navendu Mondal and Anunay Samanta, Highly Luminescent Violet- and Blue-Emitting Stable Perovskite Nanocrystals. *ACS Materials Lett.* **2019**, *1*, 116-122. *(Chapter 2)*
3. Apurba De, Navendu Mondal and Anunay Samanta, Hole Transfer Dynamics from Photoexcited Cesium Lead Halide Perovskite Nanocrystals: 1-Aminopyrene as Hole Acceptor. *J. Phys. Chem. C* **2018**, *122*, 13617-13623. *(Chapter 3)*
4. Apurba De, Navendu Mondal and Anunay Samanta, Luminescence Tuning and Exciton Dynamics of Mn-Doped $CsPbCl_3$ Nanocrystals. *Nanoscale* **2017**, *9*, 16722-16727. *(Chapter 1)*

Other Publications

5. Tasnim Ahmed, Apurba De, Sumanta Paul and Anunay Samanta, Individual Particle-Level Picture of Charge Carrier Recombination in Bi-Doped $CsPbBr_3$ Nanocrystals. (Communicated)
6. Navendu Mondal, Apurba De, Sudipta Seth, Tasnim Ahmed, Somnath Das, Sumanta Paul, Rajesh Kumar Gautam and Anunay Samanta, Dark Excitons of the Perovskites and Sensitization of Molecular Triplets. (to be communicated) *(Perspective)*
7. Somnath Das, Apurba De and Anunay Samanta, Ambient Condition Mg^{2+}-Doping Producing Highly Luminescent Green- and Violet-Emitting Perovskite Nanocrystals with Reduced Toxicity and Enhanced Stability. *J. Phys. Chem. Lett.* **2020**, *11*, 1178-1188.
8. Sudipta Seth, Tasnim Ahmed, Apurba De and Anunay Samanta, Tackling the Defects, Stability and Photoluminescence of $CsPbX_3$ Perovskite Nanocrystals. *ACS Energy Lett.* **2019**, *4*, 1610-1618. *(Perspective)*

9. Navendu Mondal, Apurba De, Somnath Das, Sumanta Paul and Anunay Samanta, Ultrafast Carrier Dynamics of Metal Halide Perovskite Nanocrystals and Perovskite-composites. *Nanoscale* **2019**, *11*, 9796-9818. *(Review)*
10. Navendu Mondal, Apurba De and Anunay Samanta, Achieving Near-Unity Photoluminescence Efficiency for Blue-Violet-Emitting Perovskite Nanocrystals. *ACS Energy Lett.* **2019**, *4*, 32-39.
11. Navendu Mondal, Apurba De and Anunay Samanta, Biexciton Generation and Dissociation Dynamics in Formamidinium and Chloride-Doped Cesium Lead Iodide Perovskite Nanocrystals. *J. Phys. Chem. Lett.* **2018**, *9*, 3673-3679.
12. M. Chandra Sekhar, Sneha Paul, Apurba De and Anunay Samanta, An Ultrafast Transient Absorption Study of Charge Separation and Recombination Dynamics in CdSe QDs and Methyl Viologen: Dependence on Surface Stoichiometry. *ChemistrySelect* **2018**, *3*, 2675-2682.
13. Navendu Mondal, Apurba De and Anunay Samanta, All-inorganic Perovskite Nanocrystal Assisted Extraction of Hot Electrons and Biexcitons from Photoexcited CdTe Quantum Dots. *Nanoscale* **2018**, *10*, 639-645.
14. Anamika Ray, Apurba De and Sumanta Bhattacharya, Study of energy transfer phenomenon between quantum dots and zinc porphyrin in solution. *Journal of Molecular Liquids* **2017**, *246*, 17-24.
15. M. Chandra Sekhar, Apurba De, Sk. Saddam Hossain and Anunay Samanta, Roles of the Methyl and Methylene Groups of Mercapto Acids in the Photoluminescence Efficiency and Carrier Trapping Dynamics of CdTe QDs. *Phys. Chem. Chem. Phys.* **2017**, *19*, 1536-1542.

List of Conference Presentations

Poster Presentation

1. "Hot Carrier Extraction from $CsPbBr_3$ Perovskite Nanocrystals", **International Conference on Nano Science and Technology- (ICONSAT-2020)**, S. N. Bose National Centre for Basic Sciences, Kolkata, India, March 5-7, 2020.

2. "Impact of B-cation doping on the Photoluminescence Properties of $CsPbCl_3$ Perovskite Nanocrystals: Investigating the Carrier Dynamics", **Theme meeting on Ultrafast Science (UFS 2019),** Indian Institute of Technology, Bombay, India, November 7-9, 2019. (*Best Poster Award*)

3. "Post-synthetic Treatment Yielding Blue-violet Emitting Perovskite Nanocrystals with Near-unity Photoluminescence Quantum Yield and Superior Stability", **The 10th Asian Photochemistry Conference- (APC-2018)** at Taipei, Taiwan, December 16-20, 2018.

4. "Photoinduced Hole Transfer Dynamics from Perovskite Nanocrystals ($CsPbX_3$: X= Br, I) to 1-Aminopyrene as Molecular Acceptor", **Chemfest-2018, 15th Annual In-House Symposium of the School of Chemistry,** University of Hyderabad, Hyderabad, India, March 9-10, 2018.

5. "Luminescence Tuning and Exciton Dynamics of Mn-doped $CsPbCl_3$ Nanocrystals", **14th Trombay Symposium on Radiation and Photochemistry (TSRP 2018), Bhabha Atomic Research Centre (BARC),** Mumbai, India, January 3-7, 2018.

6. "Investigating the Carrier Dynamics of Mn-doped $CsPbCl_3$ Nanocrystals with Tunable Mn Photoluminescence Band**",** **8th International Collaborative & Cooperative Chemistry Symposium,** Organized by School Of Chemistry, University of Hyderabad, India, December 18-19, 2017.

Oral Presentation

1. "Efficient Extraction of Hot Holes from $CsPbBr_3$ Perovskite Nanocrystals", **Chemfest-2020, 17th Annual In-House Symposium of the School of Chemistry,** University of Hyderabad, Hyderabad, India, February 27-28 , 2020.

List of Abbreviations

ADC	Analog to Digital Converter
BBO	β-Barium Borate
CBM	Conduction Band Minima
CFD	Constant Fraction Discriminator
EDET	Exciton-Dopant Energy Transfer
EDX	Energy Dispersive X-ray
FESEM	Field-Emission Scanning Electron Microscopy
EPR	Electron Paramagnetic Resonance
ESA	Excited State Absorption
FTIR	Fourier-Transform Infrared Spectroscopy
GSB	Ground State Bleach
GVD	Group Velocity Dispersion
HCC	Hot Carrier Cooling
HR-TEM	High Resolution-Transmission Electron Microscopy
HOMO	Highest Occupied Molecular Orbital
HTM	Hole Transporting materials
ICP-OES	Inductively Coupled Plasma-Optical Emission Spectroscopy
LBO	Lithium triborate
LEDs	Light-Emitting Diodes
LUMO	Lowest Unoccupied Molecular Orbital
MCA	Multi-channel Analyzer
MCP	Micro-Channel Plate
NCs	Nanocrystals
OPA	Optical Parametric Amplifier
PCE	Power Conversion Efficiency
PGA	Programmable Gain Amplifier
PIB	Photo Induced Bleach
PMT	Photo Multiplier Tube
PL	Photoluminescence
PLQY	Photoluminescence Quantum Yield
PL UC	Photoluminescence Upconversion
PXRD	Powdered X-ray Diffraction
QDs	Quantum Dots
RB	Round Bottom
RT	Room Temperature
SE	Stimulated Emission

SFS	Sum Frequency Signal
SHS	Second Harmonic Signal
SQ	Shockley-Queisser
TCSPC	Time Correlated Single Photon Counting
TA	Transient Absorption
TAC	Time to Amplitude Converter
TCU	Temperature Control Unit
TEM	Transmission Electron Microscopy
TGD	Timing and Delay Generator
UV-Vis	Ultraviolet-Visible
XPS	X-ray Photoelectron Spectroscopy

CHAPTER 1

Introduction

Overview

This chapter provides a brief introduction on semiconductor materials and the effect of quantum confinement on their band structures. Subsequent discussion is restricted to a particular type of semiconductors, the perovskites, which are the subject matter of this thesis. Important characteristic properties of the perovskites such as crystal structure, their formability criteria, exciton fine structure, composition dependent bandgap, surface properties and optical properties are discussed. A brief introduction on doped perovskites highlighting their importance is presented. Finally, discussion on charge (electron/hole) transfer processes in semiconductors is presented briefly.

1.1. Motivation

We cannot think of our day-to-day activities without mobile phones, computers and other electronic gadgets, which all consist of semiconductors. Besides, the semiconductor materials find application in solar cells as well. Energy crisis is one of the major concerns and promoting the use of renewable energy is a priority. Particularly, considering the rapidly growing population of India, the demand of energy is expected to be sky high in near future. With limited resources of non-renewable energy, one must look for alternative renewable energy sources like sunlight, wind, water etc. Based on the geological location of India and availability of abundant solar radiation throughout the year, utilizing solar energy can be advantageous. Though silicon solar cells have been commercialized, they are still quite expensive for large scale production and use in developing economics like India. In this context, the perovskite solar cells are expected to be cheap due to their ease of fabrication and they are already on the way towards commercialization. The last few years have witnessed tremendous progresses in perovskite-based solar cells and their efficiency has reached as high as >25%.[1] In this regard, photophysical investigations on these materials are crucial for device development and thus emerges the important role of spectroscopic tools. The major focus of the thesis revolves around the photophysics of this emerging class of materials, perovskites. The primary goal of the works described in this thesis is to study the optical responses of these materials using sophisticated spectroscopic techniques and gain insights that may be beneficial for their better utilization in photovoltaic and optoelectronic applications.

1.2. Semicondctors: From Bulk to NCs

Among solids, electrical conductivity of a semiconductor material falls between a metal and an insulator.[2] This variation in conductivity is based on their characteristic bandgap energies and band structures. For the transition of electrons from VB to CB, it requires a definite amount of energy equal or greater than the bandgap. By applying an ionizing radiation, one can excite an electron from VB to CB, leaving a hole behind in the VB. For semiconductors, which are of interest in photovoltaics, ionization is generally achieved

through optical excitation. Since conductivity depends on the mass of the photogenerated charge carriers (electron and hole), considering different kinds of interactions (such as coulombic interaction, spin-orbit coupling, relativistic effect etc.) experienced by the charge carriers, their rest masses are replaced with their effective masses,[3] as the latter determine the mobilities of the carriers within the crystal. The minimum amount of energy (E) required to produce an electron-hole pair is expressed as below[3, 4]

$$E = E_g + E_{e,kin} + E_{h,kin}$$

Where E_g is the bandgap of the material, $E_{e,kin}$ and $E_{h,kin}$ represent the kinetic energy of the photogenerated electron and hole, respectively. Not to mention that along with the energy conservation, momentum conservation also holds (i.e. $\hbar k_{CB} = \hbar k_{VB} + \hbar k_{photon}$). Under the approximation of negligible momentum of photon, vertical transition criterion is satisfied i.e. $\hbar k_{CB} = \hbar k_{VB}$.

Under Coulomb potential, the photogenerated electron and hole form an electrically neutral quasi-particle called 'exciton' whose energy ($E_{exciton}$) is given by[3, 4]

$$E_{exciton} = E_g - \frac{R_y}{n^2} + \frac{\hbar^2 k^2}{2\left(m_e^* + m_h^*\right)}$$

R_y represents Rydberg energy, n is an integer, $\hbar$ is the reduced Planck's constant and m_e^* and m_h^* represent effective masses of electron and hole, respectively. Another important parameter to consider in this context is the exciton Bohr radius (a_0), which is expressed as below[4]

$$a_0 = \frac{\hbar^2 \varepsilon}{e^2}\left(\frac{1}{m_e^*} + \frac{1}{m_h^*}\right)$$

Exciton Bohr radius is a function of the dielectric constant of the material (ε) and effective masses of electron and hole. It is an important parameter in determining the extent of confinement that a material possesses (discussed later).

The nanocrystalline forms of the semiconductor materials are quite interesting due to their unique properties compared to their bulk counterpart. Those properties arise due to 'quantum confined' nature of the excitons.[5] Henceforth by 'confinement' it is meant confinement of excitonic wavefunction. Whether a system is quantum confined or not is determined by considering the exciton Bohr radius and the size of the system.[6] Thus quantum confinement is a size dependent property, where the change in NCs diameter leads to change of electronic and optical properties. The dimensionality and size of a system has direct consequence on its band structure. Figure 1.1A shows schematic representation of a bulk (3D), two-dimensional (2D), one-dimensional (1D), and zero-dimensional (0D) nanostructures. The effect of confinement on their band structure is also shown. Increased confinement results in an increase of the bandgaps of the system. The general expression which defines the bandgap energy of such quantum confined system is as follows[5, 6]

$$E_g(QD) = E_g(Bulk) + \frac{\hbar^2\pi^2}{2m_e^*R^2} + \frac{\hbar^2\pi^2}{2m_h^*R^2} - \frac{1.786e^2}{\varepsilon R} - 0.248E_{Ry}^*$$

$$\text{where, } E_{Ry}^* = 13605.8\frac{1}{\varepsilon}\left(\frac{m_0}{m_e^*} + \frac{m_0}{m_h^*}\right)^{-1}$$

E_g(QD) and E_g(Bulk) represent the bandgap of the confined and bulk system, respectively. The second and the third terms arise due to the confinement energy associated with electron and hole, respectively. The fourth term represents the Coulombic attraction energy between the electron and hole. The final term corresponds to exciton Rydberg energy, which arises due to spatial correlation between electron and hole. The final term, which is generally neglected, becomes important for materials with very low dielectric constant. Here, under the effective-mass approximation, both electron and hole are described with spherical effective masses.[5, 6] Considering the system as spherical dots, in addition to spherically symmetric confining potentials, attractive Coulomb interaction is also included. There are two limiting scenarios depending on the ratio between the radius of the quantum dot, R, and the effective Bohr radius of the bulk exciton, a_0. For $R/a_0 \gg 1$, the exciton can be considered as a bound quasi-particle with

negligible confinement energy. Such systems are considered as weak confinement regime.[6] Whereas, for $R/a_0 \ll 1$, the confinement energy dominates and the electron and hole are considered as individual particles with only little spatial correlation between them. Such systems are said to be in the strongly confinement regime.[6] It is to be noted that the boundary of the strong-confinement regime remains valid up to about $R = 2a_0$.[6]

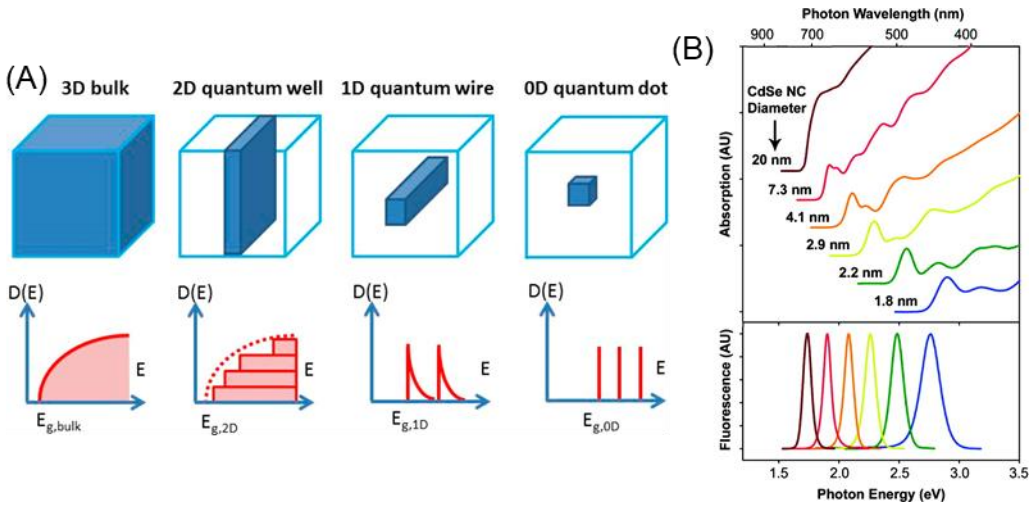

Figure 1.1. (A) Effect of quantum confinement on the bandgap and density of states of systems. Adapted with permission from ref. 7. Copyright (2019) American Chemical Society. (B) Size dependent bandgap variation and PL tunability of CdSe QDs of varying diameters. Adapted with permission from ref. 8. Copyright (2010) American Chemical Society.

A real example of this effect is highlighted in Figure 1.1B, where size dependent tunability of the bandgap of CdSe NCs is shown. A decrease in diameter of the NCs from 20 nm to 1.8 nm leads to increased confinements of the systems; consequently the PL varies over the total visible window of the electromagnetic spectrum.[8]

1.3. Perovskites

1.3.1. Background

Even though caesium lead halide perovskite NCs have been in the limelight from the last few years, its bulk counterpart of various compositions like $CsPbX_3$, Cs_4PbX_6, $CsPb_2X_5$

etc. (X represent halides) were first reported long back in 1893.[9] Perovskites being ionic in nature, studies of photoconductivity involving those materials was one of the major focuses.[10, 11] Later in 2009, following the pioneering report by Miyasaka and co-workers,[12] utilization of metal halide perovskites as solar energy harvesters took a giant leap and it became a new sensation in photovoltaic research community. Till date a PCE of >25% is reported with perovskites.[1] The applicability of the perovskites is not limited only to the solar cells. Another milestone was established in 2015, when Kovalenko and co-workers first reported that colloidal $CsPbX_3$ in their nanocrystalline form exhibiting high PLQY (50-90)%.[13] High PL of these material makes them potential candidates in display devices like LEDs.[14] Ease of preparation of these colloidal NCs attracted tremendous attention from synthetic material scientists and till date abundant literature is available highlighting various aspects of synthetic methodologies.[15] Unique properties such as defect-tolerant nature, high luminescence efficiency, high color purity, ease of bandgap tunability, large absorption coefficient and long carrier mobility make this material a front runner in various potential applications.[14-17]

1.3.2. Crystal Structure

By definition, a perovskite crystal lattice is described as a corner sharing BX_6^{4-} octahedral unit with ABX_3 (or equivalent) stoichiometry (Figure 1.2A).[18] However, a deviation from ABX_3 stoichiometry (while maintaining the charge neutrality) can be observed for several other type of perovskites namely vacancy-ordered, double or quadruple perovskites etc.[18] Here our focus will be on the ABX_3 type (where A= $CH(NH_2)_2^+$ [FA^+], $CH_3NH_3^+$ [MA^+], Cs^+ etc., B = Pb^{2+}, Sn^{2+}, etc. and X= Cl^-, Br^- or I^-) since these are the systems for all our studies described in the thesis. Figure 1.2A depicts a typical cubic ABX_3 perovskite structure. In a unit cell of cubic perovskites, the 'A' cation occupies the corner position of the unit cell and the B cation resides at the body-centered position. While 'X' anion resides on the face-centered position of the cubes. It is important to note that with variation of the size of X (Cl, Br or I) the crystal structure does not remain as perfect

cubic; crystal distortion is introduced in the structure.[19] 'A' cation residing at the octahedral void plays a crucial role in perovskite formability. Larger 'A' cation especially

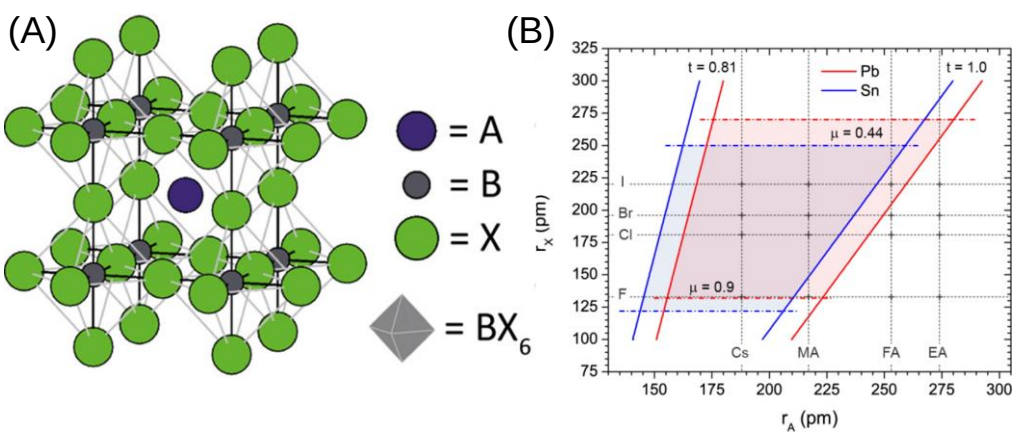

Figure 1.2. (A) Schematic representation of a cubic perovskite structure. Adapted with permission from ref. 18. Copyright (2020) American Chemical Society. (B) Formability of 3D halide perovskites as a function of A-site cation and halide anion radii. The boundaries for tolerance and octahedral factors are marked with solid and dashed lines, respectively. Adapted with permission from ref. 16. Copyright (2020) American Chemical Society.

long chain organic cation can disrupt the 3D network of the perovskite structure and leads to formation of layered perovskites.[20] The crystal stability of the perovskite structure is generally defined by the Goldschmidt tolerance factor (t) and octahedral factor (μ) and expressed as follows

$$t = \frac{r_A + r_X}{\sqrt{2}(r_B + r_X)}; \qquad \mu = \frac{r_B}{r_X}$$

Where, r_A, r_B and r_X represent the ionic radii of A, B and X, respectively. Generally, $0.81 \leq t \leq 1.0$ and $0.44 \leq \mu \leq 0.9$ values denote a favorable perovskite structure.[16, 21] Their formability can be predicted using the chart given in Figure 1.2B. If favored, they will fall under the shaded region; otherwise not.

1.3.3. Exciton Fine Structure

In lead-halide perovskites ($APbX_3$ type), the CB is formed mainly by the Pb-6*p* orbitals and the VB by the Pb-6*s* and halide-n*p* orbitals, giving an overall *p*-like and *s*-like symmetry, respectively.[22] Thus the 'A' site has no direct influence on the band structure. It is to be noted that the unlike the conventional semiconductor materials (like CdSe, GaAs etc.), the non-bonding and anti-bonding orbitals lie within the VB and CB of perovskites (Figure 1.3A).[23] This particular property makes them defect tolerant material (?) with an exceptional PL behavior (discussed later). The band structure of perovskites possesses finer characteristics called "exciton fine structure". Presence of a heavy atom (lead) introduces spin-orbit interaction between the orbitals and spin motions of the electrons, resulting into splitting of the 6-fold degenerate CB into doubly-degenerate (J_e = 1/2, m_J = ±1/2) and 4-fold degenerate (J_e = 3/2, m_J = ±3/2, ±1/2) states.[22, 24, 25] Further splitting occurs due to the electron-hole exchange interaction which leads to a singlet

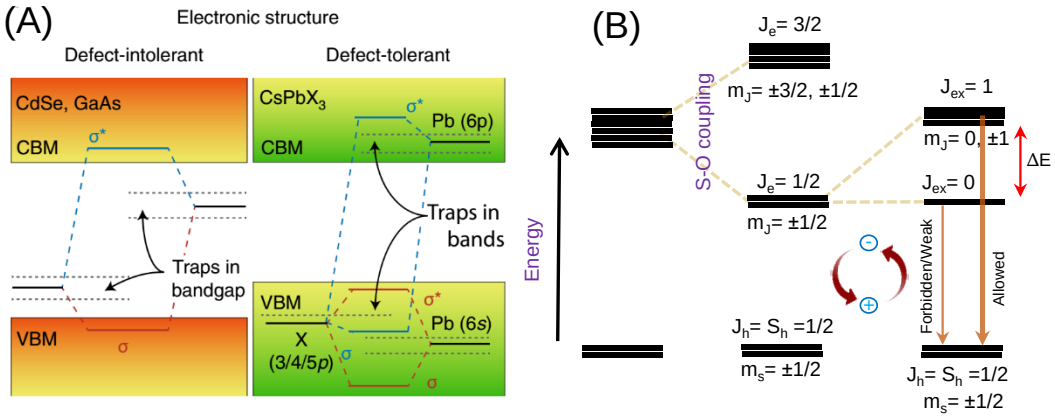

Figure 1.3. (A) Schematic representation of electronic band structure of perovskites showing their defect-intolerant tolerant nature as compared to other semiconductors. Adapted with permission from ref. 23 Copyright (2018) Springer Nature. (B) Excitonic fine structure of perovskites (Energy levels are not according to scale).

state (J_{ex} = 0) and a triply-degenerate state (J_{ex} = 1, m_J = 0, ±1).[22, 24] Thus we have three optically allowed bright, spin-allowed) transition from the J_{ex} = 1 state and one optically passive (dark, spin-forbidden) transition from J_{ex} = 0 state.[22] However, the exact positioning of the dark state in such system is of highly debated and is beyond the scope

of this thesis. Interested readers may refer to reference.[22] However, in most of the studies including those described in this thesis, simply a transition from CBM to VBM is considered. This is because, most of the studies are carried out at RT and the singlet-triplet energy separation is much lower than the thermal energy available at RT.[25] Thus observing separate transitions at RT is not possible.

1.3.4. Surface Properties and Colloidal Stability

Nanoscale analog of the perovskites i.e. the NCs are generally passivated with long alkyl chain ligands which play a crucial role in maintaining the structural integrity of the NCs.[15, 26] Presence of long hydrocarbon chain in these ligands inhibits individual NC to come close to each other in colloidal dispersion and thus aggregation is avoided. These ligands also help to passivate the surface traps which arise due to the dangling orbitals in the NCs (discussed later).[26] Perovskite NCs are conventionally passivated with two capping ligands, oleic acid and oleylamine.[26] Theoretical calculations and experimental data provide insight on their binding nature.[27] It is suggested that oleylammonium ions substitute some of the Cs-ions from the surface of the NCs and stabilize the NCs by forming hydrogen bonds between the $-NH_3^+$ moiety of oleylammonium and the surface Br^- of the NCs.[27] However, dynamic nature of binding of these ligands sometimes is detrimental for the NCs stability (Figure 1.4A).[23, 26, 28] Thus recent studies emphasize on finding alternating capping ligands having much stronger binding affinity for the NCs surface. Zwitterionic ligands in this regard are found to be helpful.[29, 30] Growing a protective shell on the surface of the NCs and incorporating the NCs into a polymer matrix are the recently developed strategies to deal with the stability issue of the perovskites NCs.[23]

Figure 1.4B depicts the surface stoichiometry of the NCs as a function of the diameter of the NCs.[31] There are two possibilities of the surface termination; [CsX] or [PbX_2]. However, as the NCs are capped with ligands, in realistic model the [PbX_2] terminated surfaces of the $CsPbX_3$ are represented as [$CsPbX_3$](PbX_2)(AX′), where the capping ligand is represented by AX′.[31]

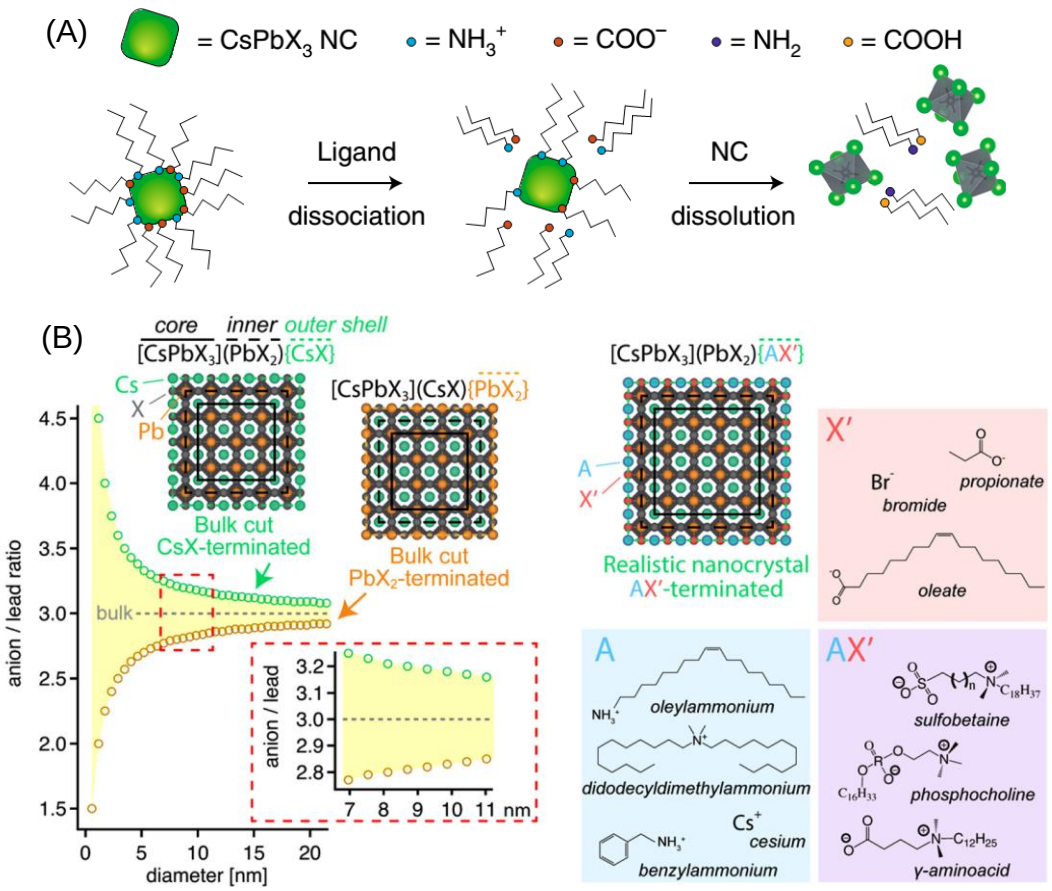

Figure 1.4. (A) Schematic illustration showing disruption of structural integrity of the NCs upon loosing weakly bound surface ligands. Adapted with permission from ref. 23. Copyright (2018) Springer Nature. (B) Models describing surface stoichiometry of typical $CsPbX_3$ type perovskite NCs. Adapted with permission from ref 31. Copyright (2019) American Chemical Society.

Here, A can be a monovalent cation such as alkylammonium and/or Cs^+ and X′ is monovalent anion such as halide and/or oleate. We will see in later sections that halide-rich surface is crucial for improved PL properties of the system.

1.3.4. Optical Properties

Though the optical transition in perovskites is not as straightforward as it seems (as described in section 1.3.3), for simplicity we will consider it as an optical transition from CBM to VBM.

For $CsPbX_3$ NCs, depending on the participating halide, the bandgap changes.[13] On replacing the halide from chloride to bromide to iodide the bandgap decreases progressively.[13] This enables excellent opportunity to tune the PL wavelength of the $CsPbX_3$ perovskite NCs as well. Moreover, this exchange of halides can easily be performed at RT,[15] which provides great ease to have materials to cover the entire visible PL window (Figure 1.5). The PLQY of these NCs varies from 1-100 %.[15] Conventionally, $CsPbCl_3$ NCs, which are the highest bandgap materials for this series possess the lowest PLQY of ~1%, whereas, the PLQY of $CsPbBr_3$ and $CsPbI_3$ can reach up to near unity. Such large variation in PLQY is due to the variation in the number/density of the trap states in them (discussed later). However, methods are now available to have near-unity PLQY for all blue-green-red emitting NCs ($APbX_3$ type).[30, 32, 33]

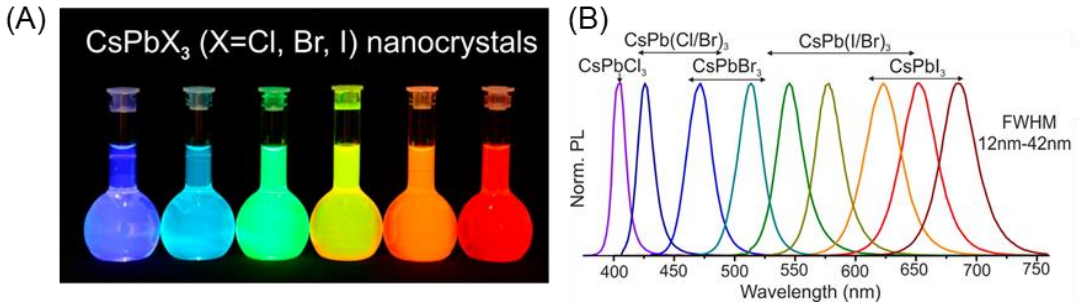

Figure 1.5. (A) Digital image of colloidal solution of $CsPbX_3$ NCs under UV radiation. (B) PL spectra of NCs with varying halide composition. Adapted with permission from ref. 13. Copyright (2015) American Chemical Society.

1.3.5. Trap States in Perovskites

Even though the perovskites are expected to be defect tolerant, they often exhibit sub-unity PLQY. It is true however that compared to the conventional semiconductor materials (such as PbSe, CdSe etc.) the perovskites are much more tolerant towards

defects. The defects in perovskites can arise for many reasons. Here we will mainly focus on its nanoscale analogue i.e. the NCs since they are of our interest. The NCs are in general protected by capping ligands, which provide the colloidal stability and passivate uncoordinated orbitals of them. For perovskite NCs, the binding of the ligands are generally weak and dynamic in nature.[28] Due to weak binding, the surface of the NCs frequently gets exposed and introduces trap states.[26, 28] Moreover, low defect formation energy favors the introduction of point defects in their crystal structures.[23] Specifically, the halide vacancies plays a major role in forming trap states and thus have a detrimental effect on the PL efficiency of the system.[23] For example, $CsPbCl_3$ NCs with halide vacant crystal structure possess PLQY in the range of 1-5%, whereas simply by adopting the halide rich synthetic protocol it can reach as high as 65%.[26] Ions occupying interstitial or antisite position also leads to the formation of trap states.[23] Hot-injection synthesis protocol often leads to the formation of lead nano-particle, residing on the surface of the

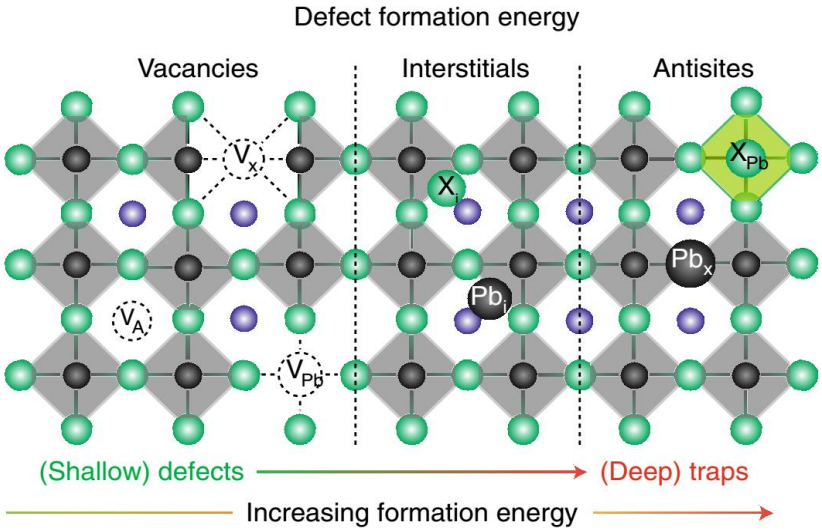

Figure 1.6. Different kinds of possible point defects in perovskites with increasing formation energy. Adapted with permission from ref. 23. Copyright (2018) Springer Nature.

synthesized NCs, that also lowers the PLQY of the system.[26, 33] Moreover, perovskites being a soft ionic crystal, dynamic lattice disorder also plays a major role in formation of

the trap states. Since the sizes of each constituent is crucial for an optimized crystal structure, introduction of any larger or smaller size ion may result in distortion in the system.[19] For example, $CsPbI_3$, because of the presence of larger size iodide, experiences a tilting of the octahedral unit (called 'octahedral tilting').[19] Such distortion often leads to formation of traps within the bandgap. Dynamic disorder may also result in self-trapping of the charge carriers. Perovskites possess active phonons (due to their soft crystal structure) which interact with the photo-generated charge carriers and form a quasi-particle called 'polaron'.[34, 35] Anharmonic X-Pb-X bending coupled with the rotating dipoles of organic cations also may lead to the formation of polaron.[34, 36] Detrimental role of polarons in the optical properties of the NCs has been suggested very recently.[34]

1.3.6. Doped Perovskites

Incorporation of small amount of impurity/foreign ions (dopants) in trace quantities is an excellent strategy to tune the PL properties of the host NCs.[17, 37] Incorporation of small amount of other halides or A cation, different from that present in the host NCs, not only improves the PL of the NCs but also their stability. Here we will focus mainly on the B-cation doping as it is one of the major themes of the thesis work. B-cation doping is attractive in the sense that it can introduce new optical, electronic and magnetic properties in the host.[17, 37] Besides, B-site substitution of Pb with other non-toxic metal ions reduces the overall toxicity of the material. Till now various homo- and hetero-valent dopants have been incorporated into the B-site of various host NCs for specific purposes (Figure 1.7).[17, 37]

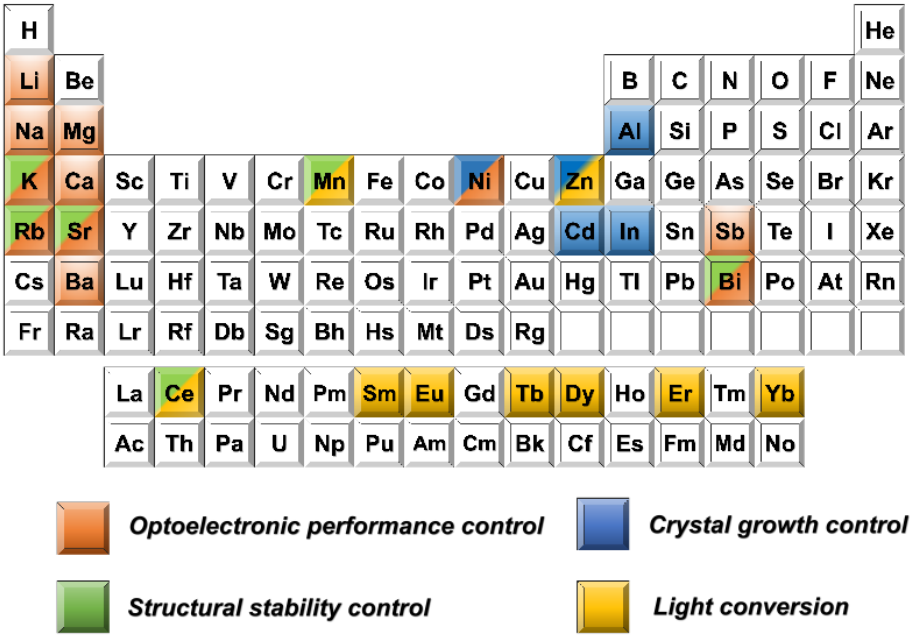

Figure 1.7. Different dopants used in perovskites to introduce new properties. Adapted with permission from ref. 17. Copyright (2018) American Chemical Society.

The strategies adopted for the exchange of B-cation in perovskite NCs are quite straightforward. These exchanges are generally performed in two ways: (i) during the synthesis of the host NCs and (ii) through post-synthetic cation exchange.[38] During the

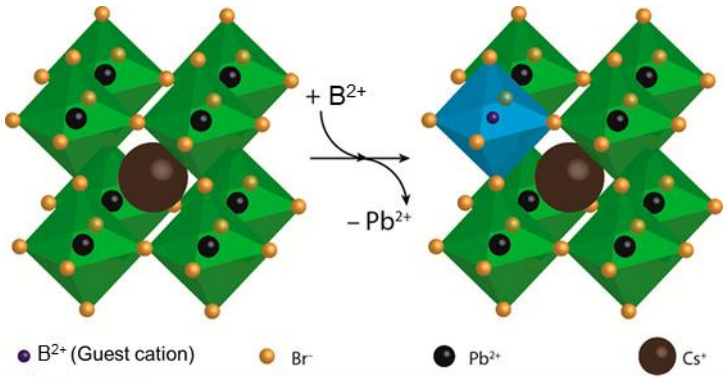

Figure 1.8. Schematic showing replacement of Pb^{2+} with a dopant B^{2+} in the octahedral site of the perovskite crystal. Adapted with permission from ref. 38. Copyright (2017) American Chemical Society.

hot injection synthesis of the NCs, addition of metal-salt of a desired dopant ion generally leads to the incorporation of it in the resulting NCs provided certain conditions are fulfilled. However, one should keep it in mind that the ionic radii of the guest cation should be such that it does not introduce too much strain in the crystal structure; otherwise the NCs will collapse.[38] Since the guest cation is going to replace Pb^{2+}, it will ultimately make bonds with the halides forming the octahedral unit. Thus, the bond energy of the guest cation and halide should favor the formability of the crystal structure. As discussed earlier, perovskite crystal structure being very soft and ionic, it provides an opportunity to exchange the B-cation in post-synthetic manner at RT as well.[38]

Among various dopants, Mn^{2+} in particular is the most attractive and extensively studied one because of its color-centered nature (due to transition from $^4T_1$ to $^6A_1$) with a long PL lifetime.[39, 40] The excitation energy is stored in this Mn-centers through Dexter-type

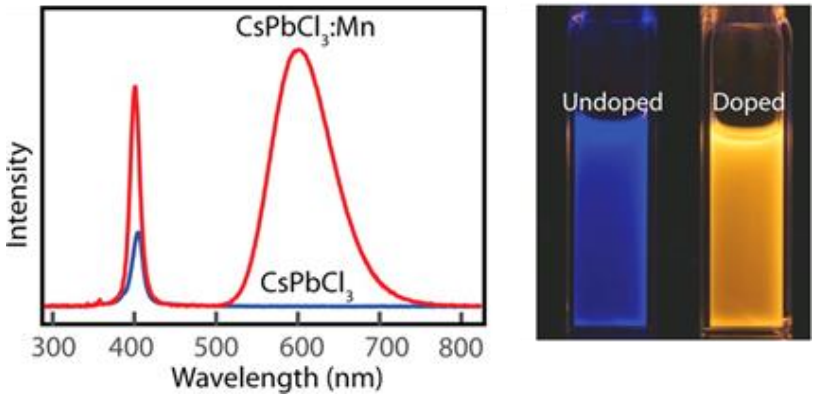

Figure 1.9. PL spectra of undoped and Mn-doped $CsPbCl_3$ NCs. Digital images of the colloidal dispersion of the NCs under UV radiation is also shown. Adapted with permission from ref. 41. Copyright (2016) American Chemical Society.

energy transfer process.[39, 40] This long-lived centers thus act as an energy reservoir, which is beneficial particularly for photovoltaic applications.[42] Moreover, Mn^{2+} being paramagnetic provides additional benefits for their potential use in spintronics.[43]

The beauty of Mn-doping has long been realized and extensive studies have been carried out with metal chalcogenide QDs as a host material.[39, 40] Mn-doping in perovskites was

first reported by Klimov and co-workers in 2016.[44] Among all $CsPbX_3$ NCs, $CsPbCl_3$ provides the ideal bandgap to have efficient emission from Mn.[41, 44] The $^4T_1$ state of Mn lies way above the conduction band edge of $CsPbI_3$ inhibiting the energy transfer process from host lattice.[44] Whereas in case of $CsPbBr_3$, back energy transfer from Mn centers limits the Mn PL efficiency.[44] With $CsPbCl_3$ as a host NC, Mn PLQY generally ranges from 25 to 50%.[41, 44] Low quantum efficiency is due to other non-radiative exciton relaxation processes (such as carrier trapping), which competes with the energy transfer process, as revealed from studies investigating the carrier dynamics of such systems.[45, 46] Suppressing these undesired non-radiative channels can enhance the exciton to dopant energy transfer efficiency and thus the Mn PLQY. This is indeed the case. Very recently, using a modified $CsPbCl_3$ host with suppressed carrier trapping process, a near-unity PLQY from the Mn is reported.[47] Apart from Mn, lanthanides are the other PL active dopants which have been investigated.[48] Incorporation of some dopants such as Cd^{2+}, Ni^{2+}, Mg^{2+}, Cu^{2+}, Zn^{2+} etc. leads to enhancement of PLQY and stability of the host materials.[26]

1.3.7. Charge Transfer Processes

Understanding the charge transfer processes from any semiconductor material of interest in photovoltaics is crucial for their better utilization. The charge carriers (electron and hole), generated upon photoexcitation, must be transferred to energy selective layers before they recombine among themselves. In most of the cases molecular adsorbates are used as model carrier acceptors. When their LUMO level lies below the CB of the energy harvester, electron transfer is a possibility.[49] Whereas, when the HOMO level lies above the VB of the material, hole transfer can take place.[49] (Figure 1.10) For a luminescent material, one of the easiest ways to check whether charge transfer is happing or not, is to monitor its PL in absence and presence of the carrier acceptor. Successful charge transfer (electron/hole) leads to PL quenching. With addition to the molecular acceptors, several wide bandgap materials (such as TiO_2, ZnO, NiO) as well as some quantum dots are also used as carrier acceptors.[50, 51] It is to be noted that, apart from the electron and hole

transfer processes, energy transfer can also leads to PL quenching;[52] thus one must be careful in assigning the actual process responsible for PL quenching.

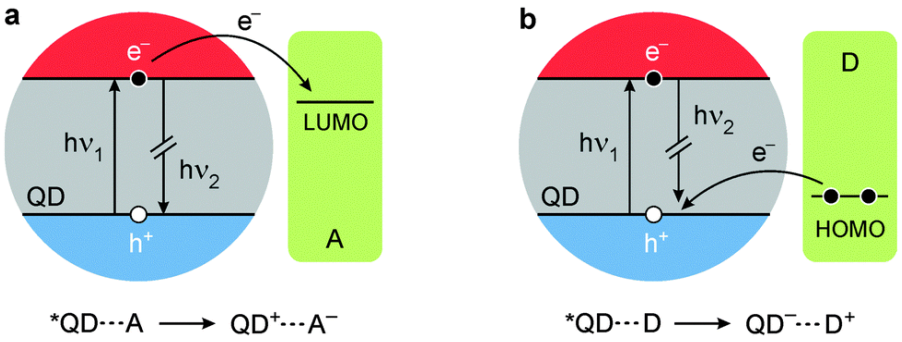

Figure 1.10. Schematic presentation of (a) electron and (b) hole transfer processes from a photoexcited QD to a molecular acceptor. Adapted with permission from ref. 49. Copyright (2014) Elsevier.

The feasibility of the charge transfer process is majorly governed by the free energy change associated with it. The free energy charge (ΔG) associated with an electron transfer process, for example, is expressed as the following[53]

$$\Delta G = eE_{D+/D} - eE_{A/A-} - eE_{0-0} - \frac{e^2}{4\pi\varepsilon_0\varepsilon_r D}$$

Where, $E_{0\text{-}0}$ corresponds to 0-0 transition of the photoexcited species, ε_0 is the vacuum permittivity, ε_r is the dielectric constant of the medium and D denotes the distance between the donor and acceptor.

As far as the perovskites NCs are concerned, from their first report,[13] till now, several charge transfer studies have been carried out.[54] While most the charge transfer studies involving perovskites are focused on carrier extraction from the band edge states, limited work has been done in harvesting the hot carriers.[55] Understanding hot carrier extraction dynamics is crucial for minimizing the energy loss when the perovskites are used as solar harvester.[55] In this thesis, we discuss some work related to hot hole and cold hole

extraction from the perovskite NCs using different molecular acceptors. With the help of ultrafast TA and PL UC measurements, these processes are probed, and a complete picture of the charge transfer processes is obtained.

1.3.9. Chapter-Wise Organization of the Thesis

This thesis is divided into seven chapters. *Chapter 1* starts with a brief introduction on semiconductor materials. Then important characteristic properties of the perovskites such as crystal structure, formability criteria, exciton fine structure, composition dependent bandgap, surface properties and optical properties are discussed. We highlight the importance of doped perovskites and finally, a brief idea of charge (electron/hole) transfer processes semiconductors are also provided. In *chapter 2*, the methodologies for preparation of the perovskites of different compositions (which have been used in the present studies), purification, characterization and methodologies for various optical measurements are described. The instruments used for steady-state absorption and emission measurements, basic working principles of several time-resolved techniques, highlighting essential components such as oscillator, regenerative amplifier, and optical parametric amplifier of the femtosecond-picosecond setups are discussed. Besides, a brief idea of other characterization techniques (such as TEM, FESEM, FTIR, PXRD etc.) is also provided. The working chapters start with *chapter 3*, in which the carrier dynamics of Mn-doped $CsPbCl_3$ NCs of varying Mn concentrations are investigated. *Chapter 4* deals with Cu-doped $CsPbCl_3$ system in which a new methodology for enhancing the PLQY of violet and blue emitting perovskites is reported. In *chapter 5*, we investigate the cold hole transfer dynamics from $CsPbBr_3$ and $CsPbI_3$ systems. In *chapter 6* hot hole transfer from perovskites using a simple molecular acceptor is demonstrated. In the last chapter (*chapter 7)*, we summarize the findings of the entire thesis work and point out possible directions for further investigations based on our findings.

References

1. NREL Best Efficiency Chart: https://www.nrel.gov/pv/assets/pdfs/best-research-cell-efficiencies.20200708.pdf.
2. YU, P.; Cardona, M., Fundamentals of Semiconductors: Physics and Materials Properties. *Springer* **2010**, ISBN 978-3-642-00710-1.
3. Henderson, B.; Imbusch, G. F., Optical Spectroscopy of Inorganic Solids. *Clarendon Press, Oxford* **1989**.
4. Gaponenko, S. V., Introduction to Nanophotonics. *Cambridge University Press* **2010**, ISBN-10: 0521763754.
5. Kayanuma, Y., Quantum-Size Effects of Interacting Electrons and Holes in Semiconductor Microcrystals with Spherical Shape. *Phys. Rev. B* **1988,** 38, 9797.
6. Einevoll, G., Confinement of Excitons in Quantum Dots. *Phys. Rev. B* **1992,** 45, 3410.
7. Katan, C.; Mercier, N.; Even, J., Quantum and Dielectric Confinement Effects in Lower-Dimensional Hybrid Perovskite Semiconductors. *Chem. Rev.* **2019,** *119*, 3140-3192.
8. Smith, A. M.; Nie, S., Semiconductor Nanocrystals: Structure, Properties, and Band Gap Engineering. *Acc. Chem. Res.* **2010,** 43, 190-200.
9. Wells, H. L., Über die Cäsium- und Kalium-Bleihalogenide. *Z. Anorg. Allg. Chem.* **1893,** *3*, 195-210.
10. Moller, C. K., A Phase Transition in Caesium Plumbochloride. *Nature* **1957,** *180*, 981-982.
11. Moller, C. K., Crystal Structure and Photoconductivity of Caesium Plumbohalides. *Nature* **1958,** *182*, 1436-1436.
12. Kojima, A.; Teshima, K.; Shirai, Y.; Miyasaka, T., Organometal Halide Perovskites as Visible-Light Sensitizers for Photovoltaic Cells. *J. Am. Chem. Soc.* **2009,** *131*, 6050-6051.
13. Protesescu, L.; Yakunin, S.; Bodnarchuk, M. I.; Krieg, F.; Caputo, R.; Hendon, C. H.; Yang, R. X.; Walsh, A.; Kovalenko, M. V., Nanocrystals of Cesium Lead Halide Perovskites ($CsPbX_3$, X = Cl, Br, and I): Novel Optoelectronic Materials Showing Bright Emission with Wide Color Gamut. *Nano Lett.* **2015,** *15*, 3692-3696.
14. Le, Q. V.; Jang, H. W.; Kim, S. Y., Recent Advances toward High-Efficiency Halide Perovskite Light-Emitting Diodes: Review and Perspective. *Small Methods* **2018,** 2, 1700419.
15. Shamsi, J.; Urban, A. S.; Imran, M.; Trizio, L. D.; Manna, L., Metal Halide Perovskite Nanocrystals: Synthesis, Post-Synthesis Modifications, and Their Optical Properties. *Chem. Rev.* **2019,** *119*, 3296-3348.
16. Manser, J. S.; Christians, J. A.; Kamat, P. V., Intriguing Optoelectronic Properties of Metal Halide Perovskites. *Chem. Rev.* **2016,** *116*, 12956-13008.
17. Zhou, Y.; Chen, J.; Bakr, O. M.; Sun, H.-T., Metal-Doped Lead Halide Perovskites: Synthesis, Properties, and Optoelectronic Applications. *Chem. Mater.* **2018,** *30*, 6589-6613.
18. Akkerman, Q. A.; Manna, L., What Defines a Halide Perovskite? *ACS Energy Lett.* **2020,** *5*, 604-610.

19. Swarnkar, A.; Mir, W. J.; Nag, A., Can B-Site Doping or Alloying Improve Thermal- and Phase-Stability of All-Inorganic $CsPbX_3$ (X = Cl, Br, I) Perovskites? *ACS Energy Lett.* **2018,** *3*, 286-289.
20. Mitzi, D. B., Templating and Structural Engineering in Organic–Inorganic Perovskites. *J. Chem. Soc., Dalton Trans* **2001**, 1-12.
21. Goldschmidt, V. M., Die Gesetze Der Krystallochemie. *Naturwissenschaften* **1926,** *14*, 477-485.
22. Becker, M.; Vaxenburg, R.; Nedelcu, G.; Sercel, P. C.; Shabaev, A.; Mehl, M. J.; Michopoulos, J. G.; Lambrakos, S. G.; Bernstein, N.; Lyons, J. L.; Stöferle, T.; Mahrt, R. F.; Kovalenko, M. V.; Norris, D. J.; Rainò, G.; Efros, A. L., Bright Triplet Excitons in Caesium Lead Halide Perovskites. *Nature* **2018,** *553*, 189-193.
23. Akkerman, Q. A.; Rainò, G.; Kovalenko, M. V.; Manna, L., Genesis, Challenges and Opportunities for Colloidal Lead Halide Perovskite Nanocrystals. *Nature Mater* **2018,** *17*, 394-405.
24. Sercel, P. C.; Lyons, J. L.; Wickramaratne, D.; Vaxenburg, R.; Bernstein, N.; Efros, A. L., Exciton Fine Structure in Perovskite Nanocrystals. *Nano Lett.* **2019,** *19*, 4068-4077.
25. Meijerink, A.; Rabouw, F. T., Shedding Light on Dark Excitons. *Nature Mater.* **2019,** 18, 660-661.
26. Seth, S.; Ahmed, T.; De, A.; Samanta, A., Tackling the Defects, Stability, and Photoluminescence of $CsPbX_3$ Perovskite Nanocrystals. *ACS Energy Lett.* **2019,** *4*, 1610-1618.
27. Ravi, V. K.; Santra, P. K.; Joshi, N.; Chugh, J.; Singh, S. K.; Rensmo, H.; Ghosh, P.; Nag, A., Origin of the Substitution Mechanism for the Binding of Organic Ligands on the Surface of $CsPbBr_3$ Perovskite Nanocubes. *J. Phys. Chem. Lett.* **2017,** *8*, 4988-4994.
28. Roo, J. D.; Ibańez, M.; Geiregat, P.; Nedelcu, G.; Walravens, W.; Maes, J.; Martins, J. C.; Driessche, I. V.; Kovalenko, M. V.; Hens, Z., Highly Dynamic Ligand Binding and Light Absorption Coefficient of Cesium Lead Bromide Perovskite Nanocrystals. *ACS Nano* **2016,** 10, 2071-2081.
29. Krieg, F.; Ochsenbein, S. T.; Yakunin, S.; Brinck, S. t.; Aellen, P.; Süess, A.; Clerc, B.; Guggisberg, D.; Nazarenko, O.; Shynkarenko, Y.; Kumar, S.; Shih, C.-J.; Infante, I.; Kovalenko, M. V., Nanocrystals 2.0: Zwitterionic Capping Ligands for Improved Durability and Stability. . *ACS Energy Lett.* **2018,** *3*, 641-646.
30. Pan, J.; Shang, Y.; Yin, J.; Bastiani, M. D.; Peng, W.; Dursun, I.; Sinatra, L.; El-Zohry, A. M.; Hedhili, M. N.; Emwas, A.-H.; Mohammed, O. F.; Ning, Z.; Bakr, O. M., Bidentate Ligand-Passivated $CsPbI_3$ Perovskite Nanocrystals for Stable Near-Unity Photoluminescence Quantum Yield and Efficient Red Light-Emitting Diodes. *J. Am. Chem. Soc.* **2018,** *140*, 562-565.
31. Bodnarchuk, M. I.; Boehme, S. C.; Brinck, S. t.; Bernasconi, C.; Shynkarenko, Y.; Krieg, F.; Widmer, R.; Aeschlimann, B.; Günther, D.; Kovalenko, M. V., Rationalizing and Controlling the Surface Structure and Electronic Passivation of Cesium Lead Halide Nanocrystals. *ACS Energy Lett.* **2019,** *4*, 63-74.
32. Mondal, N.; De, A.; Samanta, A., Achieving Near-Unity Photoluminescence Efficiency for Blue-Violet-Emitting Perovskite Nanocrystals. *ACS Energy Lett.* **2019,** *4*, 32-39.

33. Ahmed, T.; Seth, S.; Samanta, A., Boosting the Photoluminescence of $CsPbX_3$ (X = Cl, Br, I) Perovskite Nanocrystals Covering a Wide Wavelength Range by Postsynthetic Treatment with Tetrafluoroborate Salts. *Chem. Mater.* **2018,** *30*, 3633-3637.
34. Ghosh, D.; Welch, E.; Neukirch, A. J.; Zakhidov, A.; Tretiak, S., Polarons in Halide Perovskites: A Perspective. *J. Phys. Chem. Lett.* **2020,** *11*, 3271-3286.
35. Miyata, K.; Meggiolaro, D.; Trinh, M. T.; Joshi, P. P.; Mosconi, E.; Jones, S. C.; Angelis, F. D.; Zhu, X.-Y., Large Polarons in Lead Halide Perovskites. *Science* **2017,** *3*, e1701217.
36. Park, M.; Neukirch, A. J.; Reyes-Lillo, S. E.; Lai, M.; Ellis, S. R.; Dietze, D.; Neaton, J. B.; Yang, P.; Tretiak, S.; Mathies, R. A., Excited-State Vibrational Dynamics Toward the Polaron in Methylammonium Lead Iodide Perovskite. *Nat. Commun.* **2018,** 9, (2525).
37. Luo, B.; Li, F.; Xu, K.; Guo, Y.; Liu, Y.; Xia, Z.; Zhang, J. Z., B-Site Doped Lead Halide Perovskites: Synthesis, Band Engineering, Photophysics, and Light Emission Applications. *J. Mater. Chem. C* **2019,** *7*, 2781-2808.
38. Stam, W. v. d.; Geuchies, J. J.; Altantzis, T.; Bos, K. H. W. v. d.; Meeldijk, J. D.; Aert, S. V.; Bals, S.; Vanmaekelbergh, D.; Donega, C. d. M., Highly Emissive Divalent-Ion-Doped Colloidal $CsPb_{1-x}M_xBr_3$ Perovskite Nanocrystals through Cation Exchange. *J. Am. Chem. Soc.* **2017,** *139*, 4087-4097.
39. Pandey, A.; Sarma, D. D., Recent Advances in Manganese Doped II-VI Semiconductor Quantum Dots. *Z. Anorg. Allg. Chem.* **2016,** *642*, 1331-1339.
40. Norris, D. J.; Efros, A. L.; Erwin, S. C., Doped Nanocrystals. *Science* **2008,** *319*, 1776-1779.
41. Parobek, D.; Roman, B. J.; Dong, Y.; Jin, H.; Lee, E.; Sheldon, M.; Son, D. H., Exciton-to-Dopant Energy Transfer in Mn-Doped Cesium Lead Halide Perovskite Nanocrystals. *Nano Lett.* **2016,** *16*, 7376-7380.
42. Santra, P. K.; Kamat, P. V., Mn-Doped Quantum Dot Sensitized Solar Cells: A Strategy to Boost Efficiency over 5%. *J. Am. Chem. Soc.* **2012,** *134*, 2508-2511.
43. Siena, M. C. D.; Sommer, D. E.; Creutz, S. E.; Dunham, S. T.; Gamelin, D. R., Spinodal Decomposition During Anion Exchange in Colloidal Mn^{2+}-Doped $CsPbX_3$ (X = Cl, Br) Perovskite Nanocrystals. *Chem. Mater.* **2019,** 31, 7711-7722.
44. Liu, W.; Lin, Q.; Li, H.; Wu, K.; Robel, I. n.; Pietryga, J. M.; Klimov, V. I., Mn^{2+}-Doped Lead Halide Perovskite Nanocrystals with Dual-Color Emission Controlled by Halide Content. *J. Am. Chem. Soc.* **2016,** *138*, 14954-14961.
45. De, A.; Mondal, N.; Samanta, A., Luminescence Tuning and Exciton Dynamics of Mn-Doped $CsPbCl_3$ Nanocrystals. *Nanoscale* **2017,** *9*, 16722-16727.
46. Rossi, D.; Parobek, D.; Dong, Y.; Son, D. H., Dynamics of Exciton−Mn Energy Transfer in Mn-Doped $CsPbCl_3$ Perovskite Nanocrystals. *J. Phys. Chem. C* **2017,** *121*, 17143-14149.
47. Ji, S.; Yuan, X.; Cao, S.; Ji, W.; Zhang, H.; Wang, Y.; Li, H.; Zhao, J.; Zou, B., Near-Unity Red Mn^{2+} Photoluminescence Quantum Yield of Doped $CsPbCl_3$ Nanocrystals with Cd Incorporation. *J. Phys. Chem. Lett.* **2020,** *11*, 2142-2149.
48. Pan, G.; Bai, X.; Yang, D.; Chen, X.; Jing, P.; Qu, S.; Zhang, L.; Zhou, D.; Zhu, J.; Xu, W.; Dong, B.; Song, H., Doping Lanthanide into Perovskite Nanocrystals: Highly Improved and Expanded Optical Properties. *Nano Lett.* **2017,** *17*, 8005-8011.

49. Avellini, T.; Lincheneau, C.; Vera, F.; Silvi, S.; Credi, A., Hybrids of Semiconductor Quantum Dot and Molecular Species for Photoinduced Functions. *Coord. Chem. Rev.* **2014,** *263-264*, 151-160.
50. Robel, I.; Subramanian, V.; Kuno, M.; Kamat, P. V., Quantum Dot Solar Cells. Harvesting Light Energy with CdSe Nanocrystals Molecularly Linked to Mesoscopic TiO_2 Films. *J. Am. Chem. Soc.* **2006,** 128, 2385-2393.
51. Wu, X.; Yeow, E. K. L., Charge-Transfer Processes in Single CdSe/ZnS Quantum Dots with p-Type NiO Nanoparticles. *Chem. Commun.* **2010,** 46, 4390-4392.
52. Hildebrandt, N.; Spillmann, C. M.; Algar, W. R.; Pons, T.; Stewart, M. H.; Oh, E.; Susumu, K.; Díaz, S. A.; Delehanty, J. B.; Medintz, I. L., Energy Transfer with Semiconductor Quantum Dot Bioconjugates: A Versatile Platform for Biosensing, Energy Harvesting, and Other Developing Applications. *Chem. Rev.* **2017,** 117, 536-711.
53. Rehm, D.; Weller, A., Kinetics of Fluorescence Quenching by Electron and H-Atom Transfer. *Isr. J. Chem.* **1970,** 8, 259.
54. Mondal, N.; De, A.; Das, S.; Paul, S.; Samanta, A., Ultrafast Carrier Dynamics of Metal Halide Perovskite Nanocrystals and Perovskite Composites. *Nanoscale* **2019,** 11, 9796-9818.
55. Li, M.; Fu, J.; Xu, Q.; Sum, T. C., Slow Hot-Carrier Cooling in Halide Perovskites: Prospects for Hot-Carrier Solar Cells. *Adv. Mater.* **2019,** *31*, 1802486.

CHAPTER 2

Materials, Methods and Instrumentation

Overview

The methodologies for preparation, purification and characterization of the perovskites of different compositions (which have been used in the present studies), and various optical measurements are described in this chapter. The instruments used for steady-state absorption and emission measurements and basic working principles of different time-resolved techniques, highlighting the essential components, such as oscillator, regenerative amplifier, and optical parametric amplifier are discussed. The optical layout of the TA and PL UC setups are also presented. Besides, instrumental details for other measurements (such as TEM, FESEM, FTIR and PXRD etc.) for characterizing the NCs are also provided.

2.1. Materials

Cs_2CO_3 (99.995%, trace metal), formamidinium acetate (99%), $PbCl_2$ (99.998%, trace metal), $PbBr_2$ (> 98%), $MnCl_2$ (anhydrous beads, 99.99%), Cu-acetate (98%), $CuCl_2.2H_2O$ (trace metal basis, >99.995%), octadecene (ODE, 90%), oleic acid (OA, 90%), oleylamine (OLA, 70%), trioctylphosphine (TOP), benzoyl bromide (97%), 1-aminopyrene (AMP), 4-mercaptophenol (MTH) and methyl acetate (anhydrous, 99.5%) were procured from Sigma-Aldrich. PbI_2 (99%) was purchased from Alfa Aesar and methylamine (7% in tetrahydrofuran (THF), 2 mol/L) from TCI Chemicals. These chemicals were used as received. The solvents, methanol, chloroform and toluene were purchased from Merck, and purified following standard procedures before their use.[1] HPLC grade hexane, bought from Finar Chemicals, was used as received.

2.2 Methods

2.2.1. Preparation of the NCs

2.2.1.1. $CsPbX_3$ (X= Cl, Br and I) NCs

$CsPbX_3$ NCs were prepared by following a reported procedure.[2] In brief, 0.16 g of Cs_2CO_3, 6 mL of ODE, and 0.5 mL of OA were mixed in a 50 mL double-necked RB and was heated at 120°C for an hour under vacuum. It was then transferred under nitrogen atmosphere until all Cs_2CO_3 reacted with OA to form a transparent solution of Cs-oleate complex. For its later use, this solution was maintained at temperature >100°C to avoid precipitation. In another 50 mL double-necked RB, 0.052 g $PbCl_2$ (for $CsPbCl_3$) or 0.069 g of $PbBr_2$ (for $CsPbBr_3$) or 0.084 g PbI_2 (for $CsPbI_3$) along with 5 mL of ODE, 0.5 mL of OA and 0.5 mL of OLA were mixed and heated under vacuum at 120°C for an hour. For $CsPbCl_3$ additional 1 mL of TOP was added for the complete dissolution of $PbCl_2$. The temperature was then increased to 165°C (185°C for $CsPbCl_3$) and 0.45 mL of pre-heated Cs-oleate solution was injected swiftly followed by immediate cooling (1 min for $CsPbCl_3$) of the solution in ice-cold water. The NCs were obtained by collecting the

precipitate upon centrifuging the whole dispersion at ~6500 rpm and dispersing it in toluene/hexane for further studies.

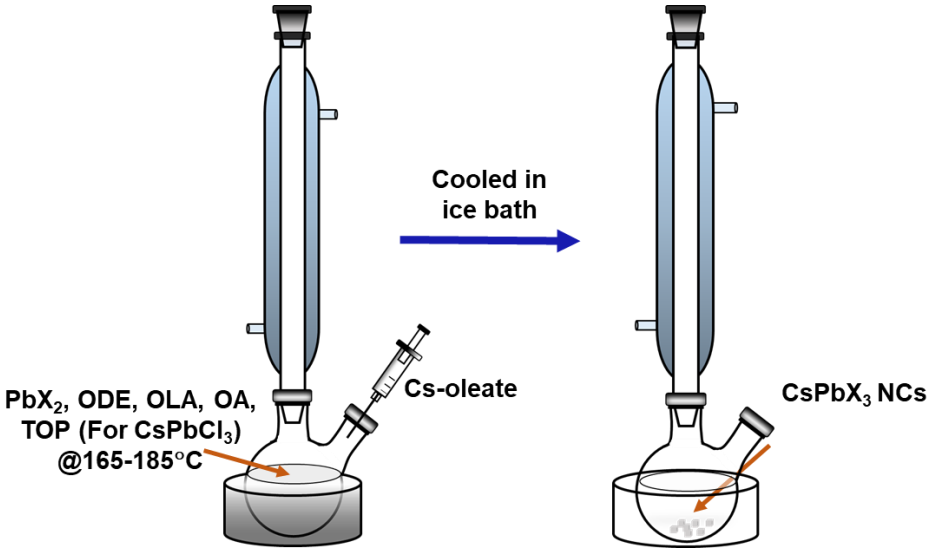

Figure 2.1. Schematic representation of the general methodology for the preparation of $CsPbX_3$ NCs.

2.2.1.2. $FAPbBr_3$ NCs

$FAPbBr_3$ NCs were prepared by following a reported procedure.[3] First, formamidinium acetate (0.130 g) was loaded into a 50 mL RB along with 5 mL OA and degassed for 10 minutes at RT. It was then heated under nitrogen atmosphere at 130ºC until the solution becomes transparent and then it was dried under vacuum for 30 min at 50ºC. In another 50 mL 2-necked RB, 0.069 g of $PbBr_2$, 1 mL OA and 0.5 mL OLA were mixed and heated at 120ºC under vacuum condition. After complete solubilization of $PbBr_2$, the temperature was raised to 165ºC and then 2.5 mL of pre-prepared (kept at 100 ºC) FA-oleate solution was quickly injected and the reaction mixture was cooled in ice-cold water after ~5s. The NCs were obtained by collecting the precipitate upon centrifuging the whole dispersion at ~7000 rpm and dispersed in hexane for further measurements.

2.2.1.3. $MAPbBr_3$ NCs

$MAPbBr_3$ NCs were synthesized by following a reported procedure.[4] Briefly, 5 mL ODE, 0.069 g $PbBr_2$, 0.8 mL of OA and 0.2 mL of OLA were mixed together into a 50 mL 2-necked RB and heated to 120ºC under vacuum. The temperature was then increased to 170ºC and once reached, methylamine solution (170 µL of 2M solution in THF and 0.7 mL of OA) was rapidly injected into it. Then it was quenched immediately in ice-cold water. The NCs were obtained by collecting the precipitate upon centrifuging the whole dispersion at ~8000 rpm and was dispersed in hexane for further measurements.

2.2.1.4. Mn-doped $CsPbCl_3$ NCs

For the preparation of Mn-doped $CsPbCl_3$ NCs,[5] a varying amount of $MnCl_2$ was added in an RB consisting of 0.052 g $PbCl_2$, 5 mL of ODE, 0.5 mL OA and 0.5 mL of OLA. The mixture was then heated under vacuum at 120°C for 1 hour. For the complete dissolution of the reactants, 1 mL of TOP under a N_2 atmosphere was added. Then the reaction temperature was raised to 185°C, and 0.45 mL of Cs-oleate (prepared by following a method described in Section 2.2.1.1.) was swiftly injected into it. The whole solution was quenched in ice water after 1 minute. The resulting solution was then centrifuged at ~6800 rpm and the supernatant liquid was discarded. The precipitated NCs were then dispersed in toluene for further studies.

2.2.1.5. Cu-doped $CsPbCl_3$ NCs

For the preparation of Cu-doped $CsPbCl_3$ NCs,[6] an additional amount of $CuCl_2{\cdot}2H_2O$ (0.22 mmol) was added to the reaction mixture consisting of 0.188 mmol $PbCl_2$, 5 mL of ODE, 0.7 mL OA and 0.7 mL of OLA. The mixture was then heated under vacuum at 120°C for 45 min. The blue solution turned colorless upon the addition of 1 mL of TOP under N_2 atmosphere. After raising the temperature to 185°C, 0.45 mL of Cs-oleate (prepared by following a method described in Section 2.2.1.1.) was swiftly injected into it; then, after a minute, the mixture was quenched in ice water. The resulting solution was then centrifuged at ~6800 rpm and the supernatant liquid was discarded. The precipitated NCs were dissolved in toluene and then washed with methyl acetate before further studies.

2.2.2. Purification of the Solvents

Solvents were purified prior to their use following standard procedures.[1] For each solvent, a specific method was followed for this purpose.[1] For example, dried toluene was obtained by refluxing the crude toluene first with metallic sodium and benzophenone, followed by distillation under moisture free condition. Whereas chloroform was just stirred with $CaCl_2$ for overnight and collected by distillation. All the solvents were kept in a reagent bottle with molecular sieves in it. Acetone was refluxed at ~70°C without any drying agent and collected through distillation.

2.2.3. Measurement of PLQY

The relative PLQY of the synthesized NCs were calculated using appropriate molecular dyes. For violet-blue emitting NCs [$CsPbCl_3$ or $CsPb(Br/Cl)_3$], either quinine sulphate (PLQY = 0.546 in 1.0 N aqueous H_2SO_4 solution) or 9,10-diphenylanthracene (PLQY = 0.93 in hexane solution) was used.[7] Ethanolic solution of coumarin 153 (PLQY = 0.55) was used for green-emitting $CsPbBr_3$ and for red-emitting $CsPbI_3$ NCs,[8] rhodamine 6G (PLQY = 0.95 in aqueous medium) was used.[9] The relative PLQY was calculated using the following equation:

$$QY_S = QY_R \times (I_S/I_R) \times (OD_R/OD_S) \times (\eta_S^2/\eta_R^2)$$

Where, integrated area of the PL spectrum is denoted by I, OD denotes the optical density at theexcitation wavelength and η represents the refracive index of the respective solvents. The subscripts “S” and “R” denote “sample” and “reference”, respectively.

2.2.4. Standard Error Limits

Standard error limits for various experimentally determined parameters are listed below:

λ_{max} (absorption/emission): ± 2 nm

PLQY: ± 3%

PL lifetime: ± 4%

NCs edge length: ± 3%

EDX composition: ± 8%

The error limits associated with the different parameters obtained in TA and PL UC measurements are given in the respective chapters. The error values provided there were directly obtained from the analysis using standard software (IGOR Pro/Origin).

2.3. Optical Measurements and Instrumentation

2.3.1. Steady-State Measurements

Steady-state absorptions were measured with a dual-lamp UV-Vis spectrophotometer (Cary 100, Varian) which consisted of a tungsten and a deuterium lamp which served as visible and UV-light sources, respectively. A PMT served as detector. Before measuring the true absorbance of the sample, baseline correction was made (to eliminate any contribution from solvents or cuvettes) by measuring the absorbance while placing two cuvettes in the double compartment filled with the solvent. Then, the sample absorbance was recorded by replacing the solvent from one cuvette with the sample solution. We used 3 mL quartz cuvettes with 1 cm path length for all measurements.

Steady-state emission spectra were recorded using a fluorescence spectrometer (FluoroLog-3, Horiba Jobin Yvon). Here a high-pressure xenon arc lamp was used as excitation source which covered a wide illumination range (250 nm to infrared). A monochromator was used for the selection of excitation wavelength. The sample fluorescence was collected at the right angled position with respect to the incident beam. The fluorescence signal was passed through a motorized monochromator which scanned a pre-selected wavelength range and finally, the fluorescence was detected by a photomultiplier.

2.3.2. TCSPC Technique

TCSPC is commonly used for recording the fluorescence decay profile of a photoexcited sample.[10] The sample is excited with a short laser pulse (*δ-pulse*) and then sample's fluorescence response is recorded as a function of time. After deconvolution of the decay profile, parameters characterizing the *δ-pulse* response are obtained.

TCSPC measurements rely on the concept that the probability distribution for emission of a single photon following pulse-excitation yields the actual intensity against the time distribution of all the photons emitted.[10] The probability distribution is constructed by sampling these single photon emission after a large number of excitations. Thus to maintain precision, it requires a laser source with relatively high repetition rate (generally > kHz) such that large number of events within a short time window is recorded.

The basic components of a typical TCSPC setup are shown in Figure 2.2. The working principle of a TCSPC is like a stop-watch, where a *START* signal is triggered either by the photons from excitation pulse or by the photons coming from the fluorescence of the sample. Depending on the triggering process the functioning method can be categorized as forward (when *START* signal is triggered by excitation pulse) or reverse mode (when fluorescence triggers the *START* signal). The process is illustrated in Figure 2.2 using a reverse mode of triggering, which is done though an electrical pulse associated with the optical signal and it passes through CFD1 to trigger the TAC. The photons associated with the fluorescence signal passes through a monochromator and then reaches CFD2. This *START* pulse initiates the charging of the capacitor in the TAC and it continues charging until *STOP* pulse comes. The excitation pulse, which acts as *STOP* signal reaches the TAC (after passing through CFD) after a certain delay and then the capacitor discharges. The final voltage of the TAC output is proportional to the time delay between the *START* and *STOP* pulse. The final output is then amplified through PGA and converted to digital signal by ADC. The height analysis of this output is performed by MCA.

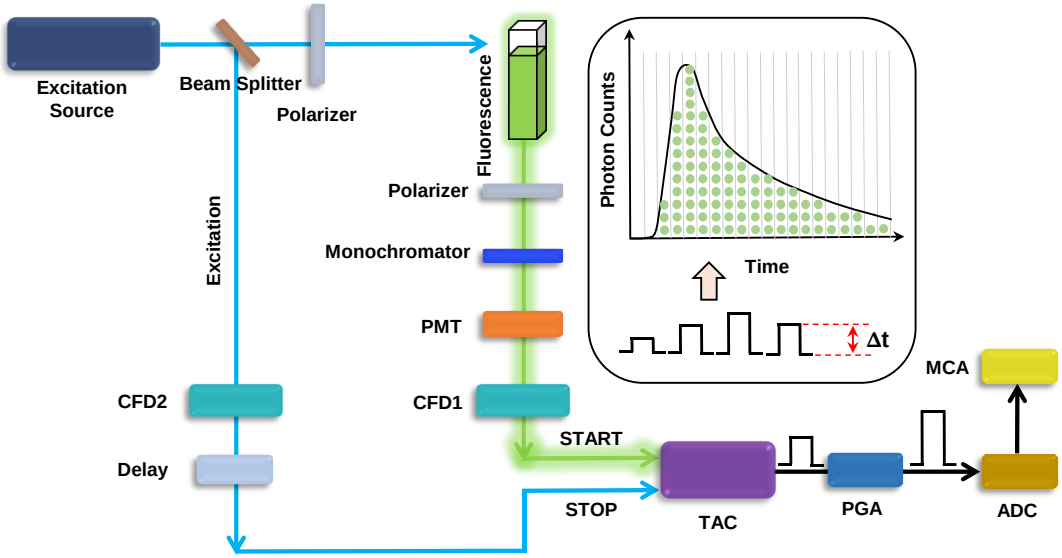

Figure 2.2. Schematic illustration of the working principle of a typical TCSPC set-up (in reverse mode).

It is important to keep the fluorescence intensity low such that the number of fluorescence photons is smaller than the number of excitation pulse; this ensures low probability of detecting two fluorescence photons coming from the sample upon each excitation. Otherwise 'pileup effect' will arise where the detector will be able to detect only one fluorescence photon, which comes first and the counting statistics will be erroneous.[10]

Our TCSPC setup (5000, Horiba Jobin Yvon IBH) utilized a PicoBrite laser diodes as excitation sources (375, 405, 481 nm) operating at a repetition rate of 1 MHz. The pulse width of the laser outputs was measured by recording the pulse response with a dilute aqueous solution of Ludox scatter and it varied between 60-100 ps depending on the laser diode used. A MCP photomultiplier (Hamamatsu R3809U-50) was used as a detector. Once the data was recorded, it was fitted with a non-linear least-squares iterative method using IBH DAS6 (Version 2.2) software. We kept a note of the χ^2 value to ensure the quality of the fit. For a typical n^{th} order multiexponential decay, the *δ-pulse* response is given as-

$$I(t) = \sum_{i=1}^{n} \alpha_i \exp(-t/\tau_i)$$

where, α_i, τ_i represent the amplitude and lifetime of the ith component, respectively.

2.3.3. Femtosecond Transient Absorption Measurement

Principle

TA spectroscopy, which is also known as pump-probe spectroscopy, is one of the most useful techniques for ultrafast-time-resolved studies.[11,12] In this technique, the system is photo-excited with a (pump) laser pulse of a given wavelength to generate the *transient* species, which is then investigated by a broad band probe pulse, which comes after a certain delay (Figure 2.3).[14] By varying the pump-probe delay one can capture the spectral and temporal evolution of the transient species.[14]

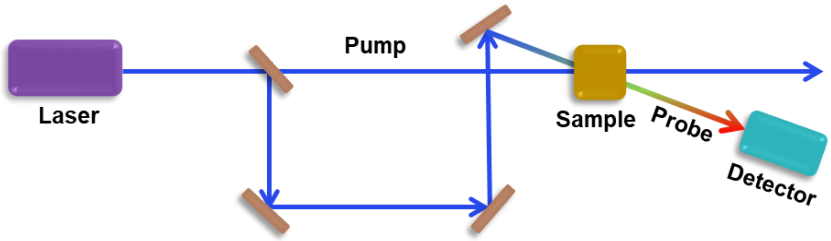

Figure 2.3. Basic schematic outline of TA measurement technique.

When pump is in play, the probe records the absorbance of the photoexcited sample and to record the absorbance of unexcited sample, pump beam is blocked by an external chopper. The transmitted intensity of the probe beam is used to calculate the differential absorbance (ΔA) i.e. absorbance of the excited minus unexcited sample. Then, by adjusting the pump-probe delay one can record the time evolution of ΔA. Mathematically, ΔA is defined as follows[14]

$$\Delta A = (\lambda, t) = A_{pump-on} - A_{pump-off} = A_{ex}(\lambda, t) - A_{gs}(\lambda)$$

$$\Delta A(\lambda, t) = \log\left(\frac{I_{0,ex}(\lambda)}{I_{ex}(\lambda, t)}\right) - \log\left(\frac{I_{0,gs}(\lambda)}{I_{gs}(\lambda)}\right) = \log\left(\frac{I_{gs}(\lambda)}{I_{ex}(\lambda, t)}\right)$$

Where, A_{ex} and A_{gs} are the respective absorbance of the excited state and ground state species. I_0 and I represent the intensity of the incident and transmitted light, respectively.

A typical TA spectrum can consist of several features as shown in Scheme 2.4. The main characteristic signals are generally associated with ground state bleach, excited state absorption and stimulated emission.[14]

(i) GSB: GSB signal appears as a negative signal in TA spectra in the region where the system has ground state absorption. Here, the pump pulse promotes a fraction of population of the sample to the excited state, the probe experiences a lower population in the ground state. Hence, more light is transmitted for the excited sample compared to the unexcited one explaining a negative ΔA value in the spectral region of the ground-state absorption (Figure 2.4).

(ii) SE: Upon photoexcitation by a pump pulse, when the probe pulse passes through the excited sample, it can depopulate some of the excited molecules to the ground state. As these emitted photons travel in the same direction as the probe pulse hits the detector, more transmitted light is detected under this condition (as compared to the unexcited sample). Hence, ΔA appears as a negative signal in this case too (Figure 2.4). It is to be noted that, in such cases where the Stokes shift is very small, spectral distinction between GSB signal and SE emission can be difficult and the overall feature appears as a broad negative signal.

(iii) ESA: After generation of excited state population, the broad-band probe pulse can promote some of them to higher lying optically allowed states. In such scenario, the transmitted intensity associated with that wavelength of the probe pulse will be lowered for the excited molecule as compared to the unexcited one. Lowering in transmittance is reflected in increase in absorbance and thus ΔA appears as a positive signal (Figure 2.4). Upon generation of a new transient species due to photoexcitation and if it has any characteristic absorption feature, that will also appear as a positive signal in the TA measurement.[14]

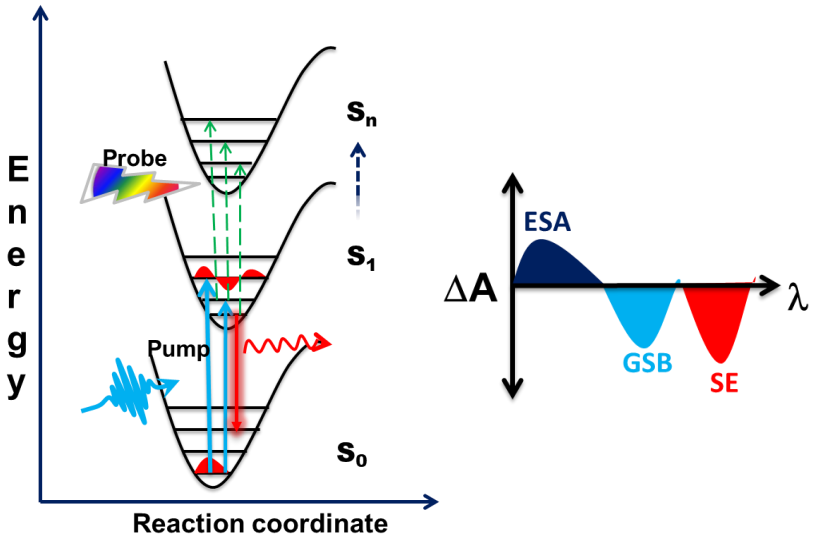

Figure 2.4. Schematic illustration of investigating a molecular system by pump-probe technique. Right panel represents different signal features associated with the measurement.

It is noteworthy that in cases where all or some of the above described signals overlap with each other, deconvolution is needed to understand the dynamics associated with each processes which is generally performed by a global analysis (multiple wavelength kinetic analysis).

Components and Optical Layout of Our TA Setup

The TA setup of the School of Chemistry, University of Hyderabad, which we used for all our studies, consisted of the following major components: (i) Ti:sapphire oscillator (MaiTai HP, Spectra-Physics, USA) (ii) nanosecond pump laser (Empower 30, Spectra-Physics, USA) (iii) regenerative amplifier (Spitfire ACE, Spectra-Physics, USA) (iv) optical parametric amplifier with optical frequency mixer (TOPAS-Prime, Spectra-Physics, USA) (V) spectrometer (CDP systems, Russia). The optical layout of the different components in the whole setup is shown below.

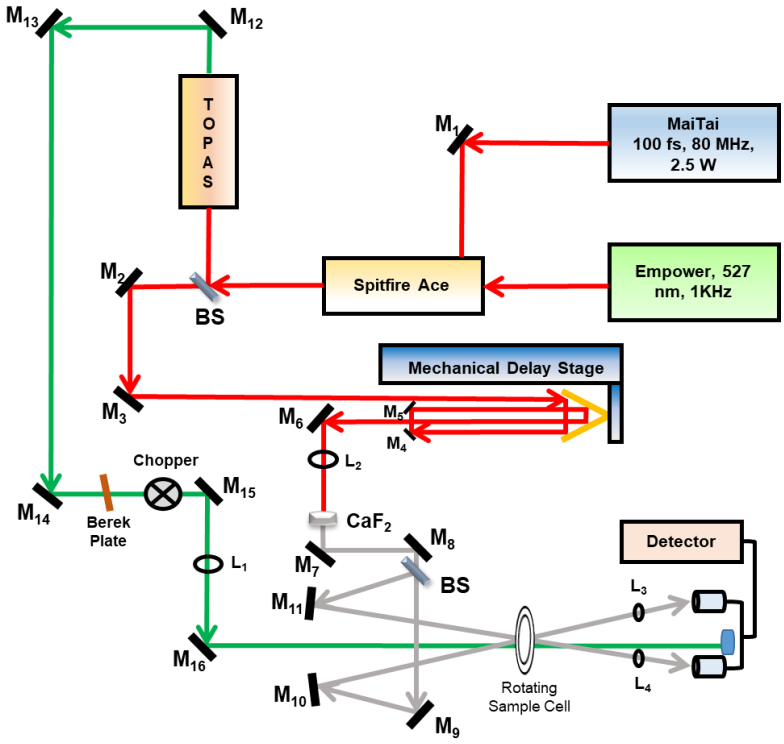

Figure 2.5. Schematic illustration of the optical layout of the TA setup of the School of Chemistry, University of Hyderabad, used for our measurements.

(i) Ti:sapphire oscillator (MaiTai HP):

The femtosecond Ti:sapphire oscillator, which is also called MaiTai, operates at a repetition rate of 80 MHz with 800 nm center wavelength. The actual lasing medium is Ti^{3+}-doped sapphire (Al_2O_3 crystal), which is a four level lasing system (Figure 2.6A).[15] The broad absorption feature in the visible region (410 to 600 nm) of the Ti:sapphire makes it a suitable active medium as it can be pumped with desired choice of visible laser (Figure 2.6B). Moreover, the broad emission window (690 to 1040 nm) also makes it a tunable laser too.[15] Another advantage of using Ti:sapphire is the large Stokes shift, which minimizes the reabsorption loss during operating condition.

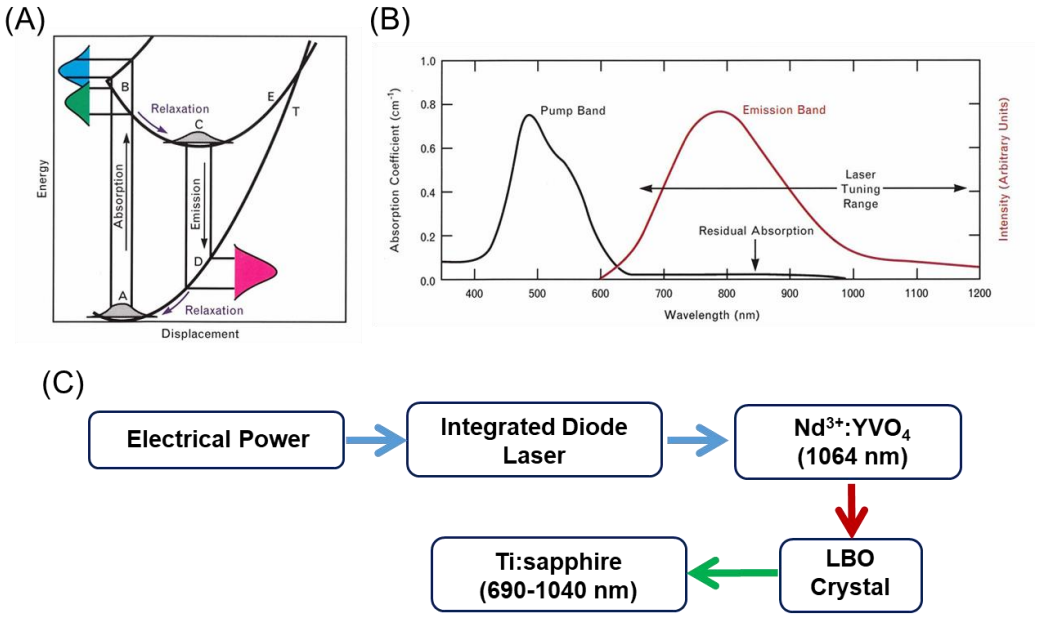

Figure 2.6. Electronic energy level diagram (A) and absorption and emission spectra (B) of Ti:sapphire. Adapted from ref. 15. (C) Outline of the operation sequence for the excitation of the Ti:sapphire.

In our system, Ti:sapphire was pumped by a second-harmonic output of Nd^{3+}:YVO_4 (532 nm) laser. Nd^{3+}:YVO_4 was pumped with two integrated diode lasers, which were operated through electrical power. The entire process is schematically presented in Figure 2.6C.

(ii) Regenerative amplifier (Spitfire ACE): The average power output of the MaiTai laser was several nJ and this needed to be amplified to achieve an excitation wavelength covering a wide range and also to generate a broadband probe. This amplification of laser pulse was performed in Spitfire ACE by adopting a method called chirped pulse amplification.[16] The basic idea of this method was to first stretch the input pulse (with reduced peak power), then amplify its power and finally, the amplified pulse was compressed again back to its short temporal resolution (Figure 2.7A). Pulse stretching was needed before amplification as direct amplification of ultrashort pulse (with high peak power) can damage its optical components.

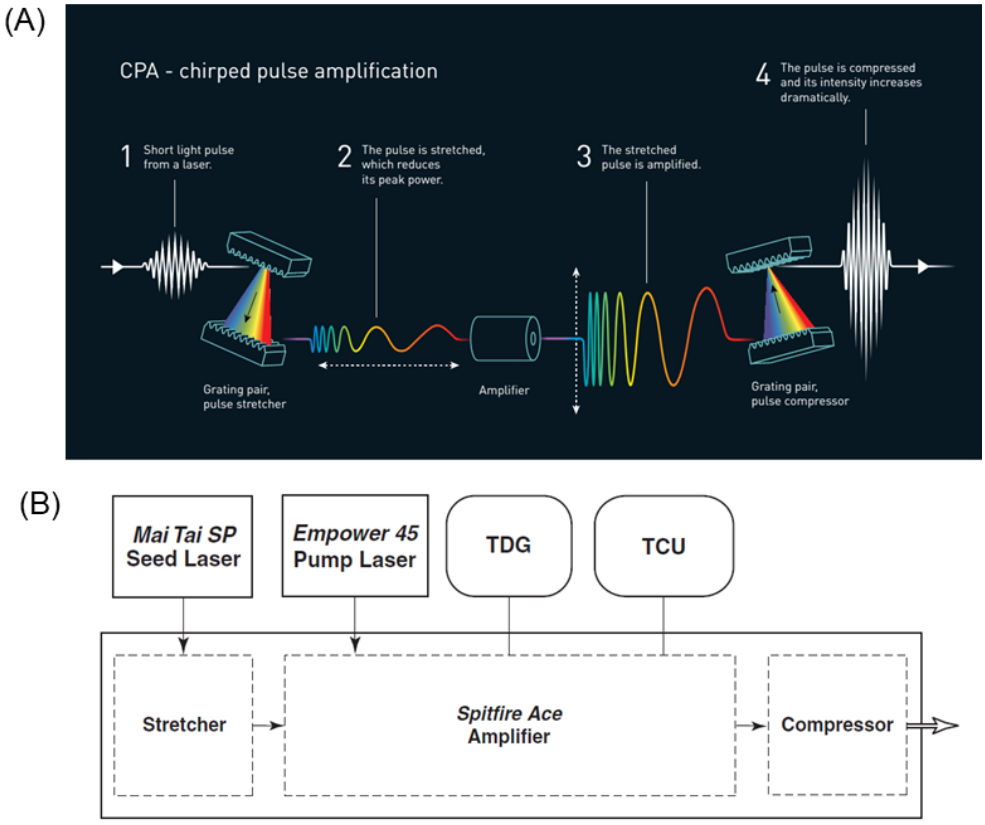

Figure 2.7. (A) Sequencial stapes involved in chirped pulse amplification process. Adopted from ref. 17. (B) Outline of the operation for the amplification process. The electronic communications between components are made through TDG and TCU.

The basic operating components involved in the amplification process in shown in Figure 2.7B. The MaiTai laser output (seed pulse) was directed into Spitfire ACE where a grating pair with positive dispersion stretches the pulse. After stretching it was then passed through a Ti:sapphire crystal, which was continuously pumped by Empower output (discussed later) and both pump and seed lasers were focused onto the crystal maintaining a strong overlap between them. Finally, the amplified output was passed through a grating pair of negative dispersion (compressor), which compresses the amplified pulse. The output of Spitfire ACE was 800 nm but with increased energy of ~4.2 mJ. The repetition rate of the resulting pulse was 1 kHz.

(iii) Empower: The empower system (Empower 30 in our case) is intercavity-doubled, Q-switched, diode pumped Nd:YLF laser which produces 527 nm output. The diode lasers pump the neodymium doped YLF crystal which emit at 1053 nm. This was then frequency-doubled by passing through a LBO crystal to generate the high-energy Q-switched pulse with 527 nm output. This high energy pulse was used for pumping the Ti:sapphire crystal in the Spitfire ACE system.

(iv) OPA with optical frequency mixer (TOPAS): OPA is one of the most complex as well as important components in the whole ultrafast TA setup. Our OPA unit (TOPAS-Prime) can generate any excitation wavelength between 280-2600 nm. TOPAS consisted of many optical parts. A portion of the (~80%) amplifier output (of 800 nm pulse) was directed to TOPAS, ~20% of which was passed through a sapphire plate for the generation of white light. A fraction of the white light was mixed with the rest of the pump light (~20%) in a BBO (BBO1) crystal to generate a signal and an idler. Any desired wavelength could be achieved by controlling the phase matching angle of the BBO crystal with respect to the seed beam. SFS could be obtained by mixing the signal output with the pump pulse in a BBO (BBO2) crystal. To generate second or fourth harmonic signal/idler, the signal and idler beam were passed through the frequency mixers and their orientation was adjusted according to the need of the pump wavelength.

(V) Spectrometer and Detection: Depending on the requirement of excitation wavelength, the TOPAS was adjusted and the beam was directed towards the rotating sample cell using a few reflectance mirrors (Figure 2.8). It is to be noted that before letting it pass through the sample, the pump was chopped with a mechanical chopper (repetition rate of 1 kHz). A portion (~20%) of the amplifier output was passed through an optical delay line (~ 4 ns) and then through a rotating CaF_2 crystal to generate a broad-band white light (350-850 nm) (Figure 2.8). This white light was then divided into two parts and focused on the rotating sample cell. One of them was used as a reference beam and another was spatially and temporally overlapped with the pump beam. For better overlap with the pump and probe beam, an angle <5° was maintained between them. Both the transmitted signal and the reference beam were directed towards two separate optical fibers and directed towards the detector (photodiode array) after passing through

polychromator. The detection was done as a differential absorption and data accusation was controlled through Excipro software (CDP system, Russia). Here it is important to note that during the measurements the intensity of the probe pulse was maintained low with respect to the pump, so that multiphoton processes can be avoided. Also, the beam diameter of the pump pulse was larger than that of probe. All measurements reported in this thesis were performed with a magic angle polarization using colloidal sample solutions. The sample solution was sandwiched between two quartz glass plates maintaining a path length of 1 mm.

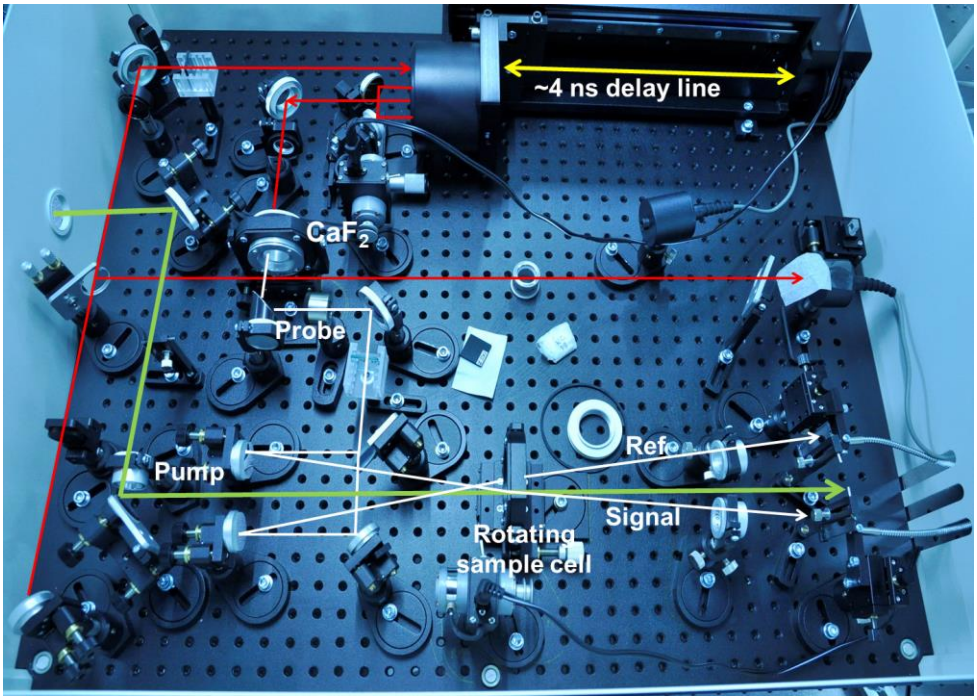

Figure 2.8. Optical layout of different components of the spectrometer of the pump-probe setup used for this study.

2.3.4. Femtosecond Fluorescence Upconversion Measurement

Principle

Fluorescence upconversion measurement is one of the few photon counting based techniques which provides best temporal resolution available till date.[10] In our case, the fluorescent sample was excited with the second harmonic (400 nm) of the MaiTai output and the resulting laser induced fluorescence signal was specially and temporally overlapped with gate pulse (800 nm) to produce a sum frequency signal (Figure 2.9). The efficiency of the sum frequency signal output depends on the phase matching angle between the gate and fluorescence beam, thus can be tuned by minute adjustment of the sum frequency crystal orientation. The temporal resolution of the measurement was governed by GVD introduced due to non-linear optical processes involved in the measurements, which in our case was ~200 fs.

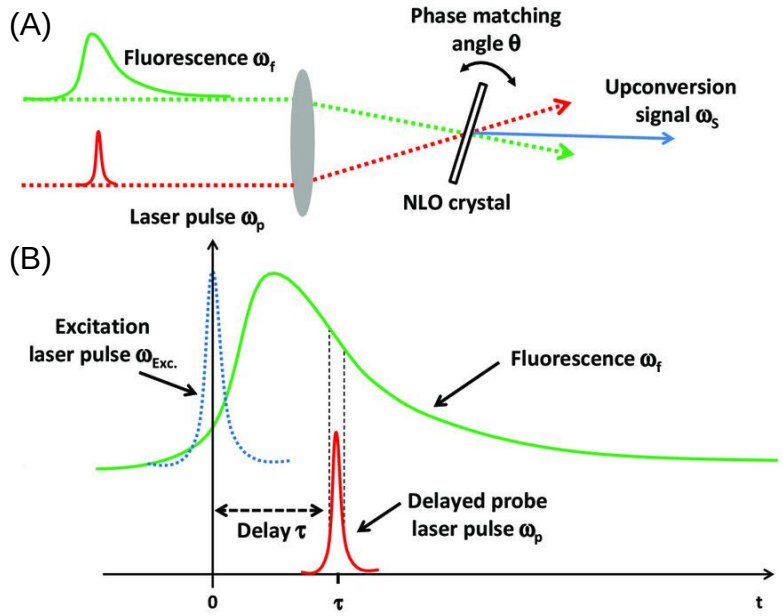

Figure 2.9. Schematic illustration of the generation of sum-frequency signal (A) and (B) measurement technique in PL UC. Reprinted with permission from ref 18.

The resulting upconverted sum frequency signal was then detected through a PMT. To obtain the kinetics, the gate pulse was delayed with respect to the excitation pulse and the time dependent changes of the sum frequency output was measured (Scheme 2.9). The intensity of the gate beam being same throughout the measurement, the time dependence

of the sum frequency output was directly correlated with intensity variation of the PL signal and thus directly provided the PL decay kinetics associated with the sample fluorescence.

Components and Optical Layout of Our PL UC Setup

The optical layout of our PL UC setup is shown in Figure 2.10. A part of the 800 nm Ti:sapphire output was directed towards the UC setup (FOG 100, CDP system, Russia). In the spectrometer, the beam was first passed through a BBO crystal to generate the second harmonic signal i.e. 400 nm. A dichroic mirror was used to reflect the 400 nm laser beam which was used as excitation source for the measurement. The transmitted 800 nm beam,

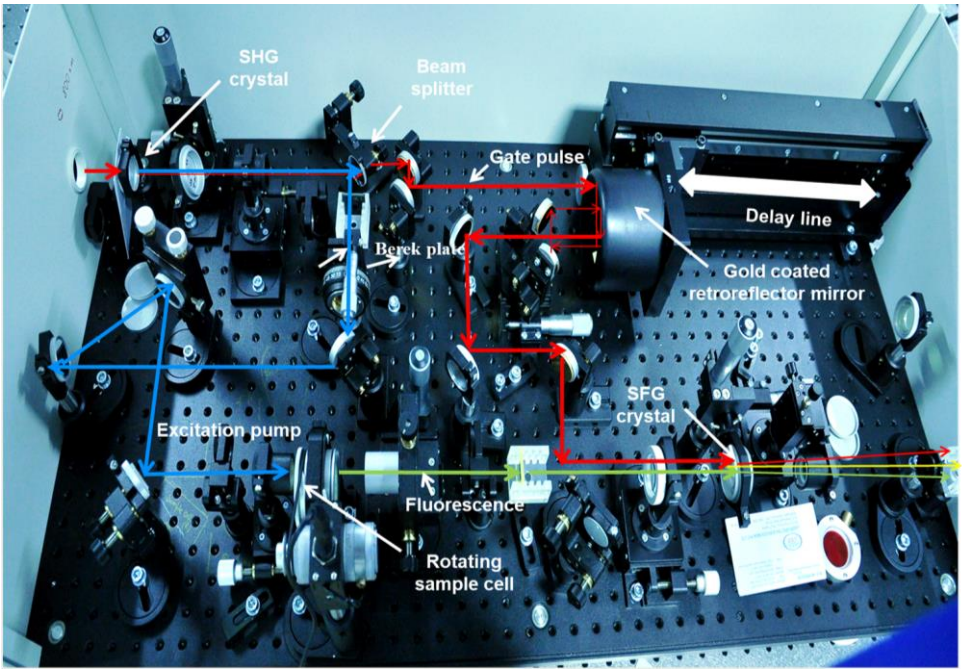

Figure 2.10. Optical layout of spectrometer part of the existing PL UP setup (FOG 100) in School of Chemistry, University of Hyderabad.

which was called the gate beam, was passed through a mechanical delay line of ~ 4 ns. Using bereck compensator, all the experiments were carried out under magic angle excitation condition. The excitation beam was focused on the rotation sample cell and the transmitted pump was cut off by placing proper filter which only allows the PL from the

sample. The scattered PL was then collimated and focused on a sum frequency mixing BBO crystal. The gate beam was also directed towards the BBO crystals and overlapped with the PL signal. Then the sum frequency output was passed through a monochromator and directed towards the PMT detector.

2.4. Other Measurements

PXRD: PXRD patterns of the thin-films of the NCs were recorded using a X-ray diffractometer (Bruker AXS D8) with Cu-Kα X-ray radiation (λ = 1.5406 Å). The samples were prepared by drop-casting colloidal dispersion of NCs solutions onto thin glass plates.

TEM: The morphology and size of the NCs were determined using a transmission electron microscope (Tecnai G2 FE1 F12) operating at an accelerating voltage of 200 kV. Samples were prepared by drop-casting a dilute solution of NCs onto carbon-coated Cu-grids. All the samples were vacuum dried before the measurements.

FESEM: FESEM images were recorded using a Carl Zeiss Ultra 55 microscope. EDX spectra and elemental mappings were performed with an Oxford Instruments X-Max^N SDD (50 mm^2) system and INCA analysis software. Samples were prepared by drop-casting a dilute solution of NCs onto carbon-coated Cu-grids/thin glass plate. All samples were vacuum dried before the measurements.

XPS: XPS measurements were performed in a Thermo Scientific K-Alpha spectrometer equipped with micro-focused monochromatic X-ray source (Al K_α, spot size ~ 400 μm) operating at 70 W. The energy resolution of the spectrometer was set at 0.5 eV at pass energy of 50 eV and 5×10^{-5} torr base pressure was maintained at the analysis chamber. Low energy electrons from the flood gun were used for charge compensation. XPS samples were prepared by drop-casting an optimum concentration of the NCs solution onto a quartz plate.

FTIR: FTIR measurements were performed using Bruker Tensor II spectrometer. A dilute solution of the NCs was drop-casted and measurement was performed once the solvent was evaporated.

ICP-OES: A Varian 720 emission spectrometer was used for ICP-OES measurements. The samples were mixed with aqua-regia [12 (N) HCl: 17 (N) HNO_3 (v/v) = 3:1] and kept overnight for complete digestion of the NCs. The resulting transparent solution was used for measurements.

EPR: A Jeol JES-FA200 spectrometer was used to record the EPR spectrum and all the measurements were carried out using colloidal dispersions of the NCs (in hexane/toluene).

References

1. Perrin, D. D.; Armerego, W. L. F.; Perrin, D. R., Purification of laboratory chemicals. *Pergamon Press: New York* 1980.
2. Protesescu, L.; Yakunin, S.; Bodnarchuk, M. I.; Krieg, F.; Caputo, R.; Hendon, C. H.; Yang, R. X.; Walsh, A.; Kovalenko, M. V. Nanocrystals of Cesium Lead Halide Perovskites ($CsPbX_3$, X = Cl, Br, and I): Novel Optoelectronic Materials Showing Bright Emission with Wide Color Gamut. *Nano Lett.* **2015**, 15, 3692-3696.
3. Protesescu, L.; Yakunin, S.; Bodnarchuk, M. I.; Bertolotti, F.; Masciocchi, N.; Guagliardi, A.; Kovalenko, M. V. Monodisperse Formamidinium Lead Bromide Nanocrystals with Bright and Stable Green Photoluminescence. *J. Am. Chem. Soc.* **2016**, 138, 14202-14205.
4. Vybornyi, O.; Yakunin, S.; Kovalenko, M. V. Polar-Solvent-Free Colloidal Synthesis of Highly Luminescent Alkylammonium Lead Halide Perovskite Nanocrystals. *Nanoscale* **2016**, 8, 6278-6283.
5. Liu, W.; Lin, Q.; Li, H.; Wu, K.; Robel, I. n.; Pietryga, J. M.; Klimov, V. I., Mn^{2+}-Doped Lead Halide Perovskite Nanocrystals with Dual-Color Emission Controlled by Halide Content. *J. Am. Chem. Soc.* **2016,** *138*, 14954-14961.
6. De, A.; Das, S.; Mondal, N; Samanta, A., Highly Luminescent Violet- and Blue-Emitting Stable Perovskite Nanocrystals. *ACS Materials Lett.* **2019**, 1, 116−122.
7. Maciejewski, A.; Steer, R. P., Spectral and Photophysical Properties of 9, 10-Diphenylanthracene in Perfluoro-n-hexane: The Influence of Solute-Solvent Interactions. *Journal of Photochemistry* **1986**, 35, 59 - 69.

8. Rurack, K.; Spieles, M., Fluorescence Quantum Yields of a Series of Red and Near-Infrared Dyes Emitting at 600-1000 nm. *Anal. Chem*. **2011**, 83, 1232–1242.
9. Kubin, R. F.; Fletcher, A. N., Fluorescence quantum yields of some rhodamine dyes. *J. Lumin.* **1982**, 27, 455-462.
10. Valeur, B., Molecular Fluorescence: Principle and Applications, 2nd edn., Wiley-VCH Verlag GmbH, Weinheim, **2001**.
11. A. M. Weiner, A.M., Ultrafast Optics, John Wiley and Sons, Inc, Hoboken, **2009**.
12. Singh, S. C.; H. Zeng, H.; Guo, C.; Cai, W., Nanomaterials: Processing and Characterization with Lasers, S. C. Singh, Wiley-VCH Verlag & Co. KGaA, Weinheim, 2012.
13. https://www.nobelprize.org/uploads/2018/10/popular-physicsprize2018.pdf
14. Ruckebusch, C.; Sliwa, M.; Pernot, P.; de Juanc, A.; Tauler, R., Comprehensive Data Analysis of Femtosecond Transient Absorption Spectra: A Review. *Journal of Photochemistry and Photobiology C: Photochemistry Reviews* 2012, 13, 1–27.
15. Wall, K. F.; Sanchez. A., Titanium Sapphire Lasers. *The Lincon Laboratory Journa*l, **1990**, 3, 447.
16. Witte, S.; Eikema, K. S. E. *IEEE Journal of Selected Topics in Quantum Electronics* **2011,** 18, 296.
17. https://www.nobelprize.org/uploads/2018/10/press-fig3-fy-en-cpa.pdf
18. Chosrowjan, H.; Taniguchi, S.; Tanaka, F. Ultrafast Fluorescence Upconversion Technique and Its Applications to Proteins *FEBS Journal*, **2015**, 282, 3003-3015.

CHAPTER 3

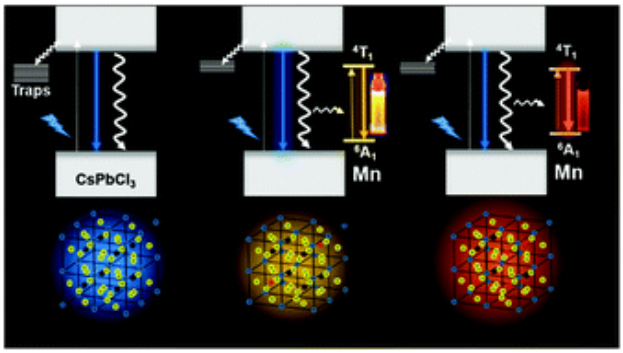

"Luminescence Tuning and Exciton Dynamics of Mn-Doped CsPbCl3 Nanocrystals"

Nanoscale, 2017, 9, 16722–16727

Overview

Mn-doped perovskite NCs are a new class of materials offering exciting opportunities to control over their optical and magnetic properties. We report a series of Mn-doped $CsPbCl_3$ NCs exhibiting tunable Mn-PL band with PL peak wavelength pushed up to 625 nm and tuned over a range of 40 nm, the largest achieved so far, by only varying the Mn content. X-band EPR data and Mn PL decay behavior of the NCs reveal that exchange interaction between Mn^{2+} ions is mainly responsible for large shift of the Mn PL band. Ultrafast pump-probe measurements show that exciton-dopant energy transfer in these NCs is slower (~ 50-100 ps) than trapping of the charge carriers (~ 8-10 ps) in host lattice. The large PL tuning reported here along with the insights provided on the mechanism of tuning and carrier dynamics are expected to boost the potential of Mn-doped $CsPbCl_3$ NCs in light-powered devices.

3.1. Introduction

Doping of semiconductor NCs by transition metal ions can generate new optical, electronic and magnetic properties through energy or charge transfer interaction between the host and dopant.[1-6] Group II-IV QDs doped with color-centered impurities like Mn^{2+} introduce dopant emission with long PL lifetime, high PLQY, large Stokes shift minimizing self-absorption and better colloidal stability over the undoped NCs.[7-9] In photo-excited Mn-doped NCs, transfer of energy from excitons to the dopant produces a PL band at ~2.12 eV corresponding to the $^4T_1$ to $^6A_1$ transition in Mn^{2+} with long PL lifetime (few ms) due to forbidden nature of the transition, thus making the system a potential candidate for efficient extraction of charge carriers.[10-12]

Recently, all-inorganic perovskite NCs, $CsPbX_3$ (X= Cl, Br, I), have emerged as promising materials in photovoltaic and optoelectronic applications.[13-16] A number of studies is undertaken on doping of all-inorganic perovskite NCs with metal ions,[17, 18] especially Mn^{2+}.[19-24] It is found that Mn-doped $CsPbCl_3$ NCs enhance the stability and efficiency of photovoltaic devices when used as energy downshift layer with the solar energy harvester.[25] Potential application of these doped NCs as display materials requires tuning of the Mn PL band position. This, however, cannot be achieved like it is done for excitonic PL by varying the size and shape of the NCs. Attempts to tune the Mn PL peak position by varying the Mn-content in $CsPbCl_3$ NCs were unsuccessful except in one case where Liu et al could tune it by 18 nm by varying the temperature and Mn-content up to 46%. [22]

Herein, we demonstrate that peak wavelength of the Mn PL band in doped $CsPbCl_3$ NCs can be tuned by 40 nm (585 to 625 nm), the highest range achieved so far, using an Mn-content of only up to 15.5 % at fixed reaction temperature. X-band EPR and Mn PL decay measurements reveal an enhancement of Mn–Mn exchange interaction at higher Mn-content in these quantum confined NCs. The ultrafast TA measurements reveal fast carrier trapping (~8-10 ps) in the host lattice and consequent reduction in the number of excitons participating in energy transfer (~50-100 ps) to the dopant sight.

3.2. Results and Discussion

3.2.1. Synthesis and characterization of the NCs

Both undoped $CsPbCl_3$ and a series of Mn-doped $CsPbCl_3$ NCs were synthesized at 185°C by suitable modification of a reported hot-injection method.[26] ICP-OES measurements show that Mn contents in these NCs are 1, 2, 7.5, 12, and 15.5 mole %, with respect to Pb, for added Mn precursor concentration of 10, 20, 30, 40 and 60%, respectively (Table A1.1). TEM images show cubic morphology of both undoped and doped NCs with average edge length of 7.0 ± 0.5 nm (Figure A1.1), which is close to the Bohr excitonic diameter (~ 5 nm) of the host NCs.[26] Estimated Goldschmidt tolerance factor (t) and octahedral factor (μ) for all Mn-doped NCs fall under the range of stable perovskite formability (Figure A1.2).[27, 28]

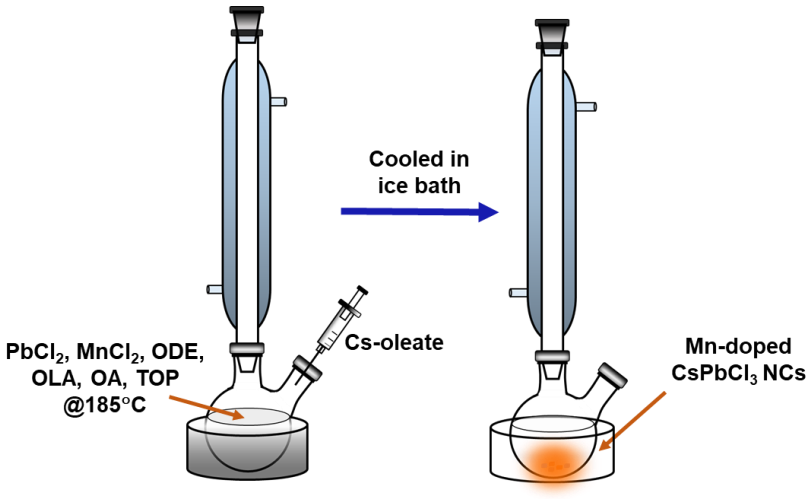

Scheme 3.1. Schematic representation of the synthesis of Mn-doped $CsPbCl_3$ NCs in the hot-injection method.

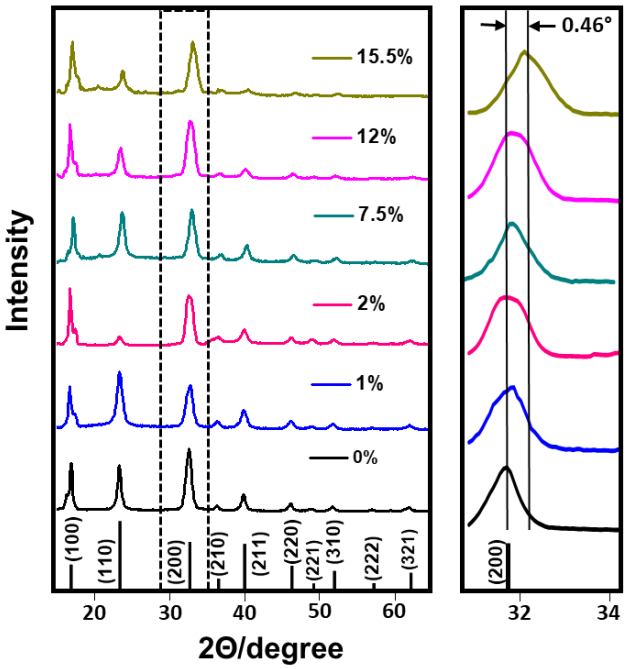

Figure 3.1. PXRD patterns of undoped and Mn-doped $CsPbCl_3$ NCs with different Mn contents. An expanded view of the (200) peak indicating the shift towards a higher angle is shown in the right panel.

PXRD patterns of the samples match with the standard cubic phase $CsPbCl_3$ (JCPDS: 84-0437, Figure 3.1), indicating intactness of the crystalline nature of NCs upon doping. A monotonic shift of the XRD peaks to higher angles with increasing Mn-content is indicative of progressive lattice contraction on substitution of Pb^{2+} (133 pm, CN=6) with smaller Mn^{2+} (97 pm, CN=6). A positive shift of the 2Θ value of 0.46° (Figure 3.1, right panel) for 15.5% Mn content is in agreement with the literature.[19]

3.2.2. Optical properties

The PL spectra of the undoped NCs exhibit a sharp excitonic PL band with peak at ~406 nm (Figure 3.2). With increase in Mn-content a gradual blue shift of the band-edge absorption (Figure A1.3) and PL is observed despite negligible variation in size of the

NCs. For undoped NC, the band gap of 3.05 eV, estimated from the Tauc plot (A1.4) is found to be consistent with earlier report.[29] With increase in dopant content, this band gap increases due to contraction of the $PbCl_6$ octahedral unit and consequent enhancement of interaction between Pb and Cl. As the CBM is dominated by Pb (6p) and Cl (3p) antibonding orbitals, the enhanced interaction results in a shift of the CBM towards higher energy.[30, 31]

For Mn-doped NCs, in addition to the excitonic band, a broad PL band typical of $^4T_1$ to $^6A_1$ electronic transition in Mn^{2+}, is observed at longer wavelength. It is evident that this band results from the transfer of excitation energy from photo-excited host NCs to Mn as the excitation spectrum corresponding to this PL band matches with the absorption spectrum of undoped NC (Figure A1.4).[32, 33]

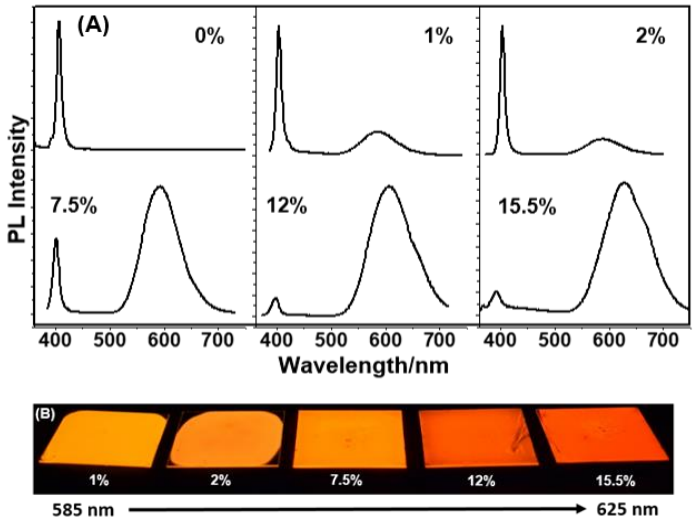

Figure 3.2. (A) PL spectra showing dual emission of sets of materials having different Mn contents (in %). (B) Digital images of films of different Mn containing NCs showing the tunability of Mn PL are highlighted.

The variation of QY of the excitonic and Mn PL on the Mn- content is depicted in Figure 3.3. Low PL QY (<1%) of undoped system is expected to be due to the mid-gap (trap) states facilitating nonradiative deactivation in wide band gap $CsPbCl_3$ NCs. On doping, the Mn PL intensity is expected to increase at the expense of excitonic PL. However, for very small Mn-content (2%), an increase in excitonic PL intensity is observed, which we

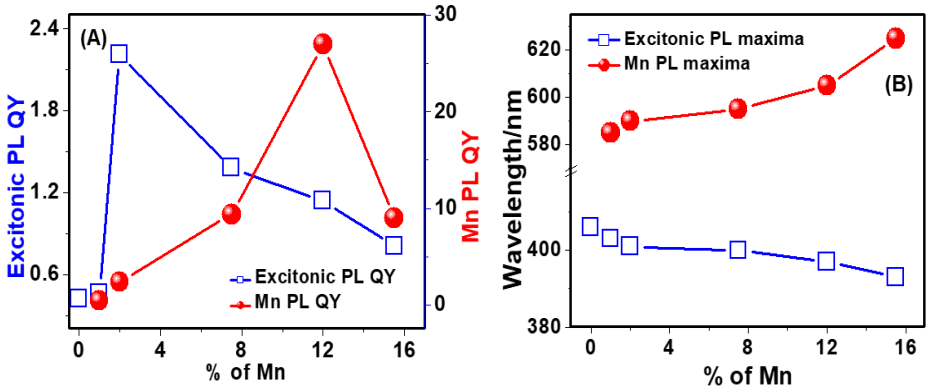

Figure 3.3. Variations in the exciton and Mn PL QY and shift in the excitonic and Mn PL maxima for different Mn containing NCs are shown in panels (A) and (B), respectively

attribute to the removal of pre-existing structural defects (chloride vacancies) in host NCs by $MnCl_2$ used in synthesis.[20] Increase in Mn-content (from 2 to 12%) leads to increase in Mn PL accompanied by a decrease of excitonic emission intensity; a signature of efficient energy transfer from host to the dopant ion. The highest Mn PL QY of ~27% is observed for 12% Mn-content, beyond which a drop is noted.[34]

Panel B of Figure 3.3 depicts the dependence of PL peak positions on Mn-content for both exciton and Mn PL band. For excitonic PL, a blue shift (406 to 393 nm) due to lattice contraction is observed. On the other hand, the Mn PL band shifts towards red with increase in Mn content in the NCs. A 40 nm shift (from 585 to 625 nm) is observed for the concentration range studied here. The spectral shift is clearly observable by naked eye, as illustrated in Figure 3.2. The wavelength tuning range demonstrated here is much larger than that (18 nm) observed very recently by Liu et al by varying the Mn-content and reaction temperature. The red shift is presumably due to the lattice contraction induced change in the crystal field strength in the host lattice thereby influencing the energy gap between Mn-emissive atomic states.[35, 36] However, we show in the following section that lattice contraction alone is not responsible for red-shift of the Mn PL band.

The Mn PL is characterized by long (~ms) lifetime (Figure 3.4., Table A1.2) consistent with spin-forbidden nature of the transition. On doping, the PL decay dynamics becomes

faster (from 1.30 to 0.51 ms) though PL intensity is increased. We also observe a change in the PL decay behavior from single to bi-exponential one for Mn-content >2%. As single exponential decay behavior is characteristic of a homogenous lattice environment experienced by Mn^{2+},[21] switching of the decay behavior to bi-exponential one for Mn-content of >2% indicates a non-uniform distribution of Mn^{2+} in the NCs. Whether this non-uniformity is restricted to the core or surface of the NCs or at both places is addressed in the next paragraph.

As a knowledge of the distribution of Mn^{2+} ions in the NCs is essential for interpretation of the above observation, we have studied the room temperature X-band EPR spectra of Mn-doped samples. The observation of six equally spaced lines of equal intensity (with hyperfine coupling constant, A = 86 G) for 1 and 2% Mn-doped NCs (Figure 3.4) is in agreement with a nuclear spin (I) of 5/2 for Mn^{2+}. Close agreement of the measured A value with that reported for bulk Mn-doped $CsPbCl_3$ suggests that Mn resides inside the NCs.[37]

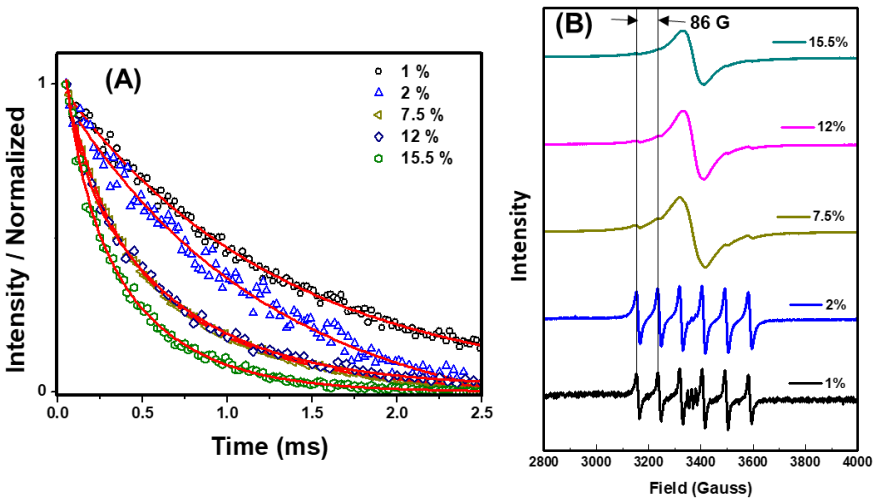

Figure 3.4. Mn PL (λ_{exc}= 330 nm) decay behavior of the samples monitored at their respective emission maxima (A), and room temperature X-band EPR spectrum of the samples (B).

The distribution of Mn^{2+} in doped $CsPbCl_3$ NCs, as indicated by the EPR spectra, is uniform up to a Mn-content of 2%. The changes in EPR spectral pattern, especially merging of individual signals leading to broadening of the spectra, with dopant

concentration clearly indicates that above 2%, Mn ions are no longer diluted in the NCs (like in for 1 and 2%) and they interact with each other.[38, 39] For highest Mn-content (15.5%) the signal collapses into an almost single broad line due to enhanced exchange interaction between Mn-pairs. It is important to note that an unchanged A-value even for highest Mn-content (15.5%) indicates that doped Mn remains inside the NCs rather on the surface.[40]

In exchange-coupled Mn^{2+} pairs, splitting of both Mn ground state ($^6A_1$, I = 5/2) and first excited state ($^4T_1$, I = 3/2) results in a reduced energy difference between the transition levels and red-shift of the emission band.[41] This coupling also partially lifts the selection rule resulting in a faster decay dynamics of Mn PL.[42] Abrupt change in both EPR pattern and Mn PL decay behavior occurs for same Mn-content (>2%), hence we conclude that in addition to the crystal field effect, the Mn-Mn exchange interaction also contributes to the red- shift of the Mn PL band at higher dopant concentrations (>2%).

3.2.3. Investigation of Carrier Dynamics

To further explore the EDET process and to determine the factors that influence it, we have studied temperature dependence of the PL. A steady decrease in PL intensity of dual bands in doped NCs (Figure 3.4) with increase in temperature from 268 to 333K is observed. The decrease of PL intensity of the excitonic band, which is very similar in both doped and undoped NCs, is mainly due to greater carrier trapping (a thermally activated process) at higher temperatures. As Mn PL intensity is determined by the rates of competitive EDET and carrier trapping processes, the observed drop of the PL intensity must be due to faster carrier trapping at higher temperature (that leaves fewer excitons to participate in EDET). As no shift of the excitonic PL band is observed with temperature, the exchange coupling between the exciton and dopant remains unaffected and plays no role in this regard.[43]

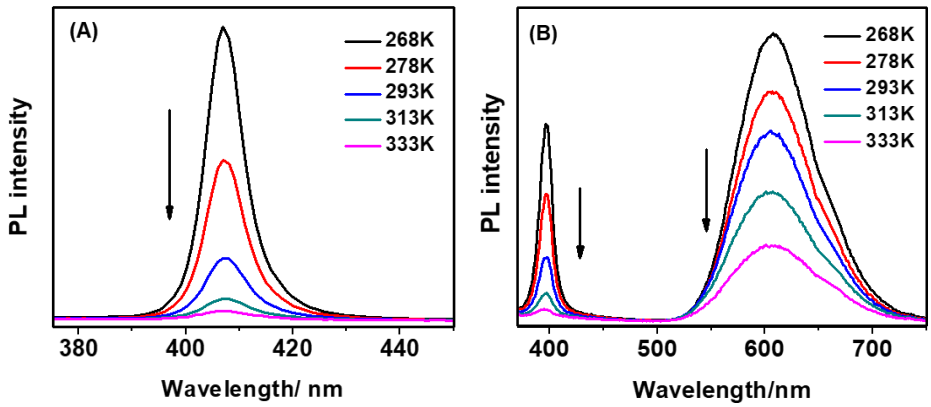

Figure 3.5. Temperature dependent PL behavior of (A) $CsPbCl_3$ and (B) Mn:$CsPbCl_3$ showing a steady decrease in PL intensity with an increase in temperature.

The competitive carrier trapping and EDET processes are corroborated by femtosecond TA measurements on undoped and doped NCs under similar excitation conditions. These spectra consist of a bleach signal around the excitonic band (~393-405 nm) and a positive photoinduced absorption band (~ 360-420 nm) (Figure A1.5). As no additional feature due to doping could be observed in doped NCs, we rely on the bleach recovery dynamics for the estimation of energy transfer rate. The bleach recovery kinetics recorded between 0-1 ns time range for all samples are found to be best represented by a bi-exponential function (as assessed by the fit residuals). In case of undoped NCs, the bleach recovery is represented by a fast (8.3 ps, 73%) and a relatively slow (160 ps, 27%) component (Table 3.1). The fast component can arise from carrier trapping or multi-exciton annihilation. However, we rule out the latter possibility considering that all TA measurements have been performed with very low excitation fluence (1.3×10^{13} photons/cm^2). The high amplitude of carrier trapping is consistent with low QY (<1%) of our samples of $CsPbCl_3$ NCs. We assign the slow component to the non-radiative recombination process based on literature.[44, 45] It is to be noted in this context that the radiative recombination time constant cannot be extracted from this data as it extends well beyond our experimental time window. For small doping content (up to 2%), the fast

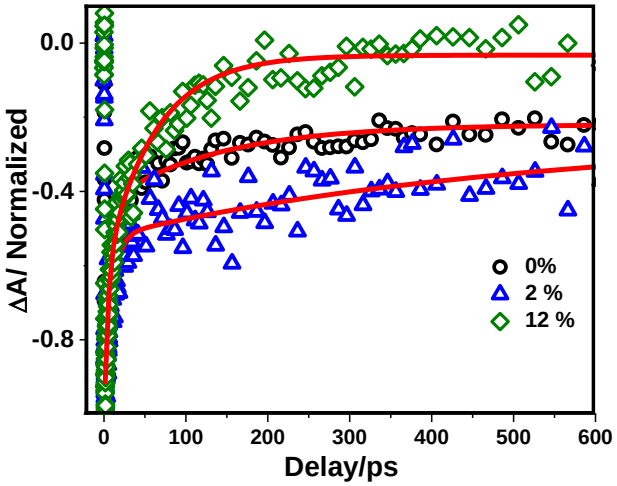

Figure 3.6. Comparison of bleach recovery kinetics of 0, 2% and 12% Mn-doped $CsPbCl_3$ NCs, monitored at their excitonic bleach maxima.

(trapping) component remains almost the same, but the recombination time and its amplitude (Table 3.1) are increased, which is also evident from the bleach recovery dynamics presented in Figure 3.6. The observation is clearly a reflection of the removal of pre-existing structural defects in the host lattice upon incorporation of small Mn-content, which is consistent with our steady state findings.

Table 3.1. Bleach recovery time constants and the corresponding amplitudes of undoped and doped NCs of varying Mn-contents.

Systems	**Recovery Components**	
	τ_1 (a_1)/ ps	**τ_2 (a_2)/ ps**
$CsPbCl_3$	8.3 ± 0.4 (0.73)	160.8 ± 10.0 (0.27)
1% Mn:$CsPbCl_3$	10.6 ± 1.8 (0.60)	450.0 ± 10.2 (0.40)
2% Mn:$CsPbCl_3$	9.0 ± 1.0 (0.59)	510.0 ± 10.0 (0.41)
7.5% Mn:$CsPbCl_3$	7.2 ± 0.8 (0.41)	138.0 ± 9.3 (0.59)
12% Mn:$CsPbCl_3$	7.0 ± 1.0 (0.43)	78.0 ± 8.3 (0.57)
15.5% Mn:$CsPbCl_3$	7.5 ± 0.5 (0.45)	48.0 ± 6.7 (0.55)

For higher dopant contents (>2%), the bleach recovery becomes faster (Figure 3.6) with no change in the fast (trapping) component (Table 3.1). Acceleration of the bleach recovery kinetics with increase in dopant content above 2% indicates additional ultrafast nonradiative (EDET) process not observable for low Mn-content (<2%) due to opposing crystal stabilization effect. It is evident that the energy transfer cannot compete with the fast trapping component rather it affects only the long component. This observation is in line with the another recent report on Mn-$CsPbCl_3$ NCs.[46] In the present case, we have estimated the energy transfer time scale from the extent of decrease in longer time constant and it is found to be ~ 92 and ~ 53 ps for 12 and 15.5% Mn-doped $CsPbCl_3$ NCs, respectively. It is also to note that, after 2% dopant content, as the host become modified (with increased τ_2); hence the estimation of the energy transfer (for 12 and 15.5%) is carried out with respect to 2% rather than 0%.

The above findings seem to suggest that the EDET efficiency can be further improved by reducing the trap centers in the host lattice. To validate this assignment we have carried out similar experiments with $CsPb(Cl/Br)_3$ as a host which offers higher excitonic PL QY with less trap centers compared to $CsPbCl_3$. However, Mn PL QY in Mn:$CsPb(Cl/Br)_3$ is found to be much lower than that in Mn:$CsPbCl_3$ (Figure A1.6). The bleach recovery dynamics is also not affected by the Mn-content (Figure A1.6) suggesting poor coupling between the exciton and dopant due to a lower band gap of the host lattice. Hence, the strength of coupling between the host and the dopant ions is one of the key factors that determines the efficiency of the EDET process. Before drawing the conclusion, we attempt to rationalize our findings considering the recent studies, where small/no tuning of the Mn PL band could be observed.[19,20,22] We think the key to achieving large tuning in our case is the stronger confinement in our NCs (~7 nm) as compared to the others (>10 nm). Close proximity of the Mn^{2+} ions in the confined space gives rise to Mn-Mn exchange coupling, which modulates the Mn PL energy gap. The other factor contributing to the shift of Mn PL band is lattice contraction induced by smaller size Mn. The Mn PL QY of the doped NCs is determined by the net effect of two opposing factors, EDET and Mn-Mn exchange interaction. Hence, the drop in Mn PL QY at highest Mn content is due to the dominating Mn-Mn exchange interaction over the EDET process.

3.3. Summary

In conclusion, we have succeeded in demonstrating the largest tuning of the Mn-doped PL in perovskite NCs and identified the factors that contribute to it. Further, the exciton dynamics of these NCs provides insight into the time constants of the photo-induced processes. We expect these findings will help improving the optical response of these substances further, thus making them useful in practical applications.

References

1. Norris, D. J.; Efros, A. L.; Erwin, S. C. Doped Nanocrystals. *Science* **2008,** 319, 1776-1779.
2. Norris, D. J.; Yao, N.; Charnock, F. T.; Kennedy, T. A. High-Quality Manganese-Doped ZnSe Nanocrystals. *Nano Lett.* **2001,** 1, 3-7.
3. Pradhan, N.; Sarma, D., D. Advances in Light-Emitting Doped Semiconductor Nanocrystals. *J. Phys. Chem. Lett.* **2011,** 2, 2818-2826.
4. D. Mocatta; G. Cohen; J. Schattner; O. Millo; E. Rabani; Banin, U. Heavily Doped Semiconductor Nanocystal Quantum Dots. *Science* **2011,** 332, 77-81.
5. Pradhan, N.; Jana, S.; Srivastava, B., B. Doping Cu in Semiconductor Nanocrystals: Some Old and Some New Physical Insights. *J. Am. Chem. Soc.* **2011,** 133, 1007-1015.
6. Pradhan, N.; S. D. Adhikari; A. Nag; Sarma, D. D. Luminescence, Plasmonic, and Magnetic Properties of Doped Semiconductor Nanocrystals. *Angew.Chem. Int.Ed.* **2017,** 56, 7038 –7054
7. Bhargava, R. N.; Gallagher, D.; Hong, X.; Nurmikko, A. Optical properties of manganese-doped nanocrystals of ZnS. *Phys. Rev. Lett.* **1994,** 72, 416-419.
8. Pradhan, N.; Peng, X. Efficient and Color-Tunable Mn-Doped ZnSe Nanocrystal Emitters: Control of Optical Performance via Greener Synthetic Chemistry. *J. Am. Chem. Soc.* **2007,** 129, 3339-3347.
9. Nag, A.; Chakraborty, S.; Sarma, D., D. To Dope Mn^{2+} in a Semiconducting Nanocrystal. *J. Am. Chem. Soc.* **2008,** 130, 10605-10611.
10. Beaulac, R.; Archer, P. I.; Ochsenbein, S. T.; Gamelin, D. R. Mn^{2+}-Doped CdSe Quantum Dots: New Inorganic Materials for Spin-Electronics and Spin-Photonics. *Adv. Funct. Mater.* **2008,** 18, 3873-3891.
11. Beaulac, R.; Archer, P. I.; Rijssel, J. V.; Meijerink, A.; Gamelin, D. R. Exciton Storage by Mn^{2+} in Colloidal Mn^{2+}-Doped CdSe Quantum Dots. *Nano Lett.* **2008,** 8, 2949-2953.
12. Santra, P. K.; Kamat, P. V. Mn-Doped Quantum Dot Sensitized Solar Cells: A Strategy to Boost Efficiency over 5%. *J. Am. Chem. Soc.* **2012,** 134, 2508-2511.
13. Liang, J.; Wang, C.; Wang, Y.; Xu, Z.; Lu, Z.; Ma, Y.; Zhu, H.; Hu, Y.; Xiao, C.; Yi, X.; et al. All-Inorganic Perovskite Solar Cells. *J. Am. Chem. Soc.* **2016,** 138, 15829−15832.

14. Swarnkar, A.; Marshall, A. R.; Sanehira, E. M.; Chernomordik, B. D.; Moore, D. T.; Christians, J. A.; Chakrabarti, T.; Luther, J. M. Quantum dot–induced phase stabilization of a-CsPbI3 perovskite for high-efficiency photovoltaics. *Science* **2016,** 354, 92-95.
15. Song, J.; Li, J.; Li, X.; Xu, L.; Dong, Y.; Zeng, H. Quantum Dot Light-Emitting Diodes Based on Inorganic Perovskite Cesium Lead Halides ($CsPbX_3$). *Adv. Mater*. **2015,** 27, 7162–7167.
16. Wang, Y.; Li, X.; Song, J.; Xiao, L.; Zeng, H.; Sun, H. All-Inorganic Colloidal Perovskite Quantum Dots: A New Class of Lasing Materials with Favorable Characteristics. *Adv. Mater.* **2015,** 27, 7101–7108.
17. R. Begum; M. R. Parida; A. L. Abdelhady; B. Murali; N. M. Alyami; G. H. Ahmed; M. N. Hedhili; O. M. Bakr; Mohammed, O. F. Engineering Interfacial Charge Transfer in $CsPbBr_3$ Perovskite Nanocrystals by Heterovalent Doping. *J. Am. Chem. Soc.* **2017,** 139, 731-737.
18. A. Swarnkar; V. K. Ravi; Nag, A. Beyond Colloidal Cesium Lead Halide Perovskite Nanocrystals: Analogous Metal Halides and Doping. *ACS Energy Lett.* **2017,** 2, 1089-1098.
19. Liu, W.; Lin, Q.; Li, H.; Wu, K.; Robel, I. N.; Pietryga, M. J.; Klimov, V. I. Mn^{2+}-Doped Lead Halide Perovskite Nanocrystals with Dual-Color Emission Controlled by Halide Content. *J. Am. Chem. Soc.* **2016,** 138, 14954-14961.
20. Parobek, D.; Benjamin J. Roman, B. J.; Yitong Dong, Y.; Ho Jin, H.; Elbert Lee, E.; Matthew Sheldon, M.; Son, D. H. Exciton-to-Dopant Energy Transfer in Mn-Doped Cesium Lead Halide Perovskite Nanocrystals. *Nano Lett.* **2016,** 16, 7376-7380.
21. Mir, W. J.; Jagadeeswararao, M.; Shyamashis Das, S.; Nag, A. Colloidal Mn-Doped Cesium Lead Halide Perovskite Nanoplatelets. *ACS Energy Lett.* **2017,** 2, 537-543.
22. Liu, H.; Wu, Z.; Shao, J.; Yao, D.; Gao, H.; Liu, Y.; Yu, W.; Zhang, H.; Yang, B. $CsPb_xMn_{1-x}Cl_3$ Perovskite Quantum Dots with High Mn Substitution Ratio. *ACS Nano* **2017,** 11, 2239–2247.
23. G. Huang; C. Wang; S. Xu; S. Zong; J. Lu; Z. Wang; C. Lu; Cui, Y. Postsynthetic Doping of $MnCl_2$ Molecules into Preformed $CsPbBr_3$ Perovskite Nanocrystals via a Halide Exchange Driven Cation Exchange. *Adv. Mater.* **2017**, 1700095.
24. S. D. Adhikari; S. K. Dutta; A. Dutta; A. K. Guria; Pradhan, N. Chemically Tailoring the Dopant Emission in Manganese-DopedCsPbCl3Perovskite Nanocrystals. *Angew. Chem. Int. Ed.* **2017,** 56, 1-6.
25. Wang, Q.; Zhang, X.; Jin, Z.; Zhang, J.; Gao, Z.; Li, Y.; Liu, S. F. Energy-Down-Shift CsPbCl3:Mn Quantum Dots for Boosting the Efficiency and Stability of Perovskite Solar Cells. *ACS Energy Lett.* **2017,** 2, 1479-1486.
26. Protesescu, L.; Sergii Yakunin, S.; I.; B. M.; F.; F. K.; Caputo, R.; Hendon, C. H.; Yang, R. X.; Walsh, A.; Kovalenko, M. V. Nanocrystals of Cesium Lead Halide Perovskites ($CsPbX_3$, X = Cl, Br, and I): Novel Optoelectronic Materials Showing Bright Emission with Wide Color Gamut. *Nano Lett.* **2015,** 15, 3692-3696.

27. Li, C.; Lu, X.; Ding, W.; Feng, L.; Gao, Y.; Guo, Z. Formability of ABX_3 (X = F, Cl, Br, I) Halide Perovskites. *Acta Crystallogr., Sect. B: Struct. Sci.* **2008,** 64, 702−707.
28. Goldschmidt, V. M. Die Gesetze der Krystallochemie. *Die Naturwissenschaften* **1926,** 14, 477-485.
29. Ravi, V. K.; Markad, G. B.; Nag, A. Band Edge Energies and Excitonic Transition Probabilities of Colloidal CsPbX3 (X = Cl, Br, I) Perovskite Nanocrystals. *ACS Energy Lett.* **2016,** 1, 665-671.
30. Brandt, R. E.; Stevanović, V; Ginley, D. S.; Buonassisi, T. Identifying defect-tolerant semiconductors with high minority-carrier lifetimes: beyond hybrid lead halide perovskites. *MRS Commun.* **2015,** 5, 265-275.
31. Stam, W.; Geuchies, J. J.; Altantzis, T.; Bos, K. H. W.; Meeldijk, J. D.; Aert, S. V.; Bals, S.; Vanmaekelbergh, D.; Donega, C. M. Highly Emissive Divalent-Ion-Doped Colloidal $CsPb_{1-x}M_xBr_3$ Perovskite Nanocrystals through Cation Exchange. *J. Am. Chem. Soc.* **2017,** 139, 4087-4097.
32. Pradhan, N.; Goorskey, D.; Thessing, J.; Xiaogang Peng, X. An Alternative of CdSe Nanocrystal Emitters: Pure and Tunable Impurity Emissions in ZnSe Nanocrystals. *J. Am. Chem. Soc.* **2005,** 127, 17586-17587.
33. Yang, Y.; Chen, O.; Angerhofer, A.; Cao, Y. C. Radial-Position-Controlled Doping in CdS/ZnS Core/Shell Nanocrystals. *J. Am. Chem. Soc.* **2006,** 128, 12428-12429.
34. The drop of Mn PL QY for 15.5% Mn-content is due to enhancement of Mn-Mn exchange interaction and consequent increase in the nonradiative deactivation rate.
35. Pradhan, N. Red-Tuned Mn d–d Emission in Doped Semiconductor Nanocrystals. *ChemPhysChem* **2016,** 17, 1087-1094.
36. Zuo, T.; Sun, Z.; Zhao, Y.; Jiang, X.; Gao, X. The Big Red Shift of Photoluminescence of Mn Dopants in Strained CdS: A Case Study of Mn-Doped MnS−CdS Hetero nanostructures. *J. Am. Chem. Soc.* **2010,** 132, 6618-6619.
37. Cape, J. A.; White, R. L.; Feigelson, R. S. EPR Study of the Structure of $CsPbCl_3$. *J. Appl. Phys.* **1969,** 40, 5001-5005.
38. Pathak, N.; Gupta, S. K.; Ghosh, P. S.; Arya, A.; Natarajan, V.; Kadam, R. M. Probing local site environments and distribution of manganese in SrZrO3:Mn; PL and EPR spectroscopy complimented by DFT calculations. *RSC Adv.* **2015,** 5, 17501–17513.
39. Beermann, P. A. G.; McGarvey, B. R.; Muralidharan, S.; Sung, R. C. W. EPR Spectra of Mn^{2+}-doped ZnS Quantum Dots. *Chem. Mater.* **2004,** 16, 915-918.
40. Debnath, T.; Maity, P.; Maiti, S.; Ghosh, H. N. Electron Trap to Electron Storage Center in Specially Aligned MnDoped CdSe d-Dot: A Step Forward in the Design of Higher Efficient uantum-Dot Solar Cell. *J. Phys. Chem. Lett.* **2014,** 5, 2836−2842.
41. Shi, L.; Huang, Y.; Seo, H. J. Emission Red Shift and Unusual Band Narrowing of Mn^{2+} in $NaCaPO_4$ Phosphor. *J. Phys. Chem. A.* **2010,** 114, 6927-6934.
42. J. C. Zhang; L. Z. Zhao; Y. Z. Long; H. D. Zhang; B. Sun; W. P. Han; X. Yan; Wang, X. Color Manipulation of Intense Multiluminescence from CaZnOS:Mn^{2+} by Mn^{2+} Concentration Effect. *Chem. Mater.* **2015,** 27, 7481−7489.

43. Park, Y.; Son, D. H. Temperature-dependent Energy Transfer in Mn-doped CdS/ZnS Nanocrystals. *Bull. Korean Chem. Soc*. **2015**, 36, 757-761.
44. Mondal, N.; Samanta, A. Complete ultrafast charge carrier dynamics in photo-excited all-inorganic perovskite nanocrystals ($CsPbX_3$). *Nanoscale* **2017,** 9, 1878-1885.
45. Ahmed, G. H.; Liu, J.; Parida, M. R.; Murali, B.; Bose, R.; AlYami, N. M.; Hedhili, M. N.; Peng, W.; Pan, J.; Besong, T. M. D. et al. Shape-Tunable Charge Carrier Dynamics at the Interfaces between Perovskite Nanocrystals and Molecular Acceptors. *J. Phys. Chem. Lett.* **2016,** 7, 3913–3919.
46. Rossi, D.; Parobek, D.; Dong, Y.; Son, D. H. Dynamics of Exciton−Mn Energy Transfer in Mn-Doped $CsPbCl_3$ Perovskite Nanocrystals. *J. Phys. Chem. C* **2017**, 121, 17143−17149.

CHAPTER 4

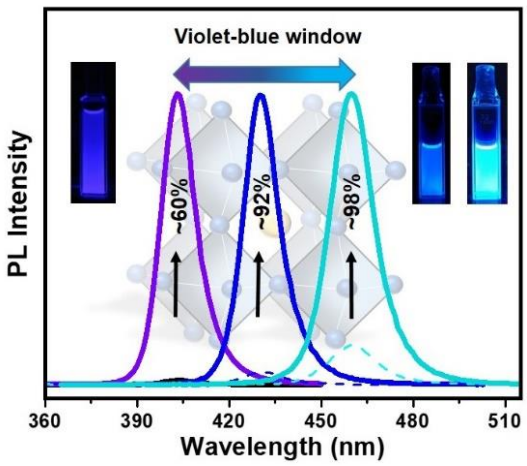

"Highly Luminescent Violet- and Blue-Emitting Stable Perovskite Nanocrystals"

ACS Materials Lett. 2019, 1, 116–122

Overview

Among the lead halide perovskites, PLQY of violet-emitting $CsPbCl_3$ NCs is the lowest (<5%). This is an impediment to the development of perovskite-based materials for optical applications covering the entire visible region. While PLQY of the green and red-emitting perovskites of this class has been raised to near-unity, achieving a similar level for violet- and blue-emitting NCs is still quite challenging. Here we report a novel method of simultaneously passivating the surface defects and crystal disorder of violet-emitting $CsPbCl_3$ NCs to dramatically enhance (by a factor of ~120) the PLQY and stability without affecting the peak wavelength (403 nm) and FWHM of the PL band. We show that addition of right quantity of $CuCl_2$ during the hot-injection synthesis of $CsPbCl_3$ NCs leads to doping of Cu^+ into the NCs, which rectifies octahedral distortion of the crystal and the Cl^- passivates the surface; combined influence of the two results in huge PL enhancement. NCs emitting throughout the blue region (430-460 nm) with near-unity PLQY (92-98%) can then be obtained by partial halide-exchange of the doped sample. Femtosecond TA studies suggest suppression of the ultrafast carrier trapping process in doped NCs. The results help extending the utility of these materials in optical applications by covering the blue-violet region as well.

4.1. Introduction

All-inorganic halide perovskites (ABX_3-type) have gained tremendous attention in recent years due to their diverse applications in photovoltaics, LEDs, lasing etc.[1-5] High PLQY and ease of tunability of the PL band position across the entire visible region make these materials quite attractive for optical applications. Interestingly, even though high PLQY (80-95%) in the green-red region is reported for the NCs without any surface modification,[6] the violet-emitting $CsPbCl_3$ NCs suffer from low PLQY (< 5%).[7-12]

Several reports describe different methods of enhancing the PLQY of these NCs as high PLQY in the violet-blue region is essential for the development of white-LEDs.[8-11, 13-18] PLQY of 60% is achieved for $CsPbCl_3$ NCs by room temperature treatment of a colloidal solution of these NCs with yttrium chloride.[9] In another study, it is shown that addition of $NiCl_2$ during hot-injection synthesis of $CsPbCl_3$ NCs leads to doping of Ni^{2+} and remarkable enhancement of PLQY (up to 96%).[10] We have shown that post-synthetic treatment of $CsPbCl_3$ NCs with $CdCl_2$ can enhance the PLQY to near-unity.[11] In a more recent study, Wang and co-workers have shown that post-synthetic treatment of $CsPbCl_3$ NCs with $CuCl_2$ enhances the PLQY up to 12%, whereas the bromide salt enhances the value to ~92.6%, it shifts the PL maximum to 460 nm.[19] In another recent work, it is reported that addition of $CuBr_2$ during hot-injection synthesis of $CsPbCl_3$ NCs leads to the formation of blue-emitting (peak between 450-460 nm) mixed-halide perovskites [$CsPb(Cl/Br)_3$] NCs with PLQY of ~80%.[20] Several metal-nitrate salts have also been used for increasing the PLQY of $CsPbCl_3$ NCs up to ~85% with an emission window of 460-470 nm.[15]

It is thus evident that though blue-emitting NCs (λ_{max} = 450-470 nm) with impressive PLQY have been achieved, obtaining stable violet-emitting NCs (peak <430 nm) with high PLQY is still a challenging exercise.[12] The halide vacancies, which create only shallow trap levels in $CsPbBr_3$, form deep trap states in $CsPbCl_3$, which promote non-radiative relaxation of the carriers and lower the PLQY of the system.[21] Besides, local structural disorder arising from halide vacancies and/or intrinsic distortion of the $[PbCl_6]^{4-}$ octahedron also contributes to carrier trapping in $CsPbCl_3$,[10, 22] unlike in $CsPbBr_3$ or $CsPb(Cl/Br)_3$, which forms near-perfect crystal structure. Hence, one needs to take care of

both halide vacancies and structural disorder to achieve a high PLQY for violet-emitting pure $CsPbCl_3$. Herein we show that when an optimum amount of $CuCl_2.2H_2O$ is added during hot-injection synthesis of the $CsPbCl_3$ NCs, the PLQY of the system is greatly enhanced without any change in the peak wavelength. An impressive PLQY of doped mixed-halide NCs emitting in the blue region (430-460 nm) is then achieved. Quantitative information on the dynamics of the nonradiative trapping processes in doped and undoped NCs that determine the PLQY of the systems, is also obtained through ultrafast TA measurements.

4.2. Results and Discussion

4.2.1. Synthesis and characterization of the NCs

While $CsPbCl_3$ NCs were prepared using a reported hot-injection method,[6] for the synthesis of Cu-doped $CsPbCl_3$ NCs, additionally $CuCl_2.2H_2O$ (0.22 mmol)[23] was added in the reaction mixture consisting of 0.188 mmol $PbCl_2$, 5 ml ODE, 0.7 mL OA and 0.7 mL OLA, and heated under vacuum at 120°C for 45 minutes. The blue solution turned colorless upon addition of 1 ml TOP under N_2 atmosphere. After raising the temperature to 185°C, 0.45 ml of Cs-oleate was swiftly injected into it and then after a minute the mixture was quenched in ice water. The process is schematically presented in scheme 4.1. The resulting solution was then centrifuged at 6,800 rpm and the supernatant liquid was discarded. The precipitated NCs were then washed with methyl acetate before dispersing them in toluene for further studies.

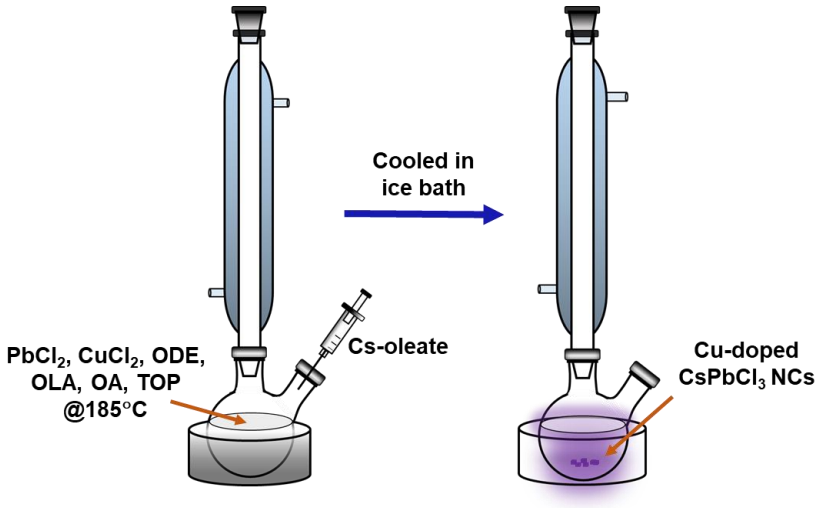

Scheme 4.1. Schematic representation of the synthesis of Cu-doped $CsPbCl_3$ NCs in the hot-injection method.

While the TEM images of $CsPbCl_3$ NCs show cubic morphology with wide size distribution and average edge length of 9 ± 2.5 nm (Figure 4.1B), the size distribution is narrower with average edge length of ~7 ± 1.0 nm (Figure 4.1A) for Cu-doped $CsPbCl_3$. Such a decrease in NCs size with increased monodispersity upon metal halide introduction during the synthesis is also noted earlier.[10,24] HR-TEM images indicate an inter-planer distances of 0.57 nm for the (100) crystal planes in both cases.

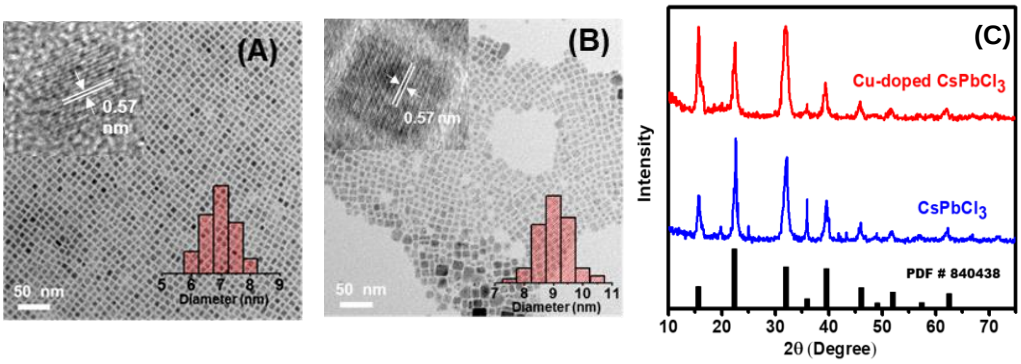

Figure 4.1. TEM images of (A) Cu-doped $CsPbCl_3$ and (B) $CsPbCl_3$ NCs. Insets show respective HRTEM images with the lattice spacing between (100) planes indicated in the image. (B) PXRD patterns of both NCs, confirming a cubic crystalline structure.

PXRD patterns show cubic crystalline structure (Figure 4.1C) for both the NCs indicating no notable influence of $CuCl_2.2H_2O$ on the crystal lattice. Elemental mapping of the FESEM images show homogenous distribution of Cu, Cs, Pb and Cl (Figure 4.2B-F) throughout the NCs. EDX measurements indicate a Cu-content of ~1.03% (i.e. ~5% substitution of Pb with Cu) (Figure 4.2A) in doped NCs. No shift of the PXRD peaks towards higher 2θ values on Cu-doping is observed in our case. This is perhaps due to small amount of Cu-incorporated in the NCs.

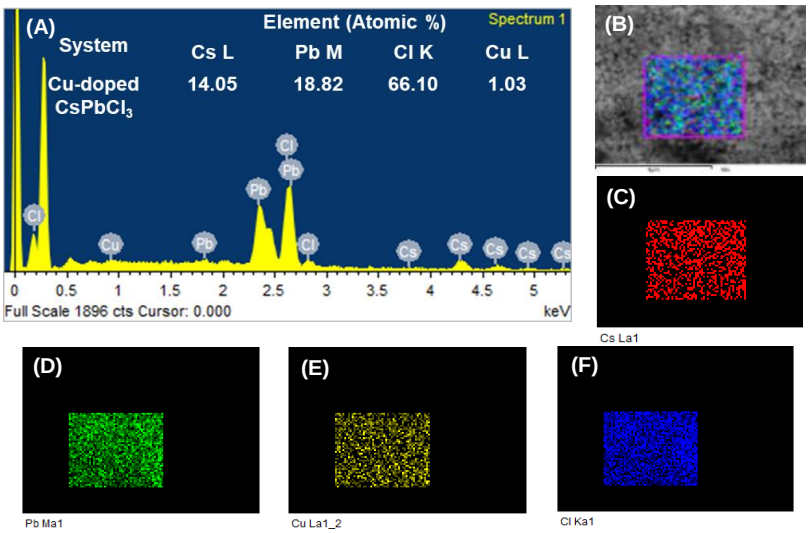

Figure 4.2. (A) EDX spectrum of Cu-doped $CsPbCl_3$ NCs. The chlorine:(lead + copper) ratio in the NCs is estimated as 3.33. (B) FESEM image of the scanning area of the NCs, showing distribution of all the elements. (C-F) Elemental mapping of Cs, Pb, Cu, and Cl in the scanned area of the NCs.

The absence of any signal due to Cu^{2+} in the EPR spectrum of the doped NCs indicates +1 oxidation state of copper in the NCs (Figure A2.1). This finding explains immediate color change of the reaction mixture from blue to colorless upon addition of TOP during the synthesis of the NCs. That TOP indeed acts as a reducing agent is confirmed by the observation that in the absence of TOP one obtains doped NCs, which exhibit

characteristic EPR signal due to Cu^{2+} (Figure A2.2) and also a PLQY of ~60% (Figure A2.3).

XPS of $CsPbCl_3$ NCs show two distinct peaks at 138.6 and 143.5 eV corresponding to Pb $4f_{7/2}$ and Pb $4f_{5/2}$, respectively (Figure A2.4). Two Cl signals corresponding to Cl $2p_{3/2}$ and Cl $2p_{1/2}$ are also observed at 198.1 and 199.7 eV, respectively. For Cu-doped $CsPbCl_3$, all peaks due to Pb 4f and Cl 2p shift to higher binding energy (Figure A2.4) indicating a halide-rich chemical environment around $[PbCl_6]^{4-}$ octahedra and stronger Pb-Cl bond.[11,25] No XPS signal due to Cu^+ could, however, be observed because of its low content or/and limited penetration of the XPS probe (typically up to ~2 nm from the surface), which is a well-known limitation of this technique.[26] A similar issue with XPS measurement failing to detect the doped metal ions was also reported earlier.[56] However, to ensure the presence of Cu in the NCs, we have performed ICP-OES measurements, which indicates a Cu content of ~7% in the NCs with respect to Pb, a value consistent with our EDX data (~5%).

4.2.2. Optical Properties

While the undoped $CsPbCl_3$ NCs show a sharp PL band (FWHM = 14 nm) with peak at 403 nm and a PLQY of only ~0.5%, the Cu-doped $CsPbCl_3$ NCs exhibit dramatically higher PLQY (~60%) with unchanged PL peak position and FWHM (Figure 4.3). As stated earlier, this maximum PLQY is observed for an optimum concentration (0.22 mmol) of $CuCl_2.2H_2O$ used during the synthesis. For higher or lower concentrations, the NCs exhibited lower PLQY values (Figure A2.5). We also examined whether post-synthetic treatment of the $CsPbCl_3$ NCs with $CuCl_2.2H_2O$ can improve the PL properties or not. Dropwise addition of $CuCl_2.2H_2O$ dissolved in OA, OLA and TOP to a toluene solution of $CsPbCl_3$ NCs under stirring condition improves the PLQY increase only up to ~16% (Figure A2.6). This finding is in agreement with recent observation of enhancement of PLQY of $CsPbCl_3$ NCs to 12% upon post-synthetic treatment with $CuCl_2$.[18]

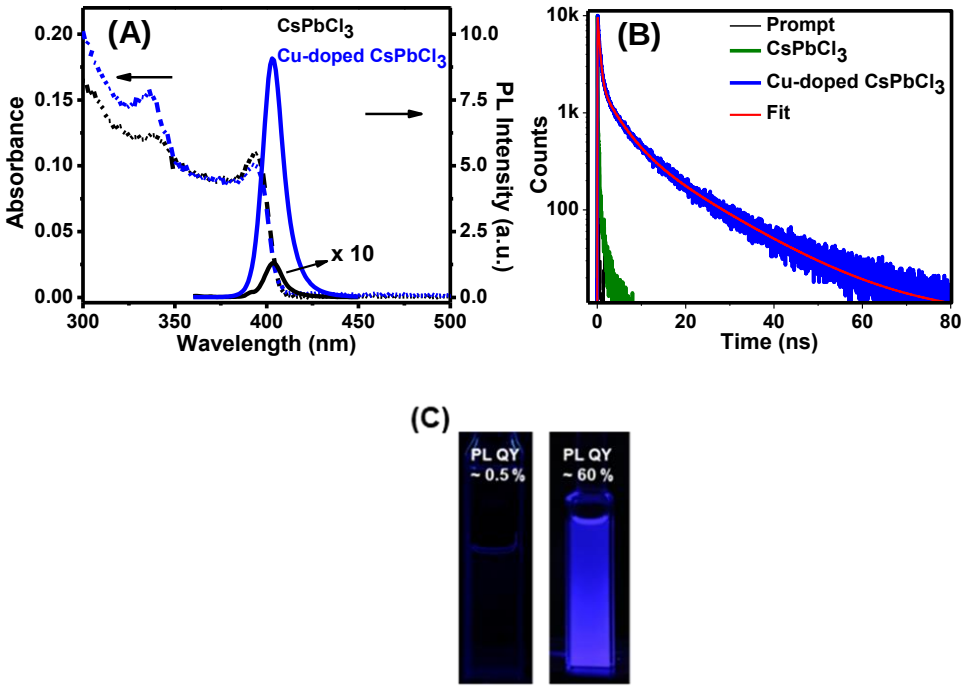

Figure 4.3. (A) Absorption and PL spectra of $CsPbCl_3$ and Cu-doped $CsPbCl_3$ NCs (B) PL decay dynamics of both the NCs (λ_{ex} = 375 nm, λ_{em} = 403 nm). (C) Digital images of the colloidal solutions of the NCs under UV light (λ_{ex} = 365 nm), where bright blue PL is clearly visible for Cu-doped $CsPbCl_3$ NCs.

Clearly, our direct hot-injection method of synthesis is much more effective in this regard. Like the colloidal dispersions (Figure 3C), a film of Cu-doped $CsPbCl_3$ NCs also exhibit strong violet PL (Figure A2.7). When checked the air-stability, the doped NCs show much more robustness by maintaining ~ 60% of its initial PL after 6 days, whereas only ~10% PL is retained in the case of undoped NCs during the same period (Figure A2.8). Unlike the undoped NCs, whose PL decay is too fast to be measured accurately in our TCSPC setup, which has a time-resolution of ~58 ps, the Cu-doped NCs show much higher PL lifetime (τ_{avg} = 1.43 ns, Figure 4.3B, Table A2.1).

Two factors contribute to high PL of the doped $CsPbCl_3$ NCs. First, the halide vacancies are well known trap centers, which facilitate nonradiative deactivation of the charge

carriers.[9,10,21] As the undoped $CsPbCl_3$ NCs are halide-deficient (evident from the Cl:Pb ratio of 2.8, Figure A2.9), but the Cu-doped ones are halide-rich Cl:(Pb+Cu) ratio of 3.3, Figure 2A), it is evident that removal of halide-vacancy associated defects in doped NCs contributes to enhanced PL of the later.[11,28,29] Secondly, it is also documented that distortion of the $[PbCl_6]^{4-}$ octahedral unit has a deleterious effect on the PL properties of $CsPbCl_3$ NCs and doping of smaller size cations (such as Cd^{2+}, Ni^{2+}) in place of Pb^{2+} (119 pm) enhances short range order in the lattice and also improves the PLQY of the NCs. [10,11 32, 57] Hence, doping of Cu^{+} (ionic radius 77 pm) helps rectification of this structural defect and also contributes to the improved PL of the NCs.

4.2.3. Investigation of Carrier Dynamics

We have also investigated the role of dopant on the carrier dynamics in the early time-scale using ultrafast TA technique.[30,31] The TA spectra obtained on 350 nm excitation of a colloidal solution of the undoped and Cu-doped NCs with femtosecond laser pulses of low pump fluence (0.12×10^{13} photons per cm^2, to avoid contribution from non-linear processes in the recorded dynamics)[32] over a time-scale of up to 500 ps, are characterized by a sharp negative signal at ~ 402 nm and positive signals on both sides of it (Figure 4.4). The negative signal represents bleach due to ground state absorption of the samples. Though the spectral features are similar in both cases, careful examination of the data reveals that bleach recovery is significantly slower in the case of Cu-doped sample.

For example, in 500 ps, the bleach recovery is only 40% for doped system compared to ~86% recovery for undoped system. Analysis of the bleach recovery kinetic traces of undoped NCs shows two fast components of 3 ps (25%) and 40.1 ps (55%) and a slower component of >850 ps (20%) (Table 4.1). The fast components are attributed to carrier trapping and long component to carrier recombination.[11,33] It should be noted here that the value of the long-time component is an approximate one as it falls beyond the time-window of the femtosecond TA-setup.

Large contribution of carrier trapping in $CsPbCl_3$ (~80%) is indeed a reflection of poor PLQY of the system.[7,11,30,34] This is predominantly due to chloride vacancies, which require little energy for its formation and generate deep trap energy levels.[21,35] In addition,

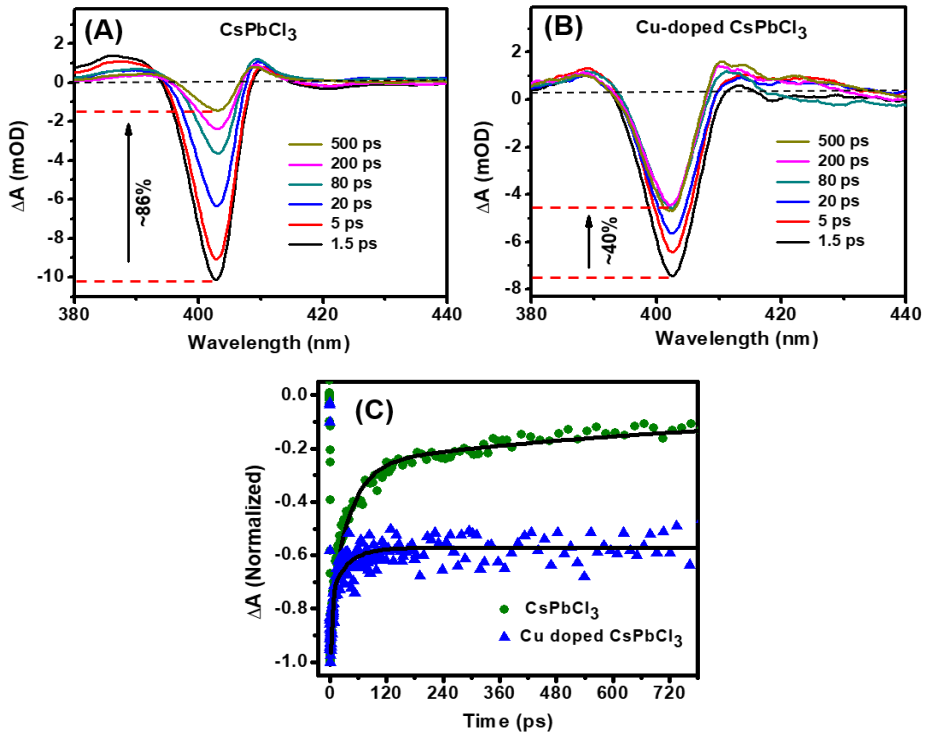

Figure 4.4. TA spectra of (A) $CsPbCl_3$ and (B) Cu-doped CsPbCl3 NCs; In both cases, samples were excited at 350 nm using a fs-laser; (C) comparison of the bleach recovery kinetics of the two samples monitored at their bleach maxima at 402 nm.

Table 4.1. Kinetic parameters of the bleach recovery dynamics of $CsPbCl_3$ and Cu-doped $CsPbCl_3$ NCs.

System	Recovery Components		
	τ_1 (a_1)/ ps	τ_2 (a_2)/ ps	τ_3 (a_3)/ ps
$CsPbCl_3$	3.0±0.2 (0.25)	40.1±2.7 (0.55)	> 850(0.20)
Cu-doped $CsPbCl_3$	3.5±0.2 (0.30)	35.0±4.5 (0.16)	> 850 (0.54)

structural disorder and strong electron-phonon interaction also contribute to carrier trapping in this system.[22] Interestingly, in doped NCs, carrier trapping is significantly suppressed (~46%) and majority of the carrier follows a longer recombination path (Table

4.1) resulting in a long PL lifetime (1.43 ns) and high PLQY as compared to the undoped sample.

If $CuBr_2$ is used in place of $CuCl_2$ during hot-injection synthesis of the NCs, doped mixed halide perovskite NCs are obtained, but controlling precisely the composition and PL peak position was difficult. However, room temperature halide exchange was found quite convenient for tuning of the PL band to access the entire blue region. For this purpose, Cu-doped $CsPbCl_3$ NCs were treated with different quantities of benzoyl bromide (as bromide source) at room temperature to adjust the PL wavelength between 430 and 460 nm.[36] The halide-exchanged doped $CsPbCl_3$ NCs exhibit a PLQY of ~ 92% (λ_{em} = 430 nm) and 98% (λ_{em} = 460 nm), while halide-exchanged undoped NCs exhibit a PLQY of only ~8% (λ_{em} = 430 nm) and 22% (λ_{em} = 460 nm) (Figure 4.5A-B). These high values are quite impressive considering that these NCs are blue emitting. Enhanced PLQY of the NCs is accompanied by increase in PL lifetime (Figure 4.5A-B Insets, Table A2.2). For Cu-doped $CsPb(Cl/Br)_3$ NCs emitting at 430 nm, the PL lifetime (4.3 ns) is much higher than that of the undoped counterpart. The doped $CsPb(Cl/Br)_3$ NCs with PL maxima at 460 nm exhibit a biexponential decay behavior with an average lifetime of 3.6 ns, which is several fold higher than that of the undoped sample (0.2 ns, Figure 5B Inset).

The TA measurements show much less bleach recovery for doped $CsPb(Cl/Br)_3$ NCs compared to the undoped sample within a given time frame (Figure 4.5C, A2.10). For example, the NCs, which emit at 460 nm, doped sample shows 10% recovery against ~70% recovery for the undoped NCs in 500 ps. The bleach recovery kinetics data shows that the contribution of the long-lifetime component (> 850 ps) is much higher (~ 84%) in doped NCs (as against 32% in undoped system) (Table A2.3) thus explaining improved PLQY of the former. The NCs, which emit at 430 nm, show a similar trend (Figure A2.10, Table A2.3).

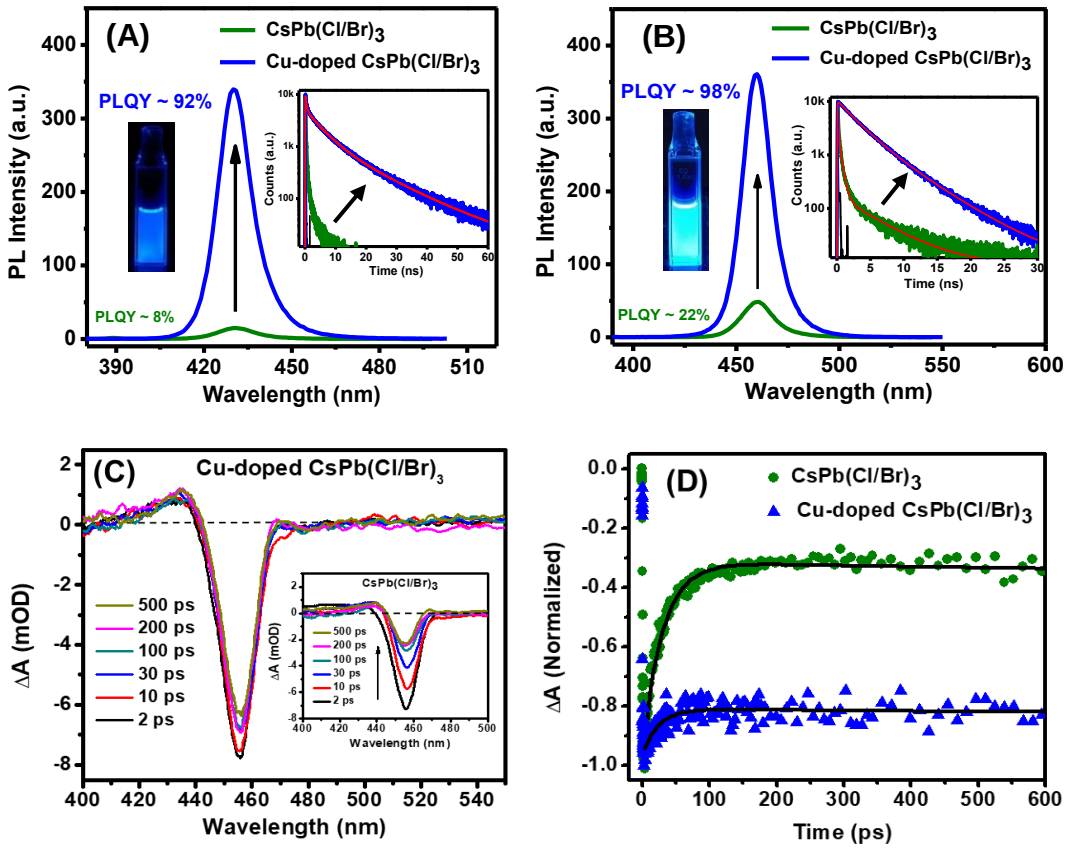

Figure 4.5. Relative PL of $CsPb(Cl/Br)_3$ and Cu-doped $CsPb(Cl/Br)_3$ NCs with PL maxima at (A) 430 nm and (B) 460 nm; PL decay profiles (λ_{ex} = 375 nm) of the NCs are compared in respective insets. Digital images of the colloidal solution of the PL improved NCs under UV light (λ_{ex} = 365 nm) are shown in both cases. (C) TA spectra of Cu-doped $CsPb(Cl/Br)_3$ NCs, which exhibit PL maxima at 460 nm (λ_{ex} = 350 nm), Inset shows of TA spectra of undoped $CsPb(Cl/Br)_3$ NCs emitting at 460 nm. (D) Comparison of bleach recovery kinetics of the two samples (λ_{em} = 460 nm) monitored at their bleach maxima at 456 nm.

Even though several metal-halide salts have been used previously for enhancing the PL of $CsPbCl_3$ NCs, both mode of function of the salts and extent of PL enhancement differ from case to case. For example, Mohammed and co-workers' room temperature post-treatment with YCl_3 enhanced the PLQY up to 60% following passivation of the Pb-Cl ion-pair defect sites by YCl_3.[9] Surprisingly, the same metal halide salt, when used during

hot-injection synthesis, did not produce significant PL enhancement despite doping of Y^{3+} in the NCs.[9] There are other instances as well. While addition of solid $CdCl_2$ into a colloidal dispersion of the $CsPbCl_3$ NCs did not influence the optical properties of the NCs greatly,[9] but when these NCs are treated with ethanol/amine solution of the same salt ($CdCl_2$) the PLQY is enhanced to near-unity.[11] This variation is most likely the outcome of how the metal-halide salts interact with the NCs in two cases. In the first case, the interaction is restricted to surface, whereas in the latter case, dissolution of the salt in ethanol/amine allows the metal ion to go inside the NCs, which helps rectification of the structural disorder in the lattice. We would like to discuss a third interesting case, which involve $NiCl_2$ salt. Its use during hot injection synthesis results in formation of Ni^{2+}-doped $CsPbCl_3$ NCs with ~ 96.5% PLQY, whereas room temperature treatment with this salt does not improve the PL properties significantly.[10,17] Very recently, it is shown that addition of $CuBr_2$ during hot-injection synthesis of $CsPbCl_3$ produces NCs with PLQY of 80-90%.[20] However, because of unavoidable halide exchange, the resulting mixed-halide NCs emit not in violet, but only in the blue region (λ_{max} = 450-460 nm). A recent post-synthetic treatment of $CsPbCl_3$ NCs with $CuCl_2$ improved the PLQY only up to 12.7% PLQY.[19] In this context, our approach of using $CuCl_2$, salt in hot-injection method is much more effective in producing highly luminescent violet-emitting $CsPbCl_3$ NCs. Additionally, one can easily get blue-emitting NCs (λ_{max}= 430-460 nm) with high PLQY (92-98%) from our PL improved NCs by following simple room temperature halide exchange protocol.

4.3. Summary

In conclusion, it is shown that one can dramatically enhance the PLQY of weakly emitting $CsPbCl_3$ NCs by using an appropriate quantity of $CuCl_2$ during the hot-injection synthesis of the NCs. The treatment leads to doping of Cu^+ into the NCs and passivation of the surface halide vacancies. Time-resolved PL and ultrafast TA measurements suggest suppression of the carrier trapping process in doped NCs. Highly luminescent (PLQY of 92-98%) NCs emitting in the blue region (430-460 nm) is also obtained by partial halide exchange of the doped NCs. The findings are likely to further enhance the potential of these promising materials in optoelectronic applications.

References

1. Liang, J.; Wang, C.; Wang, Y.; Xu, Z.; Lu, Z.; Ma, Y.; Zhu, H.; Hu, Y.; Xiao, C.; Yi, X.; Zhu, G.; Lv, H.; Ma, L.; Chen, T.; Tie, Z.; Jin, Z.; Liu, J., All-Inorganic Perovskite Solar Cells. *J. Am. Chem. Soc.* **2016,** *138*, 15829-15832.
2. Swarnkar, A.; Marshall, A. R.; Sanehira, E. M.; Chernomordik, B. D.; Moore, D. T.; Christians, J. A.; Chakrabarti, T.; Luther, J. M., Quantum dot–induced phase stabilization of α-$CsPbI_3$ perovskite for high-efficiency photovoltaics. *Science* **2016,** *354*, 92-95.
3. Li, X.; Wu, Y.; Zhang, S.; Cai, B.; Gu, Y.; Song, J.; Zeng, H., $CsPbX_3$ Quantum Dots for Lighting and Displays: Room-Temperature Synthesis, Photoluminescence Superiorities, Underlying Origins and White Light-Emitting Diodes. *Adv. Funct. Mater.* **2016,** *26*, 2435-2445.
4. Song, J.; Li, J.; Li, X.; Xu, L.; Dong, Y.; Zeng, H., Quantum Dot Light-Emitting Diodes Based on Inorganic Perovskite Cesium Lead Halides ($CsPbX_3$). *Adv. Mater.* **2015,** *27*, 7162-7167.
5. Wang, S.; Bi, C.; Yuan, J.; Zhang, L.; Tian, J., Original Core−Shell Structure of Cubic $CsPbBr_3$@Amorphous $CsPbBr_x$ Perovskite Quantum Dots with a High Blue Photoluminescence Quantum Yield of over 80%. *ACS Energy Lett.* **2018,** 3, 245-251.
6. Protesescu, L.; Yakunin, S.; Bodnarchuk, M. I.; Krieg, F.; Caputo, R.; Hendon, C. H.; Yang, R. X.; Walsh, A.; Kovalenko, M. V., Nanocrystals of Cesium Lead Halide Perovskites ($CsPbX_3$, X = Cl, Br, and I): Novel Optoelectronic Materials Showing Bright Emission with Wide Color Gamut. *Nano Lett.* **2015,** *15*, 3692-3696.
7. De, A.; Mondal, N.; Samanta, A., Luminescence Tuning and Exciton Dynamics of Mn-doped $CsPbCl_3$ Nanocrystals. *Nanoscale* **2017,** *9*, 16722-16727.
8. Ahmed, T.; Seth, S.; Samanta, A., Boosting the Photoluminescence of $CsPbX_3$ (X = Cl, Br, I) Perovskite Nanocrystals Covering a Wide Wavelength Range by Postsynthetic Treatment with Tetrafluoroborate Salts. *Chem. Mater.* **2018,** *30*, 3633-3637.
9. Ahmed, G. H.; El-Demellawi, J. K.; Yin, J.; Pan, J.; Velusamy, D. B.; Hedhili, M. N.; Alarousu, E.; Bakr, O. M.; Alshareef, H. N.; Mohammed, O. F., Giant Photoluminescence Enhancement in $CsPbCl_3$ Perovskite Nanocrystals by Simultaneous Dual-Surface Passivation. *ACS Energy Lett.* **2018,** *3*, 2301-2307.
10. Yong, Z.-J.; Guo, S.-Q.; Ma, J.-P.; Zhang, J.-Y.; Li, Z.-Y.; Chen, Y.-M.; Zhang, B.-B.; Zhou, Y.; Shu, J.; Gu, J.-L.; Zheng, L.-R.; Bakr, O. M.; Sun, a. H.-T., Doping-Enhanced Short-Range Order of Perovskite Nanocrystals for Near-Unity Violet Luminescence Quantum Yield. *J. Am. Chem. Soc.* **2018,** *140*, 9942-9951.
11. Mondal, N.; De, A.; Samanta, A., Achieving Near-Unity Photoluminescence Efficiency for Blue-Violet-Emitting Perovskite Nanocrystals. *ACS Energy Lett.* **2019,** *4*, 32-39.
12. Wu, Y.; Li, X.; Zeng, H., Highly Luminescent and Stable Halide Perovskite Nanocrystals. *ACS Energy Lett.* **2019,** *4*, 673-481.

13. Li, F.; Liu, Y.; Wang, H.; Zhan, Q.; Liu, Q.; Xia, Z., Postsynthetic Surface Trap Removal of $CsPbX_3$ (X = Cl, Br, or I) Quantum Dots via a ZnX_2/Hexane Solution toward an Enhanced Luminescence Quantum Yield. *Chem. Mater.* **2018,** *30*, 8546-8554.
14. Dutta, A.; Behera, R. K.; Dutta, S. K.; Adhikari, S. D.; Pradhan, N., Annealing $CsPbX_3$ (X = Cl and Br) Perovskite Nanocrystals at High Reaction Temperatures: Phase Change and Its Prevention. *J. Phys. Chem. Lett.* **2018,** *9*, 6599-6604.
15. Wang, S.; Wang, Y.; Zhang, Y.; Zhang, X.; Shen, X.; Zhuang, X.; Lu, P.; Yu, W. W.; Kershaw, S. V.; Rogach, A. L., Cesium Lead Chloride/Bromide Perovskite Quantum Dots with Strong Blue Emission Realized via a Nitrate-Induced Selective Surface Defect Elimination Process. *J. Phys. Chem. Lett.* **2019,** *10*, 90-96.
16. Liu, Y.; Li, F.; Liu, Q.; Xia, Z., Synergetic Effect of Postsynthetic Water Treatment on the Enhanced Photoluminescence and Stability of $CsPbX_3$ (X = Cl, Br, I) Perovskite Nanocrystals. *Chem. Mater.* **2018,** *30*, 6922-6929.
17. Behera, R. K.; Adhikari, S. D.; Dutta, S. K.; Dutta, A.; Pradhan, N., Blue-Emitting CsPbCl3 Nanocrystals: Impact of Surface Passivation for Unprecedented Enhancement and Loss of Optical Emission. *J. Phys. Chem. Lett.* **2018,** *9*, 6884-6891.
18. Dutta, A.; Behera, R. K.; Pal, P.; Baitalik, S.; Pradhan, N., Near-Unity Photoluminescence Quantum Efficiency for All $CsPbX_3$ (X = Cl, Br and I) Perovskite Nanocrystals: A Generic Synthesis Approach. *Angew. Chem. Int. Ed.* **2019,** 58, 5552-5556.
19. Chen, Y.-C.; Chou, H.-L.; Lin, J.-C.; Lee, Y.-C.; Pao, C.-W.; Chen, J.-L.; Chang, C.-C.; Chi, R.-Y.; Kuo, T.-R.; Lu, C.-W.; Wang, D.-Y., Enhanced Luminescence and Stability of Cesium Lead Halide Perovskite $CsPbX_3$ Nanocrystals by Cu^{2+}-Assisted Anion Exchange Reactions. *J. Phys. Chem. C* **2019,** 123, 2353-2360.
20. Bi, C.; Wang, S.; Li, Q.; Kershaw, S. V.; Tian, J.; Rogach, A. L., Thermally Stable Copper (II) Doped Cesium Lead Halide Perovskite Quantum Dots with a Strong Blue Emission. *J. Phys. Chem. Lett.* **2019,** *10*, 943−952.
21. Nenon, D. P.; Pressler, K.; Kang, J.; Koscher, B. A.; Olshansky, J. H.; Osowiecki, W. T.; Koc, M. A.; Alivisatos, L.-W. W. P., Design Principles for Trap-Free $CsPbX_3$ Nanocrystals: Enumerating and Eliminating Surface Halide Vacancies with Softer Lewis Bases. *J. Am. Chem. Soc.* **2018,** 140, 17760-17772.
22. Lohar, A. A.; Shinde, A.; Gahlaut, R.; Sagdeo, A.; Mahamuni, S., Enhanced Photoluminescence and Stimulated Emission in $CsPbCl_3$ Nanocrystals at Low Temperature. *J. Phys. Chem. C* **2018,** *122*, 25014-25020.
23. The particular concentration of $CuCl_2.2H_2O$ mentioned in the synthesis is determined by performing several controlled syntheses with varying amount of $CuCl_2.2H_2O$ where maximum PL enhancement of the NCs is found in case of above mentioned concentration (Figure A2.8).
24. Dong, Y.; Qiao, T.; Kim, D.; Parobek, D.; Rossi, D.; Son, D. H., Precise Control of Quantum Confinement in Cesium Lead Halide Perovskite Quantum Dots via Thermodynamic Equilibrium. *Nano Lett.* **2018,** *18*, 3716-3722.
25. Liu, M.; Zhong, G.; Yin, Y.; Miao, J.; Li, K.; Wang, C.; Xu, X.; Shen, C.; Meng, H., Aluminum-Doped Cesium Lead Bromide Perovskite Nanocrystals with

Stable Blue Photoluminescence Used for Display Backlight. *Adv. Sci.* **2017,** *4*, 1700335.

26. Bodnarchuk, M. I.; Boehme, S. C.; Brinck, S. t.; Bernasconi, C.; Shynkarenko, Y.; Krieg, F.; Widmer, R.; Aeschlimann, B.; Günther, D.; Kovalenko, M. V.; Infante, I., Rationalizing and Controlling the Surface Structure and Electronic Passivation of Cesium Lead Halide Nanocrystals. *ACS Energy Lett.* **2019,** *4*, 63-74.
27. Zhang, X.; Zhang, Y.; Zhang, X.; Yin, W.; Wang, Y.; Wang, H.; Lu, M.; Li, Z.; Gu, Z.; Yu, W. W., Yb^{3+} and Yb^{3+}/Er^{3+} doping for near-infrared emission and improved stability of $CsPbCl_3$ nanocrystals. *J. Mater. Chem. C* **2018,** 6, 10101-10105.
28. Liu, P.; Chen, W.; Wang, W.; Xu, B.; Wu, D.; Hao, J.; Cao, W.; Fang, F.; Li, Y.; Zeng, Y.; Pan, R.; Chen, S.; Cao, W.; Sun, X. W.; Wang, K., Halide-Rich Synthesized Cesium Lead Bromide Perovskite Nanocrystals for Light-Emitting Diodes with Improved Performance. *Chem. Mater.* **2017,** *29*, 5168-5173.
29. Adhikari, S. D.; Behera, R. K.; Bera, S.; Pradhan, N., Presence of Metal Chloride for Minimizing the Halide Deficiency and Maximizing the Doping Efficiency in Mn(II)-Doped $CsPbCl_3$ Nanocrystals. *J. Phys. Chem. Lett.* **2019,** 10, 1530-1536.
30. Mondal, N.; Samanta, A., Complete ultrafast charge carrier dynamics in photo-excited all-inorganic perovskite nanocrystals ($CsPbX_3$). *Nanoscale* **2017,** *9*, 1878-1885.
31. De, A.; Mondal, N.; Samanta, A., Hole Transfer Dynamics from Photoexcited Cesium Lead Halide Perovskite Nanocrystals: 1-Aminopyrene as Hole Acceptor. *J. Phys. Chem. C* **2018,** *122*, 13617-13623.
32. Mondal, N.; De, A.; Samanta, A., Biexciton Generation and Dissociation Dynamics in Formamidinium and Chloride-Doped Cesium Lead Iodide Perovskite Nanocrystals. *J. Phys. Chem. Lett.* **2018,** *9*, 3673-3679.
33. Mondal, N.; De, A.; Das, S.; Paul, S.; Samanta, A., Ultrafast Carrier Dynamics of Metal Halide Perovskite Nanocrystals and Perovskite-composites. *Nanoscale* **2019,** *11*, 9796-9818.
34. Rossi, D.; Parobek, D.; Dong, Y.; Son, D. H., Dynamics of Exciton−Mn Energy Transfer in Mn-Doped $CsPbCl_3$ Perovskite Nanocrystals. *J. Phys. Chem. C* **2017,** *121*, 17143-17149.
35. Ma, J.-P.; Chen, Y.-M.; Zhang, L.-M.; Guo, S.-Q.; Liu, J.-D.; Li, H.; Ye, B.-J.; Li, Z.-Y.; Zhou, Y.; Zhang, B.-B.; Bakr, O. M.; Zhang, J.-Y.; Sun, H.-T., Insights into the local structure of dopants, doping efficiency, and luminescence properties of lanthanide-doped $CsPbCl_3$ perovskite nanocrystals. *J. Mater. Chem. C* **2019,** *7*, 3037-3048.
36. Creutz, S. E.; Crites, E. N.; Siena, M. C. D.; Gamelin, D. R., Anion Exchange in Cesium Lead Halide Perovskite Nanocrystals and Thin Films Using Trimethylsilyl Halide Reagents. *Chem. Mater.* **2018,** *30*, 4887-4891.

CHAPTER 5

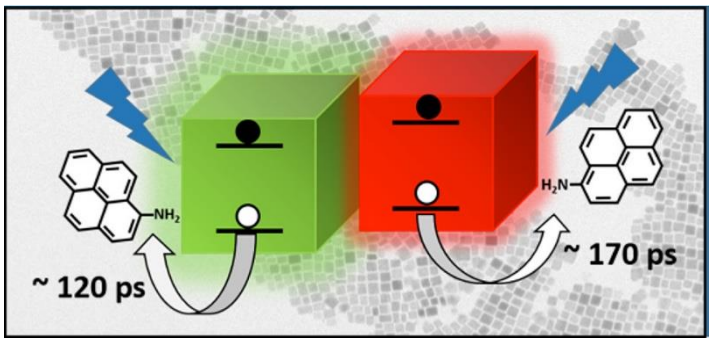

"Hole Transfer Dynamics from Photoexcited Cesium Lead Halide Perovskite Nanocrystals: 1-Aminopyrene as Hole Acceptor"

J. Phys. Chem. C 2018, 122, 13617−13623

Overview

The lead halide perovskites have emerged as promising materials for photovoltaic applications within a very short period. The key to exploitation of the full potential of these substances by achieving even higher photovoltaic conversion efficiency lies in understanding of the charge (electron/hole) separation process and their transfer across the interface. As the latter depends on the nature of the electron/hole acceptor, quest for suitable carrier acceptor is an active area in this context. Herein, we explore the hole extraction ability of AMP from two very common all-inorganic perovskite NCs, $CsPbBr_3$ and $CsPbI_3$, with different band gaps. The observation of efficient quenching of the PL of the NCs with little/negligible change in PL time-profile in the presence of AMP indicates static interaction of the two interacting species. The band alignment of the NCs relative to the HOMO-LUMO energy levels of AMP and ultrafast pump-probe measurements reveal rapid hole transfer from the photo-excited NCs to AMP. The hole transfer time constants are estimated as ~120 and ~170 ps for $CsPbBr_3$ and $CsPbI_3$ NCs, respectively. The rapid extraction of hole, as observed with the present system, appears to be the result of strong anchoring of AMP on the NCs surface and facile transfer of the hole through conducive pyrene framework. The findings reveal that judicial choice of even a simple molecular system like the present one can help rapid transfer of photo-generated carriers and contribute to the development of cost-effective solar cells in future.

5.1. Introduction

The past few years have witnessed intense activities on lead halide perovskites in various areas like in photovoltaic, [1-4] lasing, [5-6] light emitting devices etc. [7-8] with major focus as solar energy harvesting materials. Following the pioneering report by Miyasaka and co-workers in 2009,[9] the research on the perovskites has so far led to a record breaking PCE of >22%.[10] PCE is not merely determined by the light harvesting ability of the sensitizer, but also very much by the hole/electron transporting materials. In photovoltaic devices, the light harvesters are sandwiched between an electron and a hole transporting layer. The transport layers play the important role of extraction of charge carriers from the sensitizer thus minimizing internal recombination. As commonly used HTM, 2,2′,7,7′-tetrakis(N,N-di-p-methoxyphenylamine)-9,9′-spiro-bifluorene (spiro-OMeTAD) is quite expensive, the quest for an alternative HTM is an active area in this field.[11] In this regard, a few organic molecules other than spiro-OMeTAD have been studied as HTM[12-15] and the results show that both the terminal functionality and core of the molecule play important roles in the extraction of the carriers and hence, in determining the efficiency of the HTM. Liu et al. have shown how molecular engineering can improve PCE of a HTM.[12] The introduction of a phenylene spacer in phenothiazine based compound is found to influence the PCE dramatically.[13] Seok and co-workers have shown remarkable PCE of the N,N-di-p-methoxyphenylamine-substituted pyrene derivatives as HTM for $CH_3NH_3PbI_3$ attributing it to the pyrene core.[14]

As the PCE of a solar cell is governed mainly by interfacial charge (electron/hole) transfer dynamics from the perovskite NCs to their respective acceptor sites, a knowledge of other competitive processes within the NCs (excitonic recombination, carrier trapping[16-19]) is essential in this regard. Rapid dissociation of the excitons and suppression of competitive processes in NCs are key to improving the efficiency the systems. The surface trap states can further reduce the PCE.[20,21] Various surface modification treatments of the perovskite NCs have been attempted to address this issue.[22-25] For lead-based perovskites, thiophene and pyridine, which bind preferentially to surface Pb^{2+}, are found to be quite effective.[22] A recent work shows the utility of the amino functionality in

the passivation of surface trap states (by dative bond formation with Pb^{2+} on the surface) and transfer of hole.[26]

Recognizing the excellent charge transport property of the pyrene core and considering the recent report on the effectiveness of the amino functionality in the surface passivation and hole movement,[14, 26] we pick up AMP, a simple commercially available pyrene derivative with an amino functionality, to find out whether/how it can help extraction of charge carriers from photo-excited perovskite NCs, $CsPbBr_3$ and $CsPbI_3$ using femtosecond TA measurements. We note that the literature on the interfacial charge transfer dynamics from the perovskite NCs is rather limited.[27-32] While a number of electron acceptors have been tried out, to the best of our knowledge, phenothiazine and 4,5-dibromofluorescein are the only two molecular systems which have been investigated as hole acceptors from the perovskite NCs.[27, 28, 30]

5.2. Results and Discussion

5.2.1. Characterization of the NCs

The TEM images of $CsPbBr_3$ and $CsPbI_3$ NCs (Figure 5.1A,B) show a cubic morphology with an edge length of 8 ± 0.5 nm for $CsPbBr_3$ and 10 ± 0.5 nm for $CsPbI_3$ NCs. The monodispersity of the NCs is evident from the images shown in 100 nm scale bar. The PXRD patterns of the NCs (Figure 5.1C) show characteristic peaks corresponding to the cubic phase of the NCs.[33] The HR-TEM images show high crystallinity of the NCs. As $CsPbI_3$ is prone to transformation into non-emissive orthorhombic phase at room temperature,[33, 36] all studies have been performed with freshly prepared NCs dispersed in toluene.

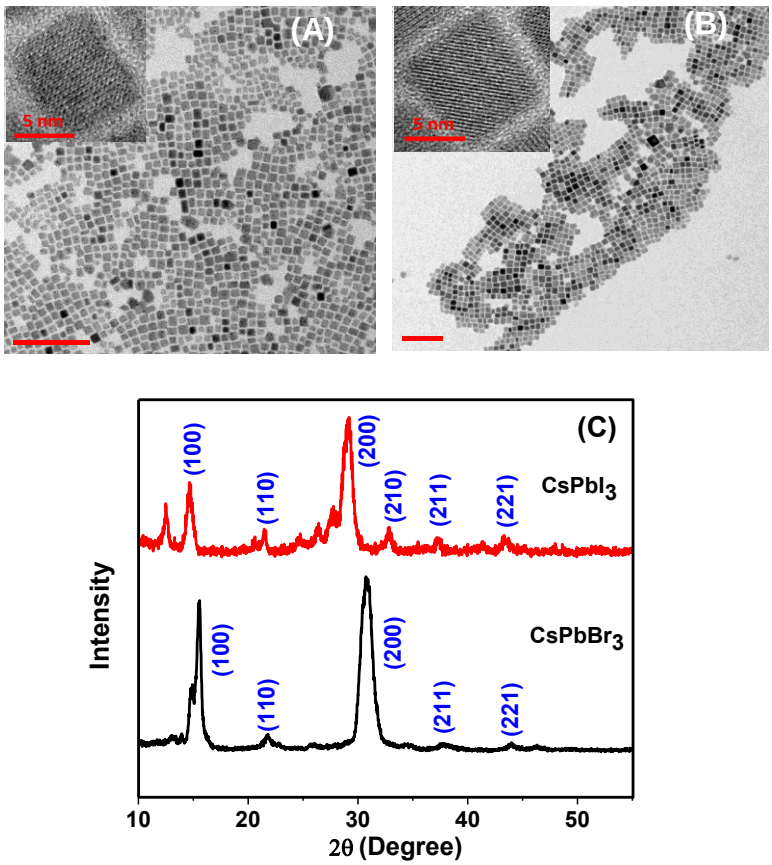

Figure 5.1. TEM images of (A) $CsPbBr_3$ and (B) $CsPbI_3$ NCs. Respective HRTEM images are given in insets. (C) PXRD patterns of both the NCs.

5.2.2. Optical properties

Individual absorption and PL spectra of $CsPbBr_3$ and $CsPbI_3$ NCs, which are characterized by well-defined excitonic peaks at ~505 and 671 nm and corresponding PL peaks at 510 and 685 nm, are shown in Figure 5.2 (A). The PL quantum yields of $CsPbBr_3$ and $CsPbI_3$ NCs are found to be ~ 68 and 60 %, respectively. Progressive addition of AMP leads to drastic decrease in the PL of the NCs (Figure 5.2B and A3.1). A noticeable red shift (~5 nm) of the peak wavelength is also noticeable. These observations are illustrated in Figure 5.2 (B) for $CsPbI_3$ NCs. The changes in the absorption spectra of

the systems in the 425-750 nm region (Figure 2B, inset), where AMP does not absorb (Figure 5.2A), clearly indicates ground-state complexation between the NCs and AMP.[29]

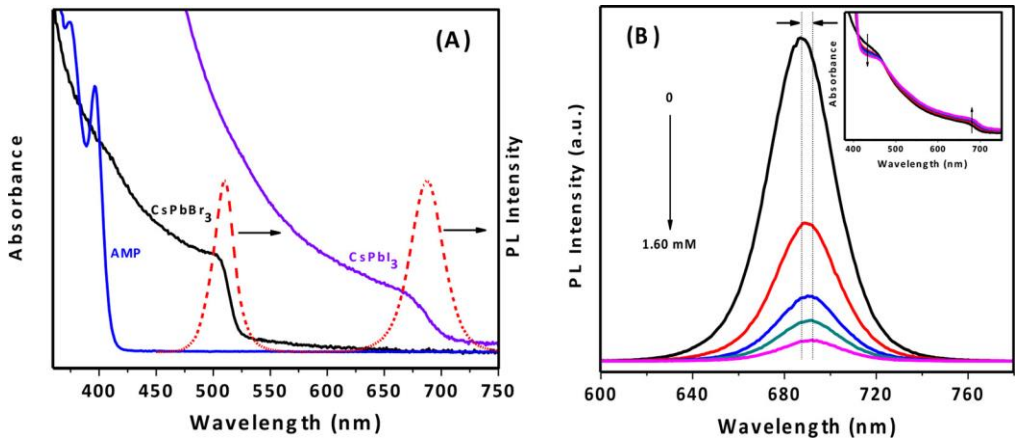

Figure 5.2. (A) Individual absorption spectra of $CsPbBr_3$, $CsPbI_3$ and AMP in toluene at room temperature and PL spectra of $CsPbBr_3$ and $CsPbI_3$ NCs. (B) PL quenching of $CsPbI_3$ NCs upon successive addition of AMP in toluene. The inset depicts the change in the corresponding absorption spectrum.

Therefore, we can attribute AMP induced PL quenching to the formation of a non-luminescent complex with the NCs. The static interaction between the two interacting species is responsible for PL quenching and further substantiated by time- resolved PL measurements in the following section.

5.2.3. Time Resolved Measurements:

The PL decay curves of $CsPbBr_3$ and $CsPbI_3$, recorded in our TCSPC setup following excitation at 485 nm using a laser diode source, are found to be multi-exponential in nature. A tri-exponential fitting to the decay profiles gave acceptable values of residuals and chi-squares. The individual lifetime components and their weightages are provided as supporting information (Table A3.1 and A3.2). The average lifetimes of $CsPbBr_3$ and $CsPbI_3$ NCs are estimated to be 5.9 ns and 41.8 ns, respectively and these values are consistent with literature.[33] Figure 5.2 and A3.2 depicts the PL decay curves in the absence and in presence of largest amount of AMP (which was used in steady state measurements). Contrary to the dramatic decrease in PL intensity the change in PL

lifetime is rather small confirming static interaction responsible for PL quenching of the system.

We have studied the charge-transfer dynamics between the NCs and AMP using femtosecond time-resolved pump-probe technique. [37] For this purpose, we have excited a toluene suspension of $CsPbBr_3$ at 470 nm and $CsPbI_3$ 530 nm to ensure that AMP is not excited when present. We have also maintained a low pump fluence in all measurements to ensure that the average number of excitons per NC is less than 0.1 and negligible contribution of the multi-exciton annihilation process to the measured dynamics.[38, 39]

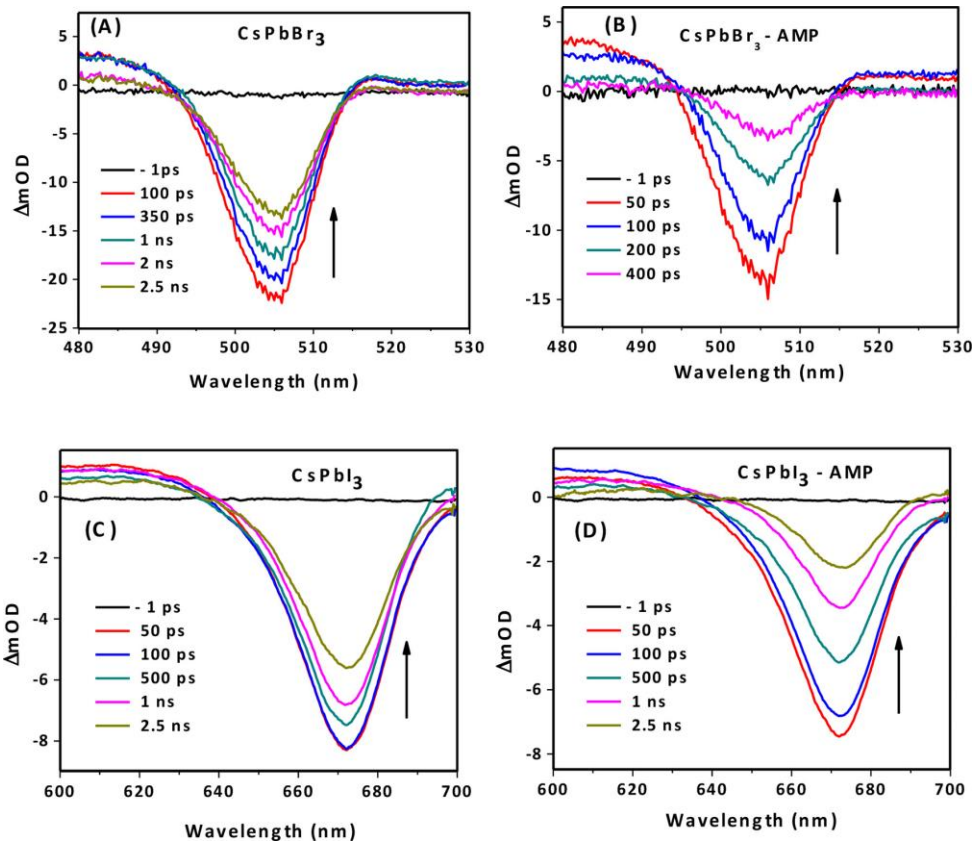

Figure 5.3. TA spectra of $CsPbBr_3$ and $CsPbI_3$ NCs without (A, C) and with (B, D) AMP. The excitations were made at 470 nm and 530 nm for $CsPbBr_3$ and $CsPbI_3$, respectively and the spectra were recorded upto 2.5 ns total delay.

As can be seen from Figure 5.3 A, the TA spectra of bare $CsPbBr_3$ NCs consist of a PIB in the ~490-512 nm wavelength region with peak at 505 nm. The PIB maximum is consistent with the excitonic peak position in the absorption spectra. As PL of these samples does not exhibit large Stokes shift, the stimulated emission signal can also contribute to the bleach signal.[40] The positive absorptions on both sides of the bleach signal arises from the lowest excitonic states, as reported in an earlier study.[16] In presence of AMP (Figure 5.3 B), one observes hardly any change in the spectral profile of $CsPbBr_3$ including the bleach position. However, the bleach recovery dynamics becomes significantly faster in presence of AMP. For example, compared to ~10% bleach recovery in 400 ps, ~90% recovery is observed in the presence of AMP during the same period.

In the case of Cd-based QDs, the bleach signal is dominated by the electrons due to high effective masses of the holes relative to the electrons (for CdTe, $m_h^*/m_e^* = 4$) and negligible/very little acceleration of bleach recovery is observed for hole extraction from those QDs.[41-43] However, as the effective masses of electrons (m_e^*) and holes (m_h^*) are quite similar for the lead halide perovskites (for $CsPbBr_3$, $m_e^* = 0.15m_0$ and $m_h^* = 0.14m_0$ where m_0 = rest mass of electron), both electrons and holes can contribute to the bleach signal.[28] However, in view of higher degeneracy of the valence band, the relative contribution of the electrons and holes towards bleach works out to be ~ 67.2 and 32.8%, for $CsPbBr_3$ NCs, respectively.[28] Therefore, in the present case, the bleach signal is sensitive to both electrons and holes and the acceleration in bleach recovery in the presence of AMP can be due to the transfer of both electron and hole or one of them. In order to determine the identity of the species being transferred from the NCs, we look into the band edge potentials of both the NCs and the HOMO-LUMO levels of AMP. The energy levels of the valence and conduction band edges of the NCs are taken from a recent literature considering similar size of the NCs. [44] In an earlier study also we used these values.[45]

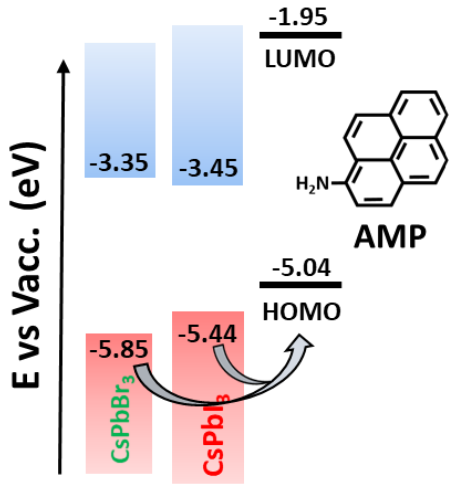

Scheme 5.1. Band alignment of $CsPbBr_3$ and $CsPbI_3$ NCs and HOMO-LUMO levels of AMP molecule.

The HOMO energy level of AMP (-5.04 eV) was estimated through cyclic voltammetry measurement. By considering the optical band gap of AMP as the energy difference between HOMO and LUMO levels, we estimated the LUMO energy as -1.95 eV. These values agree well with earlier literature.[46] It is evident from Scheme 5.1 that the LUMO level of AMP is far above the conduction band edge of both the NCs and hence, the photoinduced electron transfer from NCs to AMP can be completely ruled out. It is also evident from the figure that photo-induced hole transfer from the valence band of the NCs to the HOMO level of AMP (-5.04 eV) is the only energetically feasible process and the driving force for this process is higher for $CsPbBr_3$ compared to $CsPbI_3$. Thus we can conclude that acceleration of the bleach recovery in the presence of AMP is solely due to selective removal of holes from the photoexcited NCs. To obtain quantitative information on hole transfer dynamics, we have compared the bleach recovery kinetics of $CsPbBr_3$ in presence and absence of AMP. For bare $CsPbBr_3$ NCs, the bleach recovery is represented by a single exponential decay function with a time constant >1 ns. The single exponential nature of the decay profile with long lifetime indicates absence of any fast nonradiative

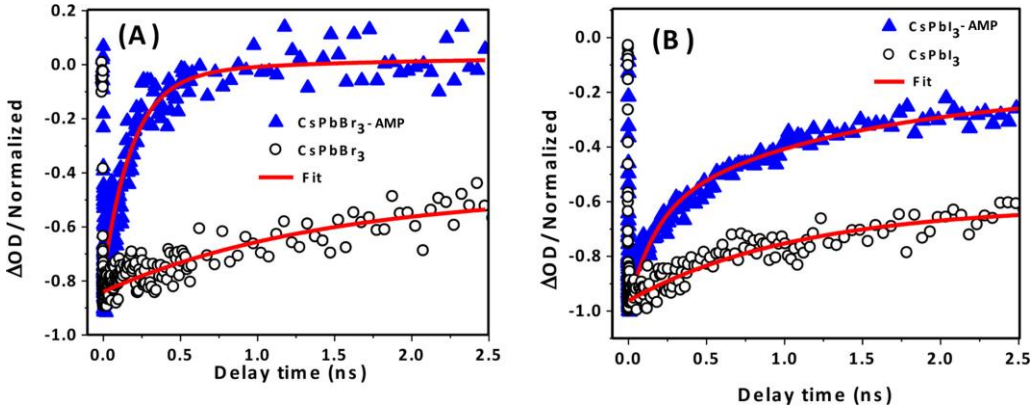

Figure 5.4. Bleach recovery kinetics of (A) $CsPbBr_3$ and (B) $CsPbI_3$ NCs without and with AMP monitored at their respective bleach maxima.

Table 5.1. Bleach Recovery Parameters of Individual NCs in the Absence and Presence of AMP.

Systems	Recovery Components	
	τ_1 (a_1)/ ps	τ_2 (a_2)/ ps
$CsPbBr_3$	--	>1
$CsPbBr_3$-AMP	120 ± 8.0 (0.70)	>1 (0.30)
$CsPbBr_3$-AMP	--	>1
$CsPbBr_3$-AMP	170 ± 10.0 (0.41)	>1 (0.59)

carrier trapping and non-linear phenomenon like exciton-exciton annihilation under this low pump fluence.[39] This long time constant must be due to electron-hole recombination process.[28] In the presence of AMP, in addition to the long time component, another short component is observable for both the NCs (Figure 5.4 and Table 5.1). This short-component is clearly due to a process induced by AMP. As it is already shown that hole transfer from the NCs is the only possibility, the observed time constant represents the hole transfer kinetics. The estimated hole transfer times from $CsPbBr_3$ and $CsPbI_3$ NCs are estimated to be 120 and 170 ps, respectively.

A faster hole transfer from $CsPbBr_3$ compared to $CsPbI_3$ is consistent with the band alignment of two NCs and a higher driving force (-ΔG) for the process. In this context, we note that in both cases we could not observe any new absorption feature due to the product of hole transfer process ($AMP^{\bullet+}$). This, however, is not surprising considering strong absorption due to both NCs throughout the monitoring window. We further note that Lian and co-workers obtained two different time scales (26 and 330 ps) for hole transfer using phenothiazine.[28] Whereas, Mandal and co-workers reported a hole transfer time scale of 137-166 ps for the same system.[30] The observed hole transfer time scale of 120-170 ps for $CsPbBr_3$ and $CsPbI_3$ to AMP is comparable or better than these two cases.

5.3. Summary

By exploiting the π-framework of the pyrene moiety and excellent surface anchoring ability of amino functionality on the perovskite NCs, it is shown here that even very simple system like AMP can exhibit promising hole transport properties. Considering this finding and recent literature report of a PCE of 12.4% in fabricated solar cell with a pyrene derivative as hole transport material,[14] we think there exists considerable scope of improving this efficiency by engineering the pyrene core with suitable functionalities and using them as cost-effective hole transport materials.

References

1. Lee, M. M.; Teuscher, J.; Miyasaka, T.; Murakami, T. N.; Snaith, H. J. Efficient Hybrid Solar Cells Based on Meso-superstructured Organometal Halide Perovskites. *Science.* **2012**, 338, 643-647.
2. Snaith, H. J. Perovskites: The Emergence of a New Era for Low-Cost, High-Efficiency Solar Cells. *J. Phys. Chem. Lett.* **2013**, 4, 3623–3630.
3. Liang, J.; Wang, C.; Wang, Y.; Xu, Z.; Lu, Z.; Ma, Y.; Zhu, H.; Hu, Y.; Xiao, C.; Yi, X. et al. All-Inorganic Perovskite Solar Cells. *J. Am. Chem. Soc*. **2016**, 138, 15829–15832.
4. Swarnkar, A.; Marshall, A. R.; Sanehira, E. M.; Chernomordik, B. D.; Moore, D. T.; Christians, J. A.; Chakrabarti T.; Luther, J. M. *Science* **2016**, 354,92–95.

5. Song, J.; Li, J.; Li, X.; Xu, L.; Dong, Y.; Zeng, H. Quantum Dot Light-Emitting Diodes Based on Inorganic Perovskite Cesium Lead Halides ($CsPbX_3$). *Adv. Mater*. **2015**, 27, 7162–7167.
6. Wang, Y.; Li, X.; Nalla, V.; Zeng, H.; Sun, H. Solution-Processed Low Threshold Vertical Cavity Surface Emitting Lasers from All-Inorganic Perovskite Nanocrystals. *Adv. Funct. Mater.* **2017**, 27, 1605088.
7. Li, X.; Wu, Y.; Zhang, S.; Cai, B.; Gu, Y.; Song, J.; Zeng, H. $CsPbX_3$ Quantum Dots for Lighting and Displays: Room-Temperature Synthesis, Photoluminescence Superiorities, Underlying Origins and White Light-Emitting Diodes. *Adv. Funct. Mater*. **2016**, 26, 2435–2445.
8. Veldhuis, S. A.; Boix, P.P.; Yantara, N.; Li, M.; Sum, T. C.; Mathews, N.; Mhaisalkar, S. G. Perovskite Materials for Light-Emitting Diodes and Lasers. *Adv. Mater*. **2016**, 28, 6804–6834.
9. Kojima, A.; Teshima, K.; Shirai, Y.; Miyasaka, T. Organometal Halide Perovskites as Visible-Light Sensitizers for Photovoltaic Cells. *J. Am. Chem. Soc*. **2009**, 131, 6050-6051.
10. https://www.nrel.gov/pv/assets/images/efficiency-chart.png
11. Burschka, J.; Pellet, N.; Moon, S.-J.; Humphry-Baker, R.; Gao, P.; Nazeeruddin, M. K.; Grätzel, M. Sequential deposition as a route to high-performance perovskite-sensitized solar cells. *Nature* **2013**, 499, 316-319.
12. Liu, X.; kong, F.; Jin, S.; Chen, W.; Yu, T.; Hayat, T.; Alsaedi, A.; Wang, H.; Tan, Z.; Chen, J. et al. Molecular Engineering of Simple Benzene−Arylamine HoleTransporting Materials for Perovskite Solar Cells. *ACS Appl. Mater. Interfaces* **2017**, 9, 27657−27663.
13. Grisorio, R.; Roose, B.; Colella, S.; Listorti, A.; Suranna, G. P.; Abate, A. Molecular Tailoring of Phenothiazine-Based Hole-Transporting Materials for High Performing Perovskite Solar Cells *ACS Energy Lett.* **2017**, 2, 1029−1034.
14. Jeon, N. J.; Lee, J.; Noh, J. H.; Nazeeruddin, M. K.; Grätzel, M.; Seok, S. I. Efficient Inorganic−Organic Hybrid Perovskite Solar Cells Based on Pyrene Arylamine Derivatives as Hole-Transporting Materials. *J. Am. Chem. Soc*. **2013**, 135, 19087−19090.
15. Guan, L.; Yin, X.; Zhao, D.; Wang, C.; An, Q.; Yu, J.; Shrestha, N.; Grice, C.R.; Awni, R.A.; Yu. Y. et al. Cost-effective hole transporting material for stable and efficient perovskite solar cells with fill factors up to 82%. *J. Mater. Chem. A* **2017**, 5, 23319-23327.
16. Mondal, N.; Samanta, A. Complete ultrafast charge carrier dynamics in photo-excited all-inorganic perovskite nanocrystals ($CsPbX_3$). *Nanoscale* **2017**, 9, 1878-1885.
17. Seth, S.; Mondal, N.; Patra, S.; Samanta, A. Fluorescence Blinking and Photoactivation of All-Inorganic Perovskite Nanocrystals $CsPbBr_3$ and $CsPbBr_2I$. *J. Phys. Chem. Lett*. **2016**, 7, 266−271.
18. Uratani, H.; Yamashita, K. Charge Carrier Trapping at Surface Defects of Perovskite Solar Cell Absorbers: A First-Principles Study *J. Phys. Chem. Lett*. **2017**, 8, 742−746.
19. Sherkar, T. S.; Momblona, C.; Gil-Escrig, L.; Ávila, J.; Sessolo, M.; Bolink, H. J.; Koster, L. J. A. Recombination in Perovskite Solar Cells: Significance of

Grain Boundaries, Interface Traps, and Defect Ions *ACS Energy Lett*. **2017**, 2, 1214−1222.
20. Han, G.; Koh, T. M.; Lim, S. S.; Goh, T. W.; Guo, X.; Leow, S. W.; Begum, R.; Sum, T. C.; Mathews, N.; Mhaisalkar, S. Facile Method to Reduce Surface Defects and Trap Densities in Perovskite Photovoltaics. *ACS Appl. Mater. Interfaces* **2017**, 9, 21292–21297.
21. Uratani, H.; Yamashita, K. harge Carrier Trapping at Surface Defects of Perovskite Solar Cell Absorbers: A First-Principles Study. *J. Phys. Chem. Lett.* 2017, 8, 742–746.
22. Noel, N.K.; Abate, A.; Stranks, S.D.; Parrott, E.S.; Burlakov, V.M.; Goriely, A.; Snaith, H.J. Enhanced Photoluminescence and Solar Cell Performance via Lewis Base Passivation of Organic–Inorganic Lead Halide Perovskites. *ACS Nano* **2014**, 8, 9815–9821.
23. Koscher, B. A.; Swabeck, J.K.; Bronstein, N.D.; Alivisatos, A.P. Essentially Trap-Free $CsPbBr_3$ Colloidal Nanocrystals by Postsynthetic Thiocyanate Surface Treatment. *J. Am. Chem. Soc*. **2017**, 139, 6566–6569.
24. Stasio, F. D.; Christodoulou, S.; Huo, N.; Konstantatos, G. Near-Unity Photoluminescence Quantum Yield in $CsPbBr_3$ Nanocrystal Solid-State Films via Postsynthesis Treatment with Lead Bromide. *Chem. Mater*. **2017**, 29, 7663–7667.
25. Woo, J. Y.; Kim, Y.; Bae, J.; Kim, T.G.; Kim, J.W.; Lee, D.C.; Jeong, S. Highly Stable Cesium Lead Halide Perovskite Nanocrystals through in Situ Lead Halide Inorganic Passivation. *Chem. Mater.* **2017**, 29, 7088–7092.
26. Wen, X.; Wu, J.; Gao, D.; Lin, C. Interfacial engineering with amino-functionalized graphene for efficient perovskite solar cells. *J. Mater. Chem. A* **2016**, 4, 13482–13487.
27. Maity, P.; Dana, J.; Ghosh, H. N. Multiple Charge Transfer Dynamics in Colloidal $CsPbBr_3$Perovskite Quantum Dots Sensitized Molecular Adsorbate. *J. Phys. Chem. C* **2016**, 120, 18348−18354.
28. Wu, K.; Liang, G.; Shang, Q.; Ren, Y.; Kong, D.; Lian, T. Ultrafast Interfacial Electron and Hole Transfer from $CsPbBr_3$ Perovskite Quantum Dots. *J. Am. Chem. Soc.* **2015**, 137, 12792−12795.
29. Ahmed, G. H.; Liu, J.; Parida, M. R.; Murali, B.; Bose, R.; AlYami, N. M.; Hedhili, M. N.; Peng, W.; Pan, J.; Besong, T. M. D. et al. Shape-Tunable Charge Carrier Dynamics at the Interfaces between Perovskite Nanocrystals and Molecular Acceptors. *J. Phys. Chem. Lett.* **2016**, 7, 3913−3919.
30. Sarkar, S.; Ravi, V. K.; Banerjee, S.; Yettapu, G. R.; Markad, G. B.; Nag, A.; Mandal, P. Terahertz Spectroscopic Probe of Hot Electron and Hole Transfer from Colloidal $CsPbBr_3$ Perovskite Nanocrystals. *Nano Lett*. **2017**, 17, 5402–5407.
31. Nair, V. C.; Muthu, C.; Rogach, A. L.; Kohara, R.; Biju, V. Channeling Exciton Migration into Electron Transfer in Formamidinium Lead Bromide Perovskite Nanocrystal/Fullerene Composites. *Angew.Chem. Int.Ed*. **2017**, 56, 1214 –1218.
32. Begum, R.; Parida, M. R.; Abdelhady, A. L.; Murali, B.; Alyami, N. M.; Ahmed, G. H.; Hedhili, M. N.; Bakr, O. M.; Mohammed, O. F. Engineering Interfacial

Charge Transfer in CsPbBr3 Perovskite Nanocrystals by Heterovalent Doping *J. Am. Chem. Soc.* **2017**, 139, 731–737.

33. Protesescu, L.; Yakunin, S.; Bodnarchuk, M.I.; Krieg, F.; Caputo, R.; Hendon, C.H.; Yang, R. X.; Walsh, A.; Kovalenko, M.V. Nanocrystals of Cesium Lead Halide Perovskites ($CsPbX_3$, X = Cl, Br, and I): Novel Optoelectronic Materials Showing Bright Emission with Wide Color Gamut. *Nano Lett.* **2015**, 15, 3692–3696.
34. Sekhar, M. C.; De, A.; Hossain, S. S.; Samanta, A. Roles of the methyl and methylene groups of mercapto acids in the photoluminescence efficiency and carrier trapping dynamics of CdTe QDs *Phys. Chem. Chem. Phys.* **2017**, 19, 1536- 1542.
35. Mondal, N.; Samanta, A. Ultrafast Charge Transfer and Trapping Dynamics in a Colloidal Mixture of Similarly Charged CdTe Quantum Dots and Silver Nanoparticles *J. Phys. Chem. C* **2016**, 120, 650–658.
36. Liu, F.; Zhang, Y.; Ding, C.; Kobayashi, S.; Izuishi, T.; Nakazawa, N.; Toyoda, T.; Ohta, T.; Hayase, S.; Minemoto, T. Highly Luminescent Phase-Stable $CsPbI_3$ Perovskite Quantum Dots Achieving Near 100% Absolute Photoluminescence Quantum Yield. *ACS Nano* **2017**, 11, 10373–10383.
37. Ponseca Jr. C.S.; Chábera, P.; Uhlig, J.; Persson, P.; Sundström, V. Ultrafast Electron Dynamics in Solar Energy Conversion. *Chem. Rev*. **2017**, 117, 10940–11024.
38. Makarov, N.S.; Guo, S.; Isaienko, O.; Liu, W.; Robel, I.; Klimov, V. I. Spectral and Dynamical Properties of Single Excitons, Biexcitons, and Trions in Cesium–Lead-Halide Perovskite Quantum Dots. *Nano Lett*. **2016**, 16, 2349–2362.
39. Aneesh, J.; Swarnkar, A.; Ravi, V.K.; Sharma, R.; Nag, A.; Adarsh, K.V. Ultrafast Exciton Dynamics in Colloidal $CsPbBr_3$ Perovskite Nanocrystals: Biexciton Effect and Auger Recombination. *J. Phys. Chem. C* **2017**, 121, 4734–4739.
40. Manser, J. S.; Christians, J. A.; Kamat, P. V. Intriguing Optoelectronic Properties of Metal Halide Perovskites. *Chem. Rev*. **2016**,116, 12956–13008.
41. Klimov, V. I.; McBranch, D. W.; Leatherdale, C. A.; Bawendi, M. G. Electron and Hole Relaxation Pathways in Semiconductor Quantum Dots. *Phys. Rev. B* **1999**, 60, 13740- 13749.
42. Sekhar, M. C.; Samanta, A. Ultrafast Transient Absorption Study of the Nature of Interaction between Oppositely Charged Photoexcited CdTe Quantum Dots and Cresyl Violet. *J. Phys. Chem. C* **2015**, 119, 15661–15668.
43. Huang, J.; Huang, Z.; Jin, S.; Lian, T. Exciton Dissociation in CdSe Quantum Dots by Hole Transfer to Phenothiazine. *J. Phys. Chem. C* **2008**, 112, 19734–19738.
44. Ravi, V. K.; Markad, G. B.; Nag, A. Band Edge Energies and Excitonic Transition Probabilities of Colloidal $CsPbX_3$ (X = Cl, Br, I) Perovskite Nanocrystals. *ACS Energy Lett.* **2016**, 1, 665–671.
45. Mondal, N.; De, A.; Samanta, A. All-Inorganic Perovskite Nanocrystals Assisted Extraction of Hot Electrons and Biexcitons from Photoexcited CdTe Quantum Dots. *Nanoscale* **2018**, 10, 639-645.

46. Kaur, M.; Kaur, P.; Dhuna, V.; Singh, S.; Singh, K. A ferrocene–pyrene based ‘turn-on’ chemodosimeter for Cr3+-application in bioimaging. *Dalton Trans.* **2014**, 43, 5707–5712.

CHAPTER 6

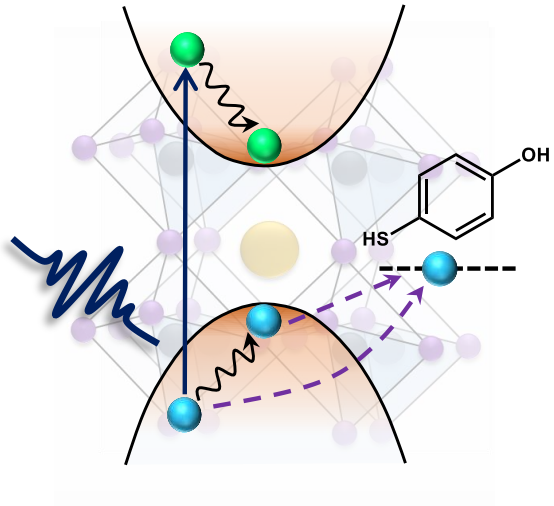

"Hot Hole Transfer Dynamics from CsPbBr3 Perovskite Nanocrystals"

ACS Energy Lett. 2020, 5, 2246-2252.

Overview

Transfer of the hot charge carriers prior to their cooling to the band-edge states can enhance the efficiency of a semiconductor-based solar cell much beyond its SQ limiting value. Herein, we explore transfer of hot holes from the $APbX_3$ NCs employing a carefully chosen molecular system, 4-mercaptophenol. Ultrafast pump-probe and fluorescence measurements indeed confirm this transfer process, whose efficiency depends on the energy content of the hole and a maximum efficiency of ~43% is achieved with $CsPbBr_3$ NCs for a photoexcitation energy of ~$1.46E_g$. While the estimated hot hole cooling and transfer rates are quite comparable, hole transfer from the band edge is found to be a significantly slower process. Findings of the present study suggests that exceeding the SQ efficiency of the solar cells based on the perovskites can indeed be a reality.

6.1. Introduction

Lead halide-based perovskites have emerged as most promising candidates for photovoltaic applications, and a solar PCE of >24% has been achieved within a short period,[1] since the pioneering work of Miyasaka and co-workers in 2009.[2] One major factor responsible for low efficiency of the conventional single junction solar cells is rapid cooling of the hot carriers, produced by solar photons of energy higher than that of the band gap, to the band edge states. Calculations show that utilization of the hot carriers can push this efficiency to ~66%, which is well-beyond the SQ limiting value (33%).[3,4] Several studies have been undertaken to understand the mechanism of relaxation of the hot charge carriers in lead halide perovskites, which indicate that the hot carriers first thermalize to a quasi-equilibrium state through carrier−carrier scattering and then attain thermal equilibrium through carrier−phonon and carrier−impurity scattering in a sub-picosecond time scale.[5−14]

These studies have revealed important factors like hot phonon bottleneck, large polaron formation, Auger heating, high carrier densities, and dielectric confinement. However, the transfer of hot carriers prior to their cooling continues to remain as a challenging task for the narrow time window available for this purpose.[15−19] Moreover, an understanding of the charge transfer dynamics involving the perovskites is also of considerable importance in photocatalytic applications.[20−24]

6.2. Results and Discussion

Herein, we focus on the transfer of hot carriers from $APbBr_3$ [A = Cs^+, $CH_3NH_3^+$ (MA^+) and $CH(NH_2)_2^+$ (FA^+)] NCs. Specifically, we investigate the dynamics and transfer efficiency of the hot holes from these NCs to a molecular system, MTH, chosen for its surface-anchoring thiol unit and energetic considerations of its HOMO and LUMO vis a vis the valence and conduction bands of the perovskite NCs, which permit only hole transfer from photoexcited NCs to MTH (Scheme 6.1). The cooling dynamics and transfer efficiency of the hot hole have been studied as a function of the excitation energy, and a maximum efficiency of ~43% from $CsPbBr_3$ NCs is achieved for

photoexcitation energy of ~1.46E_g (Eg is the band gap of the NCs). All three $APbBr_3$ [A = Cs^+, MA^+, and FA^+] NCs were prepared by reported methods,[29–31] the details of which are provided in the Supporting Information. The average edge lengths of the NCs lie

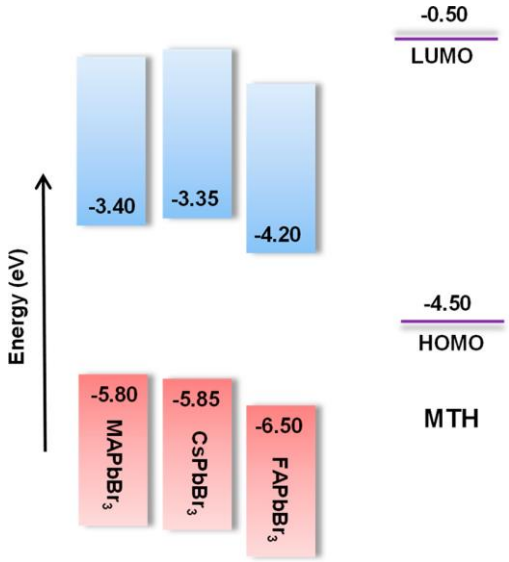

Scheme 6.1. Alignment of the Energy Levels of $APbBr_3$ NCs and MTH. The indicated energy values are obtained from refs 25-28.

between 10 and 14 nm (Figures 6.1 and A4.1). The PLQY of these NCs lie between 80 and 90%, and the PL maxima appear at ~512 nm ($CsPbBr_3$), 518 nm ($MAPbBr_3$), and 527 nm ($FAPbBr_3$). The MTH-adsorbed NCs (indicated hereafter as $APbBr_3$-MTH NCs) were obtained by a simple ligand exchange protocol (sonication of a mixture of a colloidal dispersion of the NCs and a solution of MTH in hexane; details are provided in the Supporting Information). The fact that MTH anchors onto the surface of the NCs through its thiol functionality is established by control experiments and FTIR measurements (see appendix 4) and that the morphological and structural stability of the system are unaffected after the ligand exchange is evident from the TEM image of $CsPbBr_3$-MTH (Figure 4A.2).

Even though the absorption spectra of $CsPbBr_3$ and $CsPbBr_3$-MTH NCs are almost identical (Figure 6.1A),[22] the PLQY values of the two systems differ by nearly two orders of magnitude (~90% vs <1%) (Figure 6.1B). MTH also has a pronounced effect on PL

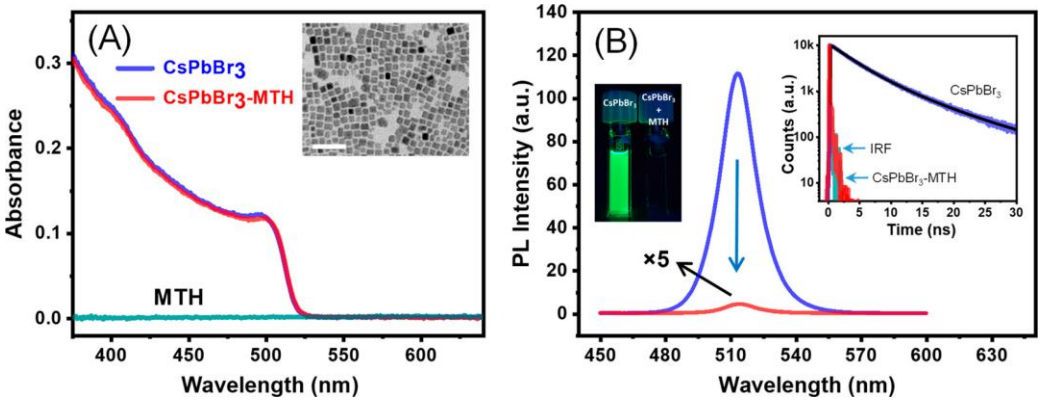

Figure 6.1. (A) Absorption spectra of $CsPbBr_3$, $CsPbBr_3$-MTH, and MTH. TEM image (in 50 nm scale) of the $CsPbBr_3$ NCs is shown in the inset. (B) PL spectra of the NCs (λ_{ex} = 400 nm). Digital images of the solutions and PL decay profiles (λ_{ex} = 405 nm) of the NCs are also provided in the insets. The concentration maintained here was ~100 nM and ~25 μM for $CsPbBr_3$ and MTH, respectively. PL data of the $MAPbBr_3$ and $FAPbBr_3$ NCs are provided in appendix 4.

decay characteristics of the NCs. TCSPC PL decay measurements show an average lifetime of 5.26 ns for $CsPbBr_3$ NCs (Figure 6.1B inset and Table A4.1). However, for $CsPbBr_3$- MTH, the PL decays too fast to measure the lifetime using this setup (see below for actual value measured by upconversion technique), which has a time-resolution of ~60 ps.[32] In the case of $MAPbBr_3$ and $FAPbBr_3$ NCs, a similar trend was observed (Figure A4.4). These PL data indicate strong interaction between the photogenerated charge carriers of the three NCs and MTH.

To determine which of the three $APbBr_3$ NCs is best suited for the transfer of a hot carrier (hot hole in the present case), we first measure their HCC time using femtosecond pump-probe technique because a system with slower HCC provides a greater opportunity for its transfer. As excitation fluence and quantum confinement can also influence the estimated HCC time,[15,33] we maintained sufficiently low pump fluence (~0.08×10^{14} photons/cm^2) in all cases to avoid nonlinear processes[33,34] and chose NCs with size larger than their exciton Bohr diameter to minimize the influence of quantum confinement.[35–37] As the HCC time depends on the energy content of the carrier,[35] during estimation of this quantity we made sure that the hot carriers possess same excess energy in all three cases. The same excess energy of the carriers (which we fixed at ~$1.46E_g$) in different systems

was maintained by varying the excitation wavelengths for the systems. For this purpose, the E_g values for different NCs were first calculated from the derivative plot of the absorption spectra (Figure A4.5), and then the excitation wavelength of the pump–probe study (Figure 6.2A) for each system was adjusted such that the excitation energy

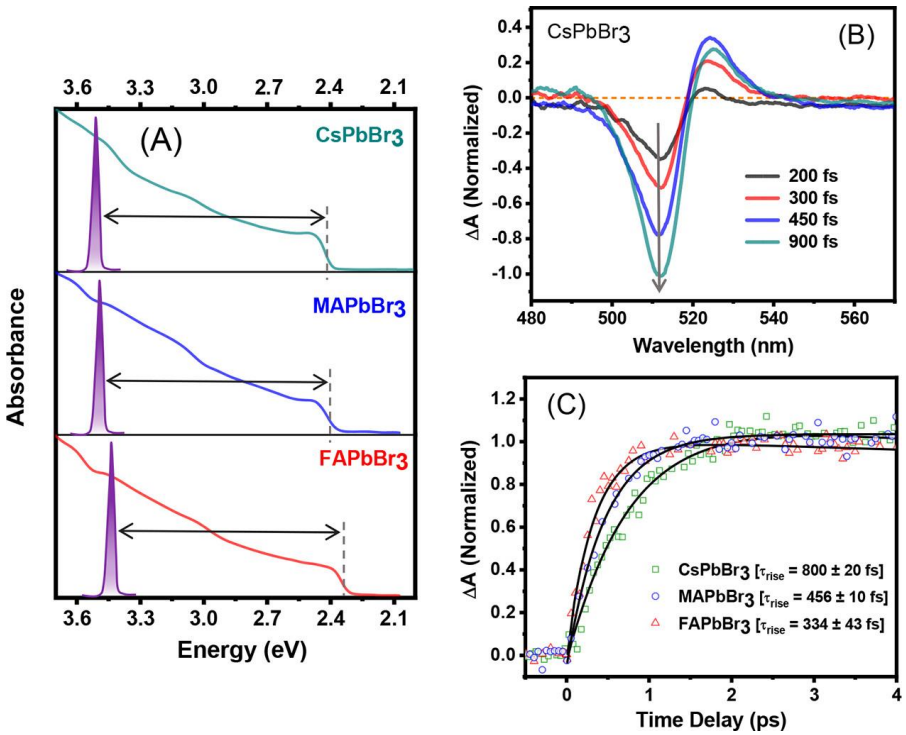

Figure 6.2. (A) Absorption spectra of the NCs. The positions of the vertical dashed lines indicate the band gaps of the systems, and the Gaussian profiles represent the pump energies used for respective samples in TA measurements. (B) Early time TA spectra of $CsPbBr_3$ NCs (upon $1.46E_g$ photoexcitation). (C) Bleach formation kinetics (monitored at respective bleach maximum) of the three NCs representing the relaxation dynamics of the hot carriers possessing the same excess energy.

corresponds to ~$1.46E_g$. Representative TA spectra of the $CsPbBr_3$ NCs at early times are shown in Figure 6.2B (TA spectra of $FAPbBr_3$ and $MAPbBr_3$ are in the Supporting Information, Figure A4.6). The spectra comprises a sharp negative (bleach) signal, which represents state-filling of the photogenerated carriers to the band-edges,[35,36,38] a positive absorption band at the lower energy side of the bleach signal due to polaron formation,[38] and a somewhat weak positive absorption band at the higher-energy side of the same due

to carrier absorption from the band edge states.[35] The HCC time is estimated by monitoring the formation of the bleach signal of the spectra.[35,38–41] The HCC times estimated from the bleach formation profiles (Figure 6.2C) are 800 ± 20, 456 ± 10, and 334 ± 43 fs for $CsPbBr_3$, $MAPbBr_3$, and $FAPbBr_3$, respectively. A faster HCC in hybrid perovskites ($FAPbBr_3$ and $MAPbBr_3$) is consistent with the literature.[33] As these results show that the carriers remain hot for the longest duration in $CsPbBr_3$ NCs, this system is expected to be most appropriate for the transfer of hot carriers, and hence, the subsequent measurements and discussion are focused on the $CsPbBr_3$ NCs. Even though the TA spectra (λ_{ex} = 350 nm) of the $CsPbBr_3$ and $CsPbBr_3$-MTH NCs are very similar (Figures 6.2B and A4.7), the bleach formation time, which represents the relaxation dynamics of the carriers, differs widely (800 ± 20 and 280 ± 18 fs, respectively) in two cases. A faster HCC in $CsPbBr_3$- MTH NCs (Figure 6.3A and Table 6.1) is a reflection of a competitive hot carrier transfer process. As the effective masses of the electron and hole are very similar (m_e^*/m_h^* = 1.07) in $CsPbBr_3$,[42,43] both hot electron and hot hole are generated in almost equal energy content on photoexcitation, and hence, the bleach formation is representative of the relaxation of both the carriers.[36,39] Even though acceleration of bleach formation in $CsPbBr_3$-MTH NCs can in principle be due to electron or/ and hole transfer process(es),[44,45] in the present case, thermodynamic consideration of the energetics of the interacting components suggests hot hole transfer from the NCs as the only possibility. An approximate rate of the transfer of hot holes is calculated (using k =

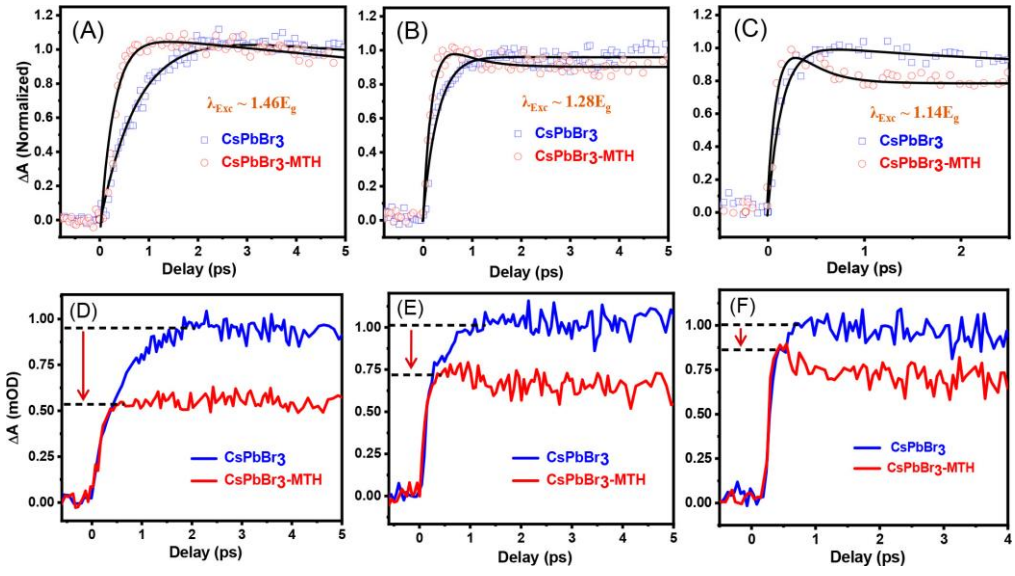

Figure 6.3. Bleach formation kinetics of $CsPbBr_3$ and $CsPbBr_3$-MTH NCs for excitation wavelengths of (A) 350 nm, (B) 400 nm, and (C) 450 nm. Panels D–F compare the bleach amplitudes of the two systems at the indicated excitation wavelengths.

Table 6.1. Bleach formation time of $CsPbBr_3$ and $CsPbBr_3$-MTH NCs for different excitation pump wavelength.

λ_{ex} (nm)	τ_{rise} [fs]/$CsPbBr_3$	τ_{rise} [fs]/ $CsPbBr_3$-MTH
350	800 ± 20	280 ± 18
400	440 ± 15	210 ± 12
450	149 ± 17	109 ± 15

$1/\tau_{NCs\text{-}MTH} - 1/\tau_{NCs)}$ as ~2.3×10^{12} s^{-1}. This high hot hole transfer rate is not surprising as it has to compete with the ultrafast hot hole relaxation rate (~1.25×10^{12} s^{-1}). We have studied the hot carrier transfer dynamics for two other excitation wavelengths, 400 and 450 nm, corresponding to energy of ~$1.28E_g$ and ~$1.14E_g$, respectively. For lower excitation energies also, the bleach formation is faster in $CsPbBr_3$-MTH NCs; however, the change is not as pronounced as it is for higher excitation energy (Figure 6.3 and Table 6.1).

As the bleach amplitude is a measure of the number of carriers relaxing to the band edge, by monitoring this quantity one can determine whether the carriers are extracted and to what extent.[15,44–46] A lower peak bleach amplitude in $CsPbBr_3$-MTH NCs (Figure 6.3) compared to $CsPbBr_3$ under identical conditions clearly indicates transfer of the hot holes to MTH. The dependence of the HC transfer efficiency on the excitation energy is $CsPbBr_3$-MTH NCs are excited further closer to the band gap, at ~$1.08E_g$ (470 nm), both bleach formation dynamics and maximum bleach amplitude are found to be very similar for the two samples (Figure A4.8), indicating no hot hole transfer from $CsPbBr_3$ NCs. Such depicted in Figure 6.4. Maximum transfer efficiency of ~43% is observed for an excitation energy of ~$1.46E_g$, and the lowest (11%) is found for ~$1.14E_g$. When $CsPbBr_3$ and an energy dependence of the hole transfer efficiency is attributed to the difference in electronic coupling of the donor-acceptor wave functions with variation in excitation

energy.[47,48] The higher the energy content of the hot hole, the larger the spread of its wave function beyond the NCs surface and consequently the greater the coupling of the hot hole wave function of the NCs with the HOMO of the organic moiety.[47,48]

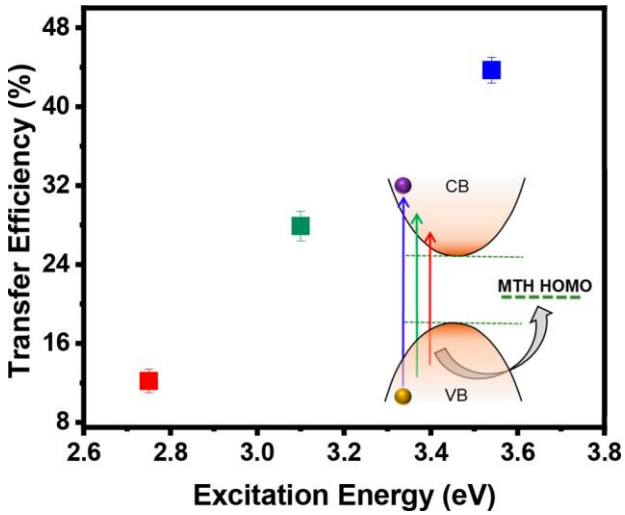

Figure 6.4. Dependence of the hot hole transfer efficiency on excitation energy.

We have examined the hot carrier transfer process also by the upconverted PL technique,[49] in which the hot carriers were generated by 400 nm (corresponding to ~1.28E_g) excitation of the NCs using ~200 fs pulses and monitoring time-dependent formation of the band-edge emission (~512 nm), which represents the cooling dynamics of the carriers.[35] The HCC time of the $CsPbBr_3$ NCs obtained by this method is found to be 460 ± 40 fs, which is in agreement with the literature[35] and also with our pump-probe measured value (440 ± 15 fs) for 400 nm excitation. However, for the $CsPbBr_3$-MTH NCs, the HCC time is much shorter (245 ± 25 fs) (Figure 6.5) and comparable to the value (210 ± 12 fs) obtained by the pump-probe technique. Comparison of the peak PL counts of the two samples indicates ~22% hot hole transfer efficiency in $CsPbBr_3$-MTH (Figure A4.9), which is consistent with our pump−probe result.

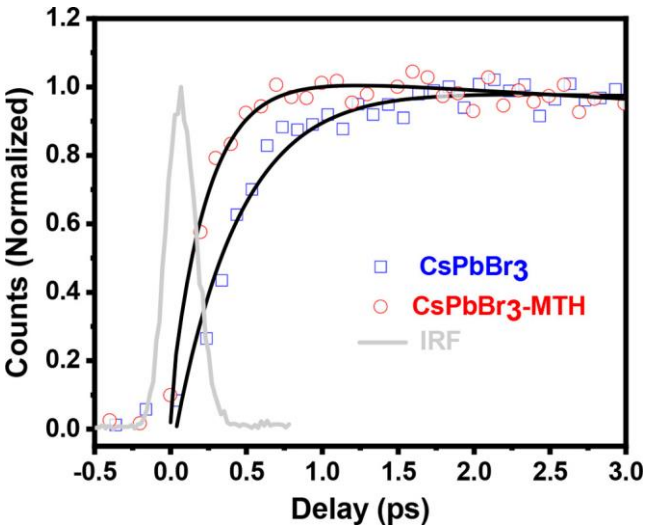

Figure 6.5. Formation kinetics of the band-edge PL of the two NCs measured by upconversion technique.

We have also examined the dynamics of transfer of the "cold" holes (i.e., those from the band-edge) by pump−probe technique by monitoring recovery of the bleach amplitude for λ_{ex} = 350 nm (Figures 6.6 and A4.10). While bleach recovery is a single exponential with τ > 1.2 ns for $CsPbBr_3$ NCs (representing the band edge electron−hole recombination time),[36,50] in the case of $CsPbBr_3$-MTH, two additional time components (14.1 ± 3 and 166.3 ± 15 ps) accompany the long component. The PL decay profile of the CsPbBr3-MTH NCs, measured by the upconversion technique, also indicates a similar picture (Figure A4.11). Two short time components (16 ± 1.4 and 160 ± 10.2 ps) are observable in addition to the long decay component of >1.2 ns. It is to be noted here that accurate estimation of the longest time component is not possible using the femtosecond time-resolved TA and PL UC setup for non-availability of a larger time window.[49,51,52] It is clear, however, that this long component arises from radiative recombination of the electron and hole.

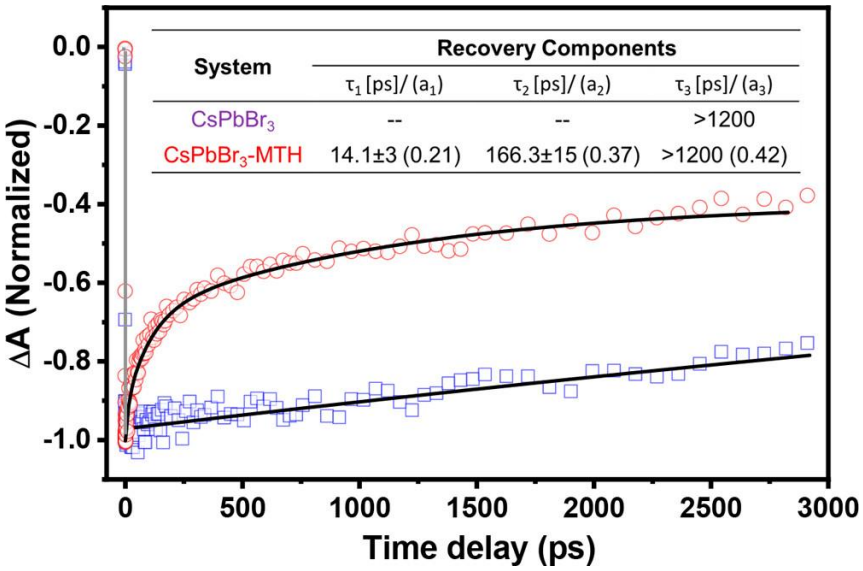

Figure 6.6. Comparison of the bleach recovery kinetics of $CsPbBr_3$ and $CsPbBr_3$-MTH NCs (λ_{ex} = 350 nm).

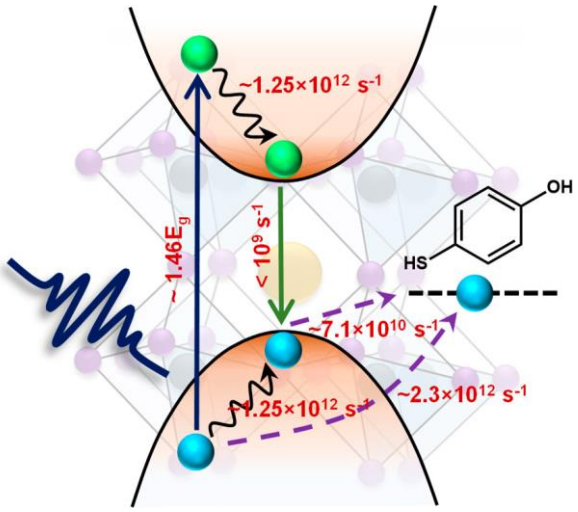

Scheme 6.2. Schematic Illustration of Carrier Relaxation Dynamics in Photoexcited (~1.46E_g) $CsPbBr_3$-MTH NCs

The short 14-16 ps component represents the hole transfer time (τ_{HT}) from the band-edge states of the NCs (corresponding to a rate of 6.2-7.6×10^{10} s^{-1}). This value is comparable

with hole transfer time from the band-edge states in other perovskites.[53] Interestingly, hole transfer from the band edge states is relatively slower than that from the higher energy levels. A faster hot hole transfer could be the result of a larger driving force (Figure A4.14) and enhanced donor-acceptor wave function coupling.[47,48] The intermediate 160-166 ps component is attributed to a negative trion, which is formed upon transfer of holes by MTH. Though positive trion formation is more common in perovskite NCs because of the intrinsic electron trap states,[54–57] formation of negative trion is also reported in the presence of strong hole scavenger.[58] Moreover, the observed negative trion lifetime agrees well with the literature data.[54]

6.3. Summary

The main findings of the present work are highlighted in Scheme 6.2 based on the above discussion. In short, we demonstrate the transfer of hot holes from $CsPbBr_3$ NCs using a molecular system. We attribute this success to intrinsic slow hot hole cooling in the system and strong electronic coupling of the deep energy levels of the valence band of the NCs with those of the localized HOMO level of the organic moiety,[17] which is facilitated by the thiol anchoring unit. The findings show that an appropriate choice of a molecular system can indeed make the transfer process quite efficient.

References

1. NREL Best Efficiency Chart: https://www.nrel.gov/pv/assets/pdfs/best-research-cell-efficiencies.20200708.pdf.
2. YU, P.; Cardona, M., Fundamentals of Semiconductors: Physics and Materials Properties. *Springer* **2010**, ISBN 978-3-642-00710-1.
3. Henderson, B.; Imbusch, G. F., Optical Spectroscopy of Inorganic Solids. *Clarendon Press, Oxford* **1989**.
4. Gaponenko, S. V., Introduction to Nanophotonics. *Cambridge University Press* **2010**, ISBN-10: 0521763754.
5. Kayanuma, Y., Quantum-Size Effects of Interacting Electrons and Holes in Semiconductor Microcrystals with Spherical Shape. *Phys. Rev. B* **1988,** 38, 9797.
6. Einevoll, G., Confinement of Excitons in Quantum Dots. *Phys. Rev. B* **1992,** 45, 3410.

7. Katan, C.; Mercier, N.; Even, J., Quantum and Dielectric Confinement Effects in Lower-Dimensional Hybrid Perovskite Semiconductors. *Chem. Rev.* **2019,** *119*, 3140-3192.
8. Smith, A. M.; Nie, S., Semiconductor Nanocrystals: Structure, Properties, and Band Gap Engineering. *Acc. Chem. Res.* **2010,** 43, 190-200.
9. Wells, H. L., Über die Cäsium- und Kalium-Bleihalogenide. *Z. Anorg. Allg. Chem.* **1893,** *3*, 195-210.
10. Moller, C. K., A Phase Transition in Caesium Plumbochloride. *Nature* **1957,** *180*, 981-982.
11. Moller, C. K., Crystal Structure and Photoconductivity of Caesium Plumbohalides. *Nature* **1958,** *182*, 1436-1436.
12. Kojima, A.; Teshima, K.; Shirai, Y.; Miyasaka, T., Organometal Halide Perovskites as Visible-Light Sensitizers for Photovoltaic Cells. *J. Am. Chem. Soc.* **2009,** *131*, 6050-6051.
13. Protesescu, L.; Yakunin, S.; Bodnarchuk, M. I.; Krieg, F.; Caputo, R.; Hendon, C. H.; Yang, R. X.; Walsh, A.; Kovalenko, M. V., Nanocrystals of Cesium Lead Halide Perovskites ($CsPbX_3$, X = Cl, Br, and I): Novel Optoelectronic Materials Showing Bright Emission with Wide Color Gamut. *Nano Lett.* **2015,** *15*, 3692-3696.
14. Le, Q. V.; Jang, H. W.; Kim, S. Y., Recent Advances toward High-Efficiency Halide Perovskite Light-Emitting Diodes: Review and Perspective. *Small Methods* **2018,** 2, 1700419.
15. Shamsi, J.; Urban, A. S.; Imran, M.; Trizio, L. D.; Manna, L., Metal Halide Perovskite Nanocrystals: Synthesis, Post-Synthesis Modifications, and Their Optical Properties. *Chem. Rev.* **2019,** *119*, 3296-3348.
16. Manser, J. S.; Christians, J. A.; Kamat, P. V., Intriguing Optoelectronic Properties of Metal Halide Perovskites. *Chem. Rev.* **2016,** *116*, 12956-13008.
17. Zhou, Y.; Chen, J.; Bakr, O. M.; Sun, H.-T., Metal-Doped Lead Halide Perovskites: Synthesis, Properties, and Optoelectronic Applications. *Chem. Mater.* **2018,** *30*, 6589-6613.
18. Akkerman, Q. A.; Manna, L., What Defines a Halide Perovskite? *ACS Energy Lett.* **2020,** *5*, 604-610.
19. Swarnkar, A.; Mir, W. J.; Nag, A., Can B-Site Doping or Alloying Improve Thermal- and Phase-Stability of All-Inorganic $CsPbX_3$ (X = Cl, Br, I) Perovskites? *ACS Energy Lett.* **2018,** *3*, 286-289.
20. Mitzi, D. B., Templating and Structural Engineering in Organic–Inorganic Perovskites. *J. Chem. Soc., Dalton Trans* **2001**, 1-12.
21. Goldschmidt, V. M., Die Gesetze Der Krystallochemie. *Naturwissenschaften* **1926,** *14*, 477-485.
22. Becker, M.; Vaxenburg, R.; Nedelcu, G.; Sercel, P. C.; Shabaev, A.; Mehl, M. J.; Michopoulos, J. G.; Lambrakos, S. G.; Bernstein, N.; Lyons, J. L.; Stöferle, T.; Mahrt, R. F.; Kovalenko, M. V.; Norris, D. J.; Rainò, G.; Efros, A. L., Bright Triplet Excitons in Caesium Lead Halide Perovskites. *Nature* **2018,** *553*, 189-193.
23. Akkerman, Q. A.; Rainò, G.; Kovalenko, M. V.; Manna, L., Genesis, Challenges and Opportunities for Colloidal Lead Halide Perovskite Nanocrystals. *Nature Mater* **2018,** *17*, 394-405.

24. Sercel, P. C.; Lyons, J. L.; Wickramaratne, D.; Vaxenburg, R.; Bernstein, N.; Efros, A. L., Exciton Fine Structure in Perovskite Nanocrystals. *Nano Lett.* **2019,** *19*, 4068-4077.
25. Meijerink, A.; Rabouw, F. T., Shedding Light on Dark Excitons. *Nature Mater.* **2019,** 18, 660-661.
26. Seth, S.; Ahmed, T.; De, A.; Samanta, A., Tackling the Defects, Stability, and Photoluminescence of $CsPbX_3$ Perovskite Nanocrystals. *ACS Energy Lett.* **2019,** *4*, 1610-1618.
27. Ravi, V. K.; Santra, P. K.; Joshi, N.; Chugh, J.; Singh, S. K.; Rensmo, H.; Ghosh, P.; Nag, A., Origin of the Substitution Mechanism for the Binding of Organic Ligands on the Surface of $CsPbBr_3$ Perovskite Nanocubes. *J. Phys. Chem. Lett.* **2017,** *8*, 4988-4994.
28. Roo, J. D.; Ibańez, M.; Geiregat, P.; Nedelcu, G.; Walravens, W.; Maes, J.; Martins, J. C.; Driessche, I. V.; Kovalenko, M. V.; Hens, Z., Highly Dynamic Ligand Binding and Light Absorption Coefficient of Cesium Lead Bromide Perovskite Nanocrystals. *ACS Nano* **2016,** 10, 2071-2081.
29. Krieg, F.; Ochsenbein, S. T.; Yakunin, S.; Brinck, S. t.; Aellen, P.; Süess, A.; Clerc, B.; Guggisberg, D.; Nazarenko, O.; Shynkarenko, Y.; Kumar, S.; Shih, C.-J.; Infante, I.; Kovalenko, M. V., Nanocrystals 2.0: Zwitterionic Capping Ligands for Improved Durability and Stability. . *ACS Energy Lett.* **2018,** *3*, 641-646.
30. Pan, J.; Shang, Y.; Yin, J.; Bastiani, M. D.; Peng, W.; Dursun, I.; Sinatra, L.; El-Zohry, A. M.; Hedhili, M. N.; Emwas, A.-H.; Mohammed, O. F.; Ning, Z.; Bakr, O. M., Bidentate Ligand-Passivated $CsPbI_3$ Perovskite Nanocrystals for Stable Near-Unity Photoluminescence Quantum Yield and Efficient Red Light-Emitting Diodes. *J. Am. Chem. Soc.* **2018,** *140*, 562-565.
31. Bodnarchuk, M. I.; Boehme, S. C.; Brinck, S. t.; Bernasconi, C.; Shynkarenko, Y.; Krieg, F.; Widmer, R.; Aeschlimann, B.; Günther, D.; Kovalenko, M. V., Rationalizing and Controlling the Surface Structure and Electronic Passivation of Cesium Lead Halide Nanocrystals. *ACS Energy Lett.* **2019,** *4*, 63-74.
32. Mondal, N.; De, A.; Samanta, A., Achieving Near-Unity Photoluminescence Efficiency for Blue-Violet-Emitting Perovskite Nanocrystals. *ACS Energy Lett.* **2019,** *4*, 32-39.
33. Ahmed, T.; Seth, S.; Samanta, A., Boosting the Photoluminescence of $CsPbX_3$ (X = Cl, Br, I) Perovskite Nanocrystals Covering a Wide Wavelength Range by Postsynthetic Treatment with Tetrafluoroborate Salts. *Chem. Mater.* **2018,** *30*, 3633-3637.
34. Ghosh, D.; Welch, E.; Neukirch, A. J.; Zakhidov, A.; Tretiak, S., Polarons in Halide Perovskites: A Perspective. *J. Phys. Chem. Lett.* **2020,** *11*, 3271-3286.
35. Miyata, K.; Meggiolaro, D.; Trinh, M. T.; Joshi, P. P.; Mosconi, E.; Jones, S. C.; Angelis, F. D.; Zhu, X.-Y., Large Polarons in Lead Halide Perovskites. *Science* **2017,** *3*, e1701217.
36. Park, M.; Neukirch, A. J.; Reyes-Lillo, S. E.; Lai, M.; Ellis, S. R.; Dietze, D.; Neaton, J. B.; Yang, P.; Tretiak, S.; Mathies, R. A., Excited-State Vibrational Dynamics Toward the Polaron in Methylammonium Lead Iodide Perovskite. *Nat. Commun.* **2018,** 9, (2525).
37. Luo, B.; Li, F.; Xu, K.; Guo, Y.; Liu, Y.; Xia, Z.; Zhang, J. Z., B-Site Doped Lead Halide Perovskites: Synthesis, Band Engineering, Photophysics, and Light Emission Applications. *J. Mater. Chem. C* **2019,** *7*, 2781-2808.

38. Stam, W. v. d.; Geuchies, J. J.; Altantzis, T.; Bos, K. H. W. v. d.; Meeldijk, J. D.; Aert, S. V.; Bals, S.; Vanmaekelbergh, D.; Donega, C. d. M., Highly Emissive Divalent-Ion-Doped Colloidal $CsPb_{1-x}M_xBr_3$ Perovskite Nanocrystals through Cation Exchange. *J. Am. Chem. Soc.* **2017,** *139*, 4087-4097.
39. Pandey, A.; Sarma, D. D., Recent Advances in Manganese Doped II-VI Semiconductor Quantum Dots. *Z. Anorg. Allg. Chem.* **2016,** *642*, 1331-1339.
40. Norris, D. J.; Efros, A. L.; Erwin, S. C., Doped Nanocrystals. *Science* **2008,** *319*, 1776-1779.
41. Parobek, D.; Roman, B. J.; Dong, Y.; Jin, H.; Lee, E.; Sheldon, M.; Son, D. H., Exciton-to-Dopant Energy Transfer in Mn-Doped Cesium Lead Halide Perovskite Nanocrystals. *Nano Lett.* **2016,** *16*, 7376-7380.
42. Santra, P. K.; Kamat, P. V., Mn-Doped Quantum Dot Sensitized Solar Cells: A Strategy to Boost Efficiency over 5%. *J. Am. Chem. Soc.* **2012,** *134*, 2508-2511.
43. Siena, M. C. D.; Sommer, D. E.; Creutz, S. E.; Dunham, S. T.; Gamelin, D. R., Spinodal Decomposition During Anion Exchange in Colloidal Mn^{2+}-Doped $CsPbX_3$ (X = Cl, Br) Perovskite Nanocrystals. *Chem. Mater.* **2019,** 31, 7711-7722.
44. Liu, W.; Lin, Q.; Li, H.; Wu, K.; Robel, I. n.; Pietryga, J. M.; Klimov, V. I., Mn^{2+}-Doped Lead Halide Perovskite Nanocrystals with Dual-Color Emission Controlled by Halide Content. *J. Am. Chem. Soc.* **2016,** *138*, 14954-14961.
45. De, A.; Mondal, N.; Samanta, A., Luminescence Tuning and Exciton Dynamics of Mn-Doped $CsPbCl_3$ Nanocrystals. *Nanoscale* **2017,** *9*, 16722-16727.
46. Rossi, D.; Parobek, D.; Dong, Y.; Son, D. H., Dynamics of Exciton−Mn Energy Transfer in Mn-Doped $CsPbCl_3$ Perovskite Nanocrystals. *J. Phys. Chem. C* **2017,** *121*, 17143-14149.
47. Ji, S.; Yuan, X.; Cao, S.; Ji, W.; Zhang, H.; Wang, Y.; Li, H.; Zhao, J.; Zou, B., Near-Unity Red Mn^{2+} Photoluminescence Quantum Yield of Doped $CsPbCl_3$ Nanocrystals with Cd Incorporation. *J. Phys. Chem. Lett.* **2020,** *11*, 2142-2149.
48. Pan, G.; Bai, X.; Yang, D.; Chen, X.; Jing, P.; Qu, S.; Zhang, L.; Zhou, D.; Zhu, J.; Xu, W.; Dong, B.; Song, H., Doping Lanthanide into Perovskite Nanocrystals: Highly Improved and Expanded Optical Properties. *Nano Lett.* **2017,** *17*, 8005-8011.
49. Avellini, T.; Lincheneau, C.; Vera, F.; Silvi, S.; Credi, A., Hybrids of Semiconductor Quantum Dot and Molecular Species for Photoinduced Functions. *Coord. Chem. Rev.* **2014,** *263-264*, 151-160.
50. Robel, I.; Subramanian, V.; Kuno, M.; Kamat, P. V., Quantum Dot Solar Cells. Harvesting Light Energy with CdSe Nanocrystals Molecularly Linked to Mesoscopic TiO_2 Films. *J. Am. Chem. Soc.* **2006,** 128, 2385-2393.
51. Wu, X.; Yeow, E. K. L., Charge-Transfer Processes in Single CdSe/ZnS Quantum Dots with p-Type NiO Nanoparticles. *Chem. Commun.* **2010,** 46, 4390-4392.
52. Hildebrandt, N.; Spillmann, C. M.; Algar, W. R.; Pons, T.; Stewart, M. H.; Oh, E.; Susumu, K.; Díaz, S. A.; Delehanty, J. B.; Medintz, I. L., Energy Transfer with Semiconductor Quantum Dot Bioconjugates: A Versatile Platform for Biosensing, Energy Harvesting, and Other Developing Applications. *Chem. Rev.* **2017,** 117, 536-711.
53. Rehm, D.; Weller, A., Kinetics of Fluorescence Quenching by Electron and H-Atom Transfer. *Isr. J. Chem.* **1970,** 8, 259.

54. Mondal, N.; De, A.; Das, S.; Paul, S.; Samanta, A., Ultrafast Carrier Dynamics of Metal Halide Perovskite Nanocrystals and Perovskite Composites. *Nanoscale* **2019,** 11, 9796-9818.
55. Li, M.; Fu, J.; Xu, Q.; Sum, T. C., Slow Hot-Carrier Cooling in Halide Perovskites: Prospects for Hot-Carrier Solar Cells. *Adv. Mater.* **2019,** *31*, 1802486.
56. Zhang, X.; Zhang, Y.; Zhang, X.; Yin, W.; Wang, Y.; Wang, H.; Lu, M.; Li, Z.; Gu, Z.; Yu, W. W., Yb^{3+} and Yb^{3+}/Er^{3+} doping for near-infrared emission and improved stability of $CsPbCl_3$ nanocrystals. *J. Mater. Chem. C* **2018,** 6, 10101-10105.
57. Yong, Z.-J.; Guo, S.-Q.; Ma, J.-P.; Zhang, J.-Y.; Li, Z.-Y.; Chen, Y.-M.; Zhang, B.-B.; Zhou, Y.; Shu, J.; Gu, J.-L.; Zheng, L.-R.; Bakr, O. M.; Sun, a. H.-T., Doping-Enhanced Short-Range Order of Perovskite Nanocrystals for Near-Unity Violet Luminescence Quantum Yield. *J. Am. Chem. Soc.* **2018,** *140*, 9942-9951.

CHAPTER 7

Concluding Remarks

7.1. Overview

The thesis is focused on the photophysical properties of an emerging class of semiconductor materials, lead halide perovskites, which have gained tremendous attention in recent years due to their potential applications in photovoltaics and light-emitting devices. We have investigated the spectral and temporal behavior of the photoinduced transients in these materials in the femtosecond-picosecond timescale. We have studied the carrier relaxation processes such as single-exciton dynamics, carrier trapping and hot carrier cooling in perovskite NCs of various compositions. In addition, we have examined charge transfer from the band edge and above-band edge states of the perovskites to various molecular acceptors. For this purpose, we have employed femtosecond TA and PL UC techniques. Besides, we have used TCSPC spectrometer for fluorescence lifetime measurements in the ps-ns time domain and UV-Vis spectrophotometer and spectrofluorimeter for various steady state optical measurements for the works described in the thesis. For characterization of the NCs, we have used several other instruments such as TEM, FESEM, FTIR, PXRD, etc. The overall finding of this work is summarized below.

$CsPbCl_3$, the least luminescent perovskite in the family of $CsPbX_3$ NCs is one of the major focuses of this thesis. Introduction of a color-centered impurity like Mn not only enhances the overall PLQY of the system but also reduces overall toxicity of the material (as it replaces Pb). Here we investigate the carrier dynamics of $CsPbCl_3$ and a series of Mn-doped $CsPbCl_3$ NCs with varying Mn-content. Our finding suggests that significant carrier trapping in $CsPbCl_3$ leads to carrier losses for radiative recombination, which decreases its PL efficiency. As this carrier trapping also hinders exciton to dopant energy transfer process in Mn-doped systems, it is evident that if one can design a host NC with reduced/suppressed carrier trapping, the energy transfer efficiency to the Mn sites and Mn PLQY can be enhanced. Apart from demonstrating this, we also show that even though the Mn PL arises due to the atomic d-d transition, its PL energy can be tuned just by varying the Mn-concentration in the NCs. Mn-Mn exchange interaction due to proximity effect is shown to be responsible for the tunable nature of the Mn PL.

For enhancing the PLQY of violet-emitting $CsPbCl_3$, we came up with a B-cation doping strategy. As crystal structure disorder and halide vacancy are the major causes of low PLQY of this system, incorporation of smaller size B-cation as halide salt can be a solution. Partial replacement of Pb with Cu serves this purpose. Use of halide salt such as $CuCl_2$ helps to fulfil the halide vacancy. As a result, the PLQY is enhanced to ~ 60% from ~1% without any change in the bandgap. Blue-emitting perovskites (with emission window of 430-460 nm) with near-unity PLQY is obtained by halide exchange of these PL-improved NCs. The suppression of carrier trapping in these systems is also clearly evident from the TA measurements data. Thus a strategic route to have a violet-blue emitting perovskites with improved PL efficiency is developed.

Understanding the charge transfer processes from perovskites is important for better utilization of these substances in photovoltaic applications. Since relatively low bandgap materials are most suitable in photovoltaics, we chose $CsPbBr_3$ and $CsPbI_3$ for this purpose. We chose amino-functionalized pyrene (1-aminopyrene) as a hole acceptor for both considering the conducting π-framework of the pyrene core and surface anchoring ability of the amino functionality. Our ultrafast TA measurements reveal successful extraction of holes from the band edge states of both NCs in ~120-170 ps. The study, which shows that even a simple molecular acceptor like aminopyrene can serve as a hole acceptor, suggests that simpler hole acceptors can be possible alternatives to commonly used expensive spiro-OMeTAD.

Above bandgap photoexcitation generates hot charge carriers, which cool down to the band edge states. During this cooling process a major portion of the excitation energy is lost. In order to minimize this loss, hot carriers need to be harvested. Using a simple molecular hole acceptor (4-mercaptophenol), we demonstrate successful extraction of hot holes from $CsPbBr_3$ NCs. We show that hole extraction efficiency varies with the energy content of the hot holes and a maximum extraction efficiency of ~43% is observed when we photo-excite the NCs with $1.46E_g$ energy. Our success of harvesting hot holes can be attributed to the intrinsic slow hot hole cooling in $CsPbBr_3$ NCs and strong binding of the acceptor molecule.

7.2. Future Scope and Challenges

Our investigations suggest that dominant carrier trapping in $CsPbCl_3$ limits the Mn-PL efficiency. Thus one needs to look for a better host material (with suppressed carrier trapping) with similar bandgap to have enhanced PLQY. Even though, we report a new and better host, its PLQY is limited to ~60%. Clearly, there lies huge scope of improving the violet-emitting perovskites with less carrier trapping with Mn PL efficiency closer to near unity. As discussed in section 1.3.6., it is shown that Cd-doping can indeed suppress the carrier trapping process in $CsPbCl_3$ system and simultaneous incorporation of Mn and Cd leads to near unity PLQY from Mn states. However, considering the toxic issue of Cd, one needs to look for alternate protocol to achieve a trap-free $CsPbCl_3$ or an alternative host with similar bandgap which will exhibit better PL efficiency of Mn PL.

There lies a great opportunity to explore the charge transfer processes from perovskites using molecular acceptors. In photovoltaic devices, spiro-OMeTAD, which is used as hole acceptor, is quite expensive. Hence, search for cheaper and simpler acceptors without compromising the performance of the device has to be made. As far as the harvesters are concerned, focus should be on low bandgap materials (such as $APbI_3$), which are of real interest in photovoltaic application. While charge transfer from the band-edge states has been explored quite extensively, little progress has been made in harvesting the hot charge carriers. Success in fabrication of the hot-carrier based devices can push the efficiency value beyond the SQ limit. As rapid hot carrier cooling makes their extraction a challenging task, systems with long hot carrier cooling time are most useful and should be investigated. With a view to minimize the energy loss, attention must be given to extraction of multi-excitons as well. In these regard, in-depth spectroscopic studies exploring the carrier dynamics of these systems need to be carried out.

Appendices

Appendix I

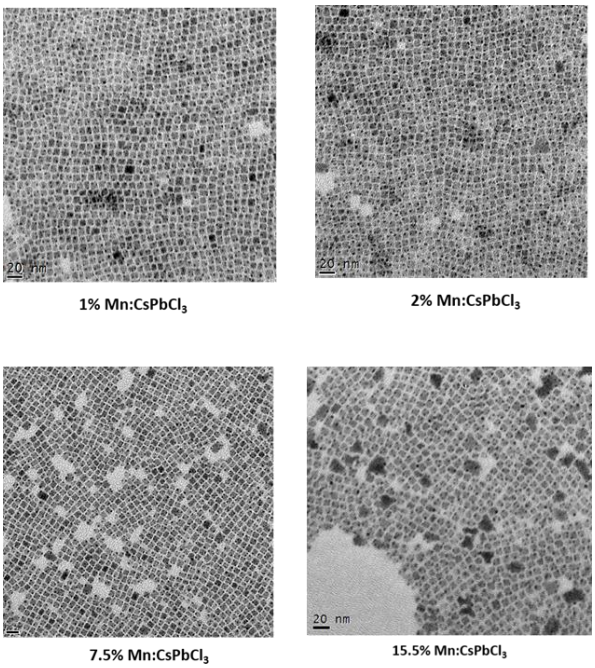

Figure A1.1. TEM images of different samples showing uniform size distribution. Scale bar shown here is of 20 nm.

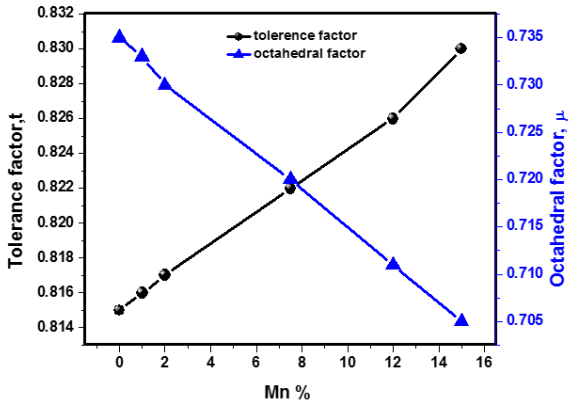

Figure A1.2. Tolerance factor and octahedral factor of different sets of synthesized materials.

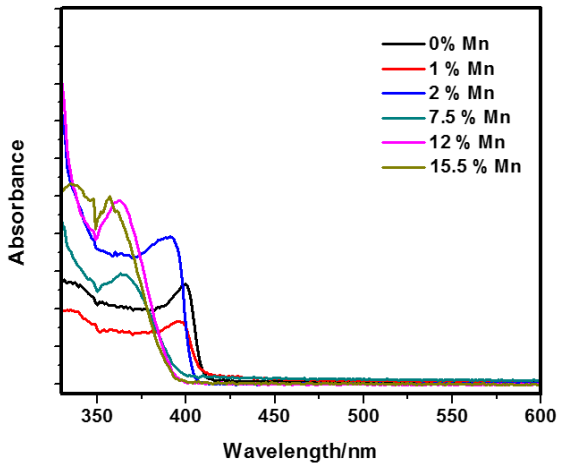

Figure A1.3. UV-Vis absorption spectra of undoped and doped $CsPbCl_3$ NCs.

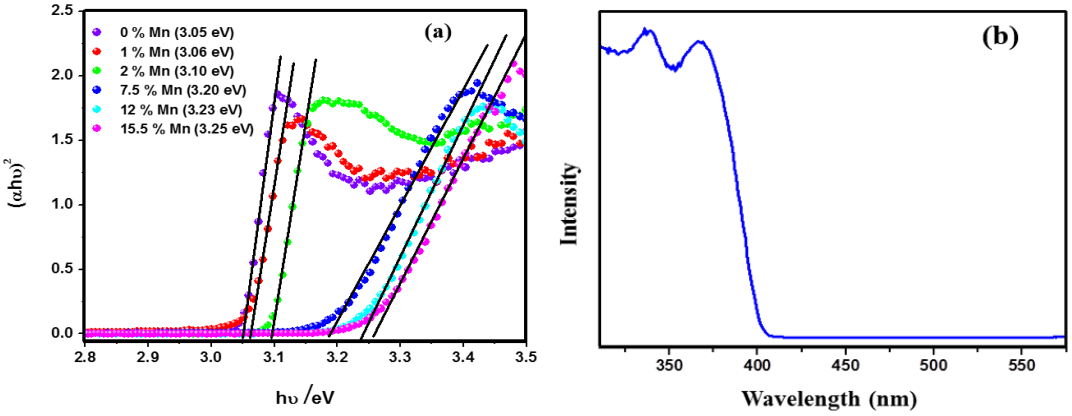

Figure A1.4. (a) Tauc plot of undoped and doped nanocrystals. Estimated band gaps are given in brackets. (b) Excitation spectra of 12% Mn:$CsPbCl_3$ recorded by monitoring at 604 nm.

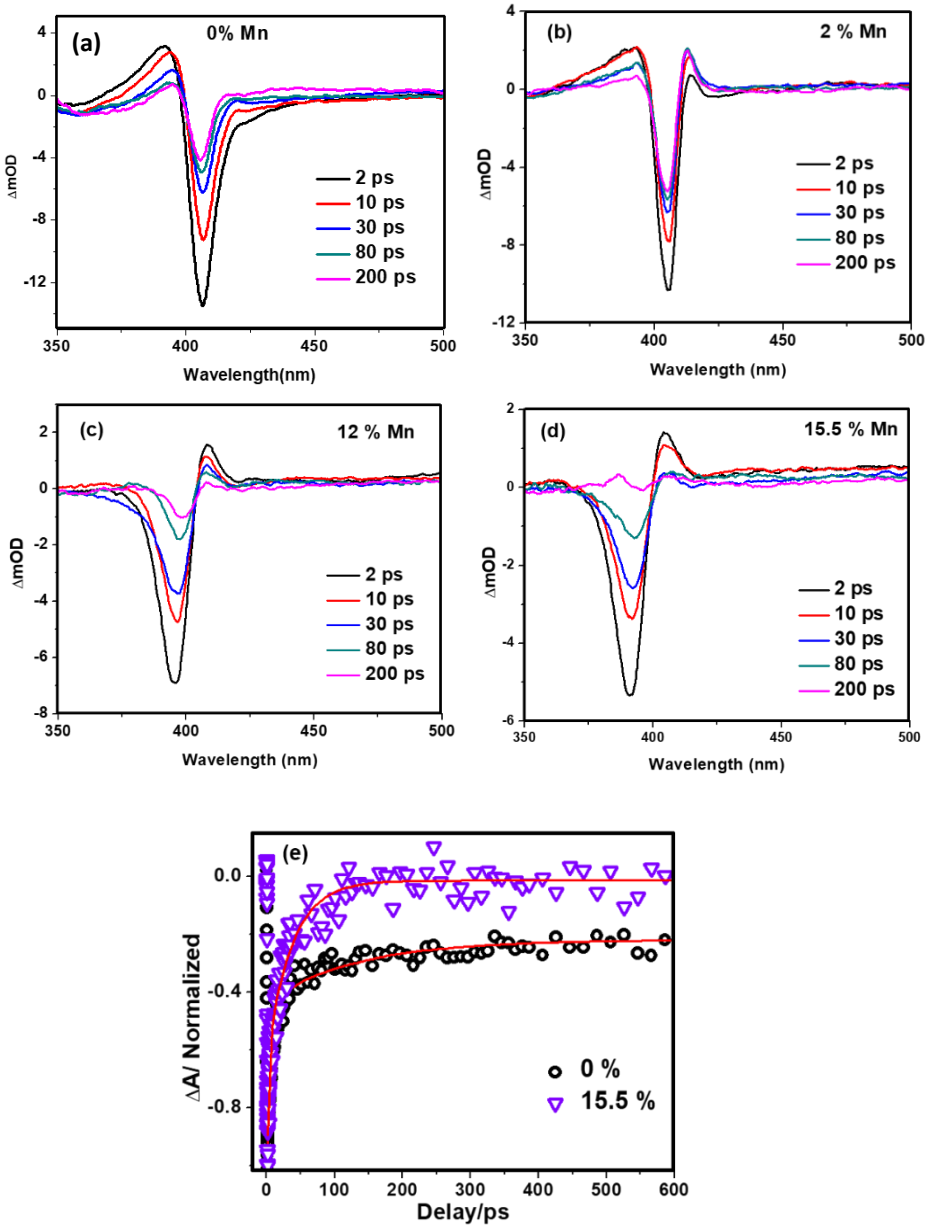

Figure A1.5. TA spectra of (a) undoped, (b) 2% Mn, (c) 12% Mn and (d) 15.5% Mn doped $CsPbCl_3$ NCs in toluene at 330 nm excitation (E) Comparison of bleach recovery kinetics of 0% and 15.5% Mn-doped $CsPbCl_3$ NCs.

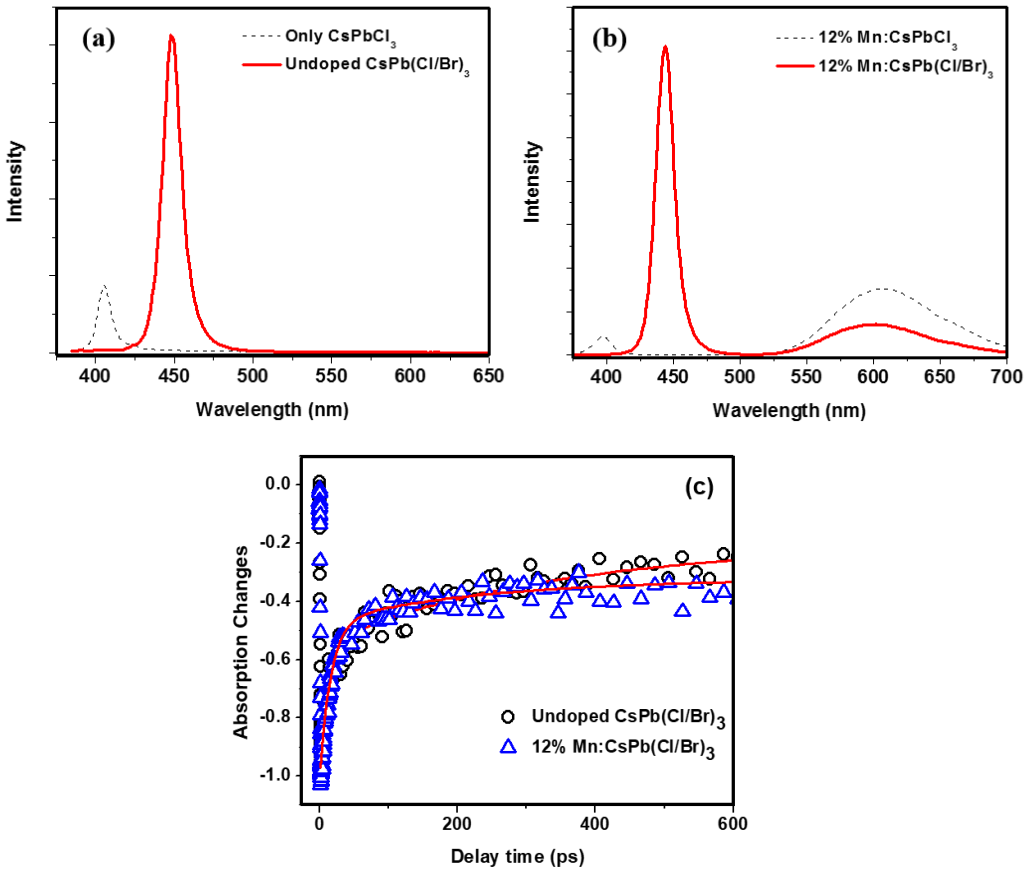

Figure A1.6. Dotted lines represent PL spectra of (a) Undoped $CsPbCl_3$ NCs (b) 12% Mn doped $CsPbCl_3$ NCs. Solid lines are for Br^- exchanged NCs for both cases. Halide (Br^-) exchange was performed by adding freshly prepared $CsPbBr_3$ NCs solution dispersed in toluene into the sample of interest. (c) Comparison of bleach recovery dynamics between undoped and 12% Mn doped $CsPb(Cl/Br)_3$ NCs.

Table A1.1. Relative Mn content estimated from ICP-OES against the precursor used during synthesis.

Precursor Ratio % (Mn/Pb)	ICP Ratio % (Mn/Pb)
10	1
20	2
30	7.5
40	12
60	15.5

Table A1.2. Mn PL decay parameters of different samples by monitoring at their respective peak position.

Sample	t_1 (b_1)	t_1 (b_1)	$\langle t_{int} \rangle$ [ms]
1% Mn:$CsPbCl_3$	1.3 ± 0.03	--	1.30
2% Mn:$CsPbCl_3$	1.24 ± 0.05	--	2
7.5% Mn:$CsPbCl_3$	0.70 ± 0.01 (0.79)	0.18 ± 0.01 (0.21)	0.66
12% Mn:$CsPbCl_3$	0.64 ± 0.03 (0.86)	0.10 ± 0.03 (0.14)	0.51
15% Mn:$CsPbCl_3$	0.45 ± 0.02 (0.82)	0.1 ± 0.01 (0.18)	0.43

Appendix II

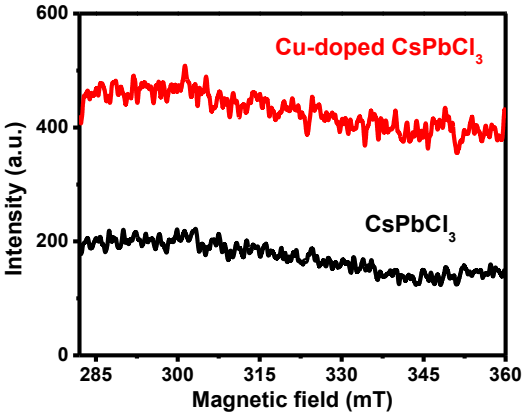

Figure A2.1. Room temperature EPR spectra of $CsPbCl_3$ and Cu-doped $CsPbCl_3$ NCs synthesized in presence of TOP. No characteristic signal of Cu^{2+} is observed.

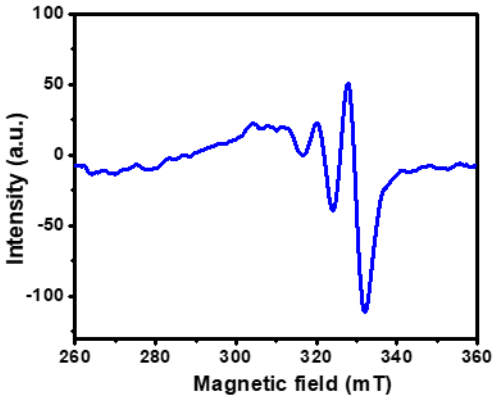

Figure A2.2. Room temperature EPR spectra of Cu-doped $CsPbCl_3$ NCs synthesized in presence of TOP. Characteristic EPR signal corresponding to Cu^{2+} is clearly observed.

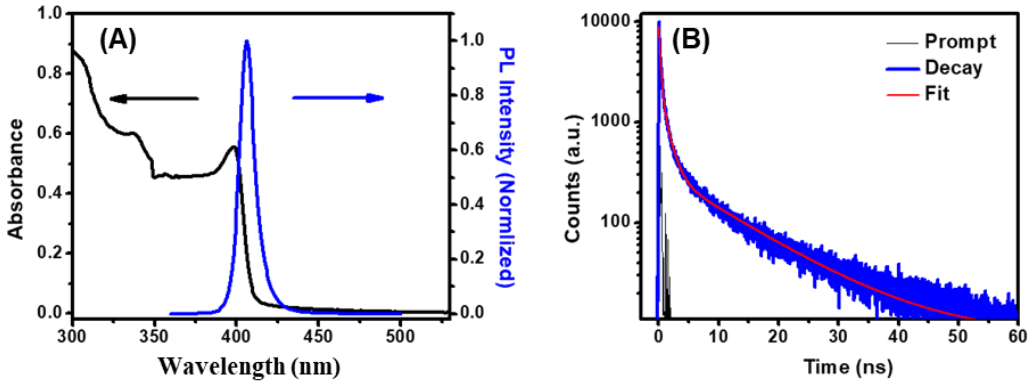

Figure A2.3. (A) Absorption and PL spectra of $CsPbCl_3$ and Cu^{2+}-doped $CsPbCl_3$ NCs (B) PL decay dynamics of NCs (λ_{ex} = 375 nm, λ_{em} = 403 nm).

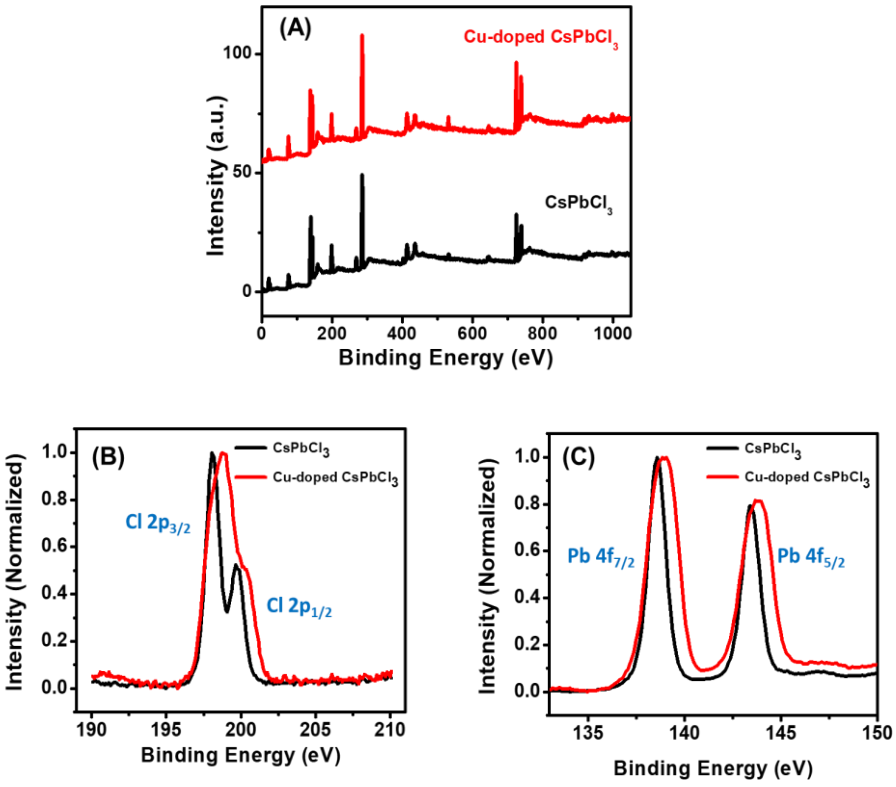

Figure A2.4. (A) XPS survey spectra of $CsPbCl_3$ and Cu-doped $CsPbCl_3$ NCs. (B) High resolution XPS spectra of Cl and Pb in undoped and doped-NCs.

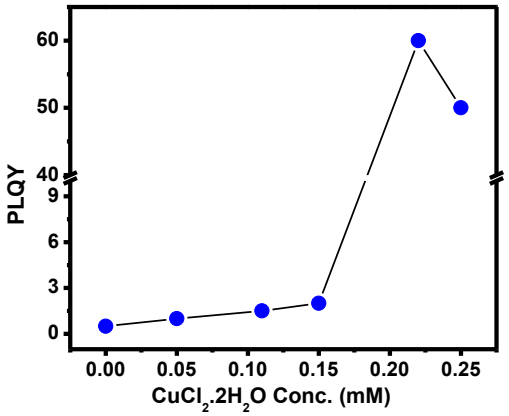

Figure A2.5. Variation of PLQY on varying content of $CuCl_2.2H_2O$ used during the synthesis of the NCs.

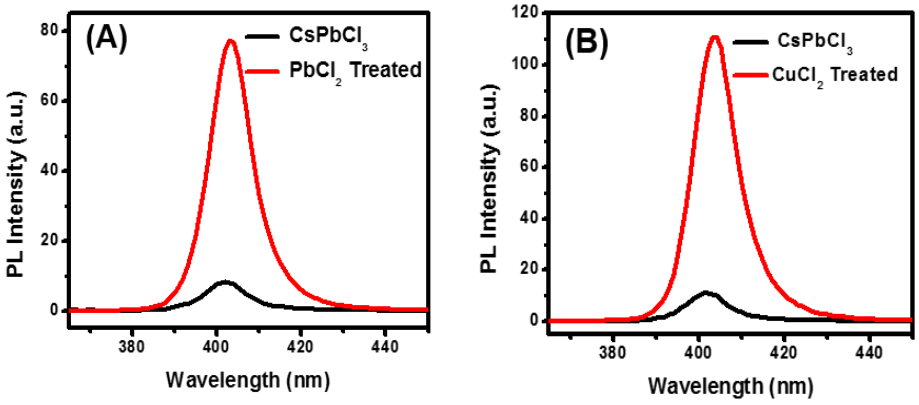

Figure A2.6. PL-enhancement of $CsPbCl_3$ NCs upon post-synthetic treatment with $PbCl_2$ (A) and $CuCl_2$. Both the salts were dissolved in toluene in presence of OA, OLA and TOP.

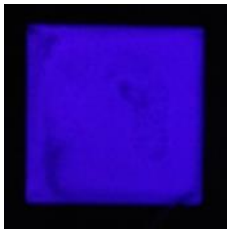

Figure A2.7. Digital image of Cu-doped $CsPbCl_3$ NCs film under UV light (365 nm).

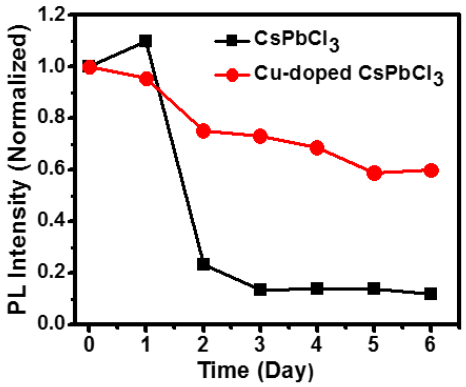

Figure A2.8. Stability of the $CsPbCl_3$ and Cu-doped $CsPbCl_3$ NCs under ambient condition, as evident form the PL of the respective systems.

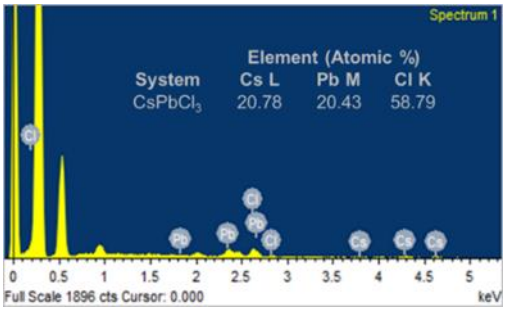

Figure A2.9. EDX spectrum and elemental atomic % of $CsPbCl_3$ NCs. The halide: lead ratio is calculated as 2.82 which indicates that the NCs are halide deficient.

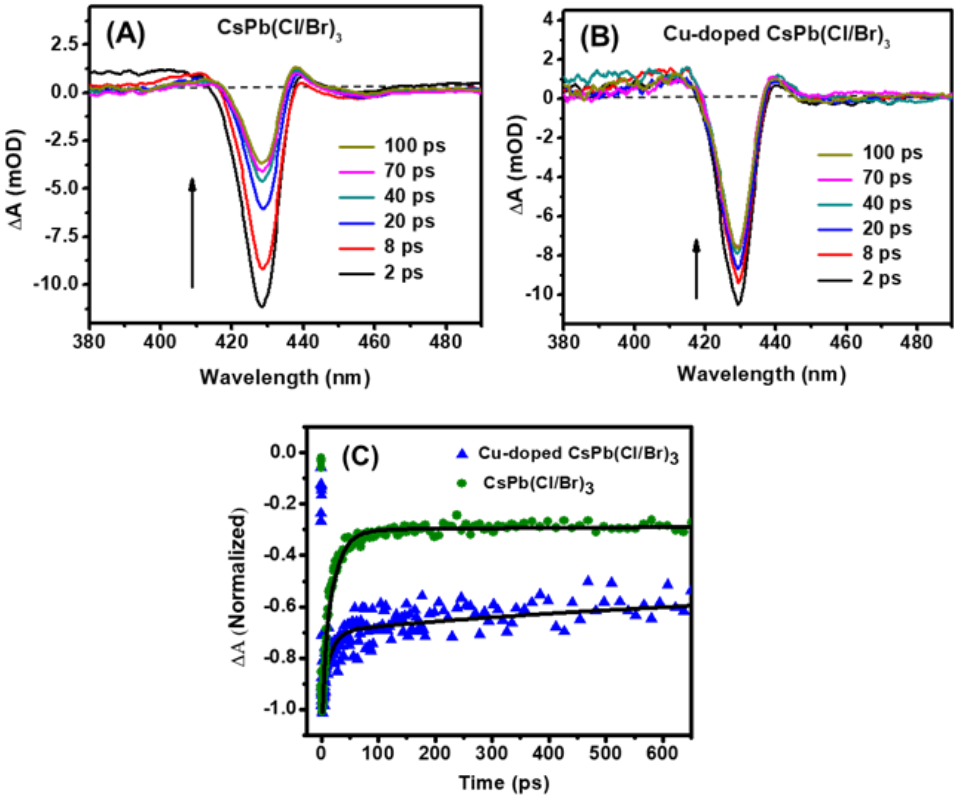

Figure A2.10. (A)-(B) TA spectra of $CsPb(Cl/Br)_3$ and Cu-doped $CsPb(Cl/Br)_3$ NCs of PL maxima of 430 nm (λ_{ex} = 350 nm) (D) Comparison of bleach recovery kinetics of the two samples monitored at their bleach maxima at 428 nm

Table A2.1. PL decay parameters of Cu-doped $CsPbCl_3$ NCs

System	τ_1 (a_1)/ ns	τ_2 (a_1)/ ns	τ_3 (a_1)/ ns	$<\tau_{amp}>$/ ns
Cu-doped $CsPbCl_3$	0.43 (0.82)	3.70 (0.13)	14.90 (0.04)	1.43

Table A2.2. PL decay parameters of halide-exchanged perovskite NCs

System	λ_{em} (nm)	τ_1 (a_1)/ ns	τ_2 (a_1)/ ns	τ_3 (a_1)/ ns	$<\tau_{amp}>$/ ns
$CsPb(Cl/Br)_3$		-	-	-	-
Cu-doped $CsPb(Cl/Br)_3$	430	0.41 (0.48)	5.00 (0.37)	14.90 (0.15)	4.3
$CsPb(Cl/Br)_3$		0.07 (0.80)	0.44 (0.19)	5.44 (0.01)	0.2
Cu-doped $CsPb(Cl/Br)_3$	460	-	2.60 (0.67)	5.60 (0.33)	3.6

Table A2.3. Kinetic parameters of bleach recovery dynamics of $CsPb(Cl/Br)_3$ and Cu-doped $CsPb(Cl/Br)_3$ NCs with PL maxima of 430 and 460 nm.

Systems	λ_{em} (nm)	Recovery components		
		$\tau_1(a_1)$ /ps	$\tau_2(a_2)$ /ps	$\tau_3(a_3)$ /ps
$CsPb(Cl/Br)_3$	430	3.5 ± 0.2 (0.21)	20.0 ± 1.7 (0.54)	> 850 (0.25)
Cu-doped $CsPb(Cl/Br)_3$		-	30.0 ± 1.5 (0.28)	> 1000 (0.72)
$CsPb(Cl/Br)_3$	460	3.1 ± 0.3 (0.16)	30.2 ± 2.0 (0.52)	> 850 (0.32)
Cu-doped $CsPb(Cl/Br)_3$		-	23.6 ± 4.1 (0.16)	> 850 (0.84)

Appendix III

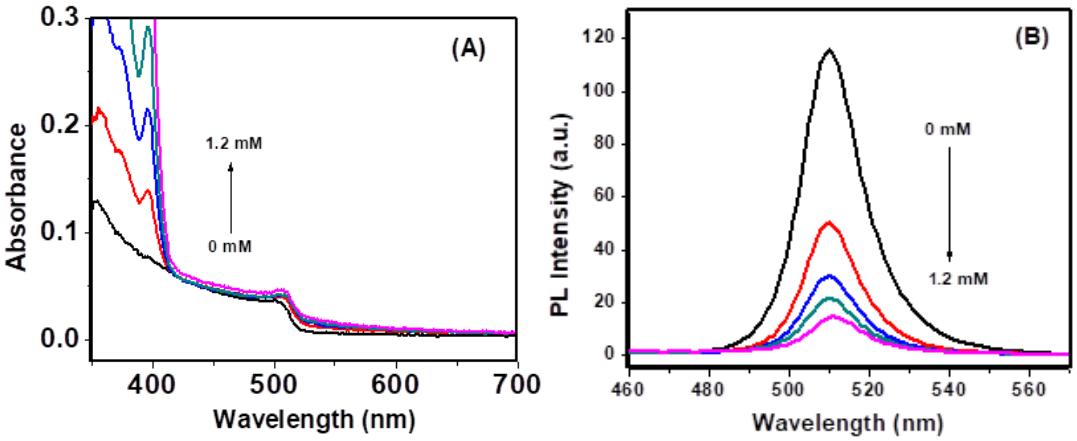

Figure A3.1. (A) Change in absorption and (B) PL spectra upon successive addition of AMP in toluene solution of $CsPbBr_3$ NCs.

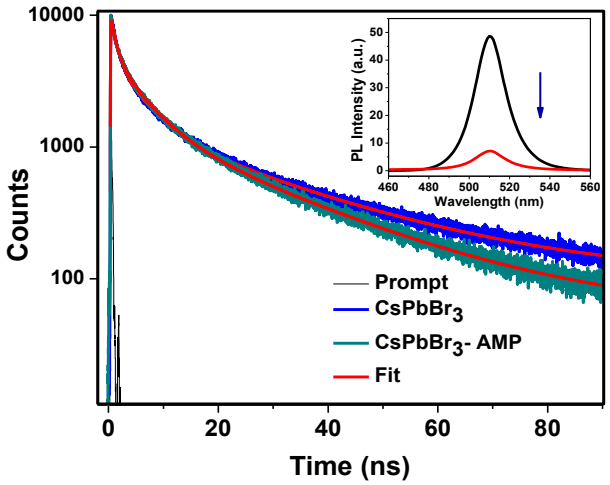

Figure A3.2. PL decay of $CsPbBr_3$ NCs, without and in presence of AMP. The shown PL decay in presence of AMP is for the maximum PL quenched sample (Corresponding PL spectra is given in insets).

Table A3.1. PL decay parameters of $CsPbBr_3$ in absence and presence of AMP.

System	τ_1 (a_1)/ ns	τ_2 (a_2)/ ns	τ_3 (a_3)/ ns	$<\tau_{amp}>$/ ns
$CsPbBr_3$	5.26 (0.32)	26.5 (0.14)	1.01 (0.54)	5.94
$CsPbBr_3$-AMP	5.40 (0.33)	23.6 (0.16)	1.06 (0.51)	6.09

Table A3.2. PL decay parameters of $CsPbI_3$ in absence and presence of AMP.

System	τ_1 (a_1)/ ns	τ_2 (a_2)/ ns	τ_3 (a_3)/ ns	$<\tau_{amp}>$/ ns
$CsPbI_3$	34.7 (0.34)	214.0 (0.13)	4.23 (0.53)	41.8
$CsPbI_3$-AMP	31.9 (0.29)	226.0 (0.12)	3.29 (0.59)	38.3

Appendix IV

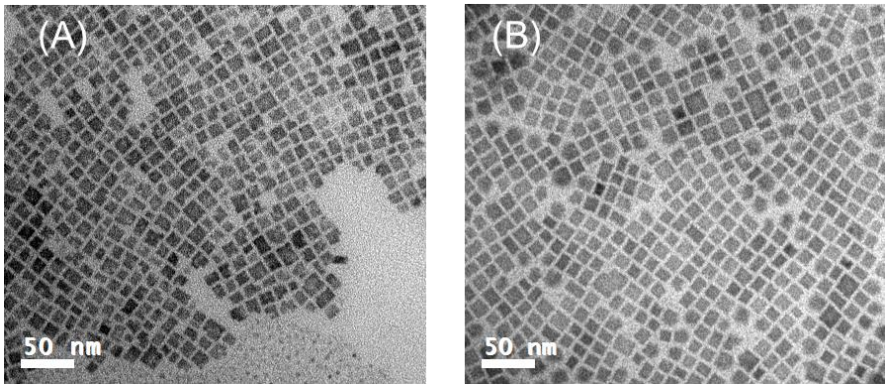

Figure A4.1. TEM images of the (A) $MAPbBr_3$ and (B) $FAPbBr_3$ NCs.

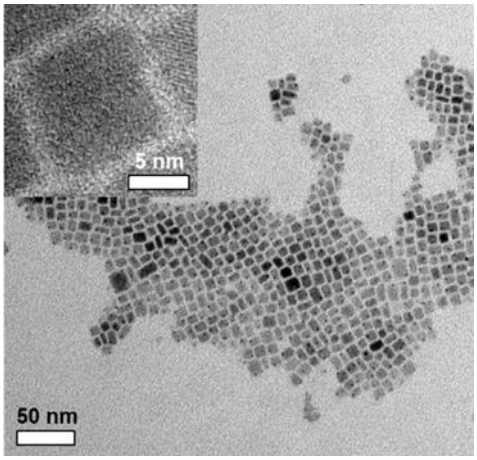

Figure A4.2. TEM image of $CsPbBr_3$-MTH showing no morphological changes upon ligand exchange.

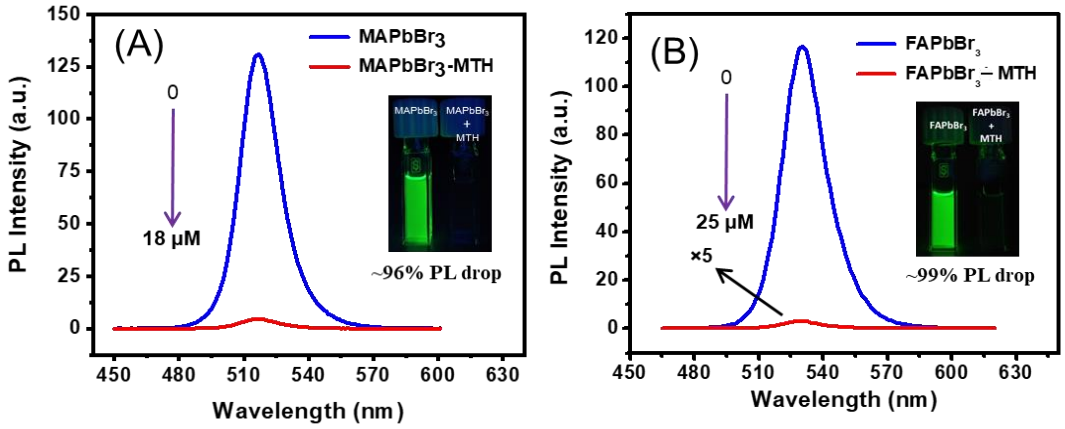

Figure A4.3. (A)-(B) PL of $APbBr_3$ (A= MA and FA) and $APbBr_3$-MTH (λ_{ex}= 400 nm). Digital images of the respective solutions are also shown.

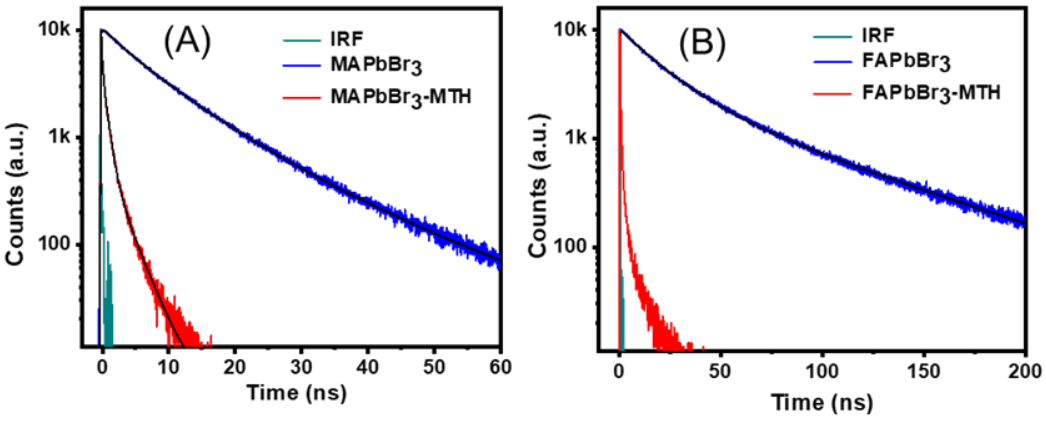

Figure A4.4. PL decay profiles (λ_{ex}=404 nm) of (A) $MAPbBr_3$ and $MAPbBr_3$-MTH and (B) $FAPbBr_3$ and $FAPbBr_3$-MTH, monitored at 519 nm and 530 nm, respectively.

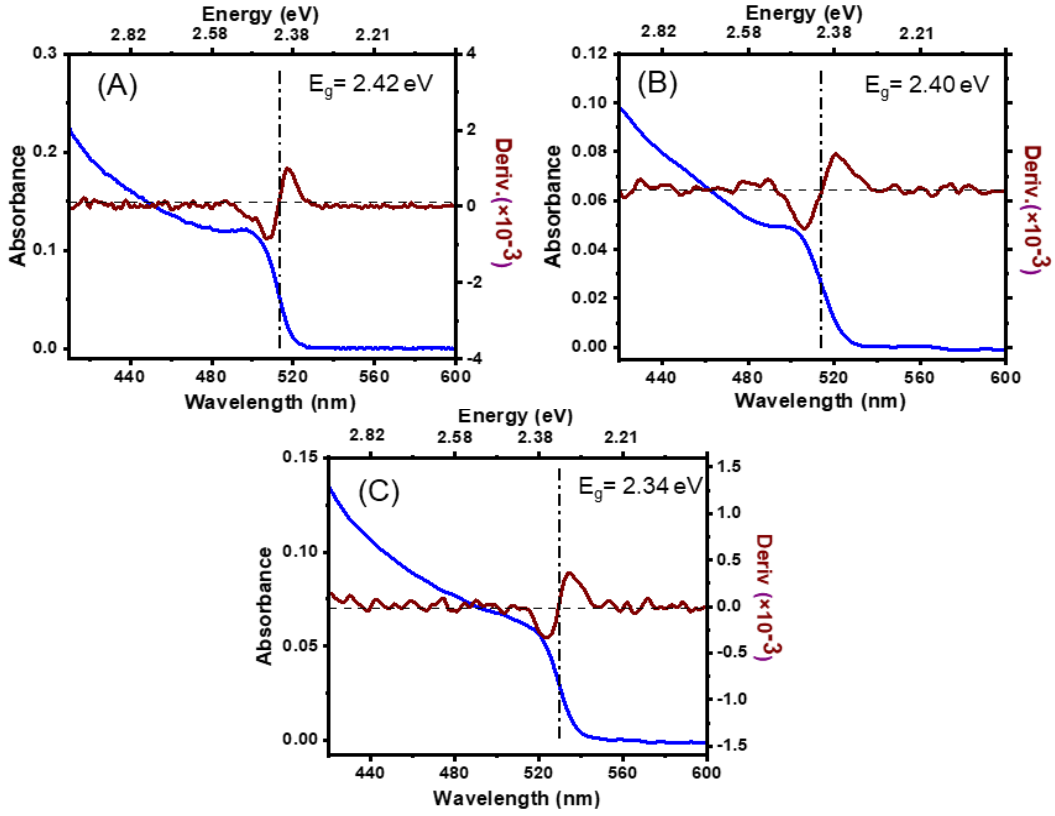

Figure A4.5. Derivative plot of the absorption spectra for the estimation of the band gap of the (A) $CsPbBr_3$, (B) $MAPbBr_3$ and (C) $FAPbBr_3$ NCs.

.

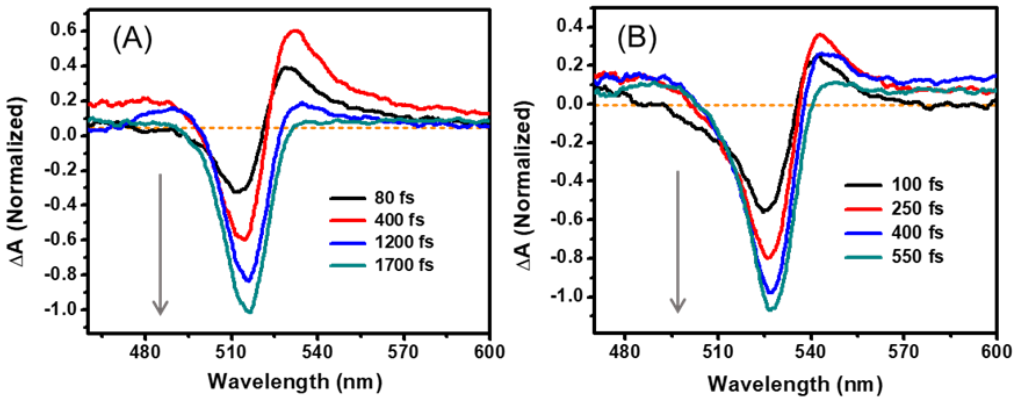

Figure A4.6. Early-time TA spectra of (A) $MAPbBr_3$ and (B) $FAPbBr_3$ NCs under 353 nm and 360 nm excitation, respectively.

.

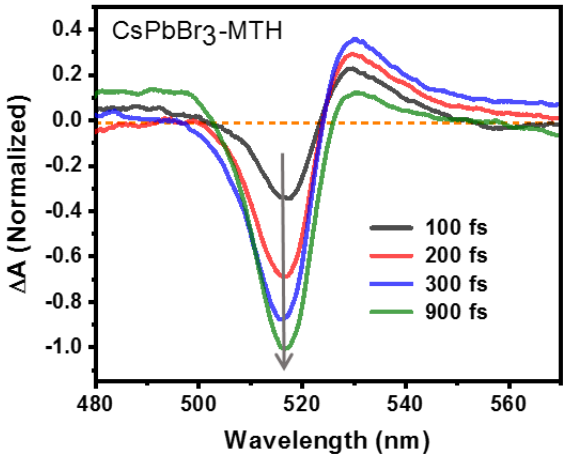

Figure A4.7. Early-time TA spectra of $CsPbBr_3$-MTH under 350 nm excitation.

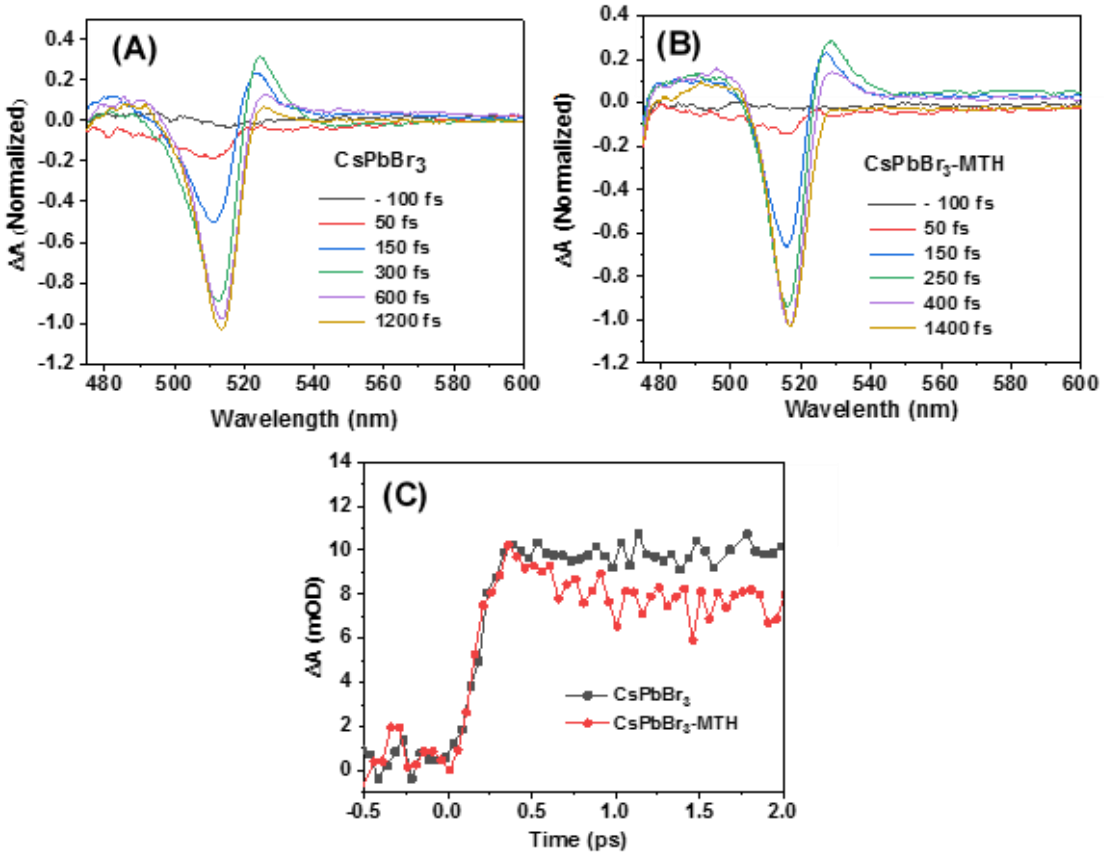

Figure A4.8. (A)-(B) Early-time TA spectra of $CsPbBr_3$ and $CsPbBr_3$-MTH under 470 nm excitation. Panel (C) represent corresponding bleach formation kinetics.

.

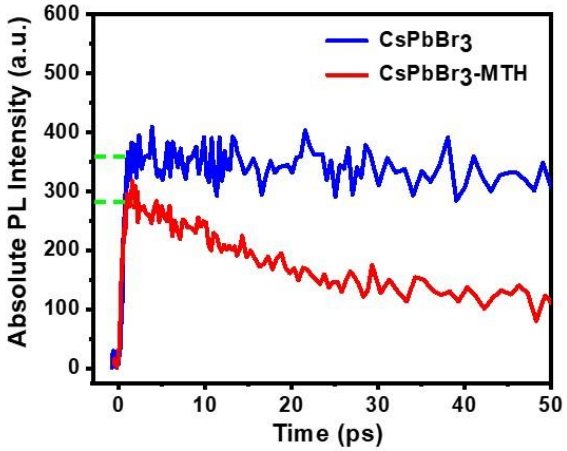

Figure A4.9. Comparison of the PL intensity counts of $CsPbBr_3$ and $CsPbBr_3$-MTH NCs.

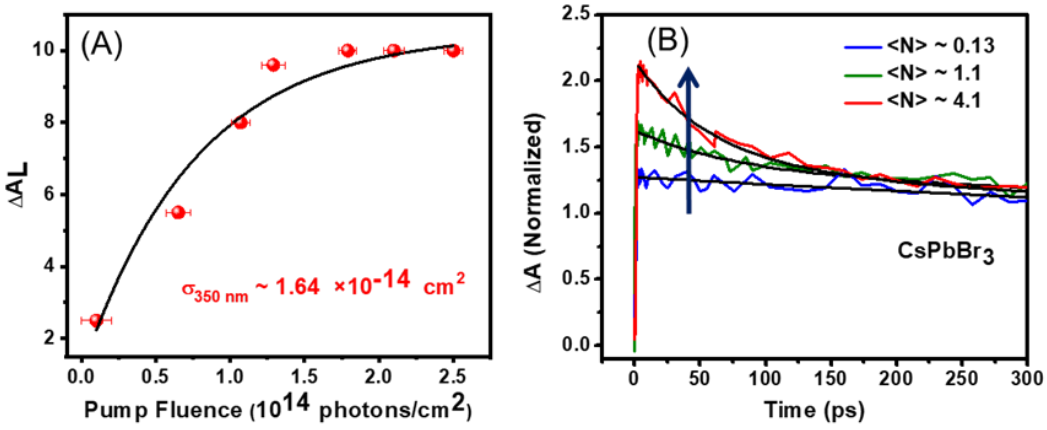

Figure A4.10. (A) Plot of late time bleach amplitude (at 500 ps) as a function of laser fluence and fit to the data with equation $\Delta A_L = [1-\exp(-J_p\sigma)]$. We obtained the value of absorption cross section (σ) of $CsPbBr_3$ NCs at 350 nm (pump wavelength), which later was multiplied with the lowest pump fluence (J_p) to obtain the value of average number of excitons (<N>). This approach to calculate the <N> is well established and have been used extensively. Under lowest pump fluence <N> is estimated as 0.13. (B) Bleach recovery kinetics of $CsPbBr_3$ NCs under varying excitation fluence

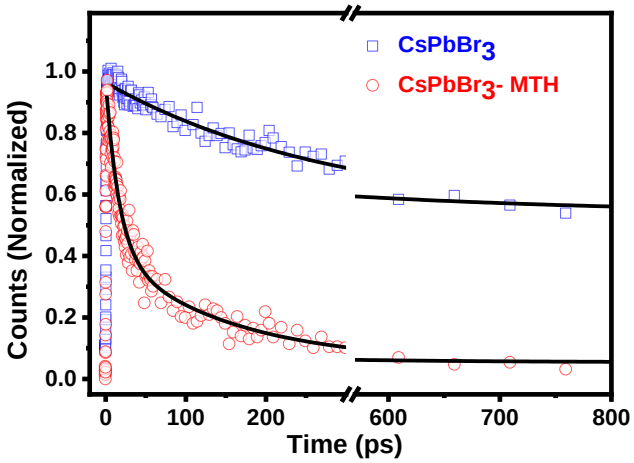

Figure A4.11. PL decay profiles (λ_{ex} = 400 nm) of $CsPbBr_3$ and $CsPbBr_3$-MTH as obtained by PL UC measurements.

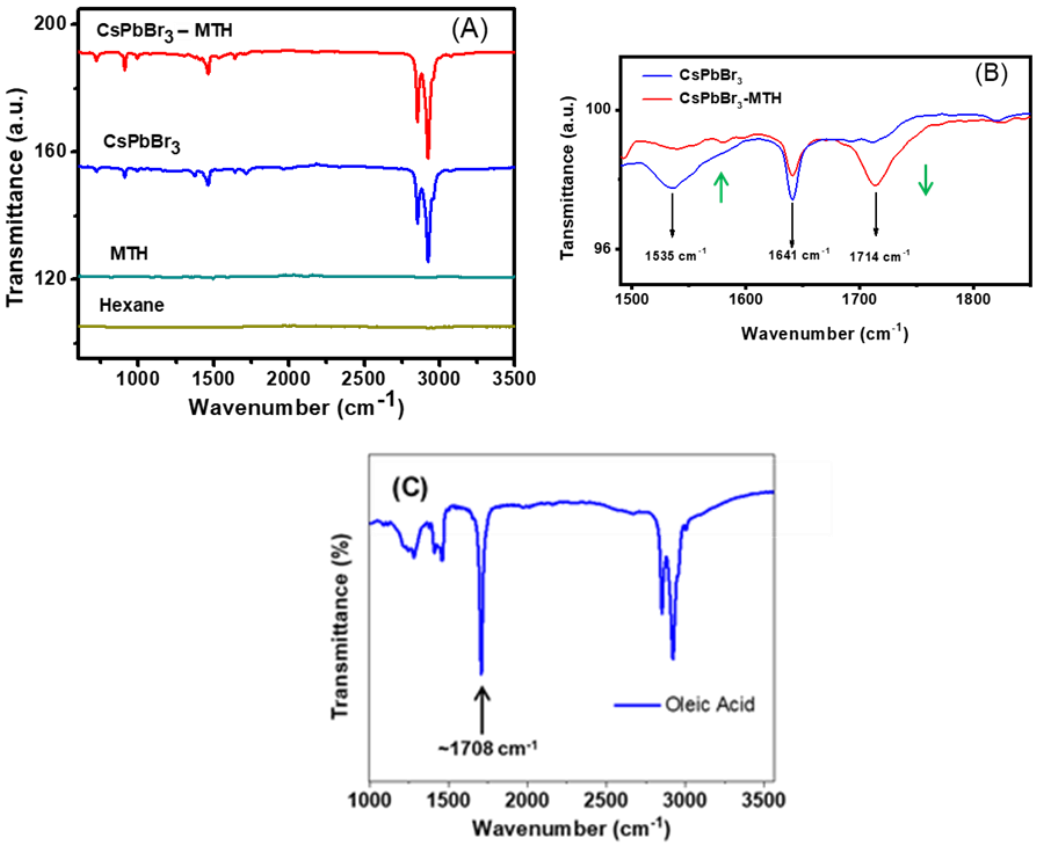

Figure A4.12. (A) FTIR spectra of $CsPbBr_3$ and $CsPbBr_3$-MTH. (B) Enlarged view FTIR spectra in the region of interest. The peak intensity around 1535 cm^{-1}, which appears in $CsPbBr_3$ NCs due to $-CO_2^-$ stretching of oleic acid (OA), gets significantly reduced in case of $CsPbBr_3$-MTH. In expense of this, a new peak at around 1714 cm^{-1} appears for $CsPbBr_3$-MTH which is due to free –C=O stretching. This is further confirmed with the IR spectra of free OA where the C=O stretching appears at ~1708 cm^{-1} (Panel C). Thus it is evident that MTH replaces some of the oleates present on the NCs surface and that is why the IR peaks corresponding to free OA appears. Replacement of some of the oleylamine (OLA) from the NCs surface may also take place (As evident from the reduced IR peak intensity at 1641 cm^{-1} which appears due to –NH stretching of OLA).

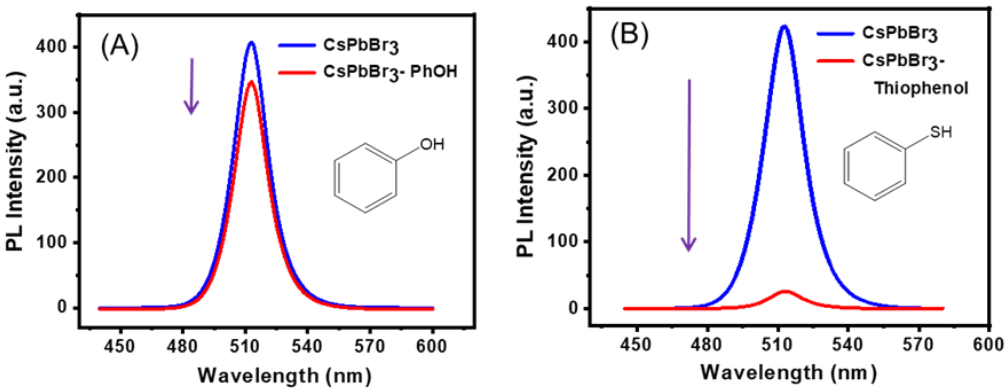

Figure A4.13. PL quenching of $CsPbBr_3$ NCs with phenol (A) and (B) thiophenol.

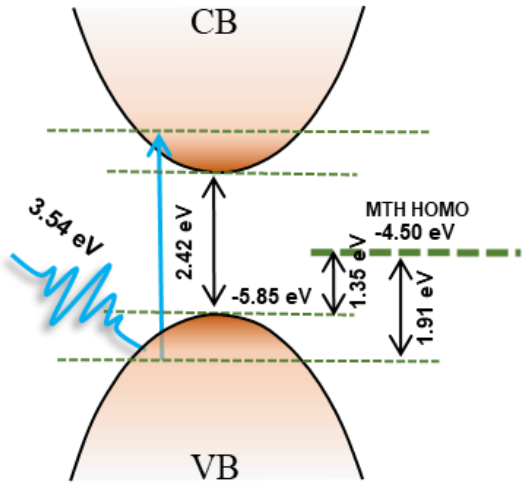

Figure A4.14. Energy schematic highlighting the driving forces for cold and hot hole transfer from $CsPbBr_3$ to MTH. Hot holes are generated upon 350 nm (3.54 eV) photoexcitation.

Table A4.1. PL decay parameters of $CsPbBr_3$, $MAPbBr_3$ and $FAPbBr_3$ NCs. In all $APbBr_3$-MTH cases the PL decay parameters could not be resolved from the IRF.

System	τ_1[ns]/ (a_1)	τ_1[ns]/ (a_1)	τ_{avg} [ns]
$CsPbBr_3$	3.72 (0.72)	9.20 (0.28)	5.26
$CsPbBr_3$-MTH	--	--	--
$MAPbBr_3$	5.73 (0.60)	13.6 (0.40)	8.87
$MAPbBr_3$-MTH	--	--	--
$FAPbBr_3$	18.9 (0.71)	65.6 (0.29)	32.44
$FAPbBr_3$-MTH	--	--	--

Nanoscale

PAPER

View Article Online
View Journal | View Issue

Check for updates

Cite this: *Nanoscale*, 2017, **9**, 16722

Luminescence tuning and exciton dynamics of Mn-doped $CsPbCl_3$ nanocrystals†

Apurba De, Navendu Mondal and Anunay Samanta *

Received 10th September 2017,
Accepted 28th September 2017

DOI: 10.1039/c7nr06745c

rsc.li/nanoscale

Mn-Doped perovskite nanocrystals (NCs) are a new class of materials offering exciting opportunities to control over their optical and magnetic properties. Herein, we report a series of Mn-doped $CsPbCl_3$ NCs exhibiting a tunable Mn photoluminescence (PL) band with a PL peak wavelength pushed up to 625 nm and tuned over a range of 40 nm, the largest achieved so far, by only varying the Mn content. The X-band EPR data and Mn PL decay behaviour of the NCs reveal that the exchange interaction between Mn^{2+} ions is mainly responsible for a large shift of the Mn PL band. Ultrafast pump–probe measurements show that exciton–dopant energy transfer in these NCs is slower (~50–100 ps) than trapping of the carriers (~8–10 ps) in the host lattice. The large PL tuning reported here along with the insights into the mechanism of tuning and carrier dynamics are expected to boost the potential of Mn-doped $CsPbCl_3$ NCs in light-powered devices.

Published on 03 October 2017. Downloaded by University of Hyderabad on 11/11/2017 07:54:08.

1. Introduction

Doping of semiconductor nanocrystals (NCs) with transition metal ions can generate new optical, electronic and magnetic properties through an energy or charge transfer interaction between the host and dopant.[1–6] Group II–IV quantum dots (QDs) doped with color-centered impurities like Mn^{2+} introduce dopant emission with a long photoluminescence (PL) lifetime, high quantum yield (QY), large Stokes shift minimizing self-absorption and better colloidal stability over undoped QDs.[7–9] In photo-excited Mn-doped NCs, transfer of energy from excitons to the dopant produces a PL band at ~2.12 eV corresponding to the $^4T_1$ to $^6A_1$ transition in Mn^{2+} with a long PL lifetime (a few ms) due to forbidden nature of the transition, thus making the system a potential candidate for efficient extraction of charge carriers.[10–12]

Recently, all-inorganic perovskite NCs, $CsPbX_3$ (X = Cl, Br, I), have emerged as promising materials for photovoltaic and optoelectronic applications.[13–16] Over the last few months, a number of studies have been undertaken on doping of all-inorganic perovskite NCs with metal ions,[17,18] especially Mn^{2+}.[19–24] It is found that Mn-doped $CsPbCl_3$ NCs enhance the stability and efficiency of photovoltaic devices when used as energy downshift layers with a solar energy harvester.[25] Potential application of these doped NCs as display materials requires tuning of the Mn PL band position. This, however, cannot be achieved like it is done for excitonic PL by varying the size and shape of the NCs. Attempts to tune the Mn PL peak position by varying the Mn-content in $CsPbCl_3$ NCs have so far been unsuccessful except in one case where Liu *et al.* could tune it by 18 nm by varying the temperature and Mn-content up to 46%.[22] Herein, we demonstrate that the peak wavelength of the Mn PL band in doped $CsPbCl_3$ NCs can be tuned by 40 nm (585 to 625 nm), the highest range achieved so far, using an Mn-content of only up to 15.5% at a fixed reaction temperature. X-band EPR and Mn PL decay measurements reveal an enhancement of the Mn–Mn exchange interaction at a higher Mn-content in these quantum confined NCs. The ultrafast transient absorption (TA) measurements reveal fast carrier trapping (~8–10 ps) in the host lattice and consequent reduction in the number of excitons participating in energy transfer (~50–100 ps) to the dopant sight.

2. Results and discussion

Both undoped $CsPbCl_3$ and a series of Mn-doped $CsPbCl_3$ NCs were synthesized at 185 °C by suitable modification of a reported hot-injection method (details are given in the Experimental section).[26] Inductively coupled plasma optical emission spectroscopy (ICP-OES) measurements show that Mn contents in these NCs are 1, 2, 7.5, 12, and 15.5 mol%, with respect to Pb, for added Mn precursor concentrations of 10, 20, 30, 40 and 60%, respectively (Table S1†). The transmission electron microscopy (TEM) images show a cubic morphology for both undoped and doped NCs with an average edge length of 7.0 ± 0.5 nm (Fig. 1B, C, and S1†), which is close to the Bohr

School of Chemistry, University of Hyderabad, Hyderabad-500 046, India.
E-mail: anunay@uohyd.ac.in

†Electronic supplementary information (ESI) available. See DOI: 10.1039/c7nr06745c

This journal is © The Royal Society of Chemistry 2017

Published on 03 October 2017. Downloaded by University of Hyderabad on 11/11/2017 07:54:08.

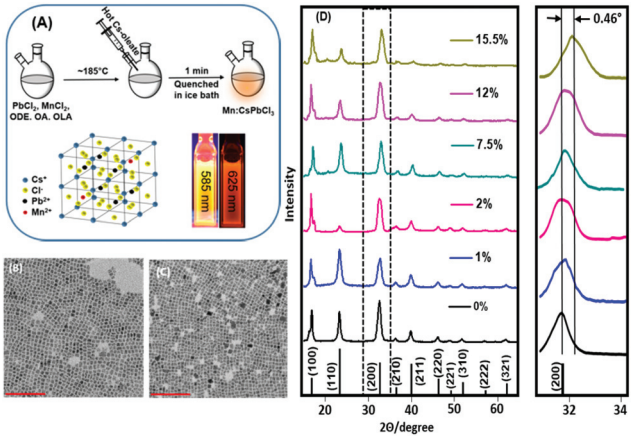

Fig. 1 (A) Schematic representation of the synthesis of Mn-doped $CsPbCl_3$ NCs. A representative model of Mn:$CsPbCl_3$ NCs showing replacement of some Pb positions by Mn is presented below. Digital images of two solutions differing in the Mn content are also shown to highlight the tunability of Mn PL. (B) and (C) TEM images of undoped and 12% Mn-doped NCs, respectively, showing a uniform size distribution. Scale bar shown here is 100 nm. (D) XRD patterns of undoped and Mn-doped $CsPbCl_3$ NCs with different Mn contents. An expanded view of the (200) peak indicating the shift towards a higher angle is shown in the right panel.

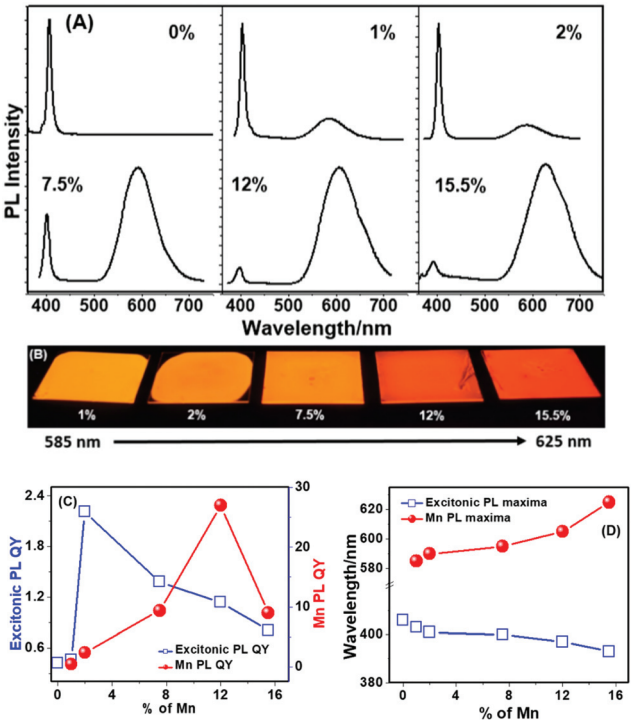

Fig. 2 (A) PL spectra showing dual emission of sets of materials having different Mn contents (in %). (B) Digital images of films of different Mn containing NCs showing the tunability of Mn PL are highlighted. Variations in the exciton and Mn PL QY and shift in the excitonic and Mn PL maxima for different Mn containing NCs are shown in panels (C) and (D), respectively.

excitonic diameter (~5 nm) of the host NCs.[26] The estimated Goldschmidt tolerance factor (t) and octahedral factor (μ) for all Mn-doped NCs fall under the range of stable perovskite formability (Fig. S2†).[27,28] The powder X-ray diffraction (XRD) patterns of the samples match with the standard cubic phase $CsPbCl_3$ (JCPDS: 84-0437, Fig. 1D), indicating the intactness of the crystalline nature of NCs upon doping. A monotonic shift of the XRD peaks to higher angles with increasing Mn-content is indicative of progressive lattice contraction on the substitution of Pb^{2+} (133 pm, CN = 6) with smaller Mn^{2+} (97 pm, CN = 6). A positive shift of the 2Θ value of 0.46° (Fig. 1D, right panel) for 15.5% Mn content is in agreement with the literature.[19]

The PL spectra of the undoped NCs exhibit a sharp excitonic PL band with a peak at ~406 nm (Fig. 2A). With increase in Mn-content a gradual blue shift of the band-edge absorption (Fig. S3†) and PL is observed despite negligible variations in the size of the NCs. For undoped NCs, the band gap of 3.05 eV, estimated from the Tauc plot (Fig. S4a†) is found to be consistent with the earlier report.[29] With increase in dopant content, this band gap increases due to the contraction of the $PbCl_6$ octahedral unit and consequent enhancement of the interaction between Pb and Cl. As the conduction band minimum (CBM) is dominated by Pb (6p) and Cl (3p) antibonding orbitals, the enhanced interaction results in a shift of the CBM towards higher energy.[30,31]

For Mn-doped NCs, in addition to the excitonic band, a broad PL band typical of $^4T_1$ to $^6A_1$ electronic transition in Mn^{2+}, is observed at a longer wavelength. It is evident that this band results from the transfer of excitation energy from photoexcited host NCs to Mn as the excitation spectrum corresponding to this PL band matches with the absorption spectrum of undoped NCs (Fig. S4b†).[32,33]

The variation of the QY of the excitonic and Mn PL on the Mn-content is depicted in Fig. 2C. A low PL QY (<1%) of an undoped system is expected to be due to the mid-gap (trap) states facilitating nonradiative deactivation in wide band gap $CsPbCl_3$ NCs. On doping, the Mn PL intensity is expected to increase at the expense of excitonic PL. However, for a very small Mn-content (2%), an increase in excitonic PL intensity is observed, which we attribute to the removal of pre-existing structural defects (chloride vacancies) in the host NCs by $MnCl_2$ used in the synthesis.[20] An increase in the Mn-content (from 2 to 12%) leads to an increase in Mn PL accompanied by a decrease of the excitonic emission intensity; a signature of efficient energy transfer from the host to the dopant ion. The highest Mn PL QY of ~27% is observed for 12% Mn-content, beyond which a drop is noted.[34]

Panel D of Fig. 2 depicts the dependence of the PL peak positions on the Mn-content for both the exciton and Mn PL bands. For excitonic PL, a blue shift (406 to 393 nm) due to lattice contraction is observed. On the other hand, the Mn PL band shifts towards red with an increase in the Mn content in the NCs. A 40 nm shift (from 585 to 625 nm) is observed for the concentration range studied here. The spectral shift is clearly observable by the naked eye, as illustrated in Fig. 2B.

Published on 03 October 2017. Downloaded by University of Hyderabad on 11/11/2017 07:54:08.

The wavelength tuning range demonstrated here is much larger than that (18 nm) observed very recently by Liu *et al.* by varying the Mn-content and reaction temperature. The red shift is presumably due to the lattice contraction induced change in the crystal field strength in the host lattice thereby influencing the energy gap between Mn-emissive atomic states.[35,36] However, we show in the following section that lattice contraction alone is not responsible for the red-shift of the Mn PL band.

The Mn PL is characterized by a long (~ms) lifetime (Fig. 3A and Table S2†) consistent with the spin-forbidden nature of the transition. On increase in dopant content, the PL decay dynamics becomes faster (from 1.30 to 0.51 ms) though the PL intensity is increased. We also observe a change in the PL decay behavior from single to bi-exponential one for a Mn-content of >2%. As single exponential decay behavior is characteristic of a homogeneous lattice environment experienced by Mn^{2+},[21] switching of the decay behavior to the bi-exponential one for the Mn-content of >2% indicates a non-uniform distribution of Mn^{2+} in the NCs. Whether this non-uniformity is restricted to the core or surface of the NCs or at both places is addressed in the next paragraph.

As a knowledge of the distribution of Mn^{2+} ions in the NCs is essential for interpretation of the above observation, we have studied the room temperature X-band EPR spectra of Mn-doped samples. The observation of six equally spaced lines of an equal intensity (with hyperfine coupling constant, A = 86 G) for 1 and 2% Mn-doped NCs (Fig. 3B) is in agreement with a nuclear spin (I) of 5/2 for Mn^{2+}. Close agreement of the measured A value with that reported for bulk Mn-doped $CsPbCl_3$ suggests that Mn resides inside the NCs.[37]

The distribution of Mn^{2+} in doped $CsPbCl_3$ NCs, as indicated by the EPR spectra, is uniform up to a Mn-content of 2%. The changes in the EPR spectral pattern, especially merging of individual signals leading to broadening of the spectra, with the dopant concentration clearly indicate that above 2%, Mn ions are no longer diluted in the NCs (like in for 1 and 2%) and they interact with each other.[38,39] For the highest Mn-content (15.5%) the signal collapses into an almost single broad line due to an enhanced exchange interaction between Mn-pairs. It is important to note that an unchanged A-value even for the highest Mn-content (15.5%) indicates that doped Mn remains inside the NCs rather on the surface.[40]

In exchange-coupled Mn^{2+} pairs, splitting of both the Mn ground state ($^6A_1$, I = 5/2) and the first excited state ($^4T_1$, I = 3/2) results in a reduced energy difference between the transition levels and red-shift of the emission band.[41] This coupling also partially lifts the selection rule resulting in a faster decay dynamics of Mn PL.[42] An abrupt change in both the EPR pattern and Mn PL decay behavior occurs for the same Mn-content (>2%), hence we conclude that in addition to the crystal field effect, the Mn–Mn exchange interaction also contributes to the red-shift of the Mn PL band at higher dopant concentrations (>2%).

To further explore the exciton–dopant energy transfer (EDET) process and to determine the factors that influence it, we have studied the temperature dependence of the PL. A steady decrease in the PL intensity of dual bands in doped NCs (Fig. 4) with an

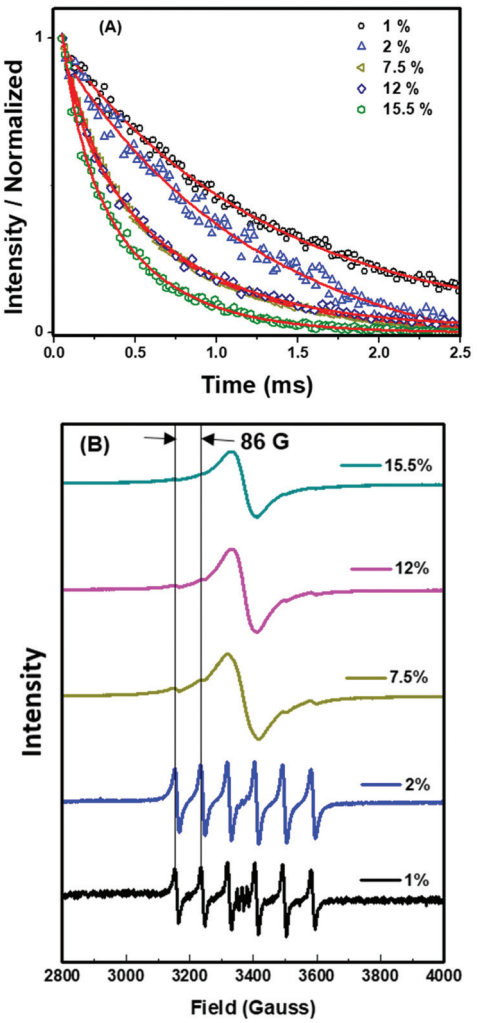

Fig. 3 Mn PL (λ_{exc} = 330 nm) decay behavior of the samples monitored at their respective emission maxima (A), and room temperature X-band EPR spectrum of the samples (B).

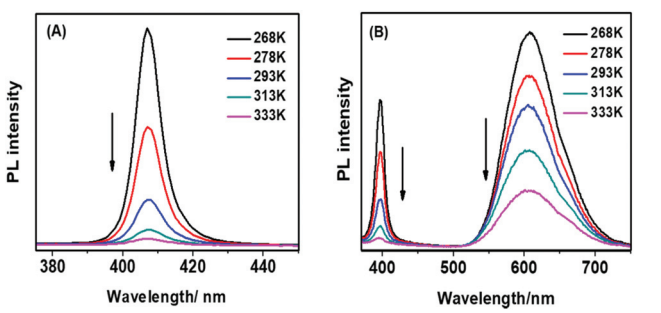

Fig. 4 Temperature dependent PL behavior of (A) $CsPbCl_3$ and (B) Mn:$CsPbCl_3$ showing a steady decrease in PL intensity with an increase in temperature.

This journal is © The Royal Society of Chemistry 2017

Published on 03 October 2017. Downloaded by University of Hyderabad on 11/11/2017 07:54:08.

increase in temperature from 268 to 333 K is observed. The decrease of the PL intensity of the excitonic band, which is very similar in both doped and undoped NCs, is mainly due to greater carrier trapping (a thermally activated process) at higher temperatures. As the Mn PL intensity is determined by the rates of competitive EDET and carrier trapping processes, the observed drop of the PL intensity must be due to faster carrier trapping at a higher temperature (that leaves fewer excitons to participate in EDET). As no shift of the excitonic PL band is observed with temperature, the exchange coupling between the exciton and dopant remains unaffected and plays no role in this regard.[43]

The competitive carrier trapping and EDET processes are corroborated by femtosecond TA measurements on undoped and doped NCs under similar excitation conditions. These spectra consist of a bleach signal around the excitonic band (~393–405 nm) and a positive photoinduced absorption band (~360–420 nm) (Fig. S5a–d†). As no additional feature due to doping could be observed in doped NCs, we rely on the bleach recovery dynamics for the estimation of the energy transfer rate. The bleach recovery kinetics recorded in the 0–1 ns time range for all samples are found to be best represented by a bi-exponential function (as assessed by the fit residuals). In the case of undoped NCs, the bleach recovery is represented by a fast (8.3 ps, 73%) and a relatively slow (160 ps, 27%) component (Table 1). The fast component can arise from carrier trapping or multi-exciton annihilation. However, we rule out the latter possibility considering that all TA measurements have been performed with very low excitation fluence (1.3×10^{13} photons per cm^2). The high amplitude of carrier trapping is consistent with a low QY (<1%) of our samples of $CsPbCl_3$ NCs. We assign the slow component to the non-radiative recombination process based on the literature.[44,45] It is to be noted in this context that the radiative recombination time constant cannot be extracted from these data as it extends well beyond our experimental time window.

For a small doping content (up to 2%), the fast (trapping) component remains almost the same, but the recombination time and its amplitude (Table 1) are increased, which is also evident from the bleach recovery dynamics presented in Fig. 5. The observation is clearly a reflection of the removal of pre-existing structural defects in the host lattice upon the incorporation of a small Mn-content, which is consistent with our steady state findings.

Table 1 Bleach recovery time constants and the corresponding amplitudes of undoped and doped NCs of varying Mn-contents

	Decay components	
Systems	τ_1 (a_1)/ps	τ_2 (a_2)/ps
Undoped $CsPbCl_3$	8.3 ± 0.4 (0.73)	160.8 ± 10.0 (0.27)
1% Mn:$CsPbCl_3$	10.6 ± 1.8 (0.60)	450.0 ± 10.2 (0.40)
2% Mn:$CsPbCl_3$	9.0 ± 1.0 (0.59)	510.0 ± 10.0 (0.41)
7.5% Mn:$CsPbCl_3$	7.2 ± 0.8 (0.41)	138.0 ± 9.3 (0.59)
12% Mn:$CsPbCl_3$	7.0 ± 1.0 (0.43)	78.0 ± 8.3 (0.57)
15.5% Mn:$CsPbCl_3$	7.2 ± 0.5 (0.45)	48.0 ± 6.7 (0.55)

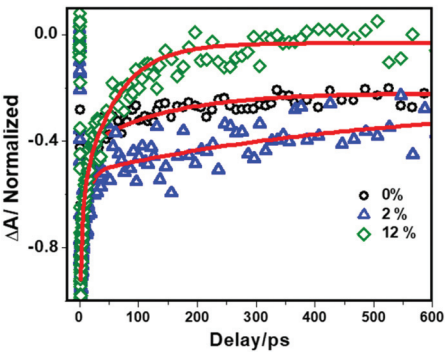

Fig. 5 Comparison of bleach recovery kinetics of 0, 2% and 12% Mn-doped $CsPbCl_3$ NCs, monitored at their excitonic bleach maxima.

For higher dopant contents (>2%), the bleach recovery becomes faster (Fig. 5) with no change in the fast (trapping) component (Table 1). Acceleration of the bleach recovery kinetics with an increase in the dopant content above 2% indicates an additional ultrafast nonradiative (EDET) process not observable for a low Mn-content (<2%) due to an opposing crystal stabilization effect. It is evident that the energy transfer cannot compete with the fast trapping component rather it affects only the long component. This observation is in line with the recent report on Mn-$CsPbCl_3$ NCs which appeared during the preparation of our manuscript.[46] In the present case, we have estimated the energy transfer time scale from the extent of a decrease in a longer time constant and it is found to be ~92 and ~53 ps for 12 and 15.5% Mn-doped $CsPbCl_3$ NCs, respectively. It is also to be noted that, after 2% dopant content, the host becomes modified (with increased τ_2); hence the estimation of the energy transfer (for 12 and 15.5%) is carried out with respect to 2% rather than 0%.

The above findings seem to suggest that the EDET efficiency can be further improved by reducing the trap centers in the host lattice. To validate this assignment we have carried out similar experiments with $CsPb(Cl/Br)_3$ as a host which offers a higher excitonic PL QY with less trap centers compared to $CsPbCl_3$. However, the Mn PL QY in Mn:$CsPb(Cl/Br)_3$ is found to be much lower than that in Mn:$CsPbCl_3$ (Fig. S6a and b†). The bleach recovery dynamics is also not affected by the Mn-content (Fig. S6c†) suggesting poor coupling between the exciton and dopant due to a lower band gap of the host lattice. Hence, the strength of coupling between the host and the dopant ions is one of the key factors that determines the efficiency of the EDET process.

3. Conclusions

Before drawing the conclusion, we attempt to rationalize our findings considering the recent studies, where small/no tuning of the Mn PL band could be observed.[19,20,22] We think the key to achieving large tuning in our case is the stronger confinement in our NCs (~7 nm) as compared to the others

Published on 03 October 2017. Downloaded by University of Hyderabad on 11/11/2017 07:54:08.

(>10 nm). The close proximity of the Mn^{2+} ions in the confined space gives rise to Mn–Mn exchange coupling, which modulates the Mn PL energy gap. The other factor contributing to the shift of the Mn PL band is lattice contraction induced by smaller Mn size. The Mn PL QY of the doped NCs is determined by the net effect of two opposing factors, the EDET and Mn–Mn exchange interaction. Hence, the drop in the Mn PL QY at the highest Mn content is due to the dominating Mn–Mn exchange interaction over the EDET process.

In conclusion, we demonstrate the largest tuning of the Mn-doped PL band in perovskite NCs and identify the factors that contribute to it. Further, the exciton dynamics of these NCs provides insight into the time constants of the photo-induced processes. We expect these findings will help improving the optical response of these substances further, thus making them useful in practical applications.

4. Experimental section

4.1 Chemicals used

Cesium carbonate (99.9%), lead chloride (99.999%), manganese(II) chloride (anhydrous, beads, 99.99%), octadecene (ODE, 90%), oleic acid (OA, 90%) and oleylamine (OLA, 70%) were purchased from Sigma-Aldrich. These chemicals were used for synthesis without further purification. Dried toluene was used as solvent in all optical studies.

4.2 Synthesis

$CsPbCl_3$ NCs were synthesized by following the hot injection method reported by Protesescu *et al.* with some minor modifications.[26] In brief, 0.16 g Cs_2CO_3, 6 ml ODE and 0.5 ml OA were taken in a double-necked round-bottom flask (RB) and the mixture was dried under vacuum for 1 hour at 120 °C. Then it was heated under a N_2 atmosphere until all Cs_2CO_3 reacted with OA to form cesium-oleate, which was kept at 120 °C before its use to avoid precipitation.

0.052 g of $PbCl_2$, 5 ml ODE, 0.5 ml OA, and 0.5 ml OLA were loaded in a 50 ml RB and the mixture was heated under vacuum at 105 °C. 1 ml TOP was injected for better solubility of $PbCl_2$. Then the temperature was increased to 185 °C and once it is reached, 0.45 ml of Cs-oleate was swiftly injected. After one minute the solution was cooled in an ice bath. The synthesized NCs were precipitated out of ODE by centrifugation and the supernatant liquid was discarded. The product was dispersed in dried toluene for further use.

For the synthesis of Mn-doped $CsPbCl_3$ NCs, $MnCl_2$ was used additionally in the mixture of $PbCl_2$, OLA and OA following the method described already. The $MnCl_2$ beads were ground well prior to their use. In contrast to the earlier study, where a higher temperature (210 °C) was used for the incorporation of Mn into the NCs,[22] we employed a moderate temperature (185 °C) and varied the Mn precursor content for the synthesis of Mn-doped NCs. The actual Mn-content in the synthesized NCs is determined through ICP-OES measurement. Detailed characterization of the NCs has been discussed in the ESI.†

Conflicts of interest

There are no conflicts to declare.

Acknowledgements

This work is supported by Grant No. EMR/2015/000582 and J. C. Bose Fellowship (to AS) of the Science and Engineering Research Board (SERB), Department of Science and Technology (DST), India. We also acknowledge the UPE support to our University from UGC and Femtosecond Laser Facility of the School. AD and NM thank UGC-BSR and CSIR, respectively, for Fellowships. Thanks are also due to the CCMB, Hyderabad for extending their TEM facility.

Notes and references

1 D. J. Norris, A. L. Efros and S. C. Erwin, *Science*, 2008, **319**, 1776–1779.
2 D. J. Norris, N. Yao, F. T. Charnock and T. A. Kennedy, *Nano Lett.*, 2001, **1**, 3–7.
3 N. Pradhan and D. D. Sarma, *J. Phys. Chem. Lett.*, 2011, **2**, 2818–2826.
4 D. Mocatta, G. Cohen, J. Schattner, O. Millo, E. Rabani and U. Banin, *Science*, 2011, **332**, 77–81.
5 N. Pradhan, S. Jana and B. B. Srivastava, *J. Am. Chem. Soc.*, 2011, **133**, 1007–1015.
6 N. Pradhan, S. D. Adhikari, A. Nag and D. D. Sarma, *Angew. Chem., Int. Ed.*, 2017, **56**, 7038–7054.
7 R. N. Bhargava, D. Gallagher, X. Hong and A. Nurmikko, *Phys. Rev. Lett.*, 1994, **72**, 416–419.
8 N. Pradhan and X. Peng, *J. Am. Chem. Soc.*, 2007, **129**, 3339–3347.
9 A. Nag, S. Chakraborty and D. D. Sarma, *J. Am. Chem. Soc.*, 2008, **130**, 10605–10611.
10 R. Beaulac, P. I. Archer, S. T. Ochsenbein and D. R. Gamelin, *Adv. Funct. Mater.*, 2008, **18**, 3873–3891.
11 R. Beaulac, P. I. Archer, J. V. Rijssel, A. Meijerink and D. R. Gamelin, *Nano Lett.*, 2008, **8**, 2949–2953.
12 P. K. Santra and P. V. Kamat, *J. Am. Chem. Soc.*, 2012, **134**, 2508–2511.
13 J. Liang, C. Wang, Y. Wang, Z. Xu, Z. Lu, Y. Ma, H. Zhu, Y. Hu, C. Xiao, X. Yi, G. Zhu, H. Lv, L. Ma, T. Chen, Z. Tie, Z. Jin and J. Liu, *J. Am. Chem. Soc.*, 2016, **138**, 15829–15832.
14 A. Swarnkar, A. R. Marshall, E. M. Sanehira, B. D. Chernomordik, D. T. Moore, J. A. Christians, T. Chakrabarti and J. M. Luther, *Science*, 2016, **354**, 92–95.
15 J. Song, J. Li, X. Li, L. Xu, Y. Dong and H. Zeng, *Adv. Mater.*, 2015, **27**, 7162–7167.
16 Y. Wang, X. Li, J. Song, L. Xiao, H. Zeng and H. Sun, *Adv. Mater.*, 2015, **27**, 7101–7108.
17 R. Begum, M. R. Parida, A. L. Abdelhady, B. Murali, N. M. Alyami, G. H. Ahmed, M. N. Hedhili, O. M. Bakr and O. F. Mohammed, *J. Am. Chem. Soc.*, 2017, **139**, 731–737.

 This journal is © The Royal Society of Chemistry 2017

Published on 03 October 2017. Downloaded by University of Hyderabad on 11/11/2017 07:54:08.

18 A. Swarnkar, V. K. Ravi and A. Nag, *ACS Energy Lett.*, 2017, **2**, 1089–1098.
19 W. Liu, Q. Lin, H. Li, K. Wu, I. N. Robel, M. J. Pietryga and V. I. Klimov, *J. Am. Chem. Soc.*, 2016, **138**, 14954–14961.
20 D. Parobek, B. J. Roman, Y. Dong, H. Jin, E. Lee, M. Sheldon and D. H. Son, *Nano Lett.*, 2016, **16**, 7376–7380.
21 W. J. Mir, M. Jagadeeswararao, S. Das and A. Nag, *ACS Energy Lett.*, 2017, **2**, 537–543.
22 H. Liu, Z. Wu, J. Shao, D. Yao, H. Gao, Y. Liu, W. Yu, H. Zhang and B. Yang, *ACS Nano*, 2017, **11**, 2239–2247.
23 G. Huang, C. Wang, S. Xu, S. Zong, J. Lu, Z. Wang, C. Lu and Y. Cui, *Adv. Mater.*, 2017, **29**, 1700095.
24 S. D. Adhikari, S. K. Dutta, A. Dutta, A. K. Guria and N. Pradhan, *Angew. Chem., Int. Ed.*, 2017, **56**, 8746–8750.
25 Q. Wang, X. Zhang, Z. Jin, J. Zhang, Z. Gao, Y. Li and S. F. Liu, *ACS Energy Lett.*, 2017, **2**, 1479–1486.
26 L. Protesescu, S. Yakunin, M. I. Bodnarchuk, F. Krieg, R. Caputo, C. H. Hendon, R. X. Yang, A. Walsh and M. V. Kovalenko, *Nano Lett.*, 2015, **15**, 3692–3696.
27 C. Li, X. Lu, W. Ding, L. Feng, Y. Gao and Z. Guo, *Acta Crystallogr., Sect. B: Struct. Sci.*, 2008, **64**, 702–707.
28 V. M. Goldschmidt, Die Gesetze der Krystallochemie, *Naturwissenschaften*, 1926, **14**, 477–485.
29 V. K. Ravi, G. B. Markad and A. Nag, *ACS Energy Lett.*, 2016, **1**, 665–671.
30 R. E. Brandt, V. Stevanović, D. S. Ginley and T. Buonassisi, *MRS Commun.*, 2015, **5**, 265–275.
31 W. Stam, J. J. Geuchies, T. Altantzis, K. H. W. Bos, J. D. Meeldijk, S. V. Aert, S. Bals, D. Vanmaekelbergh and C. M. Donega, *J. Am. Chem. Soc.*, 2017, **139**, 4087–4097.
32 N. Pradhan, D. Goorskey, J. Thessing and X. Peng, *J. Am. Chem. Soc.*, 2005, **127**, 17586–17587.
33 Y. Yang, O. Chen, A. Angerhofer and Y. C. Cao, *J. Am. Chem. Soc.*, 2006, **128**, 12428–12429.
34 The drop of the Mn PL QY for the 15.5% Mn-content is due to enhancement of the Mn–Mn exchange interaction and a consequent increase in the nonradiative deactivation rate.
35 N. Pradhan, *ChemPhysChem*, 2016, **17**, 1087–1094.
36 T. Zuo, Z. Sun, Y. Zhao, X. Jiang and X. Gao, *J. Am. Chem. Soc.*, 2010, **132**, 6618–6619.
37 J. A. Cape, R. L. White and R. S. Feigelson, *J. Appl. Phys.*, 1969, **40**, 5001–5005.
38 N. Pathak, S. K. Gupta, P. S. Ghosh, A. Arya, V. Natarajan and R. M. Kadam, *RSC Adv.*, 2015, **5**, 17501–17513.
39 P. A. G. Beermann, B. R. McGarvey, S. Muralidharan and R. C. Sung, *Chem. Mater.*, 2004, **16**, 915–918.
40 A. Nag, S. Sapra, S. S. Gupta, A. Prakash, A. Ghangrekar, N. Periswamy and D. D. Sarma, *Bull. Mater. Sci.*, 2008, **31**, 561–568.
41 L. Shi, Y. Huang and H. J. Seo, *J. Phys. Chem. A*, 2010, **114**, 6927–6934.
42 J. C. Zhang, L. Z. Zhao, Y. Z. Long, H. D. Zhang, B. Sun, W. P. Han, X. Yan and X. Wang, *Chem. Mater.*, 2015, **27**, 7481–7489.
43 Y. Park and D. H. Son, *Bull. Korean Chem. Soc.*, 2015, **36**, 757–761.
44 N. Mondal and A. Samanta, *Nanoscale*, 2017, **9**, 1878–1885.
45 G. H. Ahmed, J. Liu, M. R. Parida, B. Murali, R. Bose, N. M. AlYami, M. N. Hedhili, W. Peng, J. Pan, T. M. D. Besong, O. M. Bakr and O. F. Mohammed, *J. Phys. Chem. Lett.*, 2016, **7**, 3913–3919.
46 D. Rossi, D. Parobek, Y. Dong and D. Hee Son, *J. Phys. Chem. C*, 2017, **121**, 17143–17149.

This article is made available for a limited time sponsored by ACS under the ACS Free to Read License, which permits copying and redistribution of the article for non-commercial scholarly purposes.

ACS MATERIALS LETTERS

Cite This: ACS Materials Lett. 2019, 1, 116−122

www.acsmaterialslett.org

LETTER

Highly Luminescent Violet- and Blue-Emitting Stable Perovskite Nanocrystals

Apurba De, Somnath Das, Navendu Mondal,† and Anunay Samanta*

School of Chemistry, University of Hyderabad, Hyderabad 500046, India

Supporting Information

ABSTRACT: Among the lead halide perovskites, photoluminescence quantum yield (PLQY) of violet-emitting $CsPbCl_3$ nanocrystals (NCs) is the lowest (<5%). This is an impediment to the development of perovskite-based materials for optical applications covering the entire visible region. While PLQY of the green- and red-emitting perovskites of this class has been raised to near-unity, achieving a similar level for violet- and blue-emitting NCs is still quite challenging. Herein, we report a novel method of simultaneously passivating the surface defects and crystal disorder of violet-emitting $CsPbCl_3$ NCs to dramatically enhance (by a factor of ∼120) the PLQY and stability without affecting the peak wavelength (403 nm) and full-width at half-maximum (FWHM) of the photoluminescence (PL) band. We show that the addition of the correct quantity of $CuCl_2$ during the hot-injection synthesis of $CsPbCl_3$ NCs leads to doping of Cu^+ into the NCs, which rectifies octahedral distortion of the crystal and the Cl^- passivates the surface; the combined influence of the two results in huge PL enhancement. NCs emitting throughout the blue region (430-460 nm) with near-unity PLQY (92%−98%) can then be obtained by partial halide-exchange of the doped sample. Femtosecond transient absorption studies suggest suppression of the ultrafast carrier trapping process in doped NCs. The results help extending the utility of these materials in optical applications by covering the violet−blue region as well.

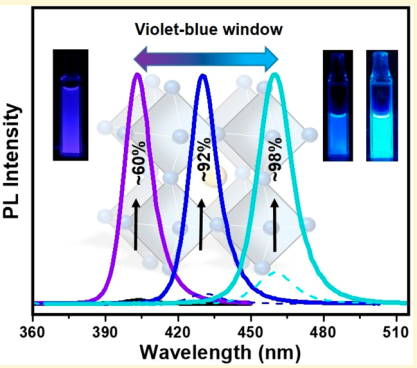

All-inorganic halide perovskites (ABX_3-type) have gained tremendous attention in recent years, because of their diverse applications in photovoltaics, light-emitting devices (LEDs), lasing, etc.[1−5] High photoluminescence quantum yield (PLQY) and ease of tunability of the photoluminescence (PL) band position across the entire visible region make these materials quite attractive for optical applications. Interestingly, although high PLQY (80%−95%) in the green−red region is reported for the nanocrystals (NCs) without any surface modification,[6] the violet-emitting $CsPbCl_3$ NCs suffer from low PLQY (<5%).[7−12]

Several reports have appeared during the past few months describing different methods of enhancing the PLQY of these NCs as high PLQY in the violet−blue region is essential for the development of white LEDs.[8−11,13−18] Recently, a PLQY of 60% is achieved for $CsPbCl_3$ NCs by room-temperature treatment of a colloidal solution of these NCs with yttrium chloride.[9] In another study, it is shown that addition of $NiCl_2$ during hot-injection synthesis of $CsPbCl_3$ NCs leads to doping of Ni^{2+} and remarkable enhancement of PLQY (up to 96%).[10] We have shown that post-synthetic treatment of $CsPbCl_3$ NCs with $CdCl_2$ can enhance the PLQY to near-unity.[11] In a more-recent study, Wang and co-workers have shown that post-synthetic treatment of $CsPbCl_3$ NCs with $CuCl_2$ enhances the PLQY up to 12%, whereas the bromide salt enhances the value to ∼92.6%, it shifts the PL maximum to 460 nm.[19] In another recent work, it is reported that the addition of $CuBr_2$ during hot-injection synthesis of $CsPbCl_3$ NCs leads to the formation of blue-emitting (peak between 450-460 nm) mixed-halide perovskites [$CsPb(Cl/Br)_3$] NCs with a PLQY of ∼80%.[20] Several metal-nitrate salts have also been used to increase the PLQY of $CsPbCl_3$ NCs up to ∼85% with an emission window of 460−470 nm.[15]

Thus, it is evident that, although blue-emitting NCs (λ_{max} = 450-470 nm) with impressive PLQY have been achieved, obtaining stable violet-emitting NCs (peak at <430 nm) with high PLQY is still a challenging exercise.[12] The halide vacancies, which create only shallow trap levels in $CsPbBr_3$, form deep trap states in $CsPbCl_3$, which promote nonradiative relaxation of the carriers and lower the PLQY of the system.[21] Besides, local structural disorder arising from halide vacancies and/or intrinsic distortion of the $[PbCl_6]^{4-}$ octahedron also contributes to carrier trapping in $CsPbCl_3$,[10,22] unlike in $CsPbBr_3$ or $CsPb(Cl/Br)_3$, which forms near-perfect crystal structure. Hence, one must take care of both halide vacancies and structural disorder to achieve a high PLQY for violet-emitting pure $CsPbCl_3$.

Received: April 8, 2019
Accepted: May 24, 2019
Published: May 24, 2019

Downloaded by UNIV OF HYDERABAD at 08:01:29:523 on July 01, 2019
from https://pubs.acs.org/doi/10.1021/acsmaterialslett.9b00101.

© 2019 American Chemical Society

DOI: 10.1021/acsmaterialslett.9b00101
ACS Materials Lett. 2019, 1, 116−122

Herein, we show that, when an optimum amount of $CuCl_2 \cdot 2H_2O$ is added during hot-injection synthesis of the $CsPbCl_3$ NCs, the PLQY of the system is greatly enhanced without any change in the peak wavelength. An impressive PLQY of doped mixed-halide NCs emitting in the blue region (430-460 nm) is then achieved. Quantitative information on the dynamics of the nonradiative trapping processes in doped and undoped NCs that determine the PLQY of the systems is also obtained through ultrafast transient absorption measurements.

While $CsPbCl_3$ NCs were prepared using a reported hot-injection method (details are given in the Electronic Supporting Information (ESI)),[6] for the synthesis of Cu-doped $CsPbCl_3$ NCs, an additional amount of $CuCl_2 \cdot 2H_2O$ (0.22 mmol)[23] was added in the reaction mixture consisting of 0.188 mmol $PbCl_2$, 5 mL of octadecene (ODE), 0.7 mL of oleic acid (OA), and 0.7 mL of oleylamine (OLA), and heated under vacuum at 120°C for 45 min. The blue solution turned colorless upon the addition of 1 mL of trioctylphosphine (TOP) under a N_2 atmosphere. After raising the temperature to 185 °C, 0.45 mL of cesium oleate was swiftly injected into it; then, after a minute, the mixture was quenched in ice water. The resulting solution was then centrifuged at 6800 rpm and the supernatant liquid was discarded. The precipitated NCs were then washed with methyl acetate before dispersing them in toluene for further studies. (The synthesis process for Cu-doped $CsPbCl_3$ NCs via the hot-injection method is depicted in Scheme 1.)

Scheme 1. Schematic Representation of the Synthesis of Cu-Doped $CsPbCl_3$ NCs in the Hot-Injection Method

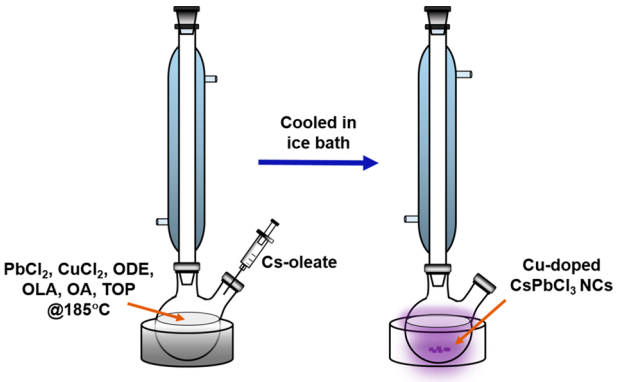

While the transmission electron microscopy (TEM) images of $CsPbCl_3$ NCs show cubic morphology with a wide size distribution and an average edge length of 9 ± 2.5 nm (Figure S1 in the ESI), the size distribution is narrower, with an average edge length of ~7 ± 1.0 nm (see Figure 1A, as well as Figure S1) for Cu-doped $CsPbCl_3$. Such a decrease in the size of the NCs size, coupled with improved monodispersity upon the introduction of metal halide during the synthesis, is consistent with previous reports.[10,24] High-resolution transmission electron microscopy (HRTEM) images indicate an interplanar distance of 0.57 nm for the (100) crystal planes in both cases.

Powdered X-ray diffraction (PXRD) patterns show cubic crystalline structure (Figure 1B) for both the NCs indicating no notable influence of $CuCl_2 \cdot 2H_2O$ on the crystal lattice. Elemental mapping of the field-emission scanning electron microscopy (FESEM) images show homogenous distribution of Cu, Cs, Pb, and Cl (Figures 2B–F) throughout the NCs. Energy-dispersive X-ray (EDX) measurements indicate a copper content of ~1.03% indicating ~5% substitution of Pb (Figure 2A) in doped NCs. No shift of the PXRD peaks toward higher 2θ values on copper doping is observed in our case. This is perhaps due to small amount of copper incorporated in the NCs.

The absence of any signal due to Cu^{2+} in the EPR spectrum of the doped NCs indicates the 1+ oxidation state of copper in the NCs (Figure S2 in the ESI). This finding explains the immediate color change of the reaction mixture from blue to colorless upon the addition of TOP during the synthesis of the NCs. The fact that TOP indeed acts as a reducing agent is confirmed by the observation that, in the absence of TOP, one obtains doped NCs, which exhibit characteristic EPR signal due to Cu^{2+} (Figure S3 in the ESI) and also a PLQY of ~60% (Figure S4 in the ESI).

X-ray photoelectron spectra (XPS) of $CsPbCl_3$ NCs show two distinct peaks at 138.6 and 143.5 eV corresponding to Pb $4f_{7/2}$ and Pb $4f_{5/2}$, respectively (Figure S5 in the SI). Two Cl signals corresponding to Cl $2p_{3/2}$ and Cl $2p_{1/2}$ are also observed at 198.1 and 199.7 eV, respectively. For Cu-doped $CsPbCl_3$, all peaks due to Pb 4f and Cl 2p shift to higher binding energy (Figure S5) indicating a halide-rich chemical environment around $[PbCl_6]^{4-}$ octahedra and a stronger Pb–Cl bond.[11,25] However, no XPS signal due to Cu^{+} could be observed, because of its low content or/and limited penetration of the XPS probe (typically up to ~2 nm from

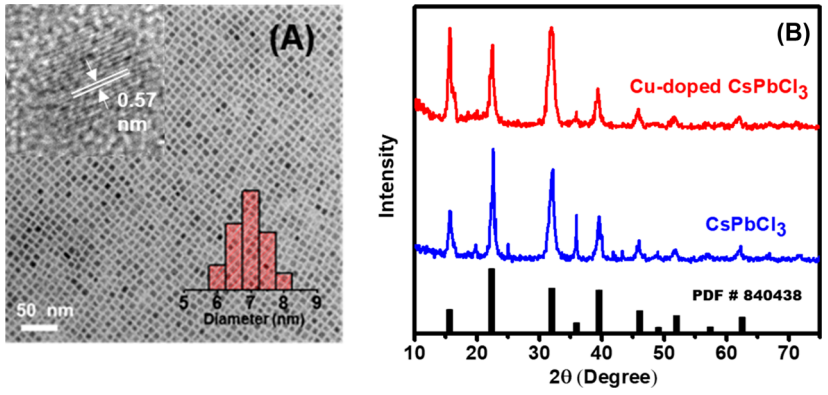

Figure 1. TEM images of (A) Cu-doped $CsPbCl_3$ NCs. Inset shows HRTEM images with the lattice spacing between (100) planes indicated in the image. (B) PXRD patterns of both NCs, confirming a cubic crystalline structure.

DOI: 10.1021/acsmaterialslett.9b00101
ACS Materials Lett. 2019, 1, 116–122

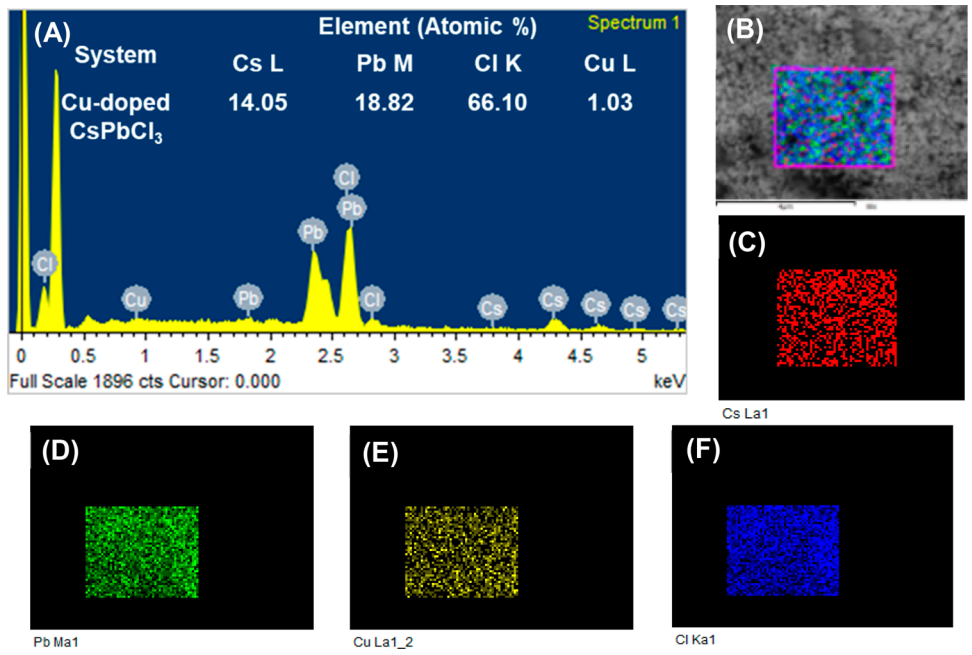

Figure 2. (A) EDX spectrum of Cu-doped $CsPbCl_3$ NCs. The chlorine:(lead + copper) ratio in the NCs is estimated as 3.33. (B) FESEM image of the scanning area of the NCs, showing distribution of all the elements. (C–F) Elemental mapping of Cs, Pb, Cu, and Cl in the scanned area of the NCs.

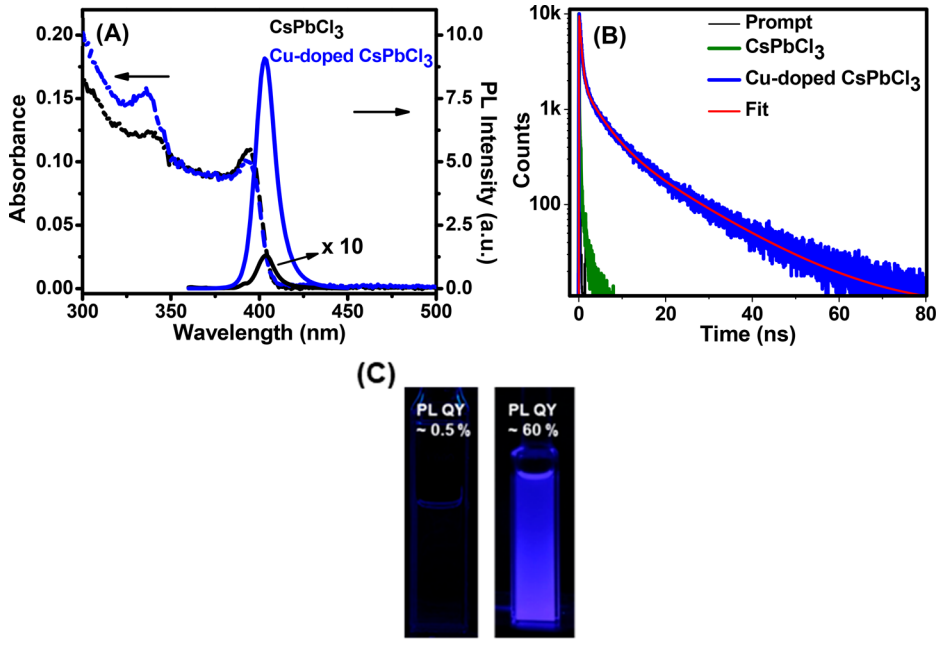

Figure 3. (A) Absorption and PL spectra of $CsPbCl_3$ and Cu-doped $CsPbCl_3$ NCs (B) PL decay dynamics of both the NCs (λ_{ex} = 375 nm, λ_{em} = 403 nm). (C) Digital images of the colloidal solutions of the NCs under UV light (λ_{ex} = 365 nm), where bright blue PL is clearly visible for Cu-doped $CsPbCl_3$ NCs.

the surface), which is a well-known limitation of this technique.[26] Not observing a dopant XPS signal, because of its low content, is not uncommon.[27] The presence of Cu (~5%) in the NCs is conclusively established by the EDX data. To further confirm the presence of Cu in the NCs, we performed inductively coupled plasma optical emission (ICP-OES) measurements, which indicates a copper content of ~7%, which is a value consistent with our EDX data.

While the undoped $CsPbCl_3$ NCs show a sharp PL band (FWHM = 14 nm) with peak at 403 nm and a PLQY of only ~0.5%, the Cu-doped $CsPbCl_3$ NCs exhibit dramatically higher PLQY (~60%) with unchanged PL peak position and FWHM (Figure 3). As stated earlier, this maximum PLQY is observed for an optimum concentration (0.22 mmol) of $CuCl_2{\cdot}.2H_2O$ used during the synthesis. For higher or lower concentrations, the NCs exhibited lower PLQY values (Figure S6 in the ESI). We also examined whether post-synthetic treatment of the $CsPbCl_3$ NCs with $CuCl_2{\cdot}2H_2O$ can improve the PL properties or not. Dropwise addition of $CuCl_2{\cdot}2H_2O$ dissolved in OA, OLA, and TOP to a toluene solution of

DOI: 10.1021/acsmaterialslett.9b00101
ACS Materials Lett. 2019, 1, 116–122

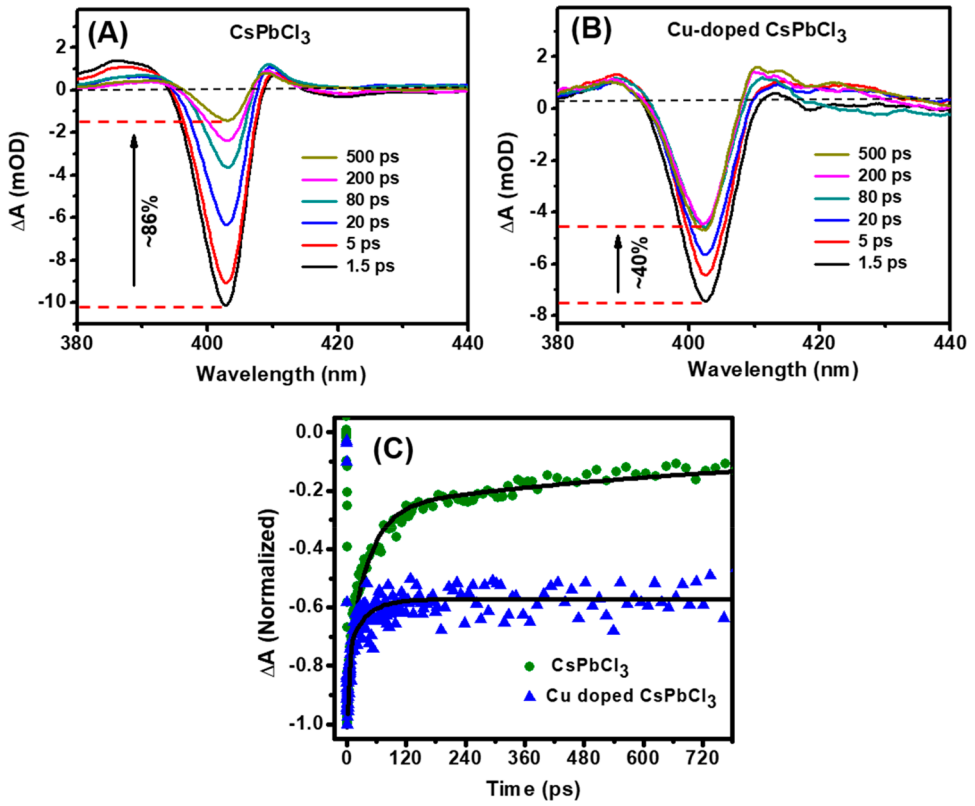

Figure 4. TA spectra of (A) $CsPbCl_3$ and (B) Cu-doped $CsPbCl_3$ NCs; In both cases, samples were excited at 350 nm using a fs-laser; (C) comparison of the bleach recovery kinetics of the two samples monitored at their bleach maxima at 402 nm.

$CsPbCl_3$ NCs under stirring condition improves the PLQY only up to ~16% (Figure S7 in the ESI). This finding is in agreement with recent observation of enhancement of PLQY of $CsPbCl_3$ NCs to 12% upon post-synthetic treatment with $CuCl_2$.[18] Clearly, our direct hot-injection method of synthesis is much more effective in this regard.

Like the colloidal dispersions (Figure 3C), a film of Cu-doped $CsPbCl_3$ NCs also exhibit strong violet PL (Figure S8 in the ESI). When the air stability was checked, the doped NCs show much more robustness by maintaining ~60% of its initial PL after 6 days, whereas only ~10% PL is retained in the case of undoped NCs during the same period (Figure S9 in the ESI). Unlike the undoped NCs, whose PL decay is too fast to be measured accurately in our time-correlated single photon-counting (TCSPC) setup, which has a time-resolution of ~58 ps, the Cu-doped NCs show much higher PL lifetime (τ_{av} = 1.43 ns; see Figure 3B, as well as Table S1 in the ESI).

Two factors contribute to high PL of the doped $CsPbCl_3$ NCs. First, the halide vacancies are well-known trap centers, which facilitate nonradiative deactivation of the charge carriers.[9,10,21] Since the undoped $CsPbCl_3$ NCs are halide-deficient (evident from the Cl:Pb ratio of 2.8, Figure S10 in the ESI), but the Cu-doped ones are halide-rich (Cl:(Pb + Cu) ratio of 3.3; see Figure 2A), it is evident that removal of halide-vacancy associated defects in doped NCs contributes to enhanced PL of the latter.[11,28,29] Second, it is also documented that distortion of the $[PbCl_6]^{4-}$ octahedral unit has a deleterious effect on the PL properties of $CsPbCl_3$ NCs and doping of smaller size cations such as Cd^{2+}, Ni^{2+} enhances short-range order in the lattice and also improves the PLQY of the NCs.[10,11] Hence, doping of Cu^{+} (ionic radius = 77 pm) helps rectification of this structural defect and also contributes to the improved PL of the NCs.

We have also investigated the role of dopant on the carrier dynamics in the early time-scale using ultrafast transient absorption technique.[30,31] The transient absorption spectra obtained on 350 nm excitation of a colloidal solution of the undoped and Cu-doped NCs with femtosecond laser pulses of low pump fluence (12.7×10^{13} photons per cm^2, to avoid contribution from nonlinear processes in the recorded dynamics)[32] over a time-scale of up to 500 ps, are characterized by a sharp negative signal at ~402 nm and positive signals on both sides of it (Figure 4). The negative signal represents bleach that is due to ground-state absorption of the samples. Although the spectral features are similar in both cases, careful examination of the data reveals that bleach recovery is significantly slower in the case of Cu-doped sample. For example, in 500 ps, the bleach recovery is only 40% for doped system, compared to ~86% recovery for undoped system. Analysis of the bleach recovery kinetic traces of undoped NCs shows two fast components of 3 ps (25%) and 40.1 ps (55%) and a slower component of >850 ps (20%) (Table 1). The fast two components are attributed to carrier

Table 1. Kinetic Parameters of the Bleach Recovery Dynamics of $CsPbCl_3$ and Cu-Doped $CsPbCl_3$ NCs

	Recovery Components		
system	τ_1 (a_1)/ ps	τ_2 (a_2)/ ps	τ_3 (a_3)/ ps
$CsPbCl_3$	3.0 ± 0.2 (0.25)	40.1 ± 2.7 (0.55)	>850 (0.20)
Cu-doped $CsPbCl_3$	3.5 ± 0.2 (0.30)	35.0 ± 4.5 (0.16)	>850 (0.54)

DOI: 10.1021/acsmaterialslett.9b00101
ACS Materials Lett. 2019, 1, 116−122

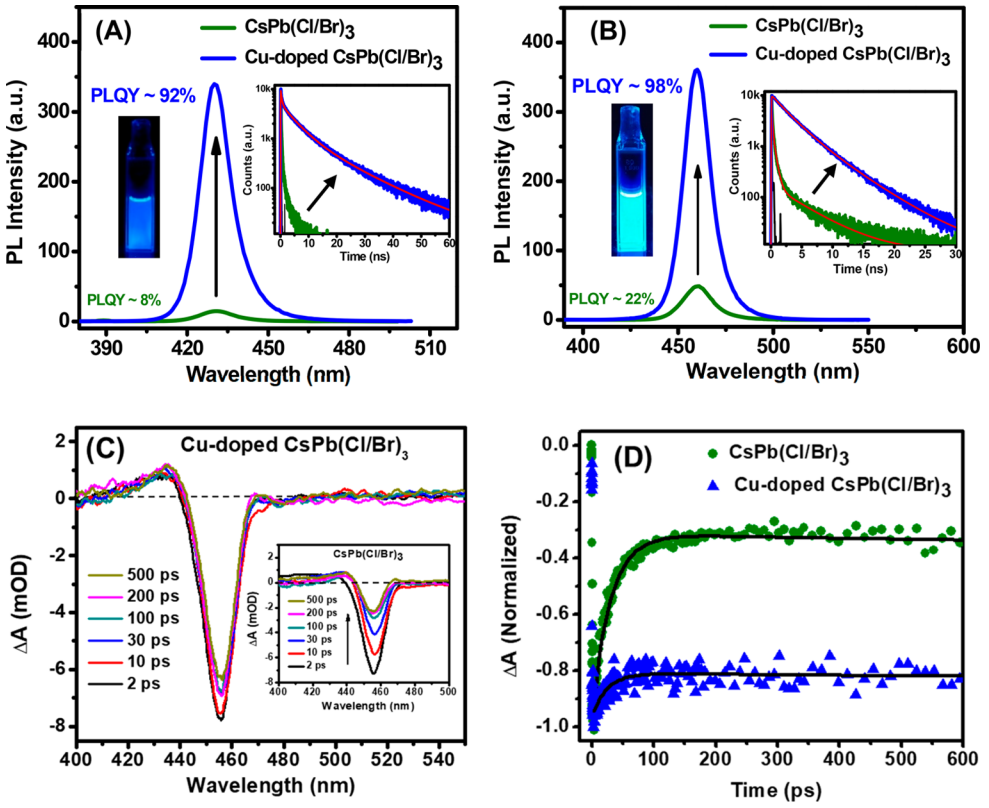

Figure 5. Relative PL of $CsPb(Cl/Br)_3$ and Cu-doped $CsPb(Cl/Br)_3$ NCs with PL maxima at (A) 430 nm and (B) 460 nm; PL decay profiles (λ_{ex} = 375 nm) of the NCs are compared in respective insets. Digital images of the colloidal solution of the PL improved NCs under UV light (λ_{ex} = 365 nm) are shown in both cases. (C) TA spectra of Cu-doped $CsPb(Cl/Br)_3$ NCs, which exhibit PL maxima at 460 nm (λ_{ex} = 350 nm), Inset shows of TA spectra of undoped $CsPb(Cl/Br)_3$ NCs emitting at 460 nm. (D) Comparison of bleach recovery kinetics of the two samples (λ_{em} = 460 nm) monitored at their bleach maxima at 456 nm.

trapping and the long-component to carrier recombination.[11,33] Here, note that the exact value of the long-time component could not be measured accurately as it falls beyond the time-window of the femtosecond TA-setup.

Large contribution of carrier trapping in $CsPbCl_3$ (~80%) is indeed a reflection of poor PLQY of the system.[7,11,30,34] This is predominantly due to chloride vacancies, which require little energy for its formation and generate deep trap energy levels.[21,35] In addition, structural disorder and strong electron-phonon interaction also contribute to carrier trapping in this system.[22] Interestingly, in doped NCs, carrier trapping is significantly suppressed (~46%) and majority of the carrier follows a longer recombination path (Table 1), resulting in a long PL lifetime (1.43 ns) and high PLQY, compared to the undoped sample.

If $CuBr_2$ is used in place of $CuCl_2$ during hot-injection synthesis of the NCs, doped mixed halide perovskite NCs are obtained, but controlling precisely the composition and PL peak position was difficult. However, room-temperature halide exchange was found quite convenient for tuning of the PL band to access the entire blue region. For this purpose, Cu-doped $CsPbCl_3$ NCs were treated with different quantities of benzoyl bromide (as bromide source) at room temperature to adjust the PL wavelength between 430 nm and 460 nm.[36] The halide-exchanged doped $CsPbCl_3$ NCs exhibit a PLQY of ~92% (λ_{em} = 430 nm) and 98% (λ_{em} = 460 nm), while halide-exchanged undoped NCs exhibit a PLQY of only ~8% (λ_{em} = 430 nm) and 22% (λ_{em} = 460 nm) (see Figures 5A and 5B). These high values are quite impressive, considering that these NCs are blue-emitting.

Enhanced PLQY of the NCs is accompanied by an increase in PL lifetime (see Figures 5A and 5B (insets), as well as Table S2 in the ESI). For Cu-doped $CsPb(Cl/Br)_3$ NCs emitting at 430 nm, the PL lifetime (4.3 ns) is much higher than that of the undoped counterpart. The doped $CsPb(Cl/Br)_3$ NCs with PL maxima at 460 nm exhibit a biexponential decay behavior with an average lifetime of 3.6 ns, which is several-fold higher than that of the undoped sample (0.2 ns; see inset in Figure 5B).

The transient absorption measurements show much slower bleach recovery for doped $CsPb(Cl/Br)_3$ NCs, compared to the undoped sample within a given time frame (see Figure 5C, as well as Figure S11 in the ESI). For example, the doped NCs sample, which emits at 460 nm, shows 10% recovery against ~70% recovery for the undoped NCs in 500 ps. The bleach recovery kinetics data show that the contribution of the long-lifetime component (> 850 ps) is much higher (~84%) in doped NCs (versus 32% in the undoped system) (Table S3 in the ESI), thus explaining the improved PLQY of the former. The NCs, which emit at 430 nm, show a similar trend (see Figure S11, as well as Table S3).

Although several metal-halide salts have been used previously to enhance the PL of $CsPbCl_3$ NCs, both the mode of function of the salts and the extent of PL enhancement differ from case to case. For example, the room-temperature post-treatment with YCl_3 that was reported by Mohammed and co-workers enhanced the PLQY up to

DOI: 10.1021/acsmaterialslett.9b00101
ACS Materials Lett. 2019, 1, 116−122

60%, following passivation of the Pb−Cl ion-pair defect sites by YCl_3.[9] Surprisingly, the same metal halide salt, when used during hot-injection synthesis, did not produce significant PL enhancement, despite the doping of Y^{3+} in the NCs.[9] There are other instances as well. While the addition of solid $CdCl_2$ into a colloidal dispersion of the $CsPbCl_3$ NCs did not influence the optical properties of the NCs greatly,[9] when these NCs are treated with ethanol/amine solution of the same salt ($CdCl_2$), the PLQY is enhanced to near-unity.[11] This variation is most likely the outcome of how the metal-halide salts interact with the NCs in two cases. In the first case, the interaction is restricted to the surface, whereas in the latter case, dissolution of the salt in ethanol/amine allows the metal ion to go inside the NCs, which helps rectification of the structural disorder in the lattice. We would like to discuss a third interesting case, which involve $NiCl_2$ salt. Its use during hot-injection synthesis results in the formation of Ni^{2+}-doped $CsPbCl_3$ NCs with ∼96.5% PLQY, whereas room-temperature treatment with this salt does not significantly improve the PL properties.[10,17] Very recently, it is shown that addition of $CuBr_2$ during hot-injection synthesis of $CsPbCl_3$ produces NCs with PLQY of 80%−90%.[20] However, because of unavoidable halide exchange, the resulting mixed-halide NCs emit not in the violet region, but only in the blue region (λ_{max} = 450−460 nm). A recent post-synthetic treatment of $CsPbCl_3$ NCs with $CuCl_2$ improved the PLQY only up to 12.7% PLQY.[19] In this context, our approach of using $CuCl_2$ salt in the hot-injection method is much more effective in producing highly luminescent violet-emitting $CsPbCl_3$ NCs. In addition, one can easily get blue-emitting NCs (λ_{max} = 430−460 nm) with high PLQY (92%−98%) from our PL improved NCs by following simple room-temperature halide exchange protocol.

In conclusion, it is shown that one can dramatically enhance the PLQY of weakly emitting $CsPbCl_3$ NCs by using an appropriate quantity of $CuCl_2$ during the hot-injection synthesis of the NCs. The treatment leads to doping of Cu^+ into the NCs and passivation of the surface halide vacancies. Time-resolved PL and ultrafast transient absorption measurements suggest suppression of the carrier trapping process in doped NCs. Highly luminescent (PLQY of 92%−98%) NCs emitting in the blue region (430−460 nm) is also obtained by partial halide exchange of the doped NCs. The findings are likely to further enhance the potential of these promising materials in optoelectronic applications.

■ ASSOCIATED CONTENT

Supporting Information

The Supporting Information is available free of charge on the ACS Publications website at DOI: 10.1021/acsmaterialslett.9b00101.

Detailed method of synthesis of $CsPbCl_3$ NCs, halide-exchange procedure, additional TEM images, absorption, emission and PL decay curves of Cu^{2+}-doped NCs, EPR data, XPS data, stability plot, EDX data of $CsPbCl_3$ NCs, TA spectra and bleach recovery kinetics of undoped and doped $CsPb(Cl/Br)_3$ NCs emitting at 430 nm; tables presenting PL decay parameters of Cu-doped $CsPbCl_3$ and undoped and doped $CsPb(Cl/Br)_3$ NCs; table with kinetic parameters of bleach recovery dynamics of $CsPb(Cl/Br)_3$ and Cu-doped $CsPb(Cl/Br)_3$ NCs (PDF)

■ AUTHOR INFORMATION

Corresponding Author

*E-mail: anunay@uohyd.ac.in.

ORCID

Apurba De: 0000-0002-3042-0642

Navendu Mondal: 0000-0001-5002-9678

Anunay Samanta: 0000-0003-1551-0209

Present Address

†Department of Physics, The University of Texas at Dallas, Richardson, TX 75080, USA.

Notes

The authors declare no competing financial interest.

■ ACKNOWLEDGMENTS

This work is supported by Grant No. EMR/2015/000582 and J. C. Bose Fellowship (to A.S.) of the Science and Engineering Research Board (SERB), Department of Science and Technology (DST), Government of India, and Mid-Career Award (to A.S.) of the University Grants Commission (UGC). The authors also acknowledge the UGC-UPE support to the University, TEM facility of the Centre for Nanotechnology, and the femtosecond pump-probe facility of the School. A.D. and S.D. thank UGC and N.M. thanks the Council of Scientific and Industrial Research (CSIR) for fellowships.

■ REFERENCES

(1) Liang, J.; Wang, C.; Wang, Y.; Xu, Z.; Lu, Z.; Ma, Y.; Zhu, H.; Hu, Y.; Xiao, C.; Yi, X.; Zhu, G.; Lv, H.; Ma, L.; Chen, T.; Tie, Z.; Jin, Z.; Liu, J. All-Inorganic Perovskite Solar Cells. *J. Am. Chem. Soc.* **2016**, *138*, 15829−15832.

(2) Swarnkar, A.; Marshall, A. R.; Sanehira, E. M.; Chernomordik, B. D.; Moore, D. T.; Christians, J. A.; Chakrabarti, T.; Luther, J. M. Quantum dot−induced phase stabilization of α-$CsPbI_3$ perovskite for high-efficiency photovoltaics. *Science* **2016**, *354*, 92−95.

(3) Li, X.; Wu, Y.; Zhang, S.; Cai, B.; Gu, Y.; Song, J.; Zeng, H. $CsPbX_3$ Quantum Dots for Lighting and Displays: Room-Temperature Synthesis, Photoluminescence Superiorities, Underlying Origins and White Light-Emitting Diodes. *Adv. Funct. Mater.* **2016**, *26*, 2435−2445.

(4) Song, J.; Li, J.; Li, X.; Xu, L.; Dong, Y.; Zeng, H. Quantum Dot Light-Emitting Diodes Based on Inorganic Perovskite Cesium Lead Halides ($CsPbX_3$). *Adv. Mater.* **2015**, *27*, 7162−7167.

(5) Wang, S.; Bi, C.; Yuan, J.; Zhang, L.; Tian, J. Original Core−Shell Structure of Cubic $CsPbBr_3$@Amorphous $CsPbBr_x$ Perovskite Quantum Dots with a High Blue Photoluminescence Quantum Yield of over 80%. *ACS Energy Lett.* **2018**, *3*, 245−251.

(6) Protesescu, L.; Yakunin, S.; Bodnarchuk, M. I.; Krieg, F.; Caputo, R.; Hendon, C. H.; Yang, R. X.; Walsh, A.; Kovalenko, M. V. Nanocrystals of Cesium Lead Halide Perovskites ($CsPbX_3$, X = Cl, Br, and I): Novel Optoelectronic Materials Showing Bright Emission with Wide Color Gamut. *Nano Lett.* **2015**, *15*, 3692−3696.

(7) De, A.; Mondal, N.; Samanta, A. Luminescence Tuning and Exciton Dynamics of Mn-doped $CsPbCl_3$ Nanocrystals. *Nanoscale* **2017**, *9*, 16722−16727.

(8) Ahmed, T.; Seth, S.; Samanta, A. Boosting the Photoluminescence of $CsPbX_3$ (X = Cl, Br, I) Perovskite Nanocrystals Covering a Wide Wavelength Range by Postsynthetic Treatment with Tetrafluoroborate Salts. *Chem. Mater.* **2018**, *30*, 3633−3637.

(9) Ahmed, G. H.; El-Demellawi, J. K.; Yin, J.; Pan, J.; Velusamy, D. B.; Hedhili, M. N.; Alarousu, E.; Bakr, O. M.; Alshareef, H. N.; Mohammed, O. F. Giant Photoluminescence Enhancement in $CsPbCl_3$ Perovskite Nanocrystals by Simultaneous Dual-Surface Passivation. *ACS Energy Lett.* **2018**, *3*, 2301−2307.

(10) Yong, Z.-J.; Guo, S.-Q.; Ma, J.-P.; Zhang, J.-Y.; Li, Z.-Y.; Chen, Y.-M.; Zhang, B.-B.; Zhou, Y.; Shu, J.; Gu, J.-L.; Zheng, L.-R.; Bakr, O.

DOI: 10.1021/acsmaterialslett.9b00101
ACS Materials Lett. 2019, 1, 116−122

M.; Sun, a. H.-T. Doping-Enhanced Short-Range Order of Perovskite Nanocrystals for Near-Unity Violet Luminescence Quantum Yield. *J. Am. Chem. Soc.* **2018**, *140*, 9942−9951.
(11) Mondal, N.; De, A.; Samanta, A. Achieving Near-Unity Photoluminescence Efficiency for Blue-Violet-Emitting Perovskite Nanocrystals. *ACS Energy Lett.* **2019**, *4*, 32−39.
(12) Wu, Y.; Li, X.; Zeng, H. Highly Luminescent and Stable Halide Perovskite Nanocrystals. *ACS Energy Lett.* **2019**, *4*, 673−481.
(13) Li, F.; Liu, Y.; Wang, H.; Zhan, Q.; Liu, Q.; Xia, Z. Postsynthetic Surface Trap Removal of $CsPbX_3$ (X = Cl, Br, or I) Quantum Dots via a ZnX_2/Hexane Solution toward an Enhanced Luminescence Quantum Yield. *Chem. Mater.* **2018**, *30*, 8546−8554.
(14) Dutta, A.; Behera, R. K.; Dutta, S. K.; Das Adhikari, S.; Pradhan, N. Annealing $CsPbX_3$ (X = Cl and Br) Perovskite Nanocrystals at High Reaction Temperatures: Phase Change and Its Prevention. *J. Phys. Chem. Lett.* **2018**, *9*, 6599−6604.
(15) Wang, S.; Wang, Y.; Zhang, Y.; Zhang, X.; Shen, X.; Zhuang, X.; Lu, P.; Yu, W. W.; Kershaw, S. V.; Rogach, A. L. Cesium Lead Chloride/Bromide Perovskite Quantum Dots with Strong Blue Emission Realized via a Nitrate-Induced Selective Surface Defect Elimination Process. *J. Phys. Chem. Lett.* **2019**, *10*, 90−96.
(16) Liu, Y.; Li, F.; Liu, Q.; Xia, Z. Synergetic Effect of Postsynthetic Water Treatment on the Enhanced Photoluminescence and Stability of $CsPbX_3$ (X = Cl, Br, I) Perovskite Nanocrystals. *Chem. Mater.* **2018**, *30*, 6922−6929.
(17) Behera, R. K.; Das Adhikari, S.; Dutta, S. K.; Dutta, A.; Pradhan, N. Blue-Emitting CsPbCl3 Nanocrystals: Impact of Surface Passivation for Unprecedented Enhancement and Loss of Optical Emission. *J. Phys. Chem. Lett.* **2018**, *9*, 6884−6891.
(18) Dutta, A.; Behera, R. K.; Pal, P.; Baitalik, S.; Pradhan, N. Near-Unity Photoluminescence Quantum Efficiency for All $CsPbX_3$ (X = Cl, Br and I) Perovskite Nanocrystals: A Generic Synthesis Approach. *Angew. Chem., Int. Ed.* **2019**, *58*, 5552−5556.
(19) Chen, Y.-C.; Chou, H.-L.; Lin, J.-C.; Lee, Y.-C.; Pao, C.-W.; Chen, J.-L.; Chang, C.-C.; Chi, R.-Y.; Kuo, T.-R.; Lu, C.-W.; Wang, D.-Y. Enhanced Luminescence and Stability of Cesium Lead Halide Perovskite $CsPbX_3$ Nanocrystals by Cu^{2+}-Assisted Anion Exchange Reactions. *J. Phys. Chem. C* **2019**, *123*, 2353−2360.
(20) Bi, C.; Wang, S.; Li, Q.; Kershaw, S. V.; Tian, J.; Rogach, A. L. Thermally Stable Copper (II) Doped Cesium Lead Halide Perovskite Quantum Dots with a Strong Blue Emission. *J. Phys. Chem. Lett.* **2019**, *10*, 943−952.
(21) Nenon, D. P.; Pressler, K.; Kang, J.; Koscher, B. A.; Olshansky, J. H.; Osowiecki, W. T.; Koc, M. A.; Wang, L.-W.; Alivisatos, A. P. Design Principles for Trap-Free $CsPbX_3$ Nanocrystals: Enumerating and Eliminating Surface Halide Vacancies with Softer Lewis Bases. *J. Am. Chem. Soc.* **2018**, *140*, 17760−17772.
(22) Lohar, A. A.; Shinde, A.; Gahlaut, R.; Sagdeo, A.; Mahamuni, S. Enhanced Photoluminescence and Stimulated Emission in $CsPbCl_3$ Nanocrystals at Low Temperature. *J. Phys. Chem. C* **2018**, *122*, 25014−25020.
(23) The particular concentration of $CuCl_2{\cdot}2H_2O$ mentioned in the synthesis is determined by performing several controlled syntheses with varying amount of $CuCl_2{\cdot}2H_2O$, where maximum PL enhancement of the NCs is found in the case of the above-mentioned concentration (see Figure S6 in the ESI).
(24) Dong, Y.; Qiao, T.; Kim, D.; Parobek, D.; Rossi, D.; Son, D. H. Precise Control of Quantum Confinement in Cesium Lead Halide Perovskite Quantum Dots via Thermodynamic Equilibrium. *Nano Lett.* **2018**, *18*, 3716−3722.
(25) Liu, M.; Zhong, G.; Yin, Y.; Miao, J.; Li, K.; Wang, C.; Xu, X.; Shen, C.; Meng, H. Aluminum-Doped Cesium Lead Bromide Perovskite Nanocrystals with Stable Blue Photoluminescence Used for Display Backlight. *Adv. Sci.* **2017**, *4*, 1700335.
(26) Bodnarchuk, M. I.; Boehme, S. C.; ten Brinck, S.; Bernasconi, C.; Shynkarenko, Y.; Krieg, F.; Widmer, R.; Aeschlimann, B.; Günther, D.; Kovalenko, M. V.; Infante, I. Rationalizing and Controlling the Surface Structure and Electronic Passivation of Cesium Lead Halide Nanocrystals. *ACS Energy Lett.* **2019**, *4*, 63−74.
(27) Zhang, X.; Zhang, Y.; Zhang, X.; Yin, W.; Wang, Y.; Wang, H.; Lu, M.; Li, Z.; Gu, Z.; Yu, W. W. Yb^{3+} and Yb^{3+}/Er^{3+} doping for near-infrared emission and improved stability of $CsPbCl_3$ nanocrystals. *J. Mater. Chem. C* **2018**, *6*, 10101−10105.
(28) Liu, P.; Chen, W.; Wang, W.; Xu, B.; Wu, D.; Hao, J.; Cao, W.; Fang, F.; Li, Y.; Zeng, Y.; Pan, R.; Chen, S.; Cao, W.; Sun, X. W.; Wang, K. Halide-Rich Synthesized Cesium Lead Bromide Perovskite Nanocrystals for Light-Emitting Diodes with Improved Performance. *Chem. Mater.* **2017**, *29*, 5168−5173.
(29) Das Adhikari, S.; Behera, R. K.; Bera, S.; Pradhan, N. Presence of Metal Chloride for Minimizing the Halide Deficiency and Maximizing the Doping Efficiency in Mn(II)-Doped $CsPbCl_3$ Nanocrystals. *J. Phys. Chem. Lett.* **2019**, *10*, 1530−1536.
(30) Mondal, N.; Samanta, A. Complete ultrafast charge carrier dynamics in photo-excited all-inorganic perovskite nanocrystals ($CsPbX_3$). *Nanoscale* **2017**, *9*, 1878−1885.
(31) De, A.; Mondal, N.; Samanta, A. Hole Transfer Dynamics from Photoexcited Cesium Lead Halide Perovskite Nanocrystals: 1-Aminopyrene as Hole Acceptor. *J. Phys. Chem. C* **2018**, *122*, 13617−13623.
(32) Mondal, N.; De, A.; Samanta, A. Biexciton Generation and Dissociation Dynamics in Formamidinium and Chloride-Doped Cesium Lead Iodide Perovskite Nanocrystals. *J. Phys. Chem. Lett.* **2018**, *9*, 3673−3679.
(33) Mondal, N.; De, A.; Das, S.; Paul, S.; Samanta, A. Ultrafast Carrier Dynamics of Metal Halide Perovskite Nanocrystals and Perovskite-composites. *Nanoscale* **2019**, *11*, 9796−9818.
(34) Rossi, D.; Parobek, D.; Dong, Y.; Son, D. H. Dynamics of Exciton−Mn Energy Transfer in Mn-Doped $CsPbCl_3$ Perovskite Nanocrystals. *J. Phys. Chem. C* **2017**, *121*, 17143−17149.
(35) Ma, J.-P.; Chen, Y.-M.; Zhang, L.-M.; Guo, S.-Q.; Liu, J.-D.; Li, H.; Ye, B.-J.; Li, Z.-Y.; Zhou, Y.; Zhang, B.-B.; Bakr, O. M.; Zhang, J.-Y.; Sun, H.-T. Insights into the local structure of dopants, doping efficiency, and luminescence properties of lanthanide-doped $CsPbCl_3$ perovskite nanocrystals. *J. Mater. Chem. C* **2019**, *7*, 3037−3048.
(36) Creutz, S. E.; Crites, E. N.; De Siena, M. C.; Gamelin, D. R. Anion Exchange in Cesium Lead Halide Perovskite Nanocrystals and Thin Films Using Trimethylsilyl Halide Reagents. *Chem. Mater.* **2018**, *30*, 4887−4891.

DOI: 10.1021/acsmaterialslett.9b00101
ACS Materials Lett. 2019, 1, 116−122

THE JOURNAL OF PHYSICAL CHEMISTRY C

Article

Cite This: J. Phys. Chem. C 2018, 122, 13617−13623

pubs.acs.org/JPCC

Hole Transfer Dynamics from Photoexcited Cesium Lead Halide Perovskite Nanocrystals: 1-Aminopyrene as Hole Acceptor

Apurba De, Navendu Mondal, and Anunay Samanta*

School of Chemistry, University of Hyderabad, Hyderabad-500 046, India

Supporting Information

ABSTRACT: The lead halide perovskites have emerged as promising materials for photovoltaic applications within a very short period. The key to exploitation of the full potential of these substances by achieving even higher photovoltaic conversion efficiency lies in understanding of the charge (electron/hole) separation process and their transfer across the interface. As the latter depends on the nature of the electron/hole acceptor, quest for suitable carrier acceptor is an active area in this context. Herein, we explore the hole extraction ability of 1-ampinopyrene (AMP) from two very common all-inorganic perovskite nanocrystals (NCs), $CsPbBr_3$ and $CsPbI_3$, with different band gaps. The observation of efficient quenching of the photoluminescence (PL) of the NCs with little/negligible change in PL time-profile in the presence of AMP indicates static interaction of the two interacting species. The band alignment of the NCs relative to the HOMO−LUMO energy levels of AMP and ultrafast pump−probe measurements reveal rapid hole transfer from the photoexcited NCs to AMP. The hole transfer time constants are estimated as 120 and 170 ps for $CsPbBr_3$ and $CsPbI_3$ NCs, respectively. The rapid extraction of the hole, as observed with the present system, appears to be the result of strong anchoring of AMP on the NCs surface and facile transfer of the hole through conducive pyrene framework. The findings reveal that judicial choice of even a simple molecular system like the present one can help rapid transfer of photogenerated carriers and contribute to the development of cost-effective solar cells in the future.

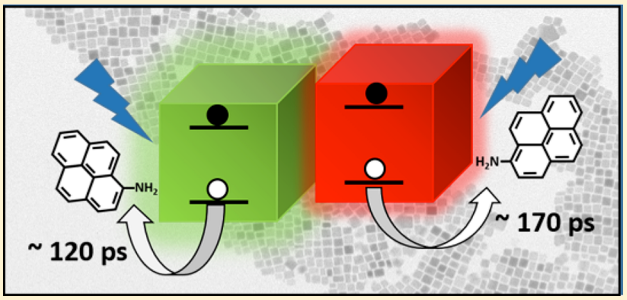

1. INTRODUCTION

The past few years have witnessed intense activities on lead halide perovskites in various areas like in photovoltaic,[1−4] lasing,[5,6] light emitting devices, etc.[7,8] with a major focus as solar energy harvesting materials. Following the pioneering report by Miyasaka and co-workers in 2009,[9] the research on the perovskites has so far led to a record breaking photoelectric conversion efficiency (PCE) of >22%.[10] PCE is not merely determined by the light harvesting ability of the sensitizer but also very much by the hole/electron transporting materials. In photovoltaic devices, the light harvesters are sandwiched between an electron and a hole transporting layer. The transport layers play the important role of extraction of charge carriers from the sensitizer thus minimizing internal recombination. As a commonly used hole transporting material (HTM), 2,2′,7,7′-tetrakis(*N*,*N*-di-*p*-methoxyphenylamine)-9,9′-spiro-bifluorene (spiro-OMeTAD), is quite expensive, the quest for an alternative HTM is an active area in this field.[11] In this regard, a few organic molecules other than spiro-OMeTAD have been studied as HTM[12−15] and the results show that both the terminal functionality and core of the molecule play important roles in the extraction of the carriers and hence, in determining the efficiency of the HTM. Liu et al. have shown how molecular engineering can improve PCE of a HTM.[12] The introduction of a phenylene spacer in phenothiazine based compound is found to influence the PCE dramatically.[13] Seok and co-workers have shown remarkable PCE of the *N*,*N*-di-*p*-methoxyphenylamine-substituted pyrene derivatives as HTM for $CH_3NH_3PbI_3$ attributing it to the pyrene core.[14]

As the PCE of a solar cell is governed mainly by interfacial charge (electron/hole) transfer dynamics from the perovskite NCs to their respective acceptor sites, a knowledge of other competitive processes within the NCs (excitonic recombination, carrier trapping[16−19]) is essential in this regard. Rapid dissociation of the excitons and suppression of competitive processes in NCs are key to improving the efficiency the systems. The surface trap states can further reduce the PCE.[20,21] Various surface modification treatments of the perovskite NCs have been attempted to address this issue.[22−25] For lead-based perovskites, thiophene and pyridine, which bind preferentially to surface Pb^{2+}, are found to be quite effective.[22] A recent work shows the utility of the amino functionality in the passivation of surface trap states (by dative bond formation with Pb^{2+} on the surface) and transfer of hole.[26]

Recognizing the excellent charge transport property of the pyrene core and considering the recent report on the

Special Issue: Prashant V. Kamat Festschrift

Received: December 30, 2017
Revised: February 7, 2018
Published: February 19, 2018

Downloaded via UNIV OF HYDERABAD on June 30, 2018 at 05:36:30 (UTC).
See https://pubs.acs.org/sharingguidelines for options on how to legitimately share published articles.

© 2018 American Chemical Society

DOI: 10.1021/acs.jpcc.7b12813
J. Phys. Chem. C 2018, 122, 13617−13623

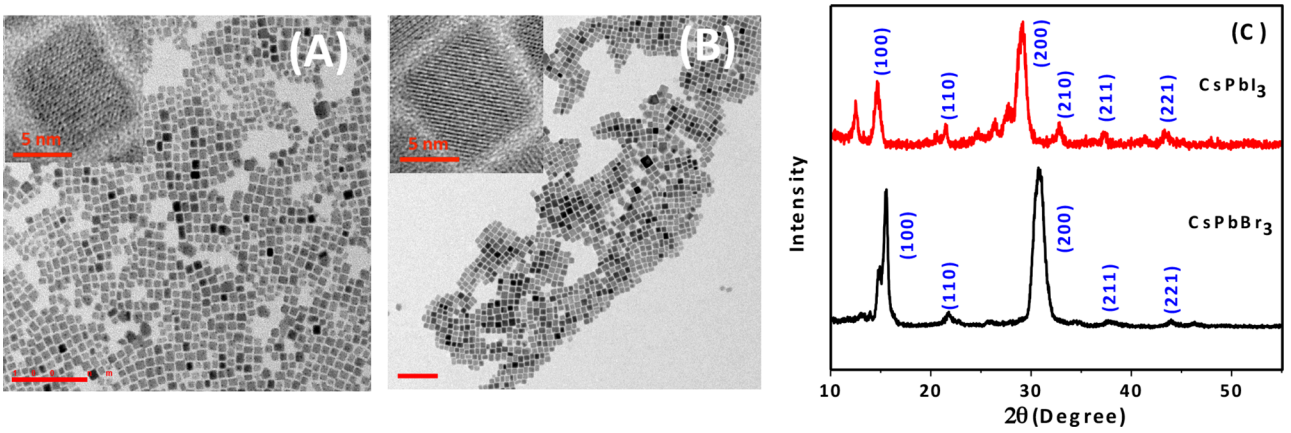

Figure 1. TEM images of (A) $CsPbBr_3$ and (B) $CsPbI_3$ NCs. Scale bar is 100 nm. Respective HRTEM images are given in insets. (C) PXRD patterns of both the NCs.

effectiveness of the amino functionality in surface passivation and hole movement,[14,26] we pick up 1-aminopyrene (AMP), a simple commercially available pyrene derivative with an amino functionality, to find out whether/how it can help extraction of charge carriers from photoexcited perovskite NCs, $CsPbBr_3$ and $CsPbI_3$ using femtosecond transient absorption (TA) measurements. We note that the literature on the interfacial charge transfer dynamics from the perovskite NCs is rather limited.[27−32] While a number of electron acceptors have been tried out, to the best of our knowledge, phenothiazine and 4,5-dibromofluorescein are the only two molecular systems which have been investigated as hole acceptors from the perovskite NCs.[27,28,30]

2. EXPERIMENTAL METHODS

2.1. Materials. Cesium carbonate (99.9%), lead bromide (>98%), octadecene (ODE, 90%), oleic acid (OA, 90%), and oleylamine (OLA, 70%) were purchased from Sigma-Aldrich. Lead iodide (99.9985%) was obtained from Alfa Aesar. All chemicals for synthesis were used without further purification. Dried toluene was used as solvent in all spectroscopic studies.

2.2. Preparation of the NCs. $CsPbBr_3$ and $CsPbI_3$ NCs were prepared by following a reported hot injection method.[33] In brief, 0.16 g of Cs_2CO_3, 6 mL of octadecene (ODE), and 0.5 mL of oleic acid (OA) were added together in a 50 mL double-necked round-bottom flask (RB), which was heated under vacuum at 120 °C for 1 h. Subsequently, it was heated at 120 °C under nitrogen atmosphere until all Cs_2CO_3 reacted with OA to form Cs-oleate complex. This solution was maintained in heating condition for its use to avoid precipitation. In another 50 mL double-necked RB, 0.069 g of $PbBr_2$ (for synthesis of $CsPbBr_3$) or 0.084 g of PbI_2 (for $CsPbI_3$) along with 5 mL of ODE, 0.5 mL of OA, and 0.5 mL of OLA were added and heated under vacuum at 105 °C for an hour. The temperature was then increased to 165 °C under nitrogen atmosphere and 0.45 mL of hot Cs−oleate solution was injected swiftly followed by immediate cooling of the solution in ice cold water. The synthesized NCs were collected by centrifuging the suspension at ∼8000 rpm and then dispersed in toluene for further study.

2.3. Structural Characterization. Transmission electron microscopy (TEM) measurements of the synthesized NCs were performed with a Tecnai G2 FE1 F12 transmission electron microscope at an accelerating voltage of 120 kV. Powdered X-ray diffraction (PXRD) patterns were recorded on a Bruker D8 Advance diffractometer using Cu Kα X-radiation (λ = 1.5406 Å).

2.4. Steady State and Time-Resolved PL Measurement. The steady-state absorption and PL spectra were measured by Cary100 (Varian) UV−visible spectrophotometer and FluoroLog-3 (Horiba Jobin Yvon) spectrofluorimeter, respectively. The PL decay profiles of the NCs were recorded by using a time-correlated single photon-counting (TCSPC) spectrometer (Horiba Jobin Yvon IBH). A diode laser (481 nm) with a repetition rate of 10 MHz was used as the excitation source and an MCP photomultiplier (Hamamatsu R3809U-50) as the detector. The instrument response function was 150 ps for this excitation source. The PL decay curves were analyzed using a nonlinear least-squares iteration procedure through decay analysis software (IBH DAS6, V 2.2).[34]

2.5. Transient Absorption Measurement. The details of the experimental setup is described elsewhere.[35] Briefly, the setup consisted of a mode-locked Ti:sapphire seed laser (Mai-Tai, Spectra Physics) with 80 MHz repetition rate and a center wavelength of 801 nm. A part of its output was directed to the regenerative amplifier (Spitfire Ace, Spectra Physics), which was pumped (at 527 nm) by a frequency doubled Nd:YLF laser (Empower, Spectra Physics). The amplified output of 801 nm (4.2 W), operating at a repetition rate of 1 kHz was then divided into two parts. One part was directed to an optical parametric amplifier (TOPAS-Prime, Spectra Physics) to generate required excitation pulse and the other was passed through a delay unit followed by a CaF_2 crystal to generate white light continuum for broad band probe pulses of 350−800 nm. The white light was split by a beam splitter to generate a signal and a reference beam. Both the beams were directed to the detector (photodiode array) to record the pump induced changes at different time delay of probe beam. The incident pump power was adjusted by neutral density filters. All spectra were chirp-corrected for group velocity dispersion of white light continuum by using the TA signals of neat ethanol. The instrument resolution was ∼100 fs. All samples were taken in a rotating sample cell (1 mm path length) in toluene and during measurements it was kept in rotating condition to ensure no photobleach of the samples.

3. RESULTS AND DISCUSSION

3.1. Characterization. The TEM images of $CsPbBr_3$ and $CsPbI_3$ NCs (Figure 1) show a cubic morphology with an edge length of 8 ± 0.5 nm for $CsPbBr_3$ and 10 ± 0.5 nm for $CsPbI_3$

DOI: 10.1021/acs.jpcc.7b12813
J. Phys. Chem. C 2018, 122, 13617−13623

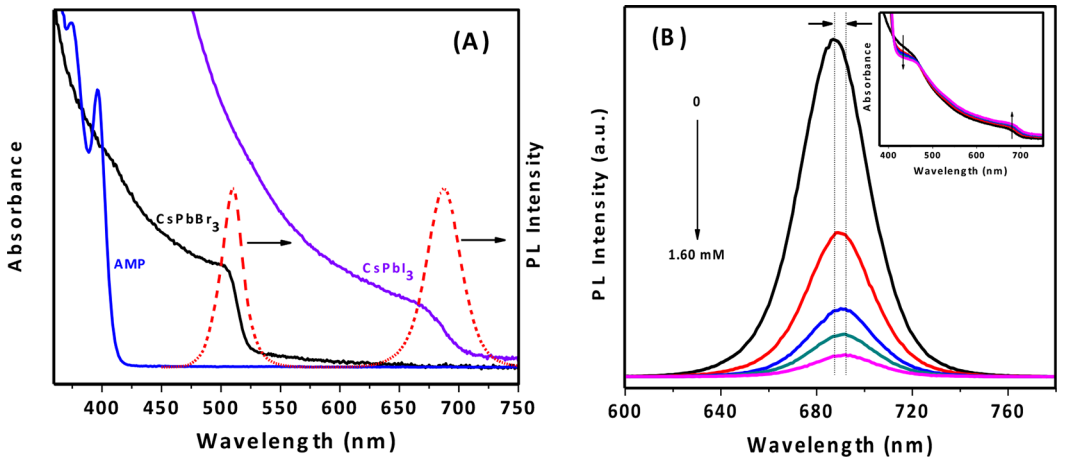

Figure 2. (A) Individual absorption spectra of $CsPbBr_3$, $CsPbI_3$ and AMP in toluene at room temperature and PL spectra of $CsPbBr_3$ and $CsPbI_3$ NCs. (B) PL quenching of $CsPbI_3$ NCs upon successive addition of AMP in toluene. The inset depicts the change in the corresponding absorption spectrum.

NCs. The monodispersity of the NCs is evident from the images shown in 100 nm scale bar. The PXRD patterns of the NCs (Figure 1C) show characteristic peaks corresponding to the cubic phase of the NCs.[33] The HRTEM images show high crystallinity of the NCs. As $CsPbI_3$ is prone to transformation into nonemissive orthorhombic phase at room temperature,[33,36] all studies have been performed with freshly prepared NCs dispersed in toluene.

3.2. Steady State Measurements. Individual absorption and PL spectra of $CsPbBr_3$ and $CsPbI_3$ NCs, which are characterized by well-defined excitonic peaks at ∼505 and 671 nm and corresponding PL peaks at 510 and 685 nm, are shown in Figure 2A. The PL quantum yields of $CsPbBr_3$ and $CsPbI_3$ NCs are found to be ∼68 and 60%, respectively. Progressive addition of AMP leads to drastic decrease in the PL of the NCs (Figures 2B and S1). A noticeable red shift (∼5 nm) of the peak wavelength is also noticeable. These observations are illustrated in Figure 2B for $CsPbI_3$ NCs. The changes in the absorption spectra of the systems in the 425−750 nm region (Figure 2B, inset), where AMP does not absorb (Figure 2A), clearly indicates ground-state complexation between the NCs and AMP.[29] Therefore, we can attribute AMP induced PL quenching to the formation of a nonluminescent complex with the NCs. The static interaction between the two interacting species is responsible for PL quenching and further substantiated by time-resolved PL measurements in the following section.

3.3. Time-Resolved Measurements. The PL decay curves of $CsPbBr_3$ and $CsPbI_3$, recorded in our TCSPC setup following excitation at 481 nm using a laser diode source, are found to be multiexponential in nature. A triexponential fitting to the decay profiles gave acceptable values of residuals and chi-squares. The individual lifetime components and their weightages are provided as Supporting Information (Tables S1 and S2). The average lifetimes of $CsPbBr_3$ and $CsPbI_3$ NCs are estimated to be 5.9 and 41.8 ns, respectively and these values are consistent with literature.[33] Figure 3 depicts the PL decay curves of $CsPbI_3$ in the absence and presence of largest amount of AMP (which was used in steady state measurements). Contrary to the dramatic decrease in PL intensity the change in PL lifetime is rather small confirming static interaction responsible for PL quenching of the system.

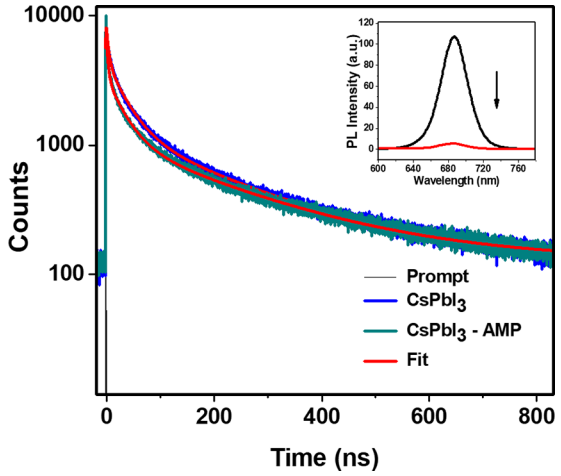

Figure 3. PL decay of $CsPbI_3$ NCs without and in the presence of AMP. The shown PL decay in the presence of AMP is for the maximum PL quenched sample (corresponding PL spectra shown as an inset).

3.4. Transient Absorption Measurement. We have studied the charge-transfer dynamics between the NCs and AMP using femtosecond time-resolved pump−probe technique.[37] For this purpose, we have excited a toluene suspension of $CsPbBr_3$ at 470 nm and $CsPbI_3$ at 530 nm to ensure that AMP is not excited when present. We have also maintained a low pump fluence in all measurements to ensure that the average number of excitons per NC is less than 0.1 and negligible contribution of the multiexciton generation process to the measured dynamics.[38,39]

As can be seen from Figure 4A, the TA spectra of bare $CsPbBr_3$ NCs consist of a photoinduced bleach (PB) in the ∼490−512 nm wavelength region with peak at 505 nm. The PB maximum is consistent with the excitonic peak position in the absorption spectra. As PL of these samples does not exhibit large Stokes shift, the stimulated emission signal can also contribute to the bleach signal.[40] The positive absorptions on both sides of the bleach signal arises from the lowest excitonic states, as reported in an earlier study.[16] In presence of AMP (Figure 4B), one observes hardly any change in the spectral profile of $CsPbBr_3$ including the bleach position. However, the

DOI: 10.1021/acs.jpcc.7b12813
J. Phys. Chem. C 2018, 122, 13617−13623

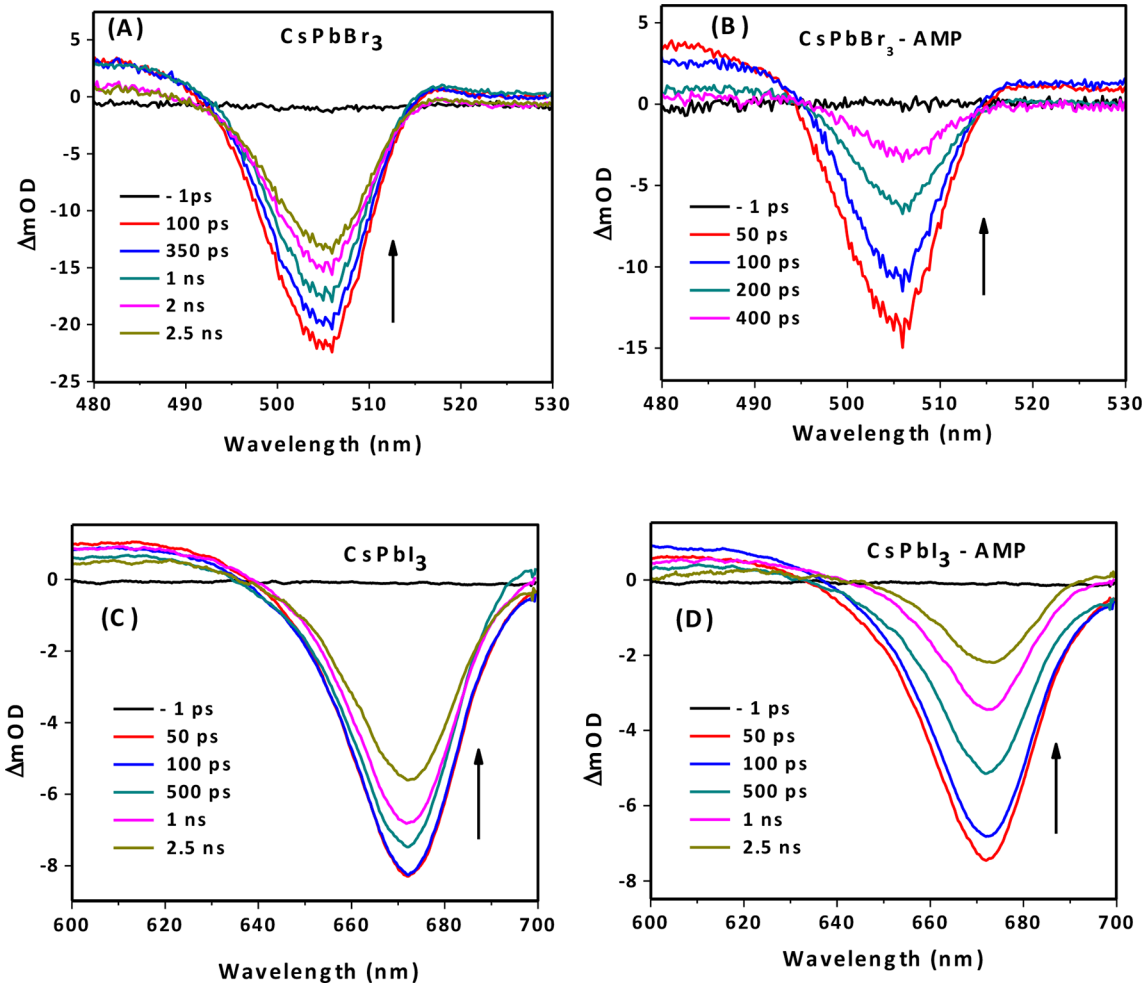

Figure 4. TA spectra of $CsPbBr_3$ and $CsPbI_3$ NCs without (A, C) and with (B, D) AMP. The excitations were made at 470 and 530 nm for $CsPbBr_3$ and $CsPbI_3$, respectively and the spectra were recorded up to 2.5 ns total delay.

bleach recovery dynamics becomes significantly faster in the presence of AMP. For example, compared to ∼10% bleach recovery in 400 ps, ∼90% recovery is observed in the presence of AMP during the same period.

In the case of Cd-based quantum dots (QDs), the bleach signal is dominated by the electrons due to high effective masses of the holes relative to the electrons (for CdTe, $m_h^*/m_e^* = 4$) and negligible/very little acceleration of bleach recovery is observed for hole extraction from those QDs.[41−43] However, as the effective masses of electrons (m_e^*) and holes (m_h^*) are quite similar for the lead halide perovskites (for $CsPbBr_3$, $m_e^* = 0.15m_0$ and $m_h^* = 0.14m_0$, where m_0 = rest mass of electron), both electrons and holes can contribute to the bleach signal.[28] However, in view of higher degeneracy of the valence band, the relative contribution of the electrons and holes toward bleach works out to be ∼67.2 and 32.8%, for $CsPbBr_3$ NCs, respectively.[28] Therefore, in the present case, the bleach signal is sensitive to both electrons and holes and the acceleration in bleach recovery in the presence of AMP can be due to the transfer of both electron and hole or one of them. In order to determine the identity of the species being transferred from the NCs, we look into the band edge potentials of both the NCs and the HOMO−LUMO levels of AMP. The energy levels of the valence and conduction band edges of the NCs are taken from a recent literature considering similar size of the NCs.[44] In an earlier study also we used these values.[45]

The HOMO energy level of AMP (−5.04 eV) was estimated through cyclic voltammetry measurement. By considering the optical band gap of AMP as the energy difference between HOMO and LUMO levels, we estimated the LUMO energy as −1.95 eV. These values agree well with earlier literature.[46] It is evident from Figure 5 that the LUMO level of AMP is far above the conduction band edge of both the NCs and hence, the

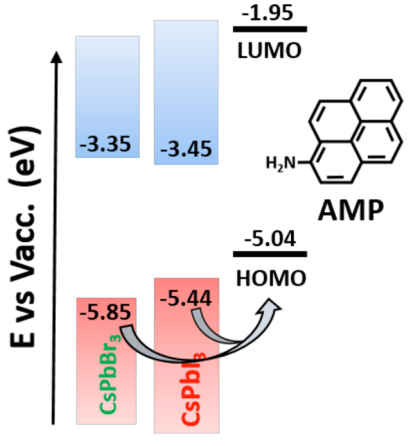

Figure 5. Band alignment of $CsPbBr_3$ and $CsPbI_3$ NCs and HOMO−LUMO levels of AMP molecule.

DOI: 10.1021/acs.jpcc.7b12813
J. Phys. Chem. C 2018, 122, 13617−13623

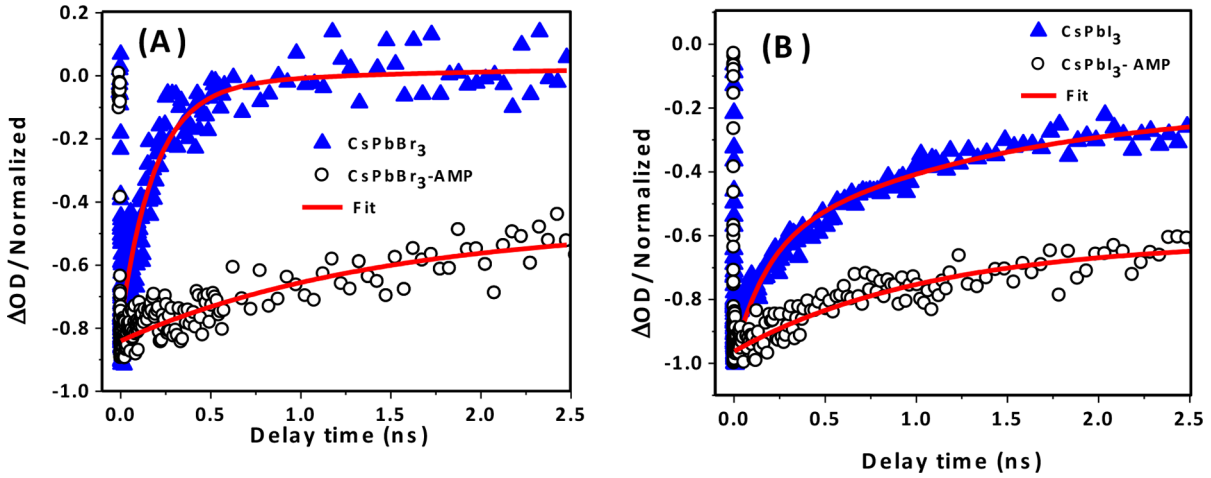

Figure 6. Bleach recovery kinetics of (A) $CsPbBr_3$ and (B) $CsPbI_3$ NCs without and with AMP monitored at their respective bleach maxima.

photoinduced electron transfer from NCs to AMP can be completely ruled out. It is also evident from Figure 5 that photoinduced hole transfer from the valence band of the NCs to the HOMO level of AMP (−5.04 eV) is the only energetically feasible process and the driving force for this process is higher for $CsPbBr_3$ compared to $CsPbI_3$. Thus, we can conclude that acceleration of the bleach recovery in the presence of AMP is solely due to selective removal of holes from the photoexcited NCs. To obtain quantitative information on hole transfer dynamics, we have compared the bleach recovery kinetics of $CsPbBr_3$ in presence and absence of AMP. For bare $CsPbBr_3$ NCs, the bleach recovery is represented by a single exponential decay function with a time constant >1 ns. The single exponential nature of the decay profile with long lifetime indicates absence of any fast nonradiative carrier trapping and nonlinear phenomenon like exciton−exciton annihilation under this low pump fluence.[39] This long time constant must be due to electron−hole recombination process.[28] In the presence of AMP, in addition to the long time component, another short component is observable for both the NCs (Figure 6 and Table 1). This short-component is

Table 1. Bleach Recovery Parameters of Individual NCs in the Absence and Presence of AMP

systems	τ_1 (a_1) [ps]	τ_2 (a_2) [ns]
$CsPbBr_3$	–	>1
$CsPbBr_3$–AMP	120 ± 8.00 (0.70)	>1 (0.30)
$CsPbI_3$	–	>1
$CsPbI_3$–AMP	170 ± 10.0 (0.41)	>1 (0.59)

clearly due to a process induced by AMP. As it is already shown that hole transfer from the NCs is the only possibility, the observed time constant represents the hole transfer kinetics. The estimated hole transfer times from $CsPbBr_3$ and $CsPbI_3$ NCs are estimated to be 120 and 170 ps, respectively.

A faster hole transfer from $CsPbBr_3$ compared to $CsPbI_3$ is consistent with the band alignment of two NCs and a higher driving force ($-\Delta G$) for the former. In this context, we note that in both cases we could not observe any new absorption feature due to the product of hole transfer process ($AMP^{+}\bullet$). This, however, is not surprising considering strong absorption due to both NCs throughout the monitoring window. We further note that Lian and co-workers obtained two different time scales (26 and 330 ps) for hole transfer using phenothiazine.[28] Whereas, Mandal and co-workers reported a hole transfer time scale of 137−166 ps for the same system.[30] The observed hole transfer time scale of 120−170 ps for $CsPbBr_3$ and $CsPbI_3$ to AMP is comparable or better than the above two cases.

4. CONCLUSION

By exploiting the π-framework of the pyrene moiety and excellent surface anchoring ability of amino functionality on the perovskite NCs, it is shown here that even very simple system like AMP can exhibit promising hole transport properties. Considering this finding and recent literature report of a PCE of 12.4% in fabricated solar cell with a pyrene derivative as hole transport material, we think there exists considerable scope of improving this efficiency by engineering the pyrene core with suitable functionalities and using them as cost-effective hole transport materials.

■ ASSOCIATED CONTENT

Supporting Information

The Supporting Information is available free of charge on the ACS Publications website at DOI: 10.1021/acs.jpcc.7b12813.

Absorption and PL spectra of $CsPbBr_3$ NCs with addition of AMP, PL decay dynamics of $CsPbBr_3$ with and without AMP, and PL decay parameters (PDF)

■ AUTHOR INFORMATION

Corresponding Author

*(A.S.) E-mail: anunay@uohyd.ac.in.

ORCID

Apurba De: 0000-0002-3042-0642

Navendu Mondal: 0000-0001-5002-9678

Anunay Samanta: 0000-0003-1551-0209

Notes

The authors declare no competing financial interest.

■ ACKNOWLEDGMENTS

This work is supported by Grant No. EMR/2015/000582 and J. C. Bose Fellowship (to AS) of the Science and Engineering Research Board (SERB), Department of Science and Technology (DST), India. We also acknowledge the UGC-UPE support to our University and Femtosecond Laser Facility

DOI: 10.1021/acs.jpcc.7b12813
J. Phys. Chem. C 2018, 122, 13617−13623

of the School. We thank our University Centre for Nanotechnology for the TEM facility. We also thank Dr. Prakriti Ranjan Bangal from IICT, Hyderabad for extending their femtosecond facility to measure some of the TA spectra of the samples. Thanks are due to Mr. Subhabrata Mukhopadhyay for the CV measurements. AD and NM thank UGC-BSR and CSIR, respectively, for Fellowships.

REFERENCES

(1) Lee, M. M.; Teuscher, J.; Miyasaka, T.; Murakami, T. N.; Snaith, H. J. Efficient Hybrid Solar Cells Based on Meso-superstructured Organometal Halide Perovskites. *Science* **2012**, *338*, 643−647.

(2) Snaith, H. J. Perovskites: The Emergence of a New Era for Low-Cost, High-Efficiency Solar Cells. *J. Phys. Chem. Lett.* **2013**, *4*, 3623−3630.

(3) Liang, J.; Wang, C.; Wang, Y.; Xu, Z.; Lu, Z.; Ma, Y.; Zhu, H.; Hu, Y.; Xiao, C.; Yi, X.; et al. All-Inorganic Perovskite Solar Cells. *J. Am. Chem. Soc.* **2016**, *138*, 15829−15832.

(4) Swarnkar, A.; Marshall, A. R.; Sanehira, E. M.; Chernomordik, B. D.; Moore, D. T.; Christians, J. A.; Chakrabarti, T.; Luther, J. M. Quantum dot−induced phase stabilization of α-$CsPbI_3$ perovskite for high-efficiency photovoltaics. *Science* **2016**, *354*, 92−95.

(5) Song, J.; Li, J.; Li, X.; Xu, L.; Dong, Y.; Zeng, H. Quantum Dot Light-Emitting Diodes Based on Inorganic Perovskite Cesium Lead Halides ($CsPbX_3$). *Adv. Mater.* **2015**, *27*, 7162−7167.

(6) Wang, Y.; Li, X.; Nalla, V.; Zeng, H.; Sun, H. Solution-Processed Low Threshold Vertical Cavity Surface Emitting Lasers from All-Inorganic Perovskite Nanocrystals. *Adv. Funct. Mater.* **2017**, *27*, 1605088.

(7) Li, X.; Wu, Y.; Zhang, S.; Cai, B.; Gu, Y.; Song, J.; Zeng, H. $CsPbX_3$ Quantum Dots for Lighting and Displays: Room-Temperature Synthesis, Photoluminescence Superiorities, Underlying Origins and White Light-Emitting Diodes. *Adv. Funct. Mater.* **2016**, *26*, 2435−2445.

(8) Veldhuis, S. A.; Boix, P. P.; Yantara, N.; Li, M.; Sum, T. C.; Mathews, N.; Mhaisalkar, S. G. Perovskite Materials for Light-Emitting Diodes and Lasers. *Adv. Mater.* **2016**, *28*, 6804−6834.

(9) Kojima, A.; Teshima, K.; Shirai, Y.; Miyasaka, T. Organometal Halide Perovskites as Visible-Light Sensitizers for Photovoltaic Cells. *J. Am. Chem. Soc.* **2009**, *131*, 6050−6051.

(10) https://www.nrel.gov/pv/assets/images/efficiency-chart.png.

(11) Burschka, J.; Pellet, N.; Moon, S.-J.; Humphry-Baker, R.; Gao, P.; Nazeeruddin, M. K.; Grätzel, M. Sequential deposition as a route to high-performance perovskite-sensitized solar cells. *Nature* **2013**, *499*, 316−319.

(12) Liu, X.; kong, F.; Jin, S.; Chen, W.; Yu, T.; Hayat, T.; Alsaedi, A.; Wang, H.; Tan, Z.; Chen, J.; et al. Molecular Engineering of Simple Benzene−Arylamine HoleTransporting Materials for Perovskite Solar Cells. *ACS Appl. Mater. Interfaces* **2017**, *9*, 27657−27663.

(13) Grisorio, R.; Roose, B.; Colella, S.; Listorti, A.; Suranna, G. P.; Abate, A. Molecular Tailoring of Phenothiazine-Based Hole-Transporting Materials for High Performing Perovskite Solar Cells. *ACS Energy Lett.* **2017**, *2*, 1029−1034.

(14) Jeon, N. J.; Lee, J.; Noh, J. H.; Nazeeruddin, M. K.; Grätzel, M.; Seok, S. I. Efficient Inorganic−Organic Hybrid Perovskite Solar Cells Based on Pyrene Arylamine Derivatives as Hole-Transporting Materials. *J. Am. Chem. Soc.* **2013**, *135*, 19087−19090.

(15) Guan, L.; Yin, X.; Zhao, D.; Wang, C.; An, Q.; Yu, J.; Shrestha, N.; Grice, C. R.; Awni, R. A.; Yu, Y.; et al. Cost-effective hole transporting material for stable and efficient perovskite solar cells with fill factors up to 82%. *J. Mater. Chem. A* **2017**, *5*, 23319−23327.

(16) Mondal, N.; Samanta, A. Complete ultrafast charge carrier dynamics in photo-excited all-inorganic perovskite nanocrystals ($CsPbX_3$). *Nanoscale* **2017**, *9*, 1878−1885.

(17) Seth, S.; Mondal, N.; Patra, S.; Samanta, A. Fluorescence Blinking and Photoactivation of All-Inorganic Perovskite Nanocrystals $CsPbBr_3$ and $CsPbBr_2I$. *J. Phys. Chem. Lett.* **2016**, *7*, 266−271.

(18) Uratani, H.; Yamashita, K. Charge Carrier Trapping at Surface Defects of Perovskite Solar Cell Absorbers: A First-Principles Study. *J. Phys. Chem. Lett.* **2017**, *8*, 742−746.

(19) Sherkar, T. S.; Momblona, C.; Gil-Escrig, L.; Ávila, J.; Sessolo, M.; Bolink, H. J.; Koster, L. J. A. Recombination in Perovskite Solar Cells: Significance of Grain Boundaries, Interface Traps, and Defect Ions. *ACS Energy Lett.* **2017**, *2*, 1214−1222.

(20) Han, G.; Koh, T. M.; Lim, S. S.; Goh, T. W.; Guo, X.; Leow, S. W.; Begum, R.; Sum, T. C.; Mathews, N.; Mhaisalkar, S. Facile Method to Reduce Surface Defects and Trap Densities in Perovskite Photovoltaics. *ACS Appl. Mater. Interfaces* **2017**, *9*, 21292−21297.

(21) Uratani, H.; Yamashita, K. harge Carrier Trapping at Surface Defects of Perovskite Solar Cell Absorbers: A First-Principles Study. *J. Phys. Chem. Lett.* **2017**, *8*, 742−746.

(22) Noel, N. K.; Abate, A.; Stranks, S. D.; Parrott, E. S.; Burlakov, V. M.; Goriely, A.; Snaith, H. J. Enhanced Photoluminescence and Solar Cell Performance via Lewis Base Passivation of Organic−Inorganic Lead Halide Perovskites. *ACS Nano* **2014**, *8*, 9815−9821.

(23) Koscher, B. A.; Swabeck, J. K.; Bronstein, N. D.; Alivisatos, A. P. Essentially Trap-Free $CsPbBr_3$ Colloidal Nanocrystals by Postsynthetic Thiocyanate Surface Treatment. *J. Am. Chem. Soc.* **2017**, *139*, 6566−6569.

(24) Di Stasio, F.; Christodoulou, S.; Huo, N.; Konstantatos, G. Near-Unity Photoluminescence Quantum Yield in $CsPbBr_3$ Nanocrystal Solid-State Films via Postsynthesis Treatment with Lead Bromide. *Chem. Mater.* **2017**, *29*, 7663−7667.

(25) Woo, J. Y.; Kim, Y.; Bae, J.; Kim, T. G.; Kim, J. W.; Lee, D. C.; Jeong, S. Highly Stable Cesium Lead Halide Perovskite Nanocrystals through in Situ Lead Halide Inorganic Passivation. *Chem. Mater.* **2017**, *29*, 7088−7092.

(26) Wen, X.; Wu, J.; Gao, D.; Lin, C. Interfacial engineering with amino-functionalized graphene for efficient perovskite solar cells. *J. Mater. Chem. A* **2016**, *4*, 13482−13487.

(27) Maity, P.; Dana, J.; Ghosh, H. N. Multiple Charge Transfer Dynamics in Colloidal $CsPbBr_3$Perovskite Quantum Dots Sensitized Molecular Adsorbate. *J. Phys. Chem. C* **2016**, *120*, 18348−18354.

(28) Wu, K.; Liang, G.; Shang, Q.; Ren, Y.; Kong, D.; Lian, T. Ultrafast Interfacial Electron and Hole Transfer from $CsPbBr_3$ Perovskite Quantum Dots. *J. Am. Chem. Soc.* **2015**, *137*, 12792−12795.

(29) Ahmed, G. H.; Liu, J.; Parida, M. R.; Murali, B.; Bose, R.; AlYami, N. M.; Hedhili, M. N.; Peng, W.; Pan, J.; Besong, T. M. D.; et al. Shape-Tunable Charge Carrier Dynamics at the Interfaces between Perovskite Nanocrystals and Molecular Acceptors. *J. Phys. Chem. Lett.* **2016**, *7*, 3913−3919.

(30) Sarkar, S.; Ravi, V. K.; Banerjee, S.; Yettapu, G. R.; Markad, G. B.; Nag, A.; Mandal, P. Terahertz Spectroscopic Probe of Hot Electron and Hole Transfer from Colloidal $CsPbBr_3$ Perovskite Nanocrystals. *Nano Lett.* **2017**, *17*, 5402−5407.

(31) Nair, V. C.; Muthu, C.; Rogach, A. L.; Kohara, R.; Biju, V. Channeling Exciton Migration into Electron Transfer in Formamidinium Lead Bromide Perovskite Nanocrystal/Fullerene Composites. *Angew. Chem., Int. Ed.* **2017**, *56*, 1214−1218.

(32) Begum, R.; Parida, M. R.; Abdelhady, A. L.; Murali, B.; Alyami, N. M.; Ahmed, G. H.; Hedhili, M. N.; Bakr, O. M.; Mohammed, O. F. Engineering Interfacial Charge Transfer in CsPbBr3 Perovskite Nanocrystals by Heterovalent Doping. *J. Am. Chem. Soc.* **2017**, *139*, 731−737.

(33) Protesescu, L.; Yakunin, S.; Bodnarchuk, M. I.; Krieg, F.; Caputo, R.; Hendon, C. H.; Yang, R. X.; Walsh, A.; Kovalenko, M. V. Nanocrystals of Cesium Lead Halide Perovskites ($CsPbX_3$, X = Cl, Br, and I): Novel Optoelectronic Materials Showing Bright Emission with Wide Color Gamut. *Nano Lett.* **2015**, *15*, 3692−3696.

(34) Chandra Sekhar, M.; De, A.; Hossain, S. S.; Samanta, A. Roles of the methyl and methylene groups of mercapto acids in the photoluminescence efficiency and carrier trapping dynamics of CdTe QDs. *Phys. Chem. Chem. Phys.* **2017**, *19*, 1536−1542.

(35) Mondal, N.; Samanta, A. Ultrafast Charge Transfer and Trapping Dynamics in a Colloidal Mixture of Similarly Charged

DOI: 10.1021/acs.jpcc.7b12813
J. Phys. Chem. C 2018, 122, 13617−13623

CdTe Quantum Dots and Silver Nanoparticles. *J. Phys. Chem. C* **2016**, *120*, 650−658.
(36) Liu, F.; Zhang, Y.; Ding, C.; Kobayashi, S.; Izuishi, T.; Nakazawa, N.; Toyoda, T.; Ohta, T.; Hayase, S.; Minemoto, T.; et al. Highly Luminescent Phase-Stable $CsPbI_3$ Perovskite Quantum Dots Achieving Near 100% Absolute Photoluminescence Quantum Yield. *ACS Nano* **2017**, *11*, 10373−10383.
(37) Ponseca, C. S., Jr.; Chábera, P.; Uhlig, J.; Persson, P.; Sundström, V. Ultrafast Electron Dynamics in Solar Energy Conversion. *Chem. Rev.* **2017**, *117*, 10940−11024.
(38) Makarov, N. S.; Guo, S.; Isaienko, O.; Liu, W.; Robel, I.; Klimov, V. I. Spectral and Dynamical Properties of Single Excitons, Biexcitons, and Trions in Cesium−Lead-Halide Perovskite Quantum Dots. *Nano Lett.* **2016**, *16*, 2349−2362.
(39) Aneesh, J.; Swarnkar, A.; Kumar Ravi, V.; Sharma, R.; Nag, A.; Adarsh, K. V. Ultrafast Exciton Dynamics in Colloidal $CsPbBr_3$ Perovskite Nanocrystals: Biexciton Effect and Auger Recombination. *J. Phys. Chem. C* **2017**, *121*, 4734−4739.
(40) Manser, J. S.; Christians, J. A.; Kamat, P. V. Intriguing Optoelectronic Properties of Metal Halide Perovskites. *Chem. Rev.* **2016**, *116*, 12956−13008.
(41) Klimov, V. I.; McBranch, D. W.; Leatherdale, C. A.; Bawendi, M. G. Electron and Hole Relaxation Pathways in Semiconductor Quantum Dots. *Phys. Rev. B: Condens. Matter Mater. Phys.* **1999**, *60*, 13740−13749.
(42) Sekhar, M. C.; Samanta, A. Ultrafast Transient Absorption Study of the Nature of Interaction between Oppositely Charged Photoexcited CdTe Quantum Dots and Cresyl Violet. *J. Phys. Chem. C* **2015**, *119*, 15661−15668.
(43) Huang, J.; Huang, Z.; Jin, S.; Lian, T. Exciton Dissociation in CdSe Quantum Dots by Hole Transfer to Phenothiazine. *J. Phys. Chem. C* **2008**, *112*, 19734−19738.
(44) Ravi, V. K.; Markad, G. B.; Nag, A. Band Edge Energies and Excitonic Transition Probabilities of Colloidal $CsPbX_3$ (X = Cl, Br, I) Perovskite Nanocrystals. *ACS Energy Lett.* **2016**, *1*, 665−671.
(45) Mondal, N.; De, A.; Samanta, A. All-Inorganic Perovskite Nanocrystals Assisted Extraction of Hot Electrons and Biexcitons from Photoexcited CdTe Quantum Dots. *Nanoscale* **2018**, *10*, 639−645.
(46) Kaur, M.; Kaur, P.; Dhuna, V.; Singh, S.; Singh, K. A ferrocene−pyrene based 'turn-on' chemodosimeter for Cr3+ − application in bioimaging. *Dalton Trans.* **2014**, *43*, 5707−5712.

DOI: 10.1021/acs.jpcc.7b12813
J. Phys. Chem. C 2018, 122, 13617−13623

ACS Energy LETTERS

http://pubs.acs.org/journal/aelccp

LETTER

Hot Hole Transfer Dynamics from $CsPbBr_3$ Perovskite Nanocrystals

Apurba De, Somnath Das, and Anunay Samanta*

Cite This: *ACS Energy Lett.* 2020, 5, 2246−2252

Read Online

ACCESS | Metrics & More | Article Recommendations | Supporting Information

ABSTRACT: Transfer of the hot charge carriers prior to their cooling to the band-edge states can enhance the efficiency of a semiconductor-based solar cell much beyond its Shockley−Queisser (SQ) limiting value. Herein, we explore transfer of hot holes from the $APbBr_3$ nanocrystals (NCs) employing a carefully chosen molecular system, 4-mercaptophenol. Ultrafast pump−probe and fluorescence measurements indeed confirm this transfer process, whose efficiency depends on the energy content of the hole, and a maximum efficiency of ∼43% is achieved with $CsPbBr_3$ NCs for a photoexcitation energy of $\sim 1.46E_g$ (E_g is the band gap of the NCs). While the estimated hot hole cooling and transfer rates are quite comparable, hole transfer from the band edge is found to be a significantly slower process. The findings of the present study suggest that exceeding the SQ efficiency of the solar cells based on the perovskites can indeed be a reality.

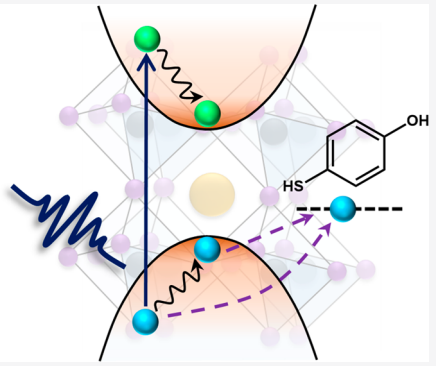

Lead halide-based perovskites have emerged as most promising candidates for photovoltaic applications, and a solar power conversion efficiency (PCE) of >24% has been achieved within a short period,[1] since the pioneering work of Miyasaka and co-workers in 2009.[2] One major factor responsible for low efficiency of the conventional single-junction solar cells is rapid cooling of the hot carriers, produced by solar photons of energy higher than that of the band gap, to the band edge states. Calculations show that utilization of the hot carriers can push this efficiency to ∼66%, which is well-beyond the Shockley−Queisser limiting value (33%).[3,4]

Several studies have been undertaken to understand the mechanism of relaxation of the hot charge carriers in lead halide perovskites, which indicate that the hot carriers first thermalize to a quasi-equilibrium state through carrier−carrier scattering and then attain thermal equilibrium through carrier−phonon and carrier−impurity scattering in a subpico-second time scale.[5−14] These studies have revealed important factors like hot phonon bottleneck, large polaron formation, Auger heating, high carrier densities, and dielectric confinement. However, the transfer of hot carriers prior to their cooling continues to remain as a challenging task for the narrow time window available for this purpose.[15−19] Moreover, an understanding of the charge transfer dynamics involving the perovskites is also of considerable importance in photocatalytic applications.[20−24]

Herein, we focus on the transfer of hot carriers from $APbBr_3$ [A = Cs^+, $CH_3NH_3^+$(MA^+) and $CH(NH_2)_2^+$ (FA^+)] nanocrystals (NCs). Specifically, we investigate the dynamics and transfer efficiency of the hot holes from these NCs to a molecular system, 4-mercaptophenol (MTH), chosen for its surface-anchoring thiol unit and energetic considerations of its HOMO and LUMO *vis a vis* the valence and conduction bands of the perovskite NCs, which permit only hole transfer from photoexcited NCs to MTH (Scheme 1). The cooling dynamics and transfer efficiency of the hot hole have been studied as a function of the excitation energy, and a maximum efficiency of ∼43% from $CsPbBr_3$ NCs is achieved for photoexcitation energy of $\sim 1.46E_g$ (E_g is the band gap of the NCs).

All three $APbBr_3$ [A = Cs^+, MA^+, and FA^+] NCs were prepared by reported methods,[29−31] the details of which are provided in the Supporting Information. The average edge lengths of the NCs lie between 10 and 14 nm (Figures 1A and S1). The photoluminescence quantum yields (PLQY) of these NCs lie between 80 and 90%, and the PL maxima appear at ∼512 nm ($CsPbBr_3$), 518 nm ($MAPbBr_3$), and 527 nm ($FAPbBr_3$). The MTH-adsorbed NCs (indicated hereafter as $APbBr_3$-MTH NCs) were obtained by a simple ligand-exchange protocol (sonication of a mixture of a colloidal dispersion of the NCs and a solution of MTH in hexane; details are provided in the Supporting Information). The fact that MTH anchors onto the surface of the NCs through its

Received: May 16, 2020
Accepted: June 8, 2020
Published: June 8, 2020

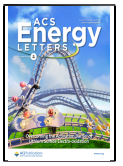

Downloaded via UNIV OF HYDERABAD on July 10, 2020 at 12:20:30 (UTC).
See https://pubs.acs.org/sharingguidelines for options on how to legitimately share published articles.

© 2020 American Chemical Society

https://dx.doi.org/10.1021/acsenergylett.0c01063
ACS Energy Lett. 2020, 5, 2246−2252

Scheme 1. Alignment of the Energy Levels of $APbBr_3$ NCs and MTH[a]

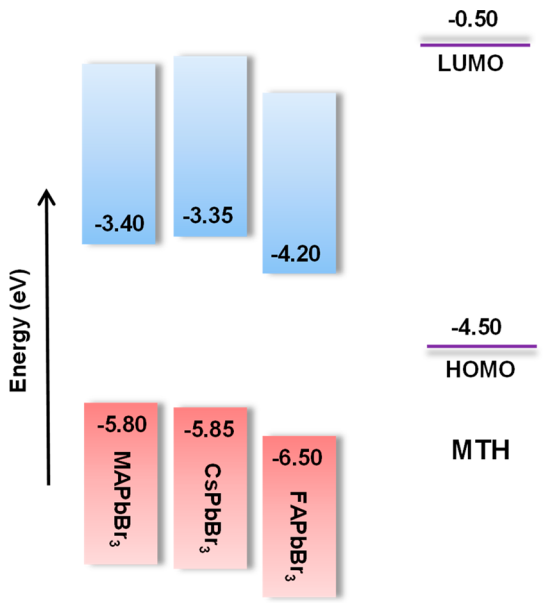

[a]The indicated energy values are obtained from refs 25−28.

thiol functionality is established by control experiments and FTIR measurements (Supporting Information) and that the morphological and structural stability of the system are unaffected after the ligand exchange is evident from the TEM image of $CsPbBr_3$-MTH (Figure S2).

Even though the absorption spectra of $CsPbBr_3$ and $CsPbBr_3$-MTH NCs are almost identical (Figure 1A),[22] the PLQY values of the two systems differ by nearly two orders of magnitude (~90% vs <1%) (Figure 1B). MTH also has a pronounced effect on PL decay characteristics of the NCs. Time-correlated single-photon counting (TCSPC) PL decay measurements show an average lifetime of 5.26 ns for $CsPbBr_3$ NCs (Figure 1B inset and Table S1). However, for $CsPbBr_3$-MTH, the PL decays too fast to measure the lifetime using this setup (see below for actual value measured by upconversion technique), which has a time-resolution of ~60 ps.[32] In the case of $MAPbBr_3$ and $FAPbBr_3$ NCs, a similar trend was observed (Figure S4). These PL data indicate strong interaction between the photogenerated charge carriers of the three NCs and MTH.

To determine which of the three $APbBr_3$ NCs is best suited for the transfer of a hot carrier (hot hole in the present case), we first measure their hot carrier cooling (HCC) time using femtosecond pump−probe technique because a system with slower HCC provides a greater opportunity for its transfer. As excitation fluence and quantum confinement can also influence the estimated HCC time,[15,33] we maintained sufficiently low pump fluence (~0.08×10^{14} photons/cm^2) in all cases to avoid nonlinear processes[33,34] and chose NCs with size larger than their exciton Bohr diameter to minimize the influence of quantum confinement.[35−37] As the HCC time depends on the energy content of the carrier,[35] during estimation of this quantity we made sure that the hot carriers possess same excess energy in all three cases. The same excess energy of the carriers (which we fixed at ~$1.46E_g$) in different systems was maintained by varying the excitation wavelengths for the systems. For this purpose, the E_g values for different NCs were first calculated from the derivative plot of the absorption spectra (Figure S5), and then the excitation wavelength of the pump−probe study (Figure 2A) for each system was adjusted such that the excitation energy corresponds to ~$1.46E_g$.

Representative transient absorption (TA) spectra of the $CsPbBr_3$ NCs at early times are shown in Figure 2B (TA spectra of $FAPbBr_3$ and $MAPbBr_3$ are in the Supporting Information, Figure S6). The spectra comprises a sharp negative (bleach) signal, which represents state-filling of the photogenerated carriers to the band-edges,[35,36,38] a positive absorption band at the lower energy side of the bleach signal due to polaron formation,[38] and a somewhat weak positive absorption band at the higher-energy side of the same due to carrier absorption from the band edge states.[35] The HCC time is estimated by monitoring the *formation* of the bleach signal of the spectra.[35,38−41] The HCC times estimated from the bleach formation profiles (Figure 2C) are 800 ± 20, 456 ± 10, and 334 ± 43 fs for $CsPbBr_3$, $MAPbBr_3$, and $FAPbBr_3$, respectively. A faster HCC in hybrid perovskites ($FAPbBr_3$ and $MAPbBr_3$) is consistent with the literature.[33] As these results show that the carriers remain hot for the longest duration in $CsPbBr_3$ NCs, this system is expected to be most appropriate for the

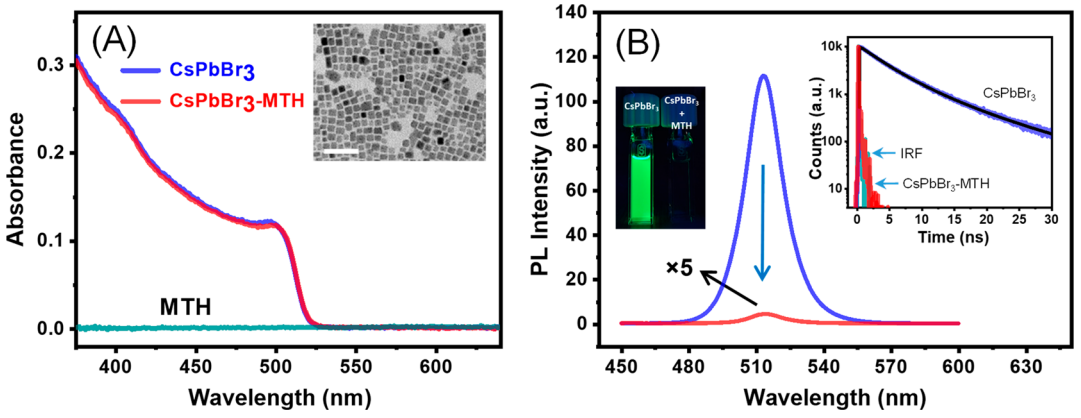

Figure 1. (A) Absorption spectra of $CsPbBr_3$, $CsPbBr_3$-MTH, and MTH. TEM image (in 50 nm scale) of the $CsPbBr_3$ NCs is shown in the inset. (B) PL spectra of the NCs (λ_{ex} = 400 nm). Digital images of the solutions and PL decay profiles (λ_{ex} = 405 nm) of the NCs are also provided in the insets. The concentration maintained here was ~100 nM and ~25 μM for $CsPbBr_3$ and MTH, respectively. PL data of the $MAPbBr_3$ and $FAPbBr_3$ NCs are provided in Supporting Information.

https://dx.doi.org/10.1021/acsenergylett.0c01063
ACS Energy Lett. 2020, 5, 2246−2252

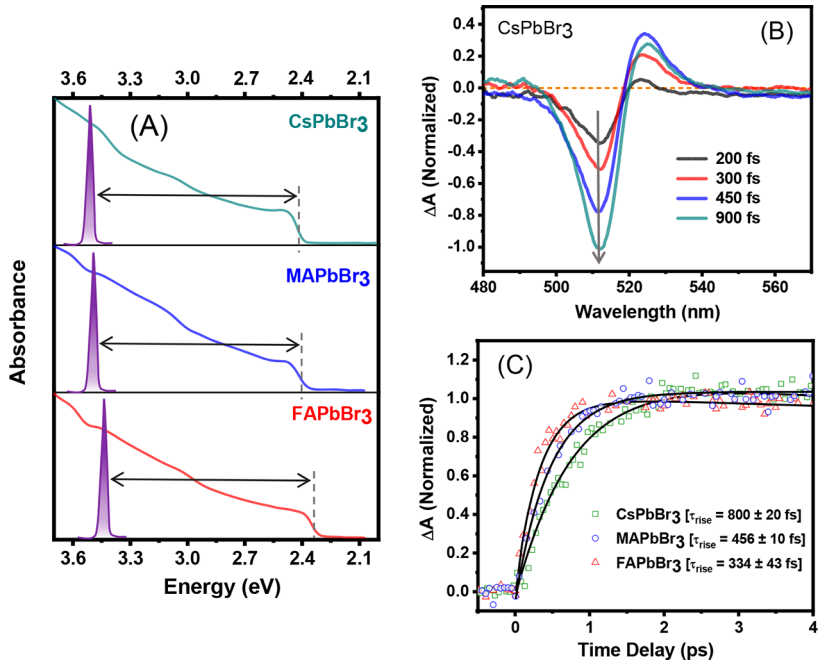

Figure 2. (A) Absorption spectra of the NCs. The positions of the vertical dashed lines indicate the band gaps of the systems, and the Gaussian profiles represent the pump energies used for respective samples in TA measurements. (B) Early time TA spectra of $CsPbBr_3$ NCs (upon $1.46E_g$ photoexcitation). (C) Bleach formation kinetics (monitored at respective bleach maximum) of the three NCs representing the relaxation dynamics of the hot carriers possessing the same excess energy.

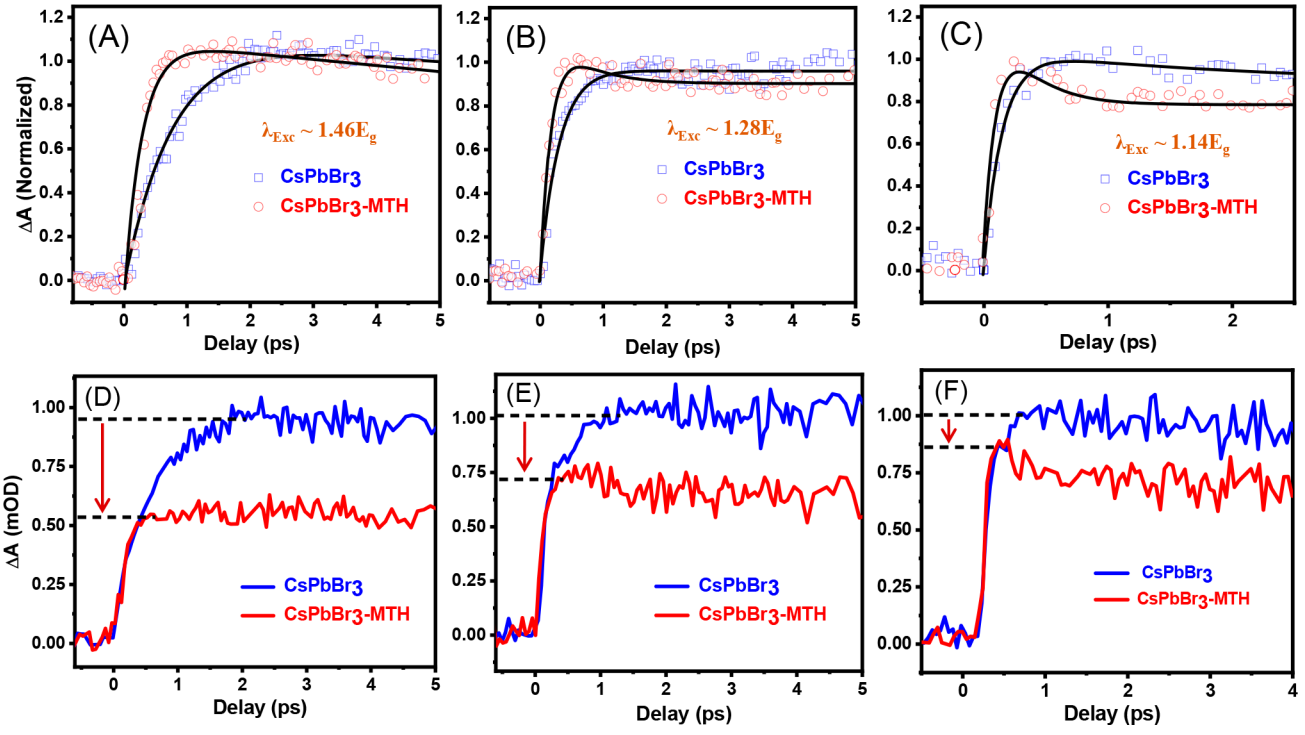

Figure 3. Bleach formation kinetics of $CsPbBr_3$ and $CsPbBr_3$-MTH NCs for excitation wavelengths of (A) 350 nm, (B) 400 nm, and (C) 450 nm. Panels D–F compare the bleach amplitudes of the two systems at the indicated excitation wavelengths.

transfer of hot carriers, and hence, the subsequent measurements and discussion are focused on the $CsPbBr_3$ NCs.

Even though the TA spectra (λ_{ex} = 350 nm) of the $CsPbBr_3$ and $CsPbBr_3$-MTH NCs are very similar (Figures 2B and S7), the bleach formation time, which represents the relaxation dynamics of the carriers, differs widely (800 ± 20 and 280 ± 18 fs, respectively) in two cases. A faster HCC in $CsPbBr_3$-MTH NCs (Figure 3A and Table 1) is a reflection of a competitive hot carrier transfer process. As the effective masses of the electron and hole are very similar (m_e^*/m_h^* = 1.07) in $CsPbBr_3$,[42,43] both hot electron and hot hole are generated in almost equal energy content on photoexcitation, and hence, the bleach formation is representative of the relaxation of both the carriers.[36,39] Even though acceleration of bleach formation

https://dx.doi.org/10.1021/acsenergylett.0c01063
ACS Energy Lett. 2020, 5, 2246−2252

Table 1. Bleach Formation Time of $CsPbBr_3$ and $CsPbBr_3$-MTH NCs for Different Excitation Pump Wavelengths

λ_{ex} (nm)	τ_{rise} [fs]/$CsPbBr_3$	τ_{rise} [fs]/ $CsPbBr_3$-MTH
350	800 ± 20	280 ± 18
400	440 ± 15	210 ± 12
450	149 ± 17	109 ± 15

in $CsPbBr_3$-MTH NCs can in principle be due to electron or/and hole transfer process(es),[44,45] in the present case, thermodynamic consideration of the energetics of the interacting components suggests hot hole transfer from the NCs as the only possibility.

An approximate rate of the transfer of hot holes is calculated (using $k = 1/\tau_{NCs\text{-}MTH} - 1/\tau_{NCs}$) as $\sim 2.3 \times 10^{12}$ s^{-1}. This high hot hole transfer rate is not surprising as it has to compete with the ultrafast hot hole relaxation rate ($\sim 1.25 \times 10^{12}$ s^{-1}). We have studied the hot carrier transfer dynamics for two other excitation wavelengths, 400 and 450 nm, corresponding to energy of $\sim 1.28E_g$ and $\sim 1.14E_g$, respectively. For lower excitation energies also, the bleach formation is faster in $CsPbBr_3$-MTH NCs; however, the change is not as pronounced as it is for higher excitation energy (Figure 3 and Table 1).

As the bleach amplitude is a measure of the number of carriers relaxing to the band edge, by monitoring this quantity one can determine whether the carriers are extracted and to what extent.[15,44−46] A lower peak bleach amplitude in $CsPbBr_3$-MTH NCs (Figure 3) compared to $CsPbBr_3$ under identical conditions clearly indicates transfer of the hot holes to MTH. The dependence of the HC transfer efficiency on the excitation energy is depicted in Figure 4. Maximum transfer

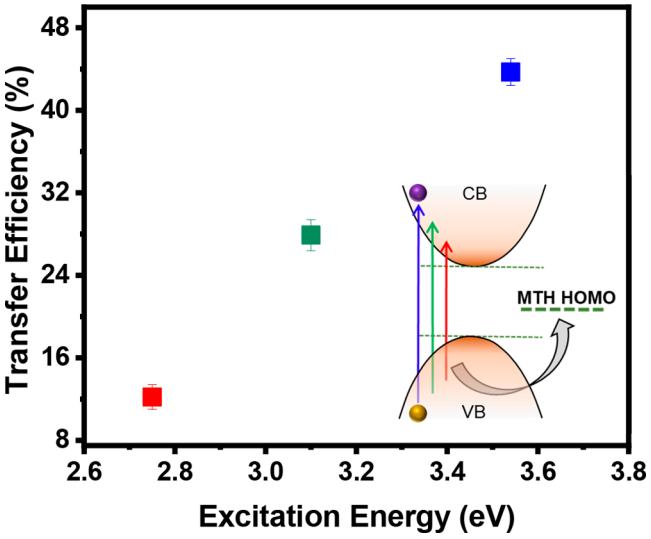

Figure 4. Dependence of the hot hole transfer efficiency on excitation energy.

efficiency of ~43% is observed for an excitation energy of $\sim 1.46E_g$, and the lowest (11%) is found for $\sim 1.14E_g$. When $CsPbBr_3$ and $CsPbBr_3$-MTH NCs are excited further closer to the band gap, at $\sim 1.08E_g$ (470 nm), both bleach formation dynamics and maximum bleach amplitude are found to be very similar for the two samples (Figure S8), indicating no hot hole transfer from $CsPbBr_3$ NCs. Such an energy dependence of the hole transfer efficiency is attributed to the difference in electronic coupling of the donor−acceptor wave functions with variation in excitation energy.[47,48] The higher the energy content of the hot hole, the larger the spread of its wave function beyond the NCs surface and consequently the greater the coupling of the hot hole wave function of the NCs with the HOMO of the organic moiety.[47,48]

We have examined the hot carrier transfer process also by the upconverted PL technique,[49] in which the hot carriers were generated by 400 nm (corresponding to $\sim 1.28E_g$) excitation of the NCs using ~200 fs pulses and monitoring time-dependent formation of the band-edge emission (~512 nm), which represents the cooling dynamics of the carriers.[35] The HCC time of the $CsPbBr_3$ NCs obtained by this method is found to be 460 ± 40 fs, which is in agreement with the literature[35] and also with our pump−probe measured value (440 ± 15 fs) for 400 nm excitation. However, for the $CsPbBr_3$-MTH NCs, the HCC time is much shorter (245 ± 25 fs) (Figure 5) and

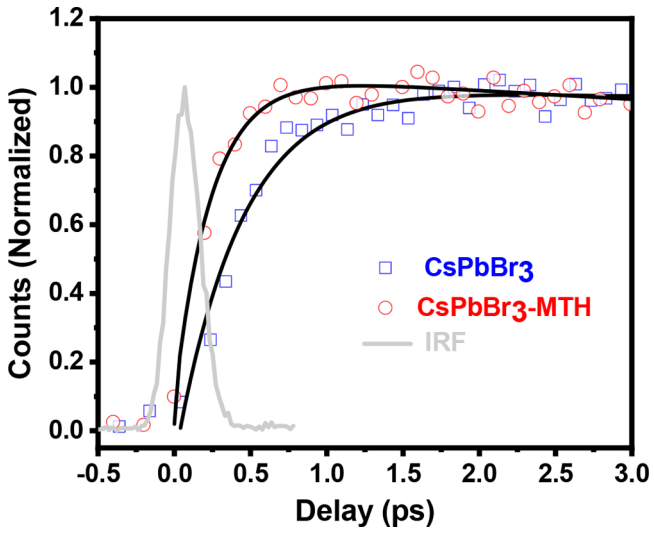

Figure 5. Formation kinetics of the band-edge PL of the two NCs measured by upconversion technique.

comparable to the value (210 ± 12 fs) obtained by the pump−probe technique. Comparison of the peak PL counts of the two samples indicates ~22% hot hole transfer efficiency in $CsPbBr_3$-MTH (Figure S9), which is consistent with our pump−probe result.

We have also examined the dynamics of transfer of the "cold" holes (i.e., those from the *band-edge*) by pump−probe technique by monitoring *recovery* of the bleach amplitude for λ_{ex} = 350 nm (Figures 6 and S10). While bleach recovery is a single exponential with τ > 1.2 ns for $CsPbBr_3$ NCs (representing the band edge electron−hole recombination time),[36,50] in the case of $CsPbBr_3$-MTH, two additional time components (14.1 ± 3 and 166.3 ± 15 ps) accompany the long component. The PL decay profile of the $CsPbBr_3$-MTH NCs, measured by the upconversion technique, also indicates a similar picture (Figure S11). Two short time components (16 ± 1.4 and 160 ± 10.2 ps) are observable in addition to the long decay component of >1.2 ns. It is to be noted here that accurate estimation of the longest time component is not possible using the femtosecond time-resolved TA and PL UC setup for nonavailability of a larger time window.[49,51,52] It is clear, however, that this long component arises from radiative recombination of the electron and hole.

https://dx.doi.org/10.1021/acsenergylett.0c01063
ACS Energy Lett. 2020, 5, 2246−2252

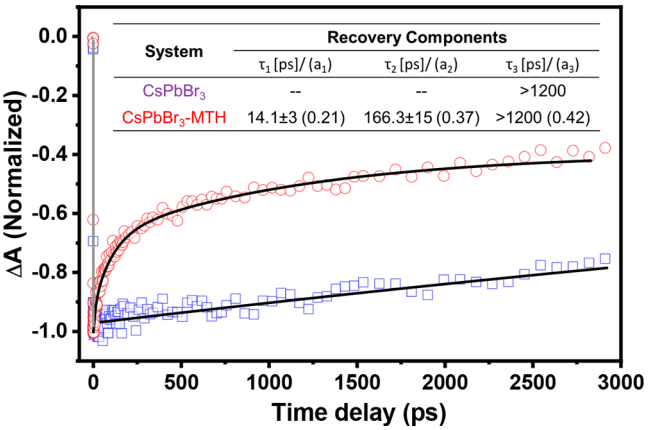

Figure 6. Comparison of the bleach recovery kinetics of $CsPbBr_3$ and $CsPbBr_3$-MTH NCs (λ_{ex} = 350 nm).

The short 14−16 ps component represents the hole transfer time (τ_{HT}) from the band-edge states of the NCs (corresponding to a rate of 6.2−7.6 × 10^{10} s^{-1}). This value is comparable with hole transfer time from the band-edge states in other perovskites.[53] Interestingly, hole transfer from the band edge states is relatively slower than that from the higher energy levels. A faster hot hole transfer could be the result of a larger driving force (Figure S14) and enhanced donor−acceptor wave function coupling.[47,48] The intermediate 160−166 ps component is attributed to a negative trion, which is formed upon transfer of holes by MTH. Though positive trion formation is more common in perovskite NCs because of the intrinsic electron trap states,[54−57] formation of negative trion is also reported in the presence of strong hole scavenger.[58] Moreover, the observed negative trion lifetime agrees well with the literature data.[54] The main findings of the present work are highlighted in Scheme 2 based on the above discussion.

In short, we demonstrate the transfer of hot holes from $CsPbBr_3$ NCs using a molecular system. We attribute this success to intrinsic slow hot hole cooling in the system and strong electronic coupling of the deep energy levels of the valence band of the NCs with those of the localized HOMO level of the organic moiety,[17] which is facilitated by the thiol anchoring unit. The findings show that an appropriate choice of a molecular system can indeed make the transfer process quite efficient.

Scheme 2. Schematic Illustration of Carrier Relaxation Dynamics in Photoexcited (~1.46E_g) $CsPbBr_3$-MTH NCs

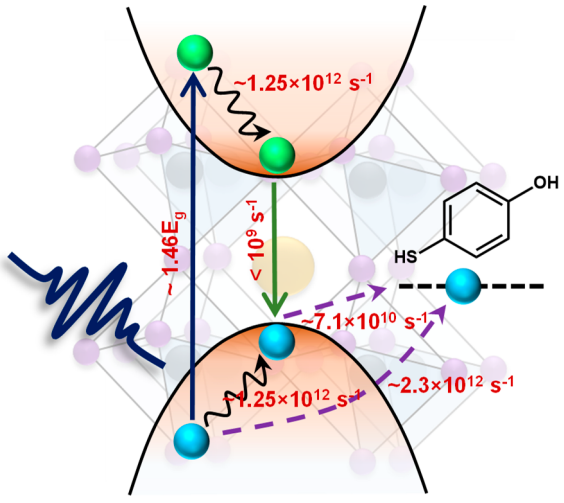

ASSOCIATED CONTENT

Supporting Information

The Supporting Information is available free of charge at https://pubs.acs.org/doi/10.1021/acsenergylett.0c01063.

Preparation and characterization of the $APbBr_3$ (A = Cs, MA and FA) and $APbBr_3$-MTH NCs, TEM images, PL spectra and decay profiles of MA/FA-$PbBr_3$ NCs, derivative plots for estimation of band gaps, TA spectra of $MAPbBr_3$ and $FAPbBr_3$NCs, TA spectra of $CsPbBr_3$-MTH, estimation of $\langle N \rangle$ through TA measurements, PL decay dynamics of $CsPbBr_3$ and $CsPbBr_3$-MTH in PL UC measurements, FTIR spectra, control experiments, and PL decay parameters (PDF)

AUTHOR INFORMATION

Corresponding Author

Anunay Samanta − *School of Chemistry, University of Hyderabad, Hyderabad 500 046, India;* orcid.org/0000-0003-1551-0209; Email: anunay@uohyd.ac.in

Authors

Apurba De − *School of Chemistry, University of Hyderabad, Hyderabad 500 046, India;* orcid.org/0000-0002-3042-0642

Somnath Das − *School of Chemistry, University of Hyderabad, Hyderabad 500 046, India*

Complete contact information is available at: https://pubs.acs.org/10.1021/acsenergylett.0c01063

Notes

The authors declare no competing financial interest.

ACKNOWLEDGMENTS

This work is supported by the J.C. Bose Fellowship (to A.S.) of the Science and Engineering Research Board (SERB), India. Financial and infrastructure support received from the University Grants Commission (UGC, through the UPE and CAS programs), Department of Science and Technology (DST, through the PURSE and FIST programs), and the University for the femtosecond pump−probe and upconversion facilities are also gratefully acknowledged. A.D. and S.D. thank UGC for Fellowships.

REFERENCES

(1) NREL Best Research-Cell Efficiencies. https://www.nrel.gov/pv/assets/pdfs/best-research-cell-efficiencies.20200406.pdf.

(2) Kojima, A.; Teshima, K.; Shirai, Y.; Miyasaka, T. Organometal Halide Perovskites as Visible-Light Sensitizers for Photovoltaic Cells. *J. Am. Chem. Soc.* **2009**, *131*, 6050−6051.

(3) Shockley, W.; Queisser, H. J. Detailed Balance Limit of Efficiency of p-n Junction Solar Cells. *J. Appl. Phys.* **1961**, *32*, 510−519.

(4) Ross, R.; Nozik, A. J. Efficiency of Hot-carrier Solar Energy Converters. *J. Appl. Phys.* **1982**, *53*, 3813−3818.

(5) Richter, J. M.; Branchi, F.; Camargo, F. V. d. A.; Zhao, B.; Friend, R. H.; Cerullo, G.; Deschler, F. Ultrafast Carrier Thermalization in Lead Iodide Perovskite Probed with Two-dimensional Electronic Spectroscopy. *Nat. Commun.* **2017**, *8*, 376.

(6) Fu, J.; Xu, Q.; Han, G.; Wu, B.; Huan, C. H. A.; Leek, M. L.; Sum, T. C. Hot Carrier Cooling Mechanisms in Halide Perovskites. *Nat. Commun.* **2017**, *8*, 1300.
(7) Kaur, G.; Babu, K. J.; Ghorai, N.; Goswami, T.; Maiti, S.; Ghosh, H. N. Polaron-Mediated Slow Carrier Cooling in a Type-1 3D/0D $CsPbBr_3$@Cs_4PbBr_6 Core-Shell Perovskite System. *J. Phys. Chem. Lett.* **2019**, *10*, 5302−5311.
(8) Boehme, S. C.; Brinck, S. t.; Maes, J.; Yazdani, N.; Zapata, F.; Chen, K.; Wood, V.; Hodgkiss, J. M.; Hens, Z.; Geiregat, P.; Infante, I. Phonon-Mediated and Weakly Size-Dependent Electron and Hole Cooling in $CsPbBr_3$ Nanocrystals Revealed by Atomistic Simulations and Ultrafast Spectroscopy. *Nano Lett.* **2020**, *20*, 1819−1829.
(9) Yin, J.; Maity, P.; Naphade, R.; Cheng, B.; He, J.-H.; Bakr, O. M.; Bredas, J.-L.; Mohammed, O. F. Tuning Hot Carrier Cooling Dynamics by Dielectric Confinement in Two-Dimensional Hybrid Perovskite Crystals Dielectric Confinement in Two-Dimensional Hybrid Perovskite Crystals. *ACS Nano* **2019**, *13*, 12621−12629.
(10) Li, Y.; Lai, R.; Luo, X.; Liu, X.; Ding, T.; Lu, X.; Wu, K. On the Absence of a Phonon Bottleneck in Strongly-Confined $CsPbBr_3$ Perovskite Nanocrystals. *Chem. Sci.* **2019**, *10*, 5983−5989.
(11) Verma, S. D.; Gu, Q.; Sadhanala, A.; Venugopalan, V.; Rao, A. Slow Carrier Cooling in Hybrid Pb-Sn Halide Perovskites. *ACS Energy Lett.* **2019**, *4*, 736−740.
(12) Hintermayr, V. A.; Polavarapu, L.; Urban, A. S.; Feldmann, J. Accelerated Carrier Relaxation through Reduced Coulomb Screening in Two Dimensional Halide Perovskite Nanoplatelets. *ACS Nano* **2018**, *12*, 10151−10158.
(13) Li, M.; Fu, J.; Xu, Q.; Sum, T. C. Slow Hot-Carrier Cooling in Halide Perovskites: Prospects for Hot-Carrier Solar Cells. *Adv. Mater.* **2019**, *31*, 1802486.
(14) Hopper, T. R.; Gorodetsky, A.; Jeong, A.; Krieg, F.; Bodnarchuk, M. I.; Maimaris, M.; Chaplain, M.; Macdonald, T. J.; Huang, X.; Lovrincic, R.; Kovalenko, M. V.; Bakulin, A. A. Hot Carrier Dynamics in Perovskite Nanocrystal Solids: Role of the Cold Carriers, Nanoconfinement, and the Surface. *Nano Lett.* **2020**, *20*, 2271−2278.
(15) Li, M.; Bhaumik, S.; Goh, T. W.; Kumar, M. S.; Yantara, N.; Gratzel, M.; Mhaisalkar, S.; Mathews, N.; Sum, T. C. Slow Cooling and Highly Efficient Extraction of Hot Carriers in Colloidal Perovskite Nanocrystals. *Nat. Commun.* **2017**, *8*, 14350.
(16) Sarkar, S.; Ravi, V. K.; Banerjee, S.; Yettapu, G. R.; Markad, G. B.; Nag, A.; Mandal, P. Terahertz Spectroscopic Probe of Hot Electron and Hole Transfer from Colloidal $CsPbBr_3$ Perovskite Nanocrystals. *Nano Lett.* **2017**, *17*, 5402−5407.
(17) Dursun, I.; Maity, P.; Yin, J.; Turedi, B.; Zhumekenov, A. A.; Lee, K. J.; Mohammed, O. F.; Bakr, O. M. Why are Hot Holes Easier to Extract than Hot Electrons from Methylammonium Lead Iodide Perovskite? *Adv. Energy Mater.* **2019**, *9*, 1900084.
(18) Lim, S. S.; Giovanni, D.; Zhang, Q.; Solanki, A.; Jamaludin, N. F.; Lim, J. W. M.; Mathews, N.; Mhaisalkar, S.; Pshenichnikov, M. S.; Sum, T. C. Hot Carrier Extraction in $CH_3NH_3PbI_3$ Unveiled by Pump-push-probe Spectroscopy. *Science Advances* **2019**, *5*, No. eaax3620.
(19) Shen, Q. S.; Ripolles, T.; Even, J.; Zhang, Y.; Ding, C.; Liu, F.; Izuishi, T.; Nakazawa, N.; Toyoda, T.; Ogomi, Y.; Hayase, S. Ultrafast Selective Extraction of Hot Holes from Cesium Lead Iodide Perovskite Films. *J. Energy Chem.* **2018**, *27*, 1170−1174.
(20) Kobosko, S. M.; DuBose, J. T.; Kamat, P. V. Perovskite Photocatalysis. Methyl Viologen Induces Unusually Long-Lived Charge Carrier Separation in $CsPbBr_3$ Nanocrystals. *ACS Energy Lett.* **2020**, *5*, 221−223.
(21) Li, Q.; Lian, T. Ultrafast Charge Separation in Two-Dimensional $CsPbBr_3$ Perovskite Nanoplatelets. *J. Phys. Chem. Lett.* **2019**, *10*, 566−573.
(22) Zhang, Y.-X.; Wang, H.-Y.; Zhang, Z.-Y.; Zhang, Y.; Sun, C.; Yue, Y.-Y.; Wang, L.; Chen, Q.-D.; Sun, H.-B. Photoluminescence Quenching of Inorganic Cesium Lead Halides Perovskite Quantum Dots ($CsPbX_3$) by Electron/Hole Acceptor. *Phys. Chem. Chem. Phys.* **2017**, *19*, 1920−1926.
(23) Zhang, Z.; He, J.; Long, R. Ultrafast Charge Separation and Recombination across a Molecule/$CsPbBr_3$ Quantum Dot Interface from First-Principles Nonadiabatic Molecular Dynamics Simulation. *J. Phys. Chem. C* **2019**, *123*, 23800−23806.
(24) DuBose, J. T.; Kamat, P. V. Probing Perovskite Photocatalysis. Interfacial Electron Transfer between $CsPbBr_3$ and Ferrocene Redox Couple. *J. Phys. Chem. Lett.* **2019**, *10*, 6074−6080.
(25) Ravi, V. K.; Markad, G. B.; Nag, A. Band Edge Energies and Excitonic Transition Probabilities of Colloidal $CsPbX_3$ (X = Cl, Br, I) Perovskite Nanocrystals. *ACS Energy Lett.* **2016**, *1*, 665−671.
(26) Yan, F.; Xing, J.; Xing, G.; Quan, L.; Tan, S. T.; Zhao, J.; Su, R.; Zhang, L.; Chen, S.; Zhao, Y.; Huan, A.; Sargent, E. H.; Xiong, Q.; Demir, H. V. Highly Efficient Visible Colloidal Lead-Halide Perovskite Nanocrystal Light-Emitting Diodes. *Nano Lett.* **2018**, *18*, 3157−3464.
(27) Perumal, A.; Shendre, S.; Li, M.; Tay, Y. K. E.; Sharma, V. K.; Chen, S.; Wei, Z.; Liu, Q.; Gao, Y.; Buenconsejo, P. J. S.; Tan, S. T.; Gan, C. L.; Xiong, Q.; Sum, T. C.; Demir, H. V. High Brightness Formamidinium Lead Bromide Perovskite Nanocrystal Light Emitting Devices. *Sci. Rep.* **2016**, *6*, 36733.
(28) Wang, L.; Han, J.; Zhu, Y.; Zhou, R.; Jaye, C.; Liu, H.; Li, Z.-Q.; Taylor, G. T.; Fischer, D. A.; Appenzeller, J.; Wong, S. S. Probing the Dependence of Electron Transfer on Size and Coverage in Carbon Nanotube-Quantum Dot Heterostructures. *J. Phys. Chem. C* **2015**, *119*, 26327−26338.
(29) Protesescu, L.; Yakunin, S.; Bodnarchuk, M. I.; Krieg, F.; Caputo, R.; Hendon, C. H.; Yang, R. X.; Walsh, A.; Kovalenko, M. V. Nanocrystals of Cesium Lead Halide Perovskites ($CsPbX_3$, X = Cl, Br, and I): Novel Optoelectronic Materials Showing Bright Emission with Wide Color Gamut. *Nano Lett.* **2015**, *15*, 3692−3696.
(30) Protesescu, L.; Yakunin, S.; Bodnarchuk, M. I.; Bertolotti, F.; Masciocchi, N.; Guagliardi, A.; Kovalenko, M. V. Monodisperse Formamidinium Lead Bromide Nanocrystals with Bright and Stable Green Photoluminescence. *J. Am. Chem. Soc.* **2016**, *138*, 14202−14205.
(31) Vybornyi, O.; Yakunin, S.; Kovalenko, M. V. Polar-solvent-free Colloidal Synthesis of Highly Luminescent Alkylammonium Lead Halide Perovskite Nanocrystals. *Nanoscale* **2016**, *8*, 6278−6283.
(32) Hossain, S. S.; Samanta, A. Solute Rotation and Translation Dynamics in an Ionic Deep Eutectic Solvent Based on Choline Chloride. *J. Phys. Chem. B* **2017**, *121*, 10556−10565.
(33) Chen, J.; Messing, M. E.; Zheng, K.; Pullerits, T. Cation-Dependent Hot Carrier Cooling in Halide Perovskite Nanocrystals. *J. Am. Chem. Soc.* **2019**, *141*, 3532−3540.
(34) De, A.; Mondal, N.; Samanta, A. Luminescence Tuning and Exciton Dynamics of Mn-doped $CsPbCl_3$ Nanocrystals. *Nanoscale* **2017**, *9*, 16722−16727.
(35) Mondal, N.; Samanta, A. Complete Ultrafast Charge Carrier Dynamics in Photo-excited All-inorganic Perovskite Nanocrystals ($CsPbX_3$). *Nanoscale* **2017**, *9*, 1878−1885.
(36) Mondal, N.; De, A.; Das, S.; Paul, S.; Samanta, A. Ultrafast Carrier Dynamics of Metal Halide Perovskite Nanocrystals and Perovskite Composites. *Nanoscale* **2019**, *11*, 9796−9818.
(37) Mondal, N.; De, A.; Samanta, A. Achieving Near-Unity Photoluminescence Efficiency for Blue-Violet-Emitting Perovskite Nanocrystals. *ACS Energy Lett.* **2019**, *4*, 32−39.
(38) Rossi, D.; Wang, H.; Dong, Y.; Qiao, T.; Qian, X.; Son, D. H. Light-Induced Activation of Forbidden Exciton Transition in Strongly Confined Perovskite Quantum Dots. *ACS Nano* **2018**, *12*, 12436−12443.
(39) Chung, H.; Jung, S. I.; Kim, H. J.; Cha, W.; Sim, E.; Kim, D.; Koh, W.-K.; Kim, J. Composition-Dependent Hot Carrier Relaxation Dynamics in Cesium Lead Halide ($CsPbX_3$, X = Br and I) Perovskite Nanocrystals. *Angew. Chem., Int. Ed.* **2017**, *56*, 4160−4164.
(40) Das, S.; De, A.; Samanta, A. Ambient Condition Mg^{2+} Doping Producing Highly Luminescent Green- and Violet-Emitting Perovskite Nanocrystals with Reduced Toxicity and Enhanced Stability. *J. Phys. Chem. Lett.* **2020**, *11*, 1178−1188.

https://dx.doi.org/10.1021/acsenergylett.0c01063
ACS Energy Lett. 2020, 5, 2246−2252

(41) Mandal, S.; Mukherjee, S.; De, C. K.; Roy, D.; Ghosh, S.; Mandal, P. K. Extent of Shallow/Deep Trap States beyond the Conduction Band Minimum in Defect-Tolerant $CsPbBr_3$ Perovskite Quantum Dot: Control over the Degree of Charge Carrier Recombination. *J. Phys. Chem. Lett.* **2020**, *11*, 1702−1707.
(42) Wu, K.; Liang, G.; Shang, Q.; Ren, Y.; Kong, D.; Lian, T. Ultrafast Interfacial Electron and Hole Transfer from $CsPbBr_3$ Perovskite Quantum Dots. *J. Am. Chem. Soc.* **2015**, *137*, 12792−12795.
(43) De, A.; Mondal, N.; Samanta, A. Hole Transfer Dynamics from Photoexcited Cesium Lead Halide Perovskite Nanocrystals: 1-Aminopyrene as Hole Acceptor. *J. Phys. Chem. C* **2018**, *122*, 13617−13623.
(44) Mondal, N.; De, A.; Samanta, A. All-inorganic Perovskite Nanocrystal Assisted Extraction of Hot Electrons and Biexcitons from Photoexcited CdTe Quantum Dots. *Nanoscale* **2018**, *10*, 639−645.
(45) Yu, P.; Wen, X.; Lee, Y.-C.; Lee, W.-C.; Kang, C.-C.; Tang, J. Photoinduced Ultrafast Charge Separation in Plexcitonic CdSe/Au and CdSe/Pt Nanorods. *J. Phys. Chem. Lett.* **2013**, *4*, 3596−3601.
(46) Mondal, N.; Paul, S.; Samanta, A. Photoinduced 2-way Electron Transfer in composites of Metal Nanoclusters and Semiconductor Quantum Dots. *Nanoscale* **2016**, *8*, 14250−14256.
(47) Grimaldi, G.; Crisp, R. W.; Brinck, S. t.; Zapata, F.; Ouwendorp, M. v.; Renaud, N.; Kirkwood, N.; Evers, W. H.; Kinge, S.; Infante, I.; Siebbeles, L. D. A.; Houtepen, A. J. Hot-electron Transfer in Quantum-dot Heterojunction films. *Nat. Commun.* **2018**, *9*, 2310.
(48) Jiang, Z.-J.; Kelley, D. F. Hot and Relaxed Electron Transfer from the CdSe Core and Core/Shell Nanorods. *J. Phys. Chem. C* **2011**, *115*, 4594−4602.
(49) Paul, S.; Ahmed, T.; Samanta, A. Influence of Divalent Counterions on the Dynamics in DNA as Probed by Using a Minor-Groove Binder. *ChemPhysChem* **2017**, *18*, 2058−2064.
(50) Ahmed, G. H.; Liu, J.; Parida, M. R.; Murali, B.; Bose, R.; AlYami, N. M.; Hedhili, M. N.; Peng, W.; Pan, J.; Besong, T. M. D.; Bakr, O. M.; Mohammed, O. F. Shape-Tunable Charge Carrier Dynamics at the Interfaces between Perovskite Nanocrystals and Molecular Acceptors. *J. Phys. Chem. Lett.* **2016**, *7*, 3913−3919.
(51) De, A.; Das, S.; Mondal, N.; Samanta, A. Highly Luminescent Violet- and Blue-Emitting Stable Perovskite Nanocrystals. *ACS Materials Lett.* **2019**, *1*, 116−122.
(52) Mondal, N.; De, A.; Samanta, A. Biexciton Generation and Dissociation Dynamics in Formamidinium and Chloride-Doped Cesium Lead Iodide Perovskite Nanocrystals. *J. Phys. Chem. Lett.* **2018**, *9*, 3673−3679.
(53) Luo, X.; Liang, G.; Wang, J.; Liu, X.; Wu, K. Picosecond Multi-hole Transfer and Microsecond Charge-separated States at the Perovskite Nanocrystal/tetracene Interface. *Chem. Sci.* **2019**, *10*, 2459−2464.
(54) Wang, J.; Ding, T.; Leng, J.; Jin, S.; Wu, K. Intact" Carrier Doping by Pump-Pump-Probe Spectroscopy in Combination with Interfacial Charge Transfer: A Case Study of $CsPbBr_3$ Nanocrystals. *J. Phys. Chem. Lett.* **2018**, *9*, 3372−3377.
(55) Seth, S.; Ahmed, T.; Samanta, A. Photoluminescence Flickering and Blinking of Single $CsPbBr_3$ Perovskite Nanocrystals: Revealing Explicit Carrier Recombination Dynamics. *J. Phys. Chem. Lett.* **2018**, *9*, 7007−7014.
(56) Ahmed, T.; Seth, S.; Samanta, A. Mechanistic Investigation of the Defect Activity Contributing to the Photoluminescence Blinking of $CsPbBr_3$ Perovskite Nanocrystals. *ACS Nano* **2019**, *13*, 13537−13544.
(57) Nakahara, S.; Tahara, H.; Yumoto, G.; Kawawaki, T.; Saruyama, M.; Sato, R.; Teranishi, T.; Kanemitsu, Y. Suppression of Trion Formation in $CsPbBr_3$ Perovskite Nanocrystals by Postsynthetic Surface Modification. *J. Phys. Chem. C* **2018**, *122*, 22188−22193.
(58) Yarita, N.; Aharen, T.; Tahara, H.; Saruyama, M.; Kawawaki, T.; Sato, R.; Teranishi, T.; Kanemitsu, Y. Observation of Positive and Negative Trions in Organic-inorganic Hybrid Perovskite Nanocrystals. *Phys. Rev. Materials* **2018**, *2*, 116003.

https://dx.doi.org/10.1021/acsenergylett.0c01063
ACS Energy Lett. 2020, 5, 2246−2252

Ultrafast Carrier Dynamics and Charge Transfer Processes in Photoexcited Perovskite Nanocrystals

by Apurba De

Submission date: 22-Oct-2020 03:34PM (UTC+0530)
Submission ID: 1422997534
File name: Thesis_Apurba_De_October_22_Plagiarism_Check_Quoted.pdf (5.04M)
Word count: 22158
Character count: 111729

Ultrafast Carrier Dynamics and Charge Transfer Processes in Photoexcited Perovskite Nanocrystals

ORIGINALITY REPORT

18%	3%	17%	2%
SIMILARITY INDEX	INTERNET SOURCES	PUBLICATIONS	STUDENT PAPERS

PRIMARY SOURCES

1	Apurba De, Somnath Das, Anunay Samanta. " Hot Hole Transfer Dynamics from CsPbBr Perovskite Nanocrystals ", ACS Energy Letters, 2020 Publication	12% Own publication.
2	Submitted to University of Hyderabad, Hyderabad Student Paper	1%
3	Apurba De, Somnath Das, Navendu Mondal, Anunay Samanta. "Highly Luminescent Violet- and Blue-Emitting Stable Perovskite Nanocrystals", ACS Materials Letters, 2019 Publication	1% Own publication.
4	mafiadoc.com Internet Source	1%
5	pubs.rsc.org Internet Source	1%
6	diposit.ub.edu Internet Source	<1%

Nano Letters, 2017
Publication

41 G. Einevoll. "Confinement of excitons in quantum dots", Physical Review B, 02/1992 <1%
Publication

Exclude quotes	On	Exclude matches	< 14 words
Exclude bibliography	On		

Ultrafast Carrier Dynamics and Charge Transfer Processes in Photoexcited Perovskite Nanocrystals

ORIGINALITY REPORT

55%	27%	54%	2%
SIMILARITY INDEX	INTERNET SOURCES	PUBLICATIONS	STUDENT PAPERS

PRIMARY SOURCES

1	Apurba De, Somnath Das, Navendu Mondal, Anunay Samanta. "Highly Luminescent Violet- and Blue-Emitting Stable Perovskite Nanocrystals", ACS Materials Letters, 2019 Publication	15%
2	Apurba De, Somnath Das, Anunay Samanta. " Hot Hole Transfer Dynamics from CsPbBr Perovskite Nanocrystals ", ACS Energy Letters, 2020 Publication	12%
3	pubs.rsc.org Internet Source	8%
4	Apurba De, Navendu Mondal, Anunay Samanta. "Hole Transfer Dynamics from Photoexcited Cesium Lead Halide Perovskite Nanocrystals: 1-Aminopyrene as Hole Acceptor", The Journal of Physical Chemistry C, 2018 Publication	6%
5	mafiadoc.com Internet Source	

Primary Sources NO: 1-7 are own papers.

28.10.2020

		5%
6	APURBA DE, Navendu Mondal, Anunay Samanta. "Luminescence Tuning and Exciton Dynamics of Mn-doped CsPbCl3 Nanocrystals", Nanoscale, 2017 Publication	3%
7	Apurba De, Navendu Mondal, Anunay Samanta. " Luminescence tuning and exciton dynamics of Mn-doped CsPbCl nanocrystals ", Nanoscale, 2017 Publication	2%
8	Submitted to University of Hyderabad, Hyderabad Student Paper	1%
9	J L Marín. Journal of Physics Condensed Matter, 02/16/1998 Publication	<1%
10	diposit.ub.edu Internet Source	<1%
11	M. Chandra Sekhar, Anunay Samanta. "Ultrafast Transient Absorption Study of the Nature of Interaction between Oppositely Charged Photoexcited CdTe Quantum Dots and Cresyl Violet", The Journal of Physical Chemistry C, 2015 Publication	<1%

	Fukata. "Downshifting of highly energetic photons and energy transfer by Mn-doped perovskite CsPbCl3 nanocrystals in hybrid organic/silicon nanostructured solar cells", Nano Energy, 2020 Publication	<1%
42	Maya Isarov, Liang Z. Tan, Maryna I. Bodnarchuk, Maksym V. Kovalenko, Andrew M. Rappe, Efrat Lifshitz. " Rashba Effect in a Single Colloidal CsPbBr Perovskite Nanocrystal Detected by Magneto-Optical Measurements ", Nano Letters, 2017 Publication	<1%
43	G. Einevoll. "Confinement of excitons in quantum dots", Physical Review B, 02/1992 Publication	<1%

Exclude quotes	Off	Exclude matches	< 14 words
Exclude bibliography	On		